**TECHNISCHE UNIVERSITÄT MÜNCHEN**

Department Chemie

Lehrstuhl für Biotechnologie

# Characterization of different Hsp90-client and chaperone-substrate interactions

**Daniel Andreas Rutz**

Vollständiger Abdruck der von der Fakultät für Chemie der Technischen Universität München zur Erlangung des akademischen Grades eines Doktors der Naturwissenschaften genehmigten Dissertation.

Vorsitzender: Prof. Dr. Ville R. I. Kaila

Prüfer der Dissertation:

1. Prof. Dr. Johannes Buchner

2. Prof. Dr. Matthias Rief

Die Dissertation wurde am 05.09.2016 bei der Technischen Universität München eingereicht und durch die Fakultät für Chemie am 07.11.2016 angenommen.

# Inventory

# 1 Introduction

## 1.1 Protein Folding

Proteins form a major group of macromolecules and are indispensable for many essential functions in the cell. Proteins consist of linear polypeptide chains of the proteinogenic amino acids and are synthesized by the ribosome *in vivo*. They have to reach a certain three-dimensional structure to fulfill their biological functions. Most of these structures are well-organized but exceptions exist where the unfolded structure is the desired state (Fink, 2005). The process of protein folding is spontaneous *in vitro* and the information for the respective structure is coded within the primary amino acid sequence of the protein, impressively shown by the pioneering experiments with Ribonuclease A of Christian Anfinsen (Anfinsen et al., 1961). Importantly, proteins cannot find their native structure on a reasonable biological time-scale by sampling all possible conformations. This problem, known as the Levinthal`s paradox, describes that a polypeptide chain with 150 amino acids would take $10^{24}$ years to find its native fold by unbiased sampling of all possible conformations (Levinthal, 1968). There has been much progress in understanding the folding of proteins since the postulation of the paradox in 1968. Protein folding heavily depends on many non-covalent interactions within the primary polypeptide chain. Hydrophobic forces seem to be of special importance as they drive the chain collapse resulting in the burial of hydrophobic side chains within the core of the structure (Kuwajima, 1989). A popular theory of describing protein folding is the so called folding funnel (Figure 1). Rather than taking a single direct way, the protein samples several folding pathways on a funnel-shaped energy surface. In the end, loss of energy and entropy lead to the native state of low energy (Dobson et al., 1998; Kim et al., 2013).

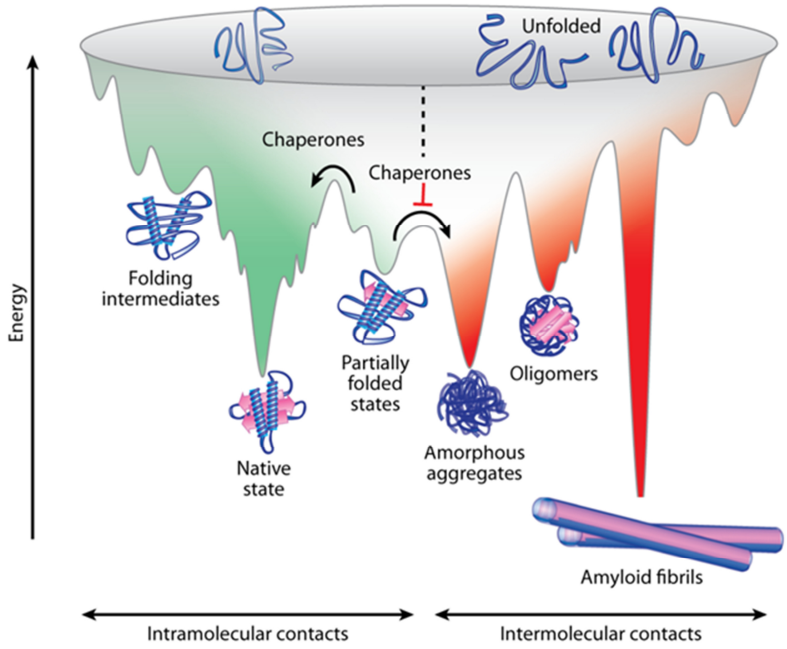


**Figure 1: The protein folding funnel;** by sampling different conformations in an energy landscape proteins achieve their native structure. Favorable native intramolecular contacts stabilize folding intermediates while the protein progresses downhill to find its native structure (green shading). Non-native, but energetically favorable contacts might lead to kinetically trapped intermediates. Chaperones help to overcome the energy barriers promoting progression of partially folded states to the native structure. By preventing unfavorable intermolecular interactions, chaperones prevent aggregation and formation of (toxic) protein deposits in the cell. Adopted from Kim et al. (2013);

By forming the required intramolecular contacts and folding intermediates proteins acquire their native structure. Other energetically favorable intramolecular contacts might lead to partially folded states that typically expose hydrophobic surfaces (Clark, 2004). Partially folded states and unfolded proteins can form non-native, but energetically favorable, intermolecular contacts leading to the formation of amorphous aggregates, oligomers or amyloid fibrils which also represent low-energy wells in the folding landscape (Figure 1). These less-ordered forms often mediate cellular toxicity (Kim et al., 2013).

## 1.2 Molecular Chaperones

Protein folding *in vivo* is far more complex than under test-tube conditions. The cellular environment is highly crowded with protein concentrations of 300-400 mg/ml (Gershenson and Gierasch, 2011; McGuffee and Elcock, 2006). Crowding effects result in favoring compact states

by limiting entropic freedom and also enhance protein aggregation due to increased affinities between proteins in general (Ellis and Minton, 2006). To prevent these unwanted processes, nature has evolved a special family of proteins, the molecular chaperones. Chaperones are ubiquitous and highly conserved among species and fulfill diverse functions in the cell (Richter et al., 2010). Molecular chaperones assist in protecting and folding of newly synthesized proteins and stabilize unfolded/partially folded intermediates but are also involved in protein degradation. Thus, chaperones are indispensable factors in protein homeostasis (McClellan et al., 2005). As the expression of molecular chaperones is often related to stress or heat shock conditions, many of them are termed stress or heat shock proteins (Hsp) (Kim et al., 2013). Members of the heat shock protein family were initially classified according to their molecular mass as Hsp40s, Hsp60s, Hsp70s, Hsp90s, Hsp100s and small Hsps (sHsps). Most members of the Hsp family function in *de novo* folding or refolding in an ATP-dependent manner. These are the so-called foldases (Hsp60s, Hsp70s and Hsp90s). An exception is the group of sHsps which are ATP-independent holdases. sHsps interact mainly with unfolded proteins to prevent their aggregation and present them to Hsp70 for subsequent refolding (Figure 2) (Haslbeck et al., 2005). In cells of higher eukaryotes, the mentioned classes of chaperones form a network for protein homeostasis (Figure 2).

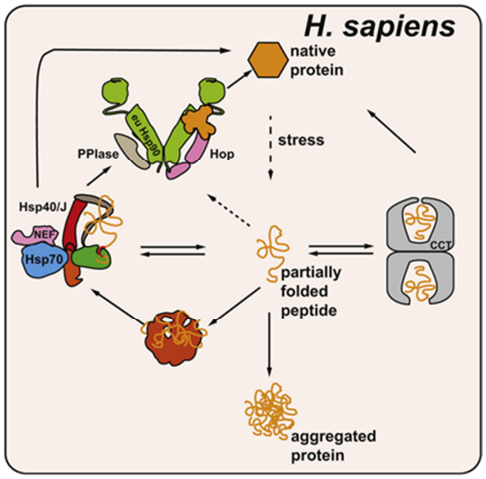


**Figure 2: Heat shock protein network in *H. sapiens*;** Hsp60/CCT (grey), sHsps (brown), Hsp70 (blue) and Hsp90 (green) are strongly connected and are able to assist protein folding in the cell. Higher eukaryotes lack the Hsp100 family proteins. Adapted from Richter et al. (2010);

Similar to the bacterial GroE, the members of the Hsp60 family, like CCT, enclose partially folded intermediates in their double ring structure and allow their folding in an environment that

is protected from the molecular crowding in the cytosol (Frydman, 2001). Hsp70 binds unfolded or partially folded proteins which are folded during its functional cycle. Hsp70 is assisted in its function by a diversity of co-chaperones including nucleotide-exchange factors (NEFs) and J-proteins (Hsp40) (Mayer and Bukau, 2005). Hsp90 binds primarily native-like proteins and shows higher selectivity than Hsp70 (Taipale et al., 2012). Hsp90 is also co-regulated by a large cohort of co-chaperones modulating its function (Taipale et al., 2010). The Hsp70 and Hsp90 system are strongly connected and protein handover from Hsp70 to Hsp90 has been shown for proteins like transcription factors or protein kinases (Mayer and Le Breton, 2015).

### 1.2.1 The Hsp70 system

#### 1.2.1.1 Structure and conformational dynamics of Hsp70

The Hsp70 family of proteins assists in a wide range of folding processes. These include folding and assembly of *de novo* synthesized proteins, refolding of misfolded proteins, membrane translocation, substrate degradation and regulatory control of substrate activities. Thus, Hsp70s fulfill housekeeping functions in folding, signal transduction and protein quality control (Mayer and Bukau, 2005). Hsp70 consists of an N-terminal nucleotide-binding domain (NBD) of 45 kDa and a C-terminal substrate-binding domain (SBD) of 25 kDa linked by a highly conserved linker of random-coil structure (Figure 3 A). The NBD displays an actin-like fold with two separate lobes containing each one subdomain. The nucleotide-binding site is positioned in the cleft between the two lobes and ATP is bound with one $Mg^{2+}$ and two $K^{+}$ ions as co-factors (Bukau and Horwich, 1998; Mayer and Bukau, 2005). The SBD is structured in a ß-sandwich subdomain containing the major interaction site for the substrate and an α-helical lid (Bukau and Horwich, 1998). The conformational changes in the NBD upon ATP binding are allosterically coupled to the substrate binding domain. Thereby, substrate binding and release are regulated by ATP-hydrolysis. When ATP binds to the NBD, the hydrophobic linker and the α-helical lid of the SBD are attached to the NBD forming the open conformation. This results in the opening of the substrate-binding cleft and high on and off rates for the substrate. Thus, the affinity for substrates in this conformation is low and the exchange fast (Figure 3) (Smock et al., 2010; Zhuravleva and Gierasch, 2011).

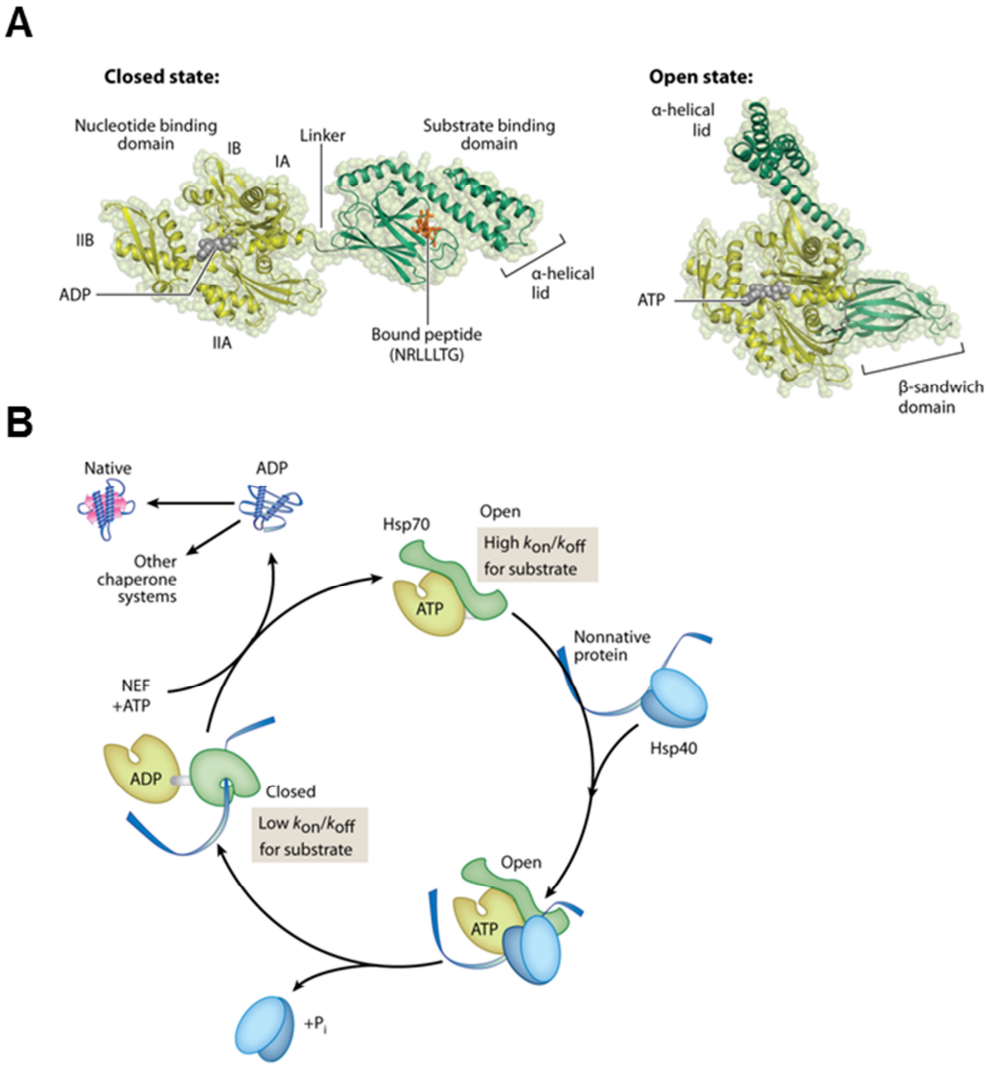


**Figure 3: Structure and conformational cycle of Hsp70; A)** Hsp70 is structured in two domains, a N-terminal nucleotide-binding domain (NBD) and a C-terminal substrate-binding domain (SBD) both connected by a highly conserved linker; Closed state of *E. coli* DnaK (PDB ID: 2KHO) on the left and the open state of *S. cerevisiae* Sse1 (PDB ID: 2QXL) on the right; **B)** Conformational cycle; ATP binding induces the open conformation. Hsp40 delivers the substrate to Hsp70 and stimulates the closed conformation by ATP-hydrolysis. NEFs stimulate ADP release and ATP re-binding induces substrate release. Adopted from Kim et al. (2013)

ATP-hydrolysis is the rate-limiting step in the conformational cycle of most Hsp70 proteins. Hydrolysis drives detachment of the α-helical lid from the NBD resulting in the closure of the SBD over the peptide substrate. In the closed state, the SBD and NBD are loosely held together by the linker that adopts a random-coil structure (Figure 3). In the ADP-bound closed state, on and off rates are significantly lower. Therefore, the affinity for substrates is high and the exchange is slow. Interestingly, it was shown that peptide substrate binding promotes the rate of

ATP-hydrolysis whereas the binding of protein substrates does not affect the ATPase activity of Hsp70 (Bertelsen et al., 2009; Mapa et al., 2010; Mayer et al., 2003). Substrate release is driven by ADP release and ATP re-binding and is thought to promote folding. Proteins that do not fold upon release are able to rebind but also can become degraded (Kim et al., 2013).

#### 1.2.1.2 Substrate binding

Most information about substrate binding to Hsp70 has been derived from a crystal structure of the SBD of *E. coli* Hsp70 (DnaK) in complex with a heptameric peptide substrate (Zhu et al., 1996). The SBD primarily binds to peptide segments of 5-7 residues in length enriched in hydrophobic and flanked by positively charged residues. The peptides segments are bound in an extended conformation by forming hydrogen-bonds between the backbone of the cavity forming loops and the peptide backbone. Additional van-der-Waals contacts are formed between the hydrophobic residues of the peptide and the substrate-binding cavity explaining the preference for hydrophobic substrates (Bukau and Horwich, 1998; Mayer, 2010). Interestingly, the central residue of the peptide segment (position 0) is deeply buried in the substrate-binding cleft which prefers large hydrophobic residues at this position (leucine) and is completely excluded from the solvent. The surface surrounding the cleft shows mainly negative potential suggesting that the flanking positively charged residues of the peptide segments promote substrate association (Zhu et al., 1996). Several structural elements are indispensable for efficient substrate binding. Removal of the α-helical lid or alterations in the hydrophobic arch enclosing the substrate lead to a significant decrease in the substrate affinity primarily by increased dissociation rates. However, the main contribution to the binding is provided by the hydrophobic cleft in the SBD. Alterations in this region result in massively decreased association rates and severely decreased affinities (Mayer and Bukau, 2005; Mayer et al., 2000; Schneider et al., 2016).

#### 1.2.1.3 Hsp70 co-chaperones

Two major groups of co-chaperones regulate the Hsp70 chaperone cycle, the Hsp40 family (J-proteins) and the nucleotide-exchange factors (NEFs) including the Bcl-2 associated athanogene (BAG) domain containing proteins. The Hsp40 family of proteins is a large group of proteins

containing more than 40 members (Kampinga and Craig, 2010). All have an N-terminal J-domain in common that binds the NBD and the linker of Hsp70. Further, all members of the Hsp40 family strongly promote ATP hydrolysis by Hsp70, driving the closed conformation and stable association with the substrate (Figure 3 B) (Kim et al., 2013; Mayer and Bukau, 2005). Apart from that, Hsp40s have diverging functions and specificities. The canonical Hsp40s (class I and II) exhibit Hsp70-independent chaperone activity used for recruiting Hsp70 to non-native substrates although the substrate transfer mechanism remains elusive. The class III Hsp40 group is much more complex and combines the J-domain with various different functionalities. These differences are also reflected in the specificity of Hsp40s for substrates. Whereas the *E. coli* DnaJ and the yeast Ydj1 are highly promiscuous, especially class III proteins show a restricted set of substrates (Kampinga and Craig, 2010).

The group of NEFs has been shown to stabilize a conformation of the NBD with an opened nucleotide-binding cleft providing the basis for ADP release and promotion of substrate exit. It seems plausible that Hsp40 and NEFs cooperate in regulating the Hsp70 chaperone cycle. By promoting cycle kinetics, substrate binding as well as release and providing substrate specificity the co-chaperones effectively expand the abilities of the Hsp70 system (Kampinga and Craig, 2010; Kim et al., 2013; Mayer and Bukau, 2005).

### 1.2.2 The Hsp90 system

The Hsp90 family of chaperones is a ubiquitously expressed, abundant group of chaperones and essential in eukaryotes. Multi-cellular eukaryotes express different Hsp90 isoforms with high homology. Hsp90α and Hsp90β are localized in the cytosol and the nucleus, Grp94 in the endoplasmic reticulum, TRAP1 in the mitochondria and Hsp90C in plastids (Johnson, 2012; Mayer and Le Breton, 2015; Taipale et al., 2010). Similar to other chaperones, Hsp90 can bind to misfolded proteins preventing their aggregation although this is not its main function as Hsp90 is not able to actively refold substrates like Hsp60 or Hsp70 (Mayer and Le Breton, 2015). Instead, Hsp90 acts with a large cohort of co-chaperones on native-like protein substrates, called clients (Johnson, 2012). Hsp90 interacts with a broad spectrum of different client proteins ranging from transcription factors like the steroid hormone receptors (SHR), protein kinases, E3-ligases to structurally unrelated proteins like Tau. An up-to-date list of client proteins can be found on the webpage of the Picard-Lab (https://www.picard.ch) (Taipale et al., 2010). Hsp90 shows despite

of this variety of structural classes high specificity in its choice of client proteins in contrast to other chaperones (Hsp70, Hsp60) involved in general protein folding. Further, the group of client proteins consists of many tumor suppressors, oncogenes as well as cancer-related proteins which are involved in crucial processes like signal transduction, proliferation and apoptosis. Thus, Hsp90 plays a central role in the regulation of essential processes and is hence of special interest as a therapeutic target (Trepel et al., 2010).

### 1.2.2.1 Structure and conformational dynamics

Hsp90 is a member of the GHKL (gyrase, Hsp90, histidine kinase and MutL) superfamily and shows structural homology with other ATPases in this group (Buchner, 1999; Pearl and Prodromou, 2006). Hsp90 is dimeric and each monomer consists of a highly conserved N-terminal domain (Hsp90-N), a middle domain (Hsp90-M) and a C-terminal dimerization domain (Hsp90-C) (Figure 4 A).

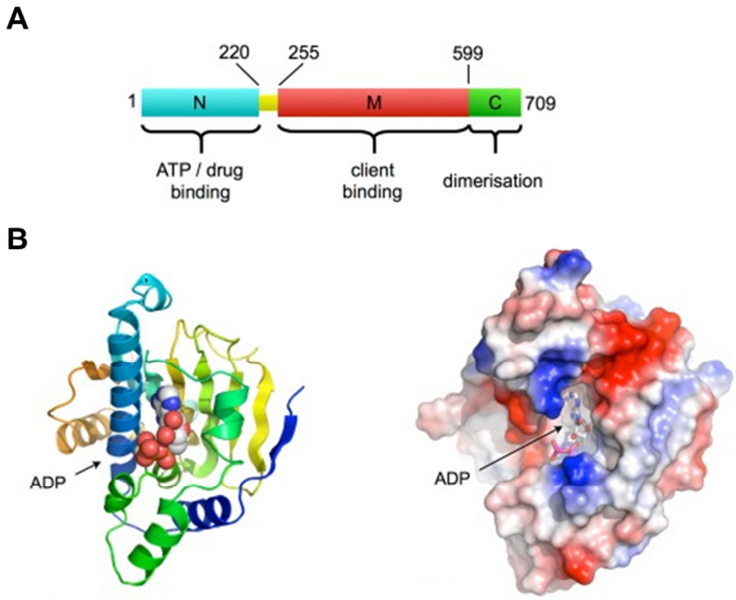


**Figure 4: Hsp90 domain organization and nucleotide binding to the Hsp90-N domain; A)** Hsp90 domain organization; The Hsp90-N domain is shown in cyan, the charged-linker region in yellow, the Hsp90-M domain in red and the Hsp90-C domain in green; Numbers indicate amino acid positions of domain borders. **B)** Nucleotide binding to the Hsp90-N domain; Cartoon representation is shown on the left and the surface representation of the Hsp90-N domain on the right. Arrows indicated position of the nucleotide. Adapted from Pearl (2016);

ATP is bound in the Hsp90-N domain and during the hydrolysis cycle, co-chaperones and client proteins associate with Hsp90. The ATP-binding site is formed by an α- and β-sandwich motif (Figure 4 B) (Ali et al., 2006). Natural inhibitors like Radicicol or Geldanamycine can effectively bind to the ATP-binding pocket and inhibit Hsp90 (Whitesell and Lindquist, 2005). Due to the strong conservation of Hsp90, these inhibitors are applicable for a large number of Hsp90s from different species (Taipale et al., 2010). The Hsp90-N domain is connected to Hsp90-M via a charged linker. Mutational studies have shown that the linker plays an important role in client binding and is also involved in the modulation of Hsp90 by co-chaperones (Hainzl et al., 2009; Jahn et al., 2014; Tsutsumi et al., 2009). The Hsp90-M domain consists of two αβα-motifs connected by a number of helices. Hsp90-M is thought to be the major site of interaction with different client proteins. Alterations at many different positions have been suggested to affect the association of Hsp90 with SHRs and protein kinases (Harris et al., 2004; Meyer et al., 2003; Sato et al., 2000; Shiau et al., 2006). The Hsp90-C domain is crucial for the structural integrity and modulation of Hsp90 by co-chaperones. Hsp90-C is a structurally mixed α-/β-domain. Two helices of each monomer form a four-helix bundle in the dimer interface, promoting dimerization of Hsp90. Further, the Hsp90-C domain contains the important MEEVD-motif at its very C-terminus which is indispensable for the interaction with tetratricopeptide-repeat (TPR) domain containing co-chaperones (Harris et al., 2004; Taipale et al., 2010).

Over the past 15 years, many structural and functional studies have improved the understanding of the processes and the conformational transitions of Hsp90 during its chaperone cycle. In the apo-form (in the absence of ATP), Hsp90 forms a wide-open V-shaped dimer with high rotational freedom between the individual subdomains (Figure 5 A). Upon binding of ATP, Hsp90 transits to a compact closed conformation. The N-terminal domain contains a lid segment that closes over the nucleotide binding site when ATP is bound and N-terminal dimerization is promoted by strand exchange between the two domains. Subsequent conformational rearrangements lead to a closed, twisted dimer in which important contacts between Hsp90-N and –M are formed (Figure 5 B) (Ali et al., 2006; Dollins et al., 2007; Krukenberg et al., 2008; Shiau et al., 2006). A non-catalytic Arginine residue from a flexible loop of Hsp90-M is crucial for ATP-hydrolysis in this closed state (Cunningham et al., 2008; Prodromou, 2012). As residues from Hsp90-N and –M are involved in the hydrolysis, Hsp90 is termed a split-ATPase (Huai et al., 2005). ATP-hydrolysis and ADP release trigger dissociation of the N-terminal domains, restoring the open conformation.

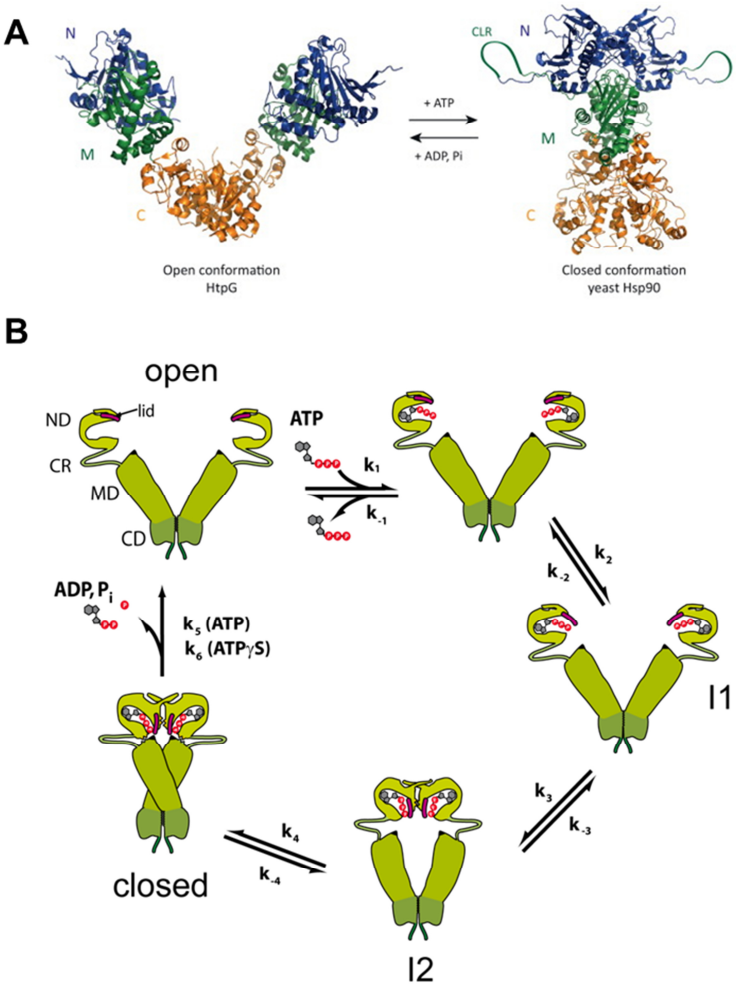


**Figure 5: The conformational cycle of Hsp90; A)** Crystal structures of open *E. coli* Hsp90 (HtpG, PDB ID: 2IOQ) and closed yeast Hsp90 in the presence of nucleotide (PDB ID: 2CG9); **B)** Schematic representation of the conformational cycle of Hsp90. Upon ATP binding, conformational changes in the N-terminal domain occur. Rearrangements include the ATP lid, which closes over the nucleotide binding pocket (I1) and dimerization of the N-terminal domains via an N-terminal strand exchange (I2, closed I). Association of the Hsp90-N and Hsp90-M domains leads to the fully closed state of the Hsp90 dimer (closed II). ATP hydrolysis and ADP release lead to dissociation of the N-terminal domains, restoring the open conformation. Adapted from Rohl et al. (2013) and Hessling et al. (2009);

ATP-hydrolysis is exceptionally slow, with yeast Hsp90 having an ATPase rate of ~ 1 $min^{-1}$ and human Hsp90 being tenfold slower (Panaretou et al., 1998; Richter et al., 2008). Interestingly, the rate limiting steps of the hydrolysis reaction are the large conformational changes occurring prior to the N-terminal dimerization and not the ATP-hydrolysis itself (Hessling et al., 2009). Some eukaryotic Hsp90s seem to be highly dynamic in switching between the described conformations especially in the apo-state. ATP binding does not ultimately lead to the closed state as

interconversion between the states seems to be possible. It has been suggested that nucleotides slightly change the energy barriers between states, shifting the continuous equilibrium of open and closed states towards a more compact conformation. Thus, it seems that members of the Hsp90 family act as probabilistic machines (Graf et al., 2009; Mickler et al., 2009; Ratzke et al., 2010). Crystal structures of *E. coli,* yeast and human Hsp90 in the absence of nucleotide and in the presence of ADP or AMP-PNP exhibited significantly different conformations but all were highly symmetric (Ali et al., 2006; Dollins et al., 2007; Shiau et al., 2006). Nevertheless, a recent structure of TRAP1 from *D. rerio* displayed a significantly asymmetric dimer conformation with one protomer arm assuming a yeast-like conformation and the other showing an altered unknown conformation (Lavery et al., 2014; Mayer and Le Breton, 2015).

#### 1.2.2.2 Hsp90 co-chaperones

Co-chaperones assist Hsp90 in fulfilling its functions and provide, besides post-translational modifications, an additional dimension of regulation. In higher eukaryotes more than 20 different co-chaperones are known with diverse functions for example in client recruitment or localization. Co-chaperones are able to stabilize certain Hsp90 conformations and bind sequentially to Hsp90 by forming asymmetric complexes. Thereby, binding of one co-chaperone stabilizes a certain conformation that promotes association with the next co-chaperone (Li et al., 2011). Thus, co-chaperones are able to control and drive the Hsp90 chaperone cycle. Most of the known co-chaperones use the TPR-domain to interact with the extreme C-terminal tail of Hsp90. The TPR-domain consists of tandem repeats of a 34 amino acid long consensus sequence forming a cleft of seven anti-parallel α-helices which binds to the C-terminal MEEVD (Hsp90) and/or EEVD (Hsp70) motif. In general, Hsp90 co-chaperones can be classified into three groups: client-recruiters, remodeling or late acting co-chaperones (Rohl et al., 2013; Smith, 2004);
The best studied client recruiting co-chaperone is the TPR-protein Sti1/Hop (stress inducible 1/ Hsp70-Hsp90 organizing protein). It is has been shown to promote the client transfer from Hsp70 to Hsp90 in general by connecting the two chaperone cycles. Sti1/Hop is structured in three TPR-domains and two DP (aspartate-proline rich)-domains and shows homology to Hip (Hsp70-interacting protein). TPR1 is linked by the DP1-domain to two TPR-domains 2A/2B which are followed by the DP2-motif. The different TPR-domains show significant specificity for Hsp70 or Hsp90. TPR2A only binds to Hsp90 whereas TPR1 and 2B are able to associate with Hsp70.

Thus, Sti1/Hop can simultaneously bind Hsp70 and Hsp90. Binding to the TPR-domains is strictly controlled by Hsp90. In the absence of Hsp90, Hsp70 binds with high affinity to TPR2A in a compact Sti1 conformation. When Hsp90 is present and bound to TPR2A, the Hsp70 binding site is shifted to TPR1 indicating regulation by Hsp90 to assure client transfer (Rohl et al., 2015b). Further, Sti1/Hop seems to be regulated by inhibitory phosphorylation (Rohl et al., 2015a). Additional contacts of Sti1/Hop with Hsp90-N and –M promote an open Hsp90 conformation in which the ATPase activity is inhibited in a non-competitive manner (Lee et al., 2012; Richter et al., 2003; Rohl et al., 2013; Schmid et al., 2012; Southworth and Agard, 2011).

Another inhibiting client-recruiting co-chaperone is Cdc37 (cell division cycle 37 homolog). Similar to Sti1/Hop, Cdc37 stabilizes an open Hsp90 conformation by blocking lid-closure and N-terminal domain association. In contrast to the generally recruiting Sti1/Hop, Cdc37 recruits specifically kinases to Hsp90 (Gaiser et al., 2010; Roe et al., 2004; Taipale et al., 2012; Verba et al., 2016).

The co-chaperone Sgt1 (suppressor of G2 allele of skp1) recruits the diverse class of nucleotide-binding Leucine-rich repeat receptors (NLR) to Hsp90. Interestingly Sgt1 contains a TPR-domain but interacts with Hsp90 with its CS (CHORD and Sgt1) domain. Sgt1 binds N-terminal in Hsp90 but does not influence the ATPase activity (Kadota et al., 2008; Kadota et al., 2010).

Similar to Sgt1, the co-chaperones Tah1 (TPR-containing protein associated with Hsp90) and Pih1 (protein interacting with Hsp90) display high client specificity. Both co-chaperones are linked to chromatin remodeling complexes and small nuclear ribonucleoprotein (RNP) maturation. In a first step, Tah1 interact with its TPR-domain with Hsp90 and recruits Pih1 to the complex. In this ternary complex, the ATPase cycle of Hsp90 is arrested (Eckert et al., 2010). By comparing the features of client recruiting co-chaperones, it seems that all recruiters prime Hsp90 for client binding by arresting the cycle kinetics (except Sgt1) and by presenting an open Hsp90 conformation to the client (Rohl et al., 2013).

As mentioned in an earlier section, transitions between the open and the closed conformation are iso-energetic and can occur spontaneously (Mickler et al., 2009). Remodeling co-chaperones are able to reduce these fluctuations by binding and stabilizing certain conformations. One of the best studied remodeling co-chaperones is Aha1 (activator of Hsp90 ATPase). Aha1 promotes the conformational changes preceding the closed conformation and stimulates the N-terminal dimerization of Hsp90 (Retzlaff et al., 2010). Together with binding to Hsp90-N and –M, Aha1 establishes the most pronounced activation of Hsp90. Interestingly only one Aha1 per Hsp90

dimer is required to establish the effect, indicating an asymmetric stimulatory mechanism. As Aha1 is relatively client unspecific, it has been thought to play a role in generally regulating the dwell-times of clients on Hsp90 (Koulov et al., 2010; Meyer et al., 2004; Retzlaff et al., 2010).

The protein phosphatase 5 (PP5) has, in contrast, an indirect effect on the conformational continuum of Hsp90. By binding to Hsp90 via its TPR-domain, the auto-inhibition of PP5 is abrogated, leading to dephosphorylation of Hsp90 and to altered client maturation *in vivo* (Rohl et al., 2013; Soroka et al., 2012). PP5 competes for its binding to Hsp90 with the large peptidyl-prolyl isomerases (PPIases) FK506 binding protein (FKBP) 51, FKBP52 and Cyclophilin 40 (Cyp40) (Johnson and Toft, 1995; Pirkl and Buchner, 2001). The large PPIases display prolyl-isomerase function but may function independent of that (Pirkl and Buchner, 2001). By using their own chaperoning function, these proteins might directly interact with clients but their exact functions remain elusive (Pirkl and Buchner, 2001). Large PPIases have been commonly observed in SHR complexes, although the SHRs seem to have preferences (Smith and Toft, 2008). FKBP52 together with PP5 was preferentially bound by GR, whereas FKBP51 was increased in PR complexes and Cyp40 in ER complexes (Barent et al., 1998; Ratajczak et al., 1990). Further, FKBP51 (inhibitory) and 52 (stimulatory) differentially influence hormone binding to GR and a role in Hsp90-dependent nuclear translocation of SHRs has been implicated (Reynolds et al., 1999; Riggs et al., 2003; Vandevyver et al., 2012).

p23/Sba1 (increased sensitivity to benzoquinone ansamycins) acts in late stages of client maturation. p23 was first identified in the context of SHRs and has been shown to stabilize Hsp90-SHR complexes (Johnson and Toft, 1995). The crystal structure of an Hsp90-p23 complex revealed the molecular basis for its functioning (Ali et al., 2006). Binding of p23 to the Hsp90-N domain interface, stabilizes the complete closure of the Hsp90 dimer. By trapping a hydrolysis-competent state the ATPase activity is inhibited enabling client activation (Johnson and Toft, 1995; Richter et al., 2004). Dissociation is linked to ATP-hydrolysis and client release (McLaughlin et al., 2006; Richter et al., 2004; Rohl et al., 2013). Interestingly, the flexible C-terminal tail conveys intrinsic chaperone function to p23 and it also functions Hsp90-independent e.g. in the context of the maintenance of telomeres (Echtenkamp et al., 2011; Weaver et al., 2000; Weikl et al., 1999).

A direct link of Hsp90 to the ubiquitin-proteasome degradation pathway exists in higher eukaryotes by the co-chaperone CHIP (carboxyl terminus of Hsp70-interacting protein). CHIP

binding to Hsp90 via its TPR-domain releases Hop and p23. Clients are ubiquitinated by its E3-ligase function and directed for degradation (Kundrat and Regan, 2010; Rohl et al., 2013).

### 1.2.2.3 Client recognition and binding sites on Hsp90

Hsp90 differs significantly from other chaperones involved in general protein folding as it binds its clients in a partially or fully folded state (Taipale et al., 2010). There is an increasing list of Hsp90 clients but still little is known about the exact mechanisms of client recognition. As the group of Hsp90 clients is structurally highly diverse and common structural features or sequence motifs are lacking, client recognition is thought to be based on general principles such as thermodynamic instability (Boczek et al., 2015; Falsone et al., 2004; Taipale et al., 2012; Wu et al., 2012). It is speculated that a typical client is arrested at a late stage of maturation, associates with Hsp90 and awaiting further signals like ligand binding or phosphorylation. These signals subsequently induce a final folding process which is assisted by Hsp90 (Mayer and Le Breton, 2015).

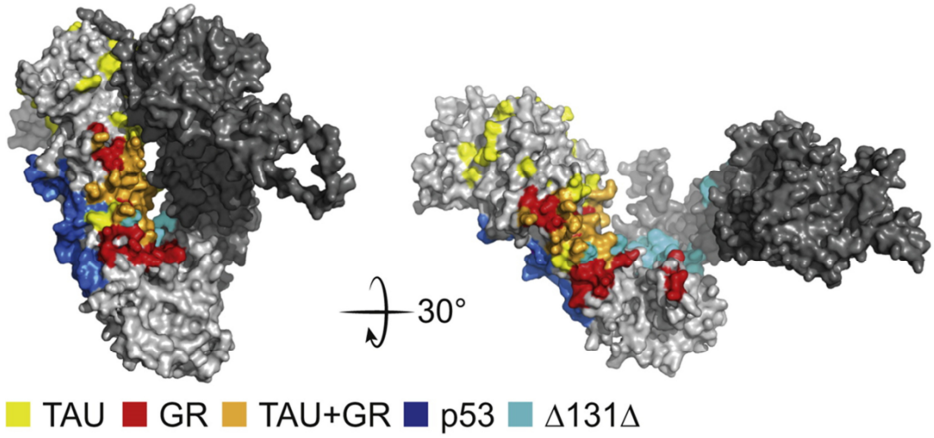


**Figure 6: Comparison of client binding sites on Hsp90;** Hsp90 residues implicated in client interaction by NMR, SAXS or HDX MS are colored; Tau in yellow, GR-LBD in red, overlay of Tau and GR-LBD in orange, p53 in blue and Δ131Δ in cyan; Adopted from Mayer and Le Breton (2015);

Due to the intrinsic instability of many Hsp90-clients, structural approaches have been challenging. Nevertheless, over the past several years an increasing body of information about the interaction of Hsp90 with several clients has been presented. A fragment of the staphylococcal nuclease, termed Δ131Δ, was extensively studied in its interaction with *E. coli* Hsp90 (Htpg) by

combining FRET, SAXS and NMR data. The results suggested that Δ131Δ is not bound when fully folded and that Hsp90 binds to locally structured regions within the protein via its of N-terminal and middle domain (Figure 6) (Street et al., 2011).

The interaction of the microtubule-associated protein Tau with human Hsp90 was studied by NMR and SAXS using full length human Hsp90 specifically labeled at isoleucines. The authors suggested that Tau binds to Hsp90 via its microtubule-binding repeats and that no significant structural changes were induced in Tau upon binding to Hsp90. Due to the limited number of isoleucines that were affected in Hsp90 by Tau, an exhaustive modeling approach was applied to establish a binding surface of Tau on Hsp90. In this model, Tau occupies a very large binding surface in Hsp90-N and-M involving charged and hydrophobic residues (Figure 6). Despite this large interaction surface, the interaction sites for most co-chaperones seemed to be unaffected (Karagöz et al., 2014).

By using isolated domains of yeast Hsp90, Hagn and co-workers could map the binding site of the tumor-suppressor p53 on Hsp90. p53 mainly interacted with Hsp90-C but also moderately affected residues in Hsp90-N and –M, in line with the notion that full-length Hsp90 is required for maturation (Figure 6) (Hagn et al., 2011). In contrast to other studies, the authors did not detect significant unfolding of p53 in the presence of Hsp90 (Park et al., 2011; Rudiger et al., 2002).

For the glucocorticoid receptor (GR), and also other SHRs, many residues in Hsp90-N, -M and –C have been identified by mutational approaches to affect GR maturation and function *in vivo* (Fang et al., 2006; Pratt and Toft, 1997). A recent NMR study using purified GR-LBD and yeast Hsp90-domains supported the mutational approaches, mapping the GR-LBD binding site mainly to Hsp90-M with contributions from Hsp90-N and –C partly overlapping with the proposed Tau binding site (Figure 6). Further the authors proved that Hsp90 interacts with a fully folded hormone-bound GR-LBD and that GR is on its own able to alter the Hsp90 cycle kinetics by inhibiting the ATPase activity in a partially closed conformation (Lorenz et al., 2014; Mayer and Le Breton, 2015).

In pioneering work, Vaughan and co-workers reconstructed the Hsp90-Cdc37-Cdk4 complex from negative-stain EM micrographs. Their work implicated Cdk4 binding to mainly the outside parts of Hsp90-N with some contacts in Hsp90-M especially involving a loop segment around tryptophan 300 (Vaughan et al., 2006). In 2016, Verba et al. could present a significantly improved reconstruction of the very same complex at 3.9 Å, drawing a completely different

picture. Due to the increased resolution, the authors could identify that Hsp90 assumes a closed conformation clamping around the partially unfolded kinase and thereby separating the kinase N- and C-lobe. Interaction of Hsp90-M with the N- and C-lobe protects the unfolded state although the exact contacts were not mentioned by the authors (Verba et al., 2016).
The previous paragraphs showed that the interaction of Hsp90 with its clients is highly diverse and no clear guideline exists of how Hsp90 acts on the clients. Thus, it can be speculated that Hsp90 is, similar to the regulation by co-chaperones, modulated by its client proteins. The clients might be able to stabilize a certain conformations and thereby adapting Hsp90 to their specific requirements (Lorenz et al., 2014; Rohl et al., 2013).

### 1.2.3 Hsp90 client proteins

#### 1.2.3.1 The Glucocorticoid receptor

Glucocorticoids (GC) play a major role in the control of many essential biological processes like growth, reproduction or immunity. This is underlined by the fact that ~ 20 % of all genes in human leukocytes are under the control of glucocorticoid-responsive elements (GRE). Further, GCs represent one of the most widely applied therapeutics used in inflammatory, autoimmune or lymphoproliferative disorders (Nicolaides et al., 2010). The action of GCs is mediated by the glucocorticoid receptor (GR), a ligand-dependent transcription factor of the steroid nuclear receptor superfamily. The GR mainly resides in the cytoplasm in the absence of its hormone but translocates into the nucleus upon ligand binding. There, it positively and negatively regulates the expression of GC-responsive genes (Chrousos, 2004; Duma et al., 2006; Zhou and Cidlowski, 2005).

##### 1.2.3.1.1 Structure and function

The GR has two highly identical isoforms, α and β. The α-isoform is the predominant in the cytoplasm. The GR is a modular structured protein containing an amino-terminal A/B region, also termed N-terminal domain (NTD), the C-domain or DNA-binding domain (DBD), the D-domain or hinge region and the E-domain or ligand-binding domain (LBD) (Figure 7).

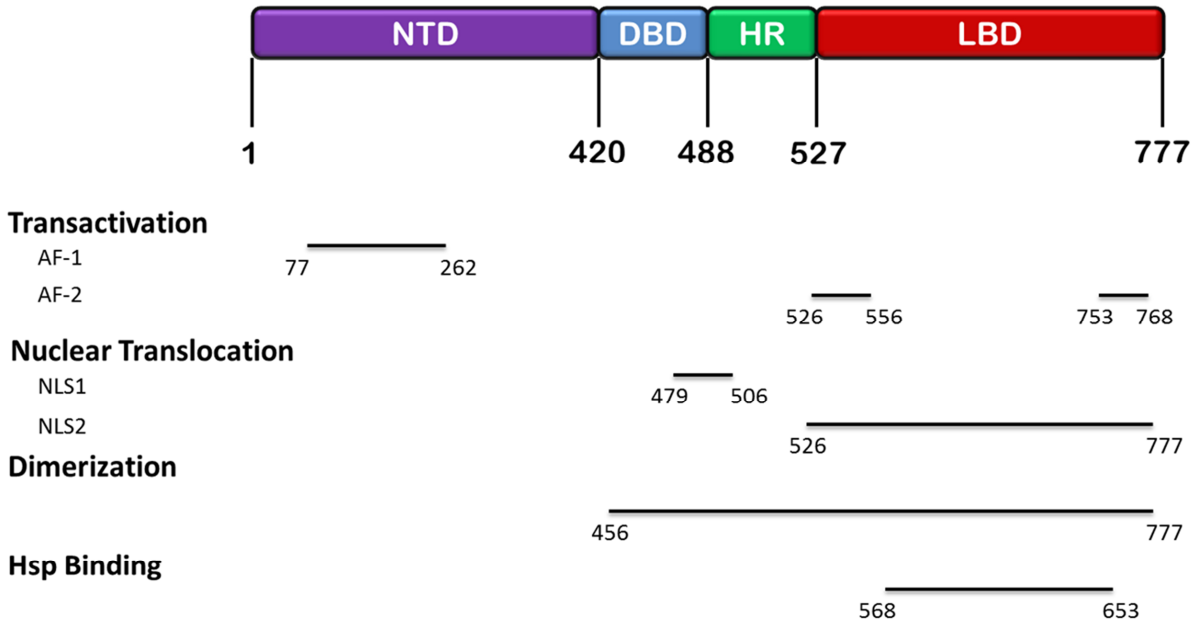


**Figure 7: Domain organization of the GR;** The GR-NTD is colored in purple, the DNA-binding domain (DBD) in blue the hinge region (HR) in green and the ligand-binding domain (LBD) in red; Numbers indicate amino acid positions of domain borders; Functional motifs in the respective domains are indicated by bars and numbers of the amino acid positions; Adapted from Nicolaides et al. (2010);

The NTD is mainly unstructured *in vitro* and contains a major transactivation domain (AF-1) important for the interaction with transcriptional co-regulators (Kumar and Thompson, 2012). The NTD seems to be post-translationally modified and recent studies indicate that it might fold upon interaction with the transcriptional machinery (Kumar and Thompson, 2012). The DBD consists of two zinc-finger motifs. The zinc ion is tetrahedrally coordinated by four cysteine residues and forms together with two α-helices the recognition site for the GREs. These elements contain two inverted hexametric repeat sequences (AGAACA) separated by three nucleotides (John et al., 2011). Importantly, the DBD contains additional motifs important for receptor dimerization and nuclear translocation. Dimerization has been conceived as a general prerequisite for GR activity. Dimerization occurs mainly on activating GREs, as repressing elements have been shown to promote binding of GR in an orientation which disconnects the dimerization interfaces (Hudson et al., 2013). The hinge region mediates flexibility to the GR and is further involved in nuclear translocation. The LBD is structured in 12 α-helices and four short β-strands and folds into a three layer helical domain (Figure 8). During ligand-binding induced activation of GR, the hormone binds to a central cavity resulting in compaction of the whole structure

(Nicolaides et al., 2010). In an agonist-bound form the important second transactivation motif AF-2 is formed by positioning of helix 12 (H12) (Figure 8 A). When antagonists, like the contraceptive Mifepristone, are bound to the LBD, the AF-2 is significantly altered by repositioning of H12 (Figure 8 B) (Schoch et al., 2010). These different conformations provide the structural basis for interaction of the LBD with different transcriptional co-regulators depending on transcriptional activation or repression. Importantly, the LBD is the major site of the interaction with molecular chaperones and is additionally required for dimerization and nuclear translocation (Bledsoe et al., 2002; Duma et al., 2006; Kauppi et al., 2003; Kumar and Thompson, 2012; Tanenbaum et al., 1998; Zhou and Cidlowski, 2005).

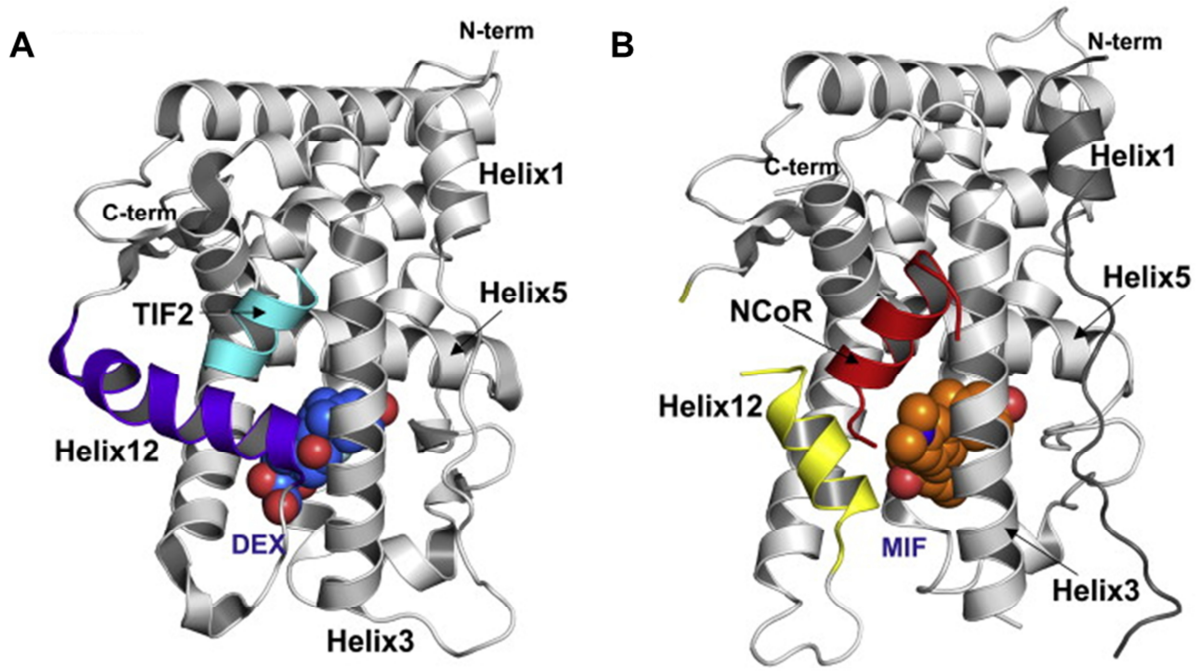


**Figure 8: Repositioning of Helix 12 and co-regulator association upon agonist (Dex) and antagonist (Mifepristone, MIF) binding to the GR-LBD; A)** Structure of GR-LBD-F602S in its agonist (Dex) conformation with bound co-activator peptide Tif2 as indicated. **B)** Structure of GR-LBD-F602S, C638D, W712S in its antagonist (MIF) conformation with bound co-repressor peptide NcoR as indicated. The position of helix 12 occupies different locations upon agonist or antagonist binding and thus creates compatible interaction sites for co-regulators. Adapted from Schoch et al. (2010);

The GR-controlled gene activation or repression is supported by many different co-factors. In the nucleus, GR binds as a homo-dimer to the promoter region of GC-responsive genes by recognizing the chromatin structure of GREs (John et al., 2011). Binding promotes recruitment of

various factors like chromatin remodeling complexes, Histone and other modifying factors. Cooperation of the different factors triggers interaction with the RNA polymerase III complex effectively initiating transcription (Acevedo and Kraus, 2004; Lemon and Tjian, 2000; Moehren et al., 2004). Such co-factors, also termed scaffolding steroid receptor co-activators (SRC), are for example SRC-1, -2 (Tif2) and SRC-3 (RAC3). The co-activators have a LXXL-motif in common for the interaction with the AF-2 in the agonist-bound LBD but also seem to associate with the AF-1 in the NTD (Figure 8) (Bledsoe et al., 2002; Khan et al., 2012). Gene repression by GR is conferred by different mechanisms like receptor cross-talk, binding to negative response elements, antagonist and/or co-repressor binding. Binding of an antagonist, like Mifepristone, leads to alterations in the AF-2 by repositioning of H12 (Figure 8 B). Thereby, co-repressors like SMRT or NcoR can associate with the LBD via their ΦXXΦΦ motif (Φ is any hydrophobic amino acid) effectively repressing transcription (Burke and Baniahmad, 2000; McKay and Cidlowski, 1999; Nagy et al., 1999; Surjit et al., 2011). Studies with other SHRs suggested that the same mechanism seems to hold true for unliganded apo receptors (Horlein et al., 1995). Of note, also chaperones were shown to modulate the transcriptional response of GR. It seems that Hsp90 and p23 are involved in receptor recycling whereas Hsp70 and cofactors seem to promote GR degradation after termination of transcription (Freeman and Yamamoto, 2002; Pratt et al., 2004).

#### 1.2.3.1.2 Maturation and interplay with chaperones

The GR is one of the most stringent Hsp90 clients and its function *in vivo* is strictly dependent on the stable interaction with Hsp90 (Picard et al., 1990). Early studies have shown that Hsp90 is required to establish and maintain a GR-conformation with high affinity for hormones (Dittmar et al., 1997). Experiments using immune-precipitated GR and other SHRs suggested that upon removal of Hsp90 the hormone binding affinity is rapidly lost but can be re-established by the addition of Hsp90, ATP and other chaperone components (Scherrer et al., 1990; Smith, 1993). *In vitro* assemblies with purified components were used to establish a minimal system to present a GR with high affinities for hormones. This minimal system is comprised of Hsp40, Hsp70, Hop, Hsp90 and p23 (Figure 9) (Morishima et al., 2000b; Pratt and Dittmar, 1998).

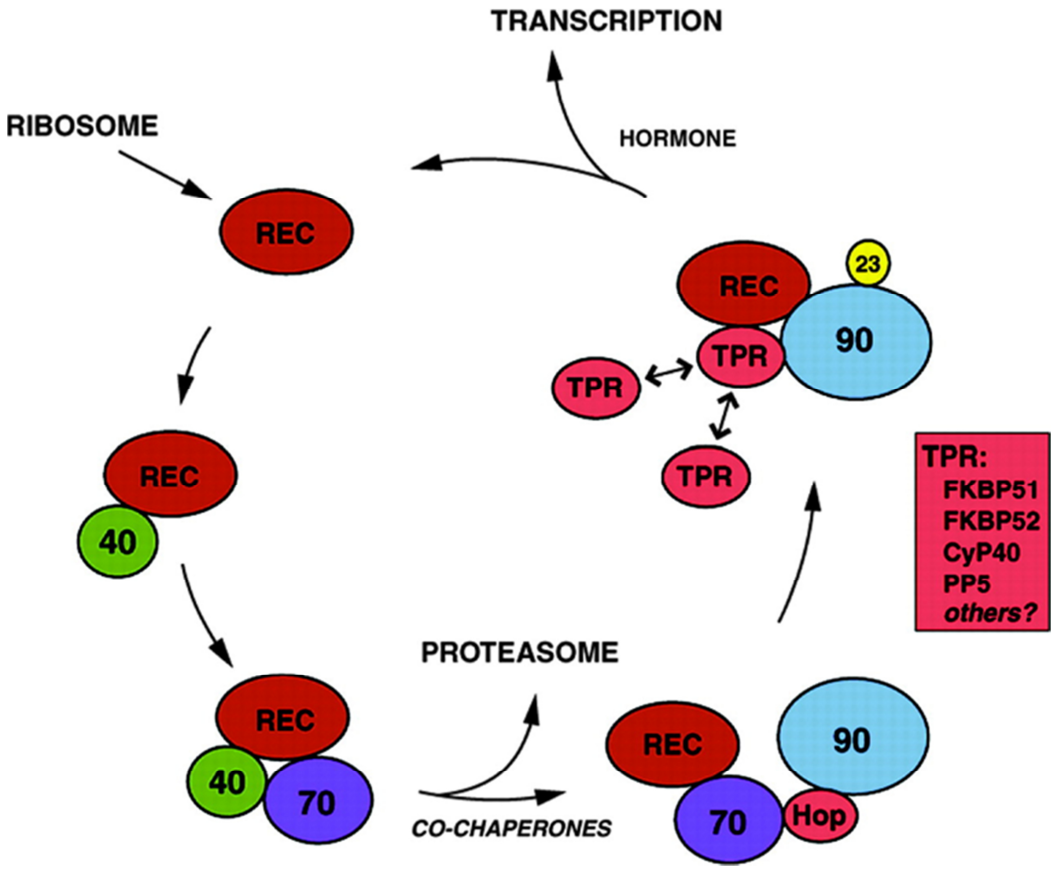


**Figure 9: Cyclic assembly of GR with molecular chaperones;** Newly synthesized GR (REC) is bound by Hsp40 and transferred to the Hsp70 system. Binding of the co-chaperone Hop together with Hsp90 promotes the transfer of GR to the Hsp90 system. Binding of p23 stabilizes the Hsp90-GR complex. TPR-domain containing co-chaperones might dynamically compete for binding to the GR-Hsp90-p23 complex. Hormone binding stimulates nuclear translocation and initiation of the transcriptional response. Adapted from Smith and Toft (2008);

Hsp40 binds the *de novo* synthesized GR and mediates the transfer to the Hsp70 system. Different Hsp70 co-chaperones like Bag1 or CHIP might act on the GR-Hsp40/Hsp70 complex, releasing GR and promoting its degradation. In a next step, Hop together with Hsp90 binds to the complex forming the intermediate transfer complex. ATP-binding to Hsp90 results in the exit of Hsp40 and Hsp70 allowing the GR to bind hormone with high affinity. Exchange of Hop by another TPR-containing co-chaperone like the large PPIases FKBP51, 52, Cyp40 or the phosphatase PP5 promotes cycle progression and entry of p23 which stabilizes the GR-Hsp90 complex (Grad and Picard, 2007; Smith and Toft, 2008). Recent studies using GR-LBD purified from *E. coli* added important aspects to the understanding of the GR-chaperone interplay. In the presence of Hsp40, Hsp70 and ATP, hormone binding to the GR-LBD was prevented presumably by Hsp70-induced alterations in the ligand binding site (Kirschke et al., 2014). The presence of

the full chaperone system (Hop, Hsp90, p23) could effectively restore and increase the hormone binding affinity of GR-LBD from Hsp40/Hsp70. In this context, it was speculated that Hsp90 might act as an ATP-dependent Hsp70 NEF promoting Hsp70 release from the client transfer complex although experimental evidence was lacking (Kirschke et al., 2014). It was generally perceived for a long time that GR dissociates from Hsp90 upon binding of hormone in a process called receptor transformation (Pratt and Toft, 1997). It was thought that upon release from Hsp90 the nuclear localization signals (NLSs) in the HR and LBD are exposed, leading to nuclear translocation by nuclear import receptors (importins) (Freedman and Yamamoto, 2004; Picard and Yamamoto, 1987). Recent progress on the interaction of hormone-bound GR (holo) with Hsp90 conveyed a significantly different picture. It was found that the holo-GR-LBD stably interacts with Hsp90, preferentially in a semi-open Hsp90 conformation in the presence of ATP (Lorenz et al., 2014). In this conformation the ATPase activity and therefore the chaperone cycle of Hsp90 was significantly inhibited by the GR-LBD. The authors could show that binding of ADP led to a decrease in the affinity of the GR-LBD for Hsp90 (Lorenz et al., 2014) supporting earlier studies suggesting that exit of GR from Hsp90 is dependent on ATP-hydrolysis and not on ligand binding (Grenert et al., 1997; Obermann et al., 1998; Panaretou et al., 1998; Smith, 1993). Further, it was observed that co-chaperones like p23 and Cpr6 (PPIase) could simultaneously bind to Hsp90 promoting the exit of Sti1 and cycle progression to the late complex. In this late complex, p23 acted synergistically with the GR-LBD by inhibiting the ATPase activity resulting in a prolonged Hsp90-client interaction (Lorenz et al., 2014). The extended association might play an important role in Hsp90-dependent receptor trafficking. Several studies have shown that GR translocation to the nucleus is inefficient in the presence of the Hsp90-inhibitor Geldanamycin suggesting an efficient Hsp90-dependent pathway (Galigniana et al., 2004; Galigniana et al., 1998). It was further shown that GR, Hsp90 and FKBP52 co-immunoprecipitated with the dynein motor complex providing experimental basis for the Hsp90-dependent translocation along microtubule tracks (Echeverria et al., 2009; Galigniana et al., 2004; Galigniana et al., 2002; Galigniana et al., 2001). This process would require a stable interaction of Hsp90 with GR as a sudden release would result in an uncontrolled hormone response supporting the idea that SHR have maintained chaperone interactions for regulatory purposes (Smith, 1993).

### 1.2.3.2 The microtubule-associated Tau

The microtubule-associated protein Tau is best known for accumulating in several neurodegenerative diseases termed tauopathies such as Alzheimer`s disease (AD) or frontotemporal dementia. Reasons for the pathogenic behavior are diverse and range from missense mutations in the Tau gene (MAPT) to environmental factors, like brain injuries and unknown origins like in age-related AD. Due to its disordered structure, Tau is subjected to heavy post-translational modifications (PTM) like phosphorylation, acetylation or proteolytic cleavage leading to various consequences for the structural dynamics of Tau. Tau is able to form β-sheet fibrils leading to formation of neurofibrillary tangles which ultimately result in cell death. So far, the process of the assembly and toxicity of Tau aggregates is poorly understood but it seems that PTMs play an important role (Sabbagh and Dickey, 2016).

#### 1.2.3.2.1 Structure, function and post-translational modifications of Tau

Tau is an intrinsically disordered protein with a strong propensity for self-aggregation into β-sheet structures.

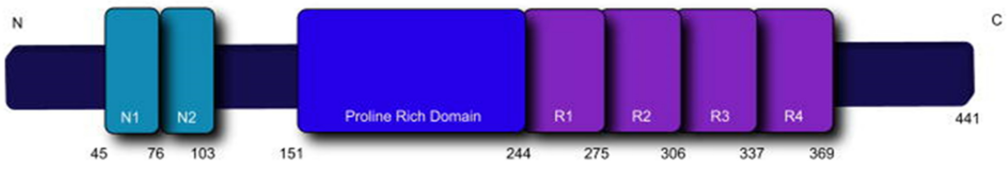


**Figure 10: Domain architecture of Tau;** Tau is comprised of an acidic N-terminal domain (N1, N2) in cyan, a Proline-rich domain in blue, and 3-4 (dependent on the isoform) microtubule binding repeat regions termed R1-R4 in purple. Adapted from (Fontaine et al., 2015)

Tau consists of several domains including an acidic N-terminal domain, a central Proline rich region, 3-4 (dependent on the isoform) mainly basic microtubule (MT) binding repeat regions and a C-terminal domain of mostly neutral amino acids. The MT binding repeats are essential for the interaction with MTs and contain a KXGS consensus motif (Figure 10). Importantly, the repeats are also involved in the formation of abnormal Tau deposits called paired helical filaments (Fontaine et al., 2015; Sabbagh and Dickey, 2016). Although Tau has been described as

an intrinsically disordered protein, it seems to retain some structural features. FRET data suggested a paper-clip like fold with the N- and C-terminus folding onto the MT binding repeats and on each other (Jeganathan et al., 2006). Specific stretches in the MT-binding repeats of Tau can serve as seeds for aggregation and are therefore thought to be critical for self-association. The VQIIYK and VQIVYK motifs have been shown to be essential for the interaction between Tau molecules resulting in oligomer formation and self-aggregation (Mukrasch et al., 2005; Peterson et al., 2008; Von Bergen et al., 2001). These motifs form additional intramolecular contacts with the proline-rich region. Thus it was speculated that proline-directed Tau phosphorylation might affect the aggregation propensity of Tau (Mukrasch et al., 2009).

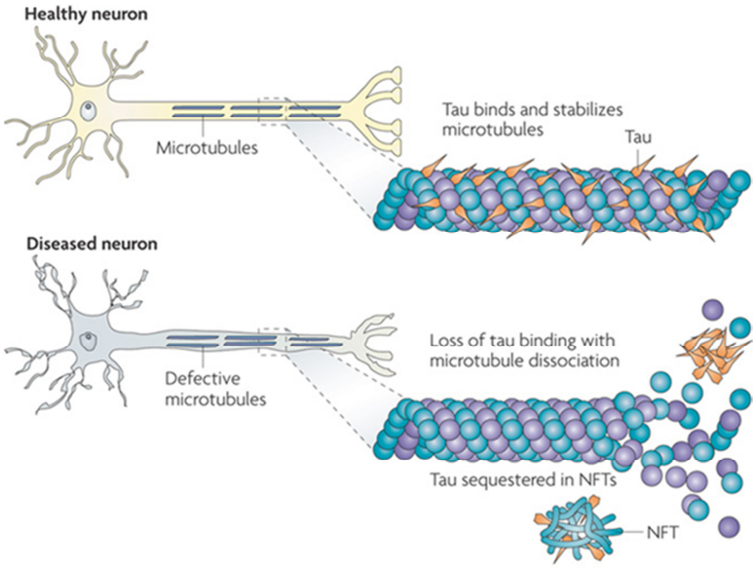


**Figure 11: Tau associates and stabilizes microtubules in healthy neurons.** Tau facilitates microtubule stabilization within cells. Tau function is compromised in Alzheimer's disease and other tauopathies. Hyperphosphorylation and Tau sequestration lead to formation of neurofibrillary tangles (NFT). The loss of Tau function leads to microtubule instability reduced axonal transport contributing to neuropathology. Adopted from Brunden et al. (2009);

It is widely accepted that Tau functions in cytoskeletal regulation by promoting MT assembly (Fontaine et al., 2015; Weingarten et al., 1975). Tau shows high affinity for MTs and associates with them via its MT binding repeats at the plus-end. Thereby, Tau stabilizes the MTs during the growth phase and the NTD might further act as a spacer to keep the MT strands in adequate distance (Breuzard et al., 2013; Bunker et al., 2004; Choi et al., 2009; Goode et al., 1997). Tauopathy-related mutants exhibit an altered phosphorylation pattern and MT binding repeat

structure resulting in reduced MT interactions and higher self-aggregation propensity. Hyperphosphorylation, promoted aggregation and sequestration of Tau in neurofibrillary tangles might lead to destabilized neurons promoting neurodegenerative cell death (Figure 11) (Brunden et al., 2009; Fontaine et al., 2015; Han and Paudel, 2009; Neumann et al., 2005).

Among PTMs like acetylation and proteolytic cleavage, phosphorylations have been shown to most significantly affect Tau binding to MTs and its aggregation propensity (Fontaine et al., 2015). Dephosphorylation of Tau was thought to promote MT association whereas phosphorylation triggers the release from the MTs by decreasing the affinity (Bramblett et al., 1993). This idea is supported by findings that Tau is also phosphorylated in the healthy brain. Several proline-directed kinases like the glycogen kinase 3 (GSK3), non-proline kinases like casein kinase but also tyrosine kinases like the c-Abl or the Src-family are among the kinases acting on Tau (Hanger et al., 1992; Vega et al., 2005). The latter are of special interest as tyrosine-phosphorylated Tau was found in brains of AD-patients. The mentioned kinases have also been identified among others to be suitable drug targets in treating tauopathies (Bramblett et al., 1993; Dolan and Johnson, 2010; Poppek et al., 2006; Watanabe et al., 1993; Yoshida and Ihara, 1993). In tauopathies, Tau becomes hyperphosphorylated especially at the KXGS motif and in particular at Ser262 in the MT binding repeats and hyperphosphorylation correlates well with AD-disease severity (Augustinack et al., 2002). pS262-Tau has been found free from MTs in amorphous aggregates indicating a pre-stage for Tau aggregation (Luna-Muñoz et al., 2007). The general conception is that hyperphosphorylation triggers aggregation as unphosphorylated Tau does not readily aggregate *in vitro* whereas phosphorylated does (Fontaine et al., 2015). Further, phosphorylation of residues near to the C-terminus was identified promote aggregation presumably by neutralizing anti-polymerizing structural properties of Tau (Crowther et al., 1994; Dolai et al., 2011; Gärtner et al., 1998; Grundke-Iqbal et al., 1986; Preuss et al., 1997)

#### 1.2.3.2.2 Interplay with chaperones

Besides PTMs, chaperones are also implicated as cellular factors affecting Tau. The evidence for the involvement of chaperones in Tau homeostasis was provided by Dou and colleagues finding that accumulation of Tau, Hsp90 and Hsp70 are inversely correlated in mice brain expressing a frontotemporal dementia-associated mutant (Dou et al., 2003).

Hsp90 seems to be involved in regulating Tau-MT interactions as it is able to bind both Tau and tubulin dimers (Garnier et al., 1998). Further it was shown that ATP-competitive Hsp90-inhibiotrs significantly reduced Tau levels by induction of the heat shock response and CHIP mediated degradation (Dickey et al., 2006; Dickey et al., 2005; Dickey et al., 2007). It was suggested that Hsp90 might promote Tau refolding thereby increasing the pool of aberrant Tau in the cell. This idea was supported by experimental evidence that direct interaction of Hsp90 with Tau induced certain conformational changes, leading to Tau with increased aggregation propensity (Dou et al., 2003; Garnier et al., 1998; Luo et al., 2007; Tortosa et al., 2009). In very recent work, a structural model for the interaction of Tau and Hsp90 has been postulated based on NMR and SAXS data. The model suggested that Tau binds to Hsp90 independently of nucleotide and does not induce a specific Hsp90 conformation. The authors speculated that Hsp90 might recognize Tau in contrast to other intrinsically disordered proteins as a late folding intermediate in which large hydrophobic clusters are buried on the inside of the protein structure but small clusters remain exposed. Further, it was suggested that Hsp70 might interact with Tau at an earlier stage by recognizing large hydrophobic patches (Karagöz et al., 2014).

Earlier studies have shown that the Hsp70 and Hsp90 binding sites overlap in the MT binding repeats and that both chaperones have opposing effects on Tau with Hsp90 increasing clearance and aggregation and Hsp70 preserving Tau and preventing aggregation. Further a role of Hsp70 has been implicated in correctly directing Tau after disassembly of MTs preventing unwanted self-aggregation. The consequences of the Hsp70-Tau interaction are dependent on the Hsp70 isoform. It seems that Hsc70 (constitutively expressed) stabilizes/preserves Tau whereas Hsp70 (stress-induced) facilitates Tau clearance. Hsp70 co-chaperones like Hsp40s, BAG proteins and the E3-ligase CHIP have been identified as Tau interactors modulating Tau aggregation (Dou et al., 2003; Jinwal et al., 2013a; Jinwal et al., 2010; Young et al., 2004).

# 2 Objective

The Hsp90 client interplay is highly complex involving various different processes like client transfer, recognition, binding and mutual influence of the client protein and its chaperone. Recent progress on the glucocorticoid receptor ligand binding domain (GR-LBD) and the microtubule-associated Tau shed some light on client binding to Hsp90 and especially for GR on the transfer from the Hsp70 system as well as the influences of the client on Hsp90. The picture emerged that Tau and GR seem to share a partly overlapping binding surface and that GR requires the full chaperone system (Hop, Hsp90, p23) to restore hormone binding when transferred form Hsp40/Hsp70. Further, it was shown that GR specifically altered Hsp90 cycle kinetics, priming the chaperone for its special requirements. However, the prerequisites for GR-controlled Hsp90 cycle kinetics, the influences of Tau on the Hsp90 cycle and a detailed picture of the GR-Hsp40/Hsp70 complex remained largely elusive. Thus, the focus of the present work was on exploring these processes in greater detail.

By using yeast Hsp90 point mutants at position 300 (W300), a residue which was previously shown to be involved in client processing in combination with biochemical, biophysical and *in silico* approaches, the prerequisites for the influence of GR on Hsp90 should be elucidated. Nuclear magnetic resonance spectroscopy (NMR) experiments should provide information whether W300 is influenced by GR-LBD binding. Yeast shuffling experiments with Hsp90 W300 and GR activity assays *in vivo* should help in understanding of the role of this special residue in general viability and GR maturation. ATPase and fluorescence resonance energy transfer (FRET) measurements should explore the influences of mutating W300 on the Hsp90 cycle kinetics in general and analyze whether the GR-LBD is able to establish its inhibitory influence in the absence of W300. To gain further insights into the functionality of the mutants, hormone-binding recovery experiments should be conducted. Analytical ultracentrifugation (AUC) coupled to fluorescence detection should give detailed information on the nucleotide-dependent binding of the GR-LBD to the Hsp90 W300 mutants. Additional ATPase and binding experiments using a defined set of Hsp90 co-chaperones should focus further on the alterations in Hsp90 due to the mutation of W300. Finally, small-angle X-ray scattering (SAXS) and atomistic molecular dynamics simulations should elucidate the conformational and atomistic principles of the prerequisites for the influence of the GR-LBD on Hsp90.

# Objective

The second part of this thesis is focused on the side-by-side comparison of the Hsp90 client interplay of two structurally unrelated client proteins, the well-folded GR-LBD and the intrinsically disordered Tau. By using identical experimental setups, detailed information concerning nucleotide-dependent binding, competition for binding sites on Hsp90, influence on the conformational cycle of Hsp90 and simultaneous co-chaperone binding should be provided. Therefore, AUC sedimentation velocity experiments should be performed to elucidate differences in the nucleotide-dependent binding. By comparing earlier NMR binding results of the GR-LBD with binding data of Tau using the identical Hsp90-domain constructs, the proposed binding site for Tau on Hsp90 and the speculation of overlapping binding patches should be stressed. NMR data should be further supported by AUC sedimentation velocity and GR-LBD-Hsp90 FRET experiments, testing simultaneous binding of both clients to Hsp90. ATPase activity measurements and Hsp90-FRET experiments should directly compare the influences of the structurally unrelated clients on the conformational cycle of Hsp90. Differential co-chaperone binding to the Hsp90-Tau complex should finally identify differences in the co-chaperone mediated regulation of the Hsp90 cycle by Tau and the GR-LBD.

The last part of this work is dedicated to the processes preceding the transfer of the GR-LBD to the Hsp90 system. By using AUC coupled to fluorescence detection, the interactions of the GR-LBD with Hsp40, Hsp70 and the combination of both should be investigated. AUC sedimentation velocity experiments using fluorescently labeled Dexamethasone (F-Dex) will give insights whether hormone-binding to the GR-LBD is possible in the detected complexes. Size-exclusion HPLC (SEC HPLC) experiments should complement the AUC results. By using a GR-LBD purified in the absence of ligand without a solubility enhancing tag (apo GR-LBD), Hormone-binding to GR-LBD in the presence of Hsp40/Hsp70 or the full chaperone system and Hsp70 ATPase activity measurements should be conducted. The experiments should reproduce the published inhibitory effect of Hsp40/Hsp70 on the hormone binding to the GR-LBD and test for influences on the ATPase cycle of Hsp70. In this context, special attention should be paid to the role of the co-chaperone Hop in these processes. To provide an experimental foundation for investigating the GR-chaperone interplay in even greater detail, single-molecule GR-LBD constructs should be designed and tested concerning conservation of chaperone interaction. Finally, initial single-molecule FRET and single-molecule force spectroscopy experiments using an optical tweezers setup should be conducted. Thereby, the influence of Hsp40 and Hsp70 on the GR-LBD on the single-molecule level should be of special interest.

# 3 Material and Methods

## 3.1 Material

### 3.1.1 Microorganisms

The following strains were used in this work.

**Table 1: Strains and organisms**

| Organism | Genotype | Source |
|---|---|---|
| *E. coli* BL21-CodonPlus(DE3)-RIL | F$^-$ *omp*T *hsd*S($r_B^-m_B^-$) *dcm*$^+$ Tet$^r$ *gal* λ(DE3) *end*A Hte [*arg*U *ile*Y *leu*W Cam$^r$] | Stratagene (La Jolla, USA) |
| *E. coli* Mach1 | F$^-$ Φ80(Δ*lac*Z)ΔM15 Δ*lac*X74 *hsd*R($r_K^-$ $m_K^+$) Δ*rec*A1398 *end*A1 *ton*A | Invitrogen (Karlsruhe, Germany) |
| *E. coli* XL-1 blue | *recA1 endA1 gyrA96 thi-1 hsdR17 supE44 relA1 lac [F´ proAB lac$I_q$ZΔM15 Tn10 (Tet$_r$)]* | Stratagene (La Jolla, USA) |
| *S. cerevisiae* BY4741 | MATa *his3Δ0 leu2Δ0 met15Δ0 ura3Δ0* | Euroscarf (Frankfurt, Germany) |
| *S. cerevisiae* ΔPCLDα | MATα *ade2 leu2 ura3 his3 trp1 hsc82*::*LEU2 hsp82*::*LEU2 (pKAT6GPD-Hsp82)* | Susan Lindquist |

### 3.1.2 Chemicals

All chemicals, if not noted otherwise, were purchased from Roth (Karlsruhe, Germany), Sigma Aldrich (St. Louis, USA) or Merck (Darmstadt, Germany) and were of p.a. grade. All media and buffers were prepared using deionized water.

| **Media** | |
|---|---|
| Agar Agar | Serva (Heidelberg, Germany) |
| Bacto Peptone | Difco (Detroit, USA) |
| Bacto Tryptone | Difco (Detroit, USA) |
| Bacto Yeast extract | Difco (Detroit, USA) |
| LB-medium powder | Serva (Heidelberg, Germany) |
| Yeast Nitrogen Base | Difco (Detroit, USA) |
| YPD- medium powder | Roth (Karlsruhe, Germany) |
| **Antibiotics** | |
| Ampicillin | Roth (Karlsruhe, Germany) |
| Kanamycin | Roth (Karlsruhe, Germany) |
| **Nucleotides** | |
| 5'–Adenylyl-ß,γ-imido-diphosphate (AMP-PNP) | Roche Diagnostic GmbH (Mannheim, Germany) |
| Adenosin-5`-[γ-thio]-triphosphate (ATPγS) tetralithium salt | Roche Diagnostic GmbH (Mannheim, Germany) |
| Adenosin-5`-triphosphate (ATP) | Roche Diagnostic GmbH (Mannheim, Germany) |
| Adenosine-5´-diphosphate (ADP), Disodium salt | Roche Diagnostic GmbH, Mannheim, Germany |
| Desoxynucleotidetriphosphates (dNTP) | New England Biolabs (Beverly, USA) |
| **Fluorophores/Labels** | |
| ATTO488-maleimide | ATTO-TEC (Siegen, |

| | |
|---|---|
| | Germany) |
| ATTO550-maleimide | ATTO-TEC (Siegen, Germany) |
| ATTO532-maleimide | ATTO-TEC (Siegen, Germany) |
| ATTO647-maleimide | ATTO-TEC (Siegen, Germany) |
| 3-Maleimido-2,2,5,5-tetramethyl-1-pyrrolidinyloxy, free radical (3-Maleimido-PROXYL) | Sigma (St. Louis, USA) |
| Sypro Orange Protein Gel Stain (5000 x in DMSO) | Thermo Scientific (Waltham, USA) |
| **Miscellaneous reagents** | |
| 1,4-Dithithreitol (DTT) | Roth (Karlsruhe, Germany) |
| 11-Deoxycorticosterone (DOC) | Sigma (St. Louis, USA) |
| 3-[(3-Cholamidopropyl)dimethylammonio]-1-propanesulfonate (CHAPS) | Roth (Karlsruhe, Germany) |
| 5-Fluorootic Acid (5-FOA) | Thermo Scientific (Waltham, USA) |
| Acrylamide (38 %, 2 % Bisacrylamide) | Serva (Heidelberg, Germany) |
| Agarose, ultra pure | Roth (Karlsruhe, Germany) |
| Ammonium-15N chloride ($^{15}NH_4Cl$) | Cambridge Isotope Laboratories, Inc. (Andover, USA) |
| Ammoniumperoxodisulfate (APS) | Roth (Karlsruhe, Germany) |
| Biotin | Sigma (St. Louis, USA) |
| Bromphenolblue S | Serva (Heidelberg, Germany) |
| Coomassie Brilliant Blue R-250 | Serva (Heidelberg, Germany) |
| Deoxyribonucleic acid, single stranded from salmon testes | Sigma (St. Louis, USA) |
| Dexamethasone (Dex) | Sigma (St. Louis, USA) |
| Dexamethasone Fluorescein (F-DEX) | Sigma (St. Louis, USA) |

| | |
|---|---|
| Dimethylsulfoxide (DMSO) | Sigma (St. Louis, USA) |
| Isopropyl-β-D-thiogalactopyranoside (IPTG) | Roth (Karlsruhe, Germany) |
| Milk powder (blotting grade) | Roth (Karlsruhe, Germany) |
| Nicotinamideadenine dinucleotide (NADH) | Roche Diagnostic GmbH (Mannheim, Germany) |
| *ortho*-Nitrophenyl-β-galactoside (ONPG) | Sigma (St. Louis, USA) |
| Phenylmethylsulfonyl fluoride (PMSF) | Sigma (St. Louis, USA) |
| Phosphoenolpyruvate (PEP) | Roche Diagnostic GmbH (Mannheim, Germany) |
| Polyethylene glycol (PEG-6000 / 4000) | Merck (Darmstadt, Germany) |
| Polyoxyethylen (20) sorbitan monolaurate (Tween 20) | Merck (Darmstadt, Germany) |
| Protease Inhibitor Mix HP | Serva (Heidelberg, Germany) |
| Radicicol | Roth (Karlsruhe, Germany) |
| Serva DNA Stain G | Serva (Heidelberg, Germany) |
| Sodium dodecyl sulfate (SDS) | Roth (Karlsruhe, Germany) |
| Tetramethylethylenediamine (TEMED) | Roth (Karlsruhe, Germany) |
| Thiamin hydrochloride | Sigma (St. Louis, USA) |
| Tris-(2-Carboxyethyl)phosphine, hydrochloride (TCEP) | Sigma (St. Louis, USA) |
| Xylencyanol | Serva (Heidelberg, Germany) |
| β-Mercaptoethanol, pure | Merck (Darmstadt, Germany) |

### 3.1.3 Buffers and solutions

**Molecular biology**

| Solution | Concentration | Ingredients |
|---|---|---|
| 2X Quick ligation buffer | 132 mM | Tris, pH 7.6 |
| | 20 mM | $MgCl_2$ |
| | 2 mM | DTT |
| | 2 mM | ATP |
| | 15 % | PEG-6000 |
| Agarose solution | 0.8-2 % (w/v) | Agarose |
| | 100 ml | TAE (1x) |
| | 1-2 µl | Serva DNA Stain G |
| Blocking solution | 5 % (w/v) | Milk powder in PBS-T |
| Competent cell solution | 13 ml | 3 M NaAc (pH 5.5) |
| | 100 ml | 1 M $CaCl_2$ |
| | 25 ml | 2.8 M $MnCl_2$ |
| | 862 ml | $H_2O$ |
| Competent cell solution + glycerol | 69 ml | Glycerol (87 %) |
| | 331 ml | CC solution |
| DNA loading buffer | 50 % (v/v) | Glycerol |
| | 10 mM | EDTA pH 8.0 |
| | 0.2 %(w/v) | Bromphenolblue |
| | 0.2 % (w/v) | Xylencyanol |
| Separating gel buffer (4x) | 250 mM | Tris/acetate pH 8.0 |
| | 0.8 % (w/v) | SDS |
| Stacking gel buffer (2x) | 250 mM | Tris/acetate pH 8.0 |
| | 0.4 % (w/v) | SDS |
| TAE (50X) | 2 M | Tris/acetate pH 8,0 |
| | 50 mM | EDTA |

| **SDS-PAGE and Western blotting** | | |
|---|---|---|
| Fairbanks A | 2.5 g | Coomassie Brilliant Blue R-250 |
| | 250 ml | Ethanol |
| | 80 ml | Acetic acid |
| | ad 1l | $H_2O$ |
| Fairbanks D | 250 ml | Ethanol |
| | 80 ml | Acetic acid |
| | ad 1l | $H_2O$ |
| Laemmli sample buffer (5X) | 312.5 mM | Tris, pH 6.8 |
| | 10 % (w/v) | SDS |
| | 50 % (v/v) | Glycerol |
| | 2.5 % (v/v) | β-Mercaptoethanol |
| | 0.05 % (w/v) | Bromphenolblue |
| PBS (10X) | 40 mM | $KH_2PO_4$ |
| | 160 mM | $Na_2HPO_4$ |
| | 1.15 M | NaCl |
| | | pH 7.4 |
| PBS-T | 0.1 % (v/v) | Tween-20 |
| | | PBS (1X) |
| SDS running buffer (10X) | 250 mM | Tris, pH 6.8 |
| | 2 M | Glycine |
| | 1 % (w/v) | SDS |
| WB transfer buffer | 36 g | Glycine |
| | 7.6 g | Tris |
| | 500 ml | Methanol |
| | 0.3 % (w/v) | SDS |
| | ad 2.5 l | $H_2O$ |
| | | pH 8.3 |

### 3.1.4 Plasmids

The following plasmids were used or created (Table 2).

**Table 2: Plasmids**

| No. | Name | Insert/Cloning site | Origin |
|---|---|---|---|
| **1** | pET28b | | Merck Biosciences GmbH (Schwalbach, Germany) |
| **2** | p413-GPD | | Mumberg et al. (1995) |
| **3** | pET-Sumo-mod | $His_6$-Sumo, BbsI(NcoI)/BamHI | Oliver Lorenz |
| **4** | pETHALO | Halo, NdeI/BamHI | Oliver Lorenz |
| **5** | pET-Sumo protease (403-621) | | Alexander Bepperling |
| **6** | pMal-C2-Tev protease (S219P) | | Addgene (Cambridge, USA) |
| **7** | pET28-yHsp90 | NdeI/BamHI | Klaus Richter |
| **8** | pET28-hHsp90ß | NdeI/BamHI | Klaus Richter |
| **9** | pET28-Sba1 | | Alexandra Rehn |
| **10** | pET28-Hop | | Andreas Schmid |
| **11** | pET28-hAha1 | | Klaus Richter |
| **12** | pRSETA-Cyp40 (Cpr6) | | Chrisostomos Prodromou |
| **13** | pET28-hGR | NcoI/XhoI | Oliver Lorenz |
| **14** | pET28-yHsp90 W300A | NdeI/BamHI | This work |
| **15** | pET28-yHsp90 W300E | NdeI/BamHI | This work |
| **16** | pET28-yHsp90 W300K | NdeI/BamHI | This work |
| **17** | pET28-yHsp90 W300F | NdeI/BamHI | This work |
| **18** | pET28-yHsp90 W300Y | NdeI/BamHI | This work |
| **19** | pET28-yHsp90 W277A | NdeI/BamHI | This work |
| **20** | pET28-hHsp90 W312A | NdeI/BamHI | This work |
| **21** | pET28-hHsp90 W312E | NdeI/BamHI | This work |

| | | | |
|---|---|---|---|
| **22** | pET28-hHsp90 W312K | NdeI/BamHI | This work |
| **23** | pET28-hHsp90 W312F | NdeI/BamHI | This work |
| **24** | pET28-hHsp90 W312Y | NdeI/BamHI | This work |
| **25** | pET28-hHsp90 W289A | NdeI/BamHI | This work |
| **26** | pET28-yHsp90 D61C | NdeI/BamHI | Martin Hessling |
| **27** | pET28-yHsp90 D61C W300A | NdeI/BamHI | This work |
| **28** | pET28-yHsp90 D61C W300E | NdeI/BamHI | This work |
| **29** | pET28-yHsp90 D61C W300K | NdeI/BamHI | This work |
| **30** | pET28-yHsp90 D61C W300F | NdeI/BamHI | This work |
| **31** | pET28-yHsp90 D61C W300Y | NdeI/BamHI | This work |
| **32** | pET28-yHsp90 D61C W277A | NdeI/BamHI | This work |
| **33** | pET28-yHsp90 E333C | NdeI/BamHI | This work |
| **34** | pET-Sumo-hHsp70 | BamHI/XhoI | Eva Kriehuber |
| **35** | pET-Sumo-Ydj1 | BamHI/XhoI | Oliver Lorenz |
| **36** | pET-Halo-GR-LBDm | BamHI/XhoI | Oliver Lorenz |
| **37** | pET-Sumo-GR-DBDLBDm | BamHI/XhoI | Oliver Lorenz |
| **38** | pET-Halo-smGR-LBD | BamHI/XhoI | This work |
| **39** | pET-Halo-SACK-GR-LBDm | BamHI/XhoI | This work |
| **39** | pET28-MBP-yHsp90MD | NdeI/BamHI | Lee Freiburger |
| **40** | pET28-TEV-Tau | NdeI/BamHI | Chad Dickey |
| **41** | p413-GPD-yHsp90 | SpeI/SalI | This work |
| **42** | p413-GPD-yHsp90 W300A | SpeI/SalI | This work |
| **43** | p413-GPD-yHsp90 W300E | SpeI/SalI | This work |
| **44** | p413-GPD-yHsp90 W300K | SpeI/SalI | This work |
| **45** | p413-GPD-yHsp90 W300F | SpeI/SalI | This work |
| **46** | p413-GPD-yHsp90 W300Y | SpeI/SalI | This work |
| **47** | p413-GPD-yHsp90 W277A | SpeI/SalI | This work |
| **48** | p413-GPD-hHsp90 | SpeI/SalI | This work |
| **49** | p413-GPD-hHsp90 W312A | SpeI/SalI | This work |
| **50** | p413-GPD-hHsp90 W312E | SpeI/SalI | This work |

| | | | |
|---|---|---|---|
| **51** | p413-GPD-hHsp90 W312K | SpeI/SalI | This work |
| **52** | p413-GPD-hHsp90 W312F | SpeI/SalI | This work |
| **53** | p413-GPD-hHsp90 W312Y | SpeI/SalI | This work |
| **54** | p413-GPD-hHsp90 W289A | SpeI/SalI | This work |
| **55** | p2A/GRGZ | | Nathan and Lindquist (1995) |

### 3.1.5 DNA oligonucleotides

The following oligonucleotides were used for cloning.

**Table 3: DNA oligonucleotides;**

| No. | Primer | Sequence (5‘-3‘) |
|---|---|---|
| **1** | 5E333C | CCAAAGAGAGCACCATTCGACTTGTTTTGTAGTAAAAAGAAGAAG |
| **2** | 3E333C | GATATTATTCTTCTTCTTTTTACTACAAAACAAGTCGAATGGTGC |
| **3** | 5`BAMTEVACKGRM | GATCGTGGATCCGAAAACCTGTATTTTCAGTCTGCGTGCAAGCAACTCACCCCTACCCTGGTGTCAC |
| **4** | 3`GRMKCLSTOPXHO | GATCTGCTCGAGTCAGAGGCACTTTTGATGAAACAGAAGTTTTTTGATATTTCC |
| **5** | 5`W300A | CTATAAGTCTATTTCAAACGACGCGGAAGACCCATTGTACGTTAAG |
| **6** | 3`W300A | CTTAACGTACAATGGGTCTTCCGCGTCGTTTGAAATAGACTTATAG |
| **7** | 5`W300E | CTATAAGTCTATTTCAAACGACGAAGAAGACCCATTGTACGTTAAG |
| **8** | 3`W300E | CTTAACGTACAATGGGTCTTCTTCGTCGTTTGAAATAGACTTATAG |
| **9** | 5`W300K | CTATAAGTCTATTTCAAACGACAAAGAAGACCCATTGTACGTTAAG |

| | | |
|---|---|---|
| **10** | 3`W300K | CTTAACGTACAATGGGTCTTCTTTGTCGTTTGAA ATAGACTTATAG |
| **11** | C638DFW | GACTCTACCCGATATGTACGACCAATG |
| **12** | C638DREV | ATTCTCTGCTCATTAATAATCAG |
| **13** | W312A-FW | CACTAATGACGCCGAAGACCACTTGGC |
| **14** | W312A-REV | AGGCTCTTGTAGAATTCTC |
| **15** | W312E-FW | CACTAATGACGAAGAAGACCACTTGGC |
| **16** | W312K-FW | CACTAATGACAAAGAAGACCACTTGGC |
| **17** | W312K-REV | AGGCTCTTGTAGAATTCTC |
| **18** | 1SMGR_NW | TCAGTCTGCGTGGAAGCAACTCA |
| **19** | 2SMGR_NW | AAATACAGGTTTTCGGATCCACG |
| **20** | 82W277A_1 | ATAAGCCTTTGGCGACTAGAAACCC |
| **21** | 82W277A_2 | GTCTTGTTTAGTTCTTCTATCTC |
| **22** | 90SSW289A_1 | CAAGCCTATTGCGACCAGAAACCC |
| **23** | 90SSW289A_2 | GTCTTGTTTAGTTCTTCCTG |
| **24** | 82_FW_SPEI | GATCGTACTAGTATGGCTAGTGAAACTTTTGAAT TTC |
| **25** | 82_RW_SALI | CTAGCAGTCGACCTAATCTACCTCTTCCATTTCG |
| **26** | 90SS_FW_SPEI | GATCGTACTAGTATGCCTGAGGAAGTGCACC |
| **27** | 90SS_RW_SALI | CTAGCAGTCGACCTAATCGACTTCTTCCATGCG |
| **28** | FW_W300Y | TTCAAACGACTATGAAGACCCATTG |
| **29** | RW_W300Y/F | ATAGACTTATAGAAAGCATTGTATTC |
| **30** | FW_W300F | TTCAAACGACTTTGAAGACCCATTG |
| **31** | FW_W312Y | CACTAATGACTATGAAGACCACTTGG |
| **32** | RW_W312Y/F | AGGCTCTTGTAGAATTCTC |
| **33** | FW_W312F | CACTAATGACTTTGAAGACCACTTG |

### 3.1.6 Media and antibiotics

| **Media for *E. coli* growth** | | |
|---|---|---|
| Name | | Composition |
| LB | | 20 g/l LB-powder<br>For plates: 15 g/l Agar Agar |
| 2YT | | 17 g/l Bacto Tryptone<br>10 g/l Bacto Yeast extract<br>5 g/l NaCl |
| ZYM-5052 auto induction media (Studier, 2005) | ZY | 10 g/l Bacto Tryptone<br>5 g/l Bacto Yeast extract |
| | M | 25 mM $Na_2HPO_4$<br>25 mM $KH_2PO_4$<br>50 mM $NH_4Cl$<br>5 mM $Na_2SO4$ |
| | 5052 | 0.5 % Glycerol<br>0.05 % D(+)-Glucose<br>0.02 % Lactose monohydrate |
| | 1000X Trace elements* | 0.2X |
| *1000X Trace elements | 50 mM $FeCl_3$, 20 mM $CaCl_2$, 10 mM $MnCl_2$ 10 mM $ZnSO_4$, 2 mM $CoCl_2$, 2 mM $CuCl_2$, 2 mM $NiCl_2$, 2 mM $Na_2MoO_4$, 2 mM $Na_2SeO_3$, 2 mM $H_3BO_3$ in 60 mM HCl | |
| Minimal media (M9) | | 7.52 g/l $Na_2HPO_4$ x 2 $H_20$<br>3 g/l $KH_2PO_4$<br>0.5 g/l NaCl<br>1 ml 1 M $MgSO_4$<br>0.3 ml 1 M $CaCl_2$<br>10 ml 0.2 g/ml D(+)-Glucose |

| | | |
|---|---|---|
| | | 1 g $^{15}NH_4Cl$<br>1 ml 1 mg/ml Biotin<br>1 ml 1 mg/ml Thiamine hydrochloride<br>10 ml 100X Trace metals*<br>ad 1 l $H_2O$ |
| *100X Trace metals | 5 g EDTA, 0.83 g $FeCl_3$ x 6 $H_2O$, 84 mg $ZnCl_2$, 13 mg $CuCl_2$ x 2 $H_2O$, 10 mg $CoCl_2$ x 6 $H_2O$, 10 mg $H_3BO_3$, 1.35 mg $MnCl_2$ x 4 $H_2O$ ad 1l, pH 7.5 | |
| **Media for yeast growth** | | |
| YPD | | 50 g/l YPD<br>For plates: 20 g/l Agar Agar |
| Dropout medium (CSM) | | 6.7 g Yeast nitrogen base<br>1 ml 1M NaOH<br>2 g selective aa-mix*<br>20 g D(+)-Glucose<br>ad 1 l<br>For plates: 20 g Agar Agar |
| *selective aa-mix | adenine (0.5 g), arginine (2.0 g), aspartic acid (2.0 g), histidine (2.0 g), leucine (10.0 g), lysine (2.0 g), methionine (2.0 g), phenylalanine (2.0 g), threonine (2.0 g), tryptophan (2.0 g), tyrosine (2.0 g), uracil (2.0 g); Depending on used auxotrophy marker(s), corresponding aa or nucleobase respectively, were eliminated from the mix. | |
| **Antibiotics and working concentration** | | |
| Ampicillin | 100 µg/ml | |
| Kanamycin | 50-100 µg/ml | |

### 3.1.7 Proteins and reagents

| Protein/reagent | |
|---|---|
| Antarctic Phosphatase | New England Biolabs (Beverly, USA) |
| Bovine serum albumin, 98% electrophoresis (BSA) | Sigma (St. Louis, USA) |
| DNase I | Roche Diagnostic GmbH (Mannheim, Germany) |
| Lactate dehydrogenase suspension | Roche Diagnostic GmbH (Mannheim, Germany) |
| OneTaq DNA Polymerase | New England Biolabs (Beverly, USA) |
| Phusion High-Fidelity DNA Polymerase | New England Biolabs (Beverly, USA) |
| Pyruvate kinase suspension | Roche Diagnostic GmbH (Mannheim, Germany) |
| Q5 High Fidelity DNA Polymerase | New England Biolabs (Beverly, USA) |
| Q5 site-directed mutagenesis kit | New England Biolabs (Beverly, USA) |
| Restriction enzymes | New England Biolabs (Beverly, USA) |
| Sumo-protease | Oliver Lorenz |
| T4-DNA Ligase | New England Biolabs (Beverly, USA) |
| Tau (isoform D) | Chad Dickey |
| TEV-protease | Oliver Lorenz, Frank Echtenkamp |
| Yeast Aha1 | Franziska Tippel, Sandrine Stiegler |
| yeast Sti1 | Franziska Tippel |
| α-GR | Pineda |
| α-Hsp90 total (4F3.E8) | Pineda |
| α-mouse-POD | Sigma (St. Louis, USA) |
| α-rabbit-POD | Sigma (St. Louis, USA) |

### 3.1.8 Standards and kits

| Standard/kit | |
|---|---|
| 1 kb DNA ladder | Peqlab (Erlangen, Germany) |
| Gel Filtration Standard | Biorad (Munich, Germany) |
| Low-Range-molecular weight marker (LMW) | Biorad (Munich, Germany) |
| Protein Marker IV ("Prestained") | VWR International GmbH (Darmstadt, Germany) |
| Q5 site-directed mutagenesis kit | New England Biolabs (Beverly, USA) |
| SERVAChrom Protein Standard III | Serva (Heidelberg, Germany) |
| Western Bright ECL Spray | Advansta (Menlo Park, USA) |
| Wizard SV Gel and PCR Clean-Up System | Promega (Madison, USA) |
| Wizard SV Mini-Preps DNA Purification System | Promega (Madison, USA) |

### 3.1.9 Chromatography columns

| Column | |
|---|---|
| GSTrap FF (5ml) | GE Healthcare (Munich, Germany) |
| HiLoad 16/60 Superdex 200 pg | GE Healthcare (Munich, Germany) |
| HiLoad 16/60 Superdex 200 pg | GE Healthcare (Munich, Germany) |
| HiLoad 16/60 Superdex 75 pg | GE Healthcare (Munich, Germany) |
| HiLoad 16/60 Superdex 75 pg | GE Healthcare (Munich, Germany) |
| His SpinTrap columns | GE Healthcare (Munich, Germany) |
| HisTrap FF (5 ml) | GE Healthcare (Munich, Germany) |
| HisTrap HP (5 ml) | GE Healthcare (Munich, Germany) |
| HiTrap Heparin HP (5ml) | GE Healthcare (Munich, Germany) |
| Hydroxyapatite | BioRad (Munich, Germany) |
| Resource Q (6 ml) | GE Healthcare (Munich, Germany) |
| Superdex 200 increase 10/300GL (HPLC) | GE Healthcare (Munich, Germany) |

### 3.1.10 Devices and additional material

| Device | |
|---|---|
| **Spectrophotometers** | |
| Circular Dichroism Spectropolarimeter Jasco J715 including PTC 343 Peltier temperature device | Jasco (Groß-Umstadt, Germany) |
| Fluorescence Spectrometer FP-8600 | Jasco (Groß-Umstadt, Germany) |
| Fluoromax 3 Fluorescence Spectrometer equipped with polarizers | Horiba Jobin Yvon GmbH (Bernsheim, Germany) |
| Spectrophotometer Nanodrop ND-1000 UV/VIS | Peqlab (Erlangen, Germany) |
| Spectrophotometer Varian Cary 50/100 Bio UV/Vis | Varian (Palo Alto, USA) |
| **Analytical balances** | |
| Sartorius 1409 MP | Sartorius (Göttingen, Germany) |
| Sartorius BL 310 | Sartorius (Göttingen, Germany) |
| Sartorius universal | Sartorius (Göttingen, Germany) |
| **Centrifuges** | |
| Analytical Ultracentrifuge XL-A equipped with absorption and fluorescence detection systems | Beckman Coulter (Krefeld, Germany) and AVIV Biomedical (Lakewood, USA) |
| Analytical Ultracentrifuge XL-I with absorbance and interference detection systems | Beckman Coulter (Krefeld, Germany) |
| Avanti J-25 and J-26 XP with rotors JA-10 and JA-25.50 | Beckman Coulter (Krefeld, Germany) |
| Benchtop Centrifuge 5418 | Eppendorf (Hamburg, Germany) |
| Eppendorf Centrifuge 5810 | Eppendorf (Hamburg, Germany) |
| Heraeus Biofuge stratos | Thermo Scientific (Waltham, USA) |

| **Chromatography devices** | |
|---|---|
| Äkta FPLC | GE Healthcare (Munich, Germany) |
| Shimadzu HPLC system equipped with autosampler | Shimadzu (Munich, Germany) |
| **Gel electrophoresis** | |
| Hoefer Mighty Small dual gel caster | Hoefer (Holliston, USA) |
| Mighty Small II SE 250/SE 260 electrophoresis unit | Hoefer (Holliston, USA) |
| **Power supply** | |
| Electrophoresis Power Supply – EPS 3501 XL | GE Healthcare (Freiburg, Germany) |
| Electrophoresis Power Supply – EPS 601 | GE Healthcare (Freiburg, Germany) |
| Electrophoresis Power Supply – EPS 1001 | GE Healthcare (Freiburg, Germany) |
| **Plate reader** | |
| Tecan Sunrise | Tecan Group Ltd. (Maennedorf, Switzerland) |
| **Additional equipment** | |
| Amicon pressure based sample concentration cell (50 ml) | Merck Millipore (Billerica USA) |
| Amicon Ultra-15 Centrifugal Filter Units | Merck Millipore (Billerica USA) |
| Amicon Ultra-4 Centrifugal Filter Units | Merck Millipore (Billerica USA) |
| Bandelin Sonopuls HD2200 | Branson (Danbury, USA) |
| Cell Disruption System Basic Z | Constant Systems (Warwick, United Kingdom) |
| Cellstar®, 15 and 50 mL | Greiner Bio One (Kremsmünster, Austria) |
| Cuvette, PS | Brand GmbH (Wertheim, Germany) |
| Cuvettes | Zefa (Munich, Germany) |
| Dialysis membranes Spectra/Por (various MWCOs) | Spectrum Laboratories (Breda, Netherlands) |
| Dialysis tubes Spectra/Por (6-8 kDa) | Spectrum (Houston, USA) |

| | |
|---|---|
| Eppendorf Thermomixer compact | Eppendorf (Hamburg, Germany) |
| Eppendorf ThermoStat plus | Eppendorf (Hamburg, Germany) |
| Fastblot B44 | Biometra (Göttingen, Germany) |
| Freezer Ultra-low temperature C760, -80 °C | New Brunswick Scientific (Nürtingen, Germany) |
| Homogenizer Heidolph DIAX 900 | Heidolph (Kelheim, Germany) |
| Ice maker 105439 | Ziegra (Isernhagen, Germany) |
| Image Quant 3000, LAS 4000 | GE Healthcare (Freiburg, Germany) |
| Incubator Binder KB 115 | Binder GmbH (Tuttlingen, Germany) |
| Incubator Certomat BS-1 | Sartorius (Göttingen, Germany) |
| Incubator Mytron WB | Mytron (Heiligenstadt, Germany) |
| Magnetic stirrer Heidolph MR 3001 | Heidolph (Kelheim, Germany) |
| Micro Fluorescence-cuvette | Hellma Analytics (Müllheim, Germany) |
| Micro UV-cuvette 10 mm | Hellma Analytics (Müllheim, Germany) |
| Mx3000P qPCR-system | Agilent Technologies Inc. (Santa Clara, USA) |
| PCR cycler BioRad T-100 thermal cycler | BioRad (Munich, Germany) |
| PCR tubes | Biorad (Munich, Germany) |
| PD10 column | GE Healthcare (Munich, Germany) |
| Petri dishes, PS, 94 mm | Greiner Bio One (Kremsmünster, Austria) |
| pH indicator | Merck (Darmstadt, Germany) |
| pH-Meter 538 MultiCal | WTW (Weilheim, Germany) |
| Platform shaker Heidolph Polymax 2040 | Heidolph (Kelheim, Germany) |
| PVDF membranes | Roth (Karlsruhe, Germany) |
| Reaction tubes, 0.5, 1.5 mL and 2 mL | Sarstedt (Nümbrecht, Germany) |
| Shaking device Certomat SII, GFL 3005 | Sartorius (Göttingen, Germany) |
| Ultracel Ultrafiltration disc 10 kDa NMWL 76 mm and 44.5 mm | Merck Millipore (Billerica USA) |
| Vortex Heidolph REAX top | Heidolph (Kelheim, Germany) |

### 3.1.11 Computer programs and online tools

| Program | |
|---|---|
| Adobe CS2 | Adobe Systems (San Jose, USA) |
| ClustalW/Omega | http://www.ebi.ac.uk/Tools/msa/clustalo/ |
| Endnote X7.5 | Thomson Reuters (New York City, USA) |
| Microsoft Office 2010 | Microsoft (Redmond, USA) |
| Mmass 2.4 | http://www.mmass.org |
| NCBI Blast | http://blast.ncbi.nlm.nih.gov/ |
| NEBaseChanger | http://nebasechanger.neb.com/ |
| Origin 9.1G | OriginLab (Nothampton, USA) |
| ProtParamTool | ExPasy (http://www.expasy.ch) |
| Pymol 1.1 | Schrödinger (Cambridge, USA) |
| SedFit 14.1 | Peter Schuck |
| Sednterp | John Philo |
| SedView 1.1 | David B. Hayes, Walter F. Stafford |
| Serial Cloner 2.6.1 | Serial Basics (USA) |
| Tm Calculator | http://tmcalculator.neb.com |

## 3.2 Molecular biological methods

### 3.2.1 Purification of DNA

#### 3.2.1.1 Plasmid-DNA amplification and purification

DNA-plasmid amplification was performed by pelleting 5-10 ml of an *E. coli* ONC. Cells were disrupted and the plasmid isolated by using the Wizard plus SV Minipreps DNA purification System according to the manufacturer`s instructions. DNA plasmids were afterwards subjected to restriction digest, sequencing or storage at -20°C in nuclease-free $H_2O$.

#### 3.2.1.2 Agarose gel electrophoresis

Agarose gel electrophoresis was applied for analytic and preparative separation of plasmid/linear DNA. Therefore samples were supplemented with 1 x DNA-loading buffer and loaded on a 1 % agarose gel in 1 x TAE containing $1:10^5$ Serva DNA stain G together with 7 µl of the 1 kb ladder as standard. Gels were developed at constant amperage of 150 mA for 15-30 min and visualized using the Image Quant 3000 system.

#### 3.2.1.3 Purification of DNA from agarose gels and reaction mixtures

DNA samples excised from agarose gels and reaction mixtures were purified using the Wizard Plus Gel Extraction Kit according to the manufacturers protocol. Isolated DNA was either stored at -20°C in nuclease-free $H_2O$ or further processed.

### 3.2.2 Determination of DNA concentration

To determine the concentration of DNA samples UV/Vis-spectroscopy was applied. Absorbance was measured at 260 nm in a Nanodrop ND-100 UV/Vis-spectrometer. The concentration was determined according to the Lambert-Beer equation:

$$\mathbf{A = \varepsilon \times c \times d}$$

**Equation 1**

With $A$ = absorbance at 260 nm, $\varepsilon$ = the extinction coefficient of DNA at 260 nm in [µl * $ng^{-1}$ * $cm^{-1}$], $c$ = the DNA concentration [ng * $\mu l^{-1}$] and $d$ = layer thickness [cm]. The extinction coefficient of double-stranded DNA is 0.02 µl * $ng^{-1}$ * $cm^{-1}$. Purity of the sample was monitored by the ratio of absorbance at 260 and 280 nm ($A_{260}/A_{280}$).

### 3.2.3 Polymerase chain reaction (PCR)

Amplification of target DNA sequences was performed by polymerase chain reaction. Used template plasmids and oligonucleotide-primers are listed in Table 2 and Table 3, respectively. Dependent on the target sequence Phusion High-Fidelity, Q5 High-Fidelity or GoTaq DNA-Polymerase were used. For standard target gene amplification the following reaction mixture was used:

| Component | Concentration |
|---|---|
| Polymerase buffer (5 x Phusion HP, 5 x Q5 Reaction Buffer, 5 x OneTaq Standard Reaction Buffer ) | 1 x |
| dNTPs (10 mM) | 200 µM |
| Forward primer (10 µM) | 0.5 µM |
| Reverse primer (10 µM) | 0.5 µM |
| Template DNA | < 20 ng for plasmid DNA |
| DNA-Polymerase (2000 units/ml) (Phusion High-Fidelity, Q5 High-Fidelity, OneTaq DNA-Polymerase) | 0.02 units/µl |
| Additives (DMSO, 5 x Q5 High GC Enhacer, 5x OneTaq High GC Enhancer) | 3 % DMSO, 1 x High GC Enhancer |
| $H_2O$ | Add to 50 µl |

PCR reactions were performed in a BioRad T-100 thermal cycler. A typical temperature program was as follows:

| Step | Temperature [°C] | Time [s] | Cycles |
|---|---|---|---|
| Initial denaturation | 98 | 30 | - |
| Denaturation | 98 | 10 | - |
| Annealing | variable | 10-30 | - |
| Elongation | 72 | variable | - |
| Number of cycles (Denaturation-Annealing-Elongation) | - | - | 30 |
| Storage | 10 | ∞ | - |

Success of PCR was probed by subsequent DNA gel electrophoresis (3.2.1.2).

### 3.2.3.1 Colony-PCR

Positive clones can be identified by colony PCR after successful transformation with ligation products. Therefore single-colonies were picked from the selective agar plates, resuspended in the following reaction mixture and PCR performed according to 3.2.3.

| Component | Concentration |
|---|---|
| 5 x Phusion HP | 1 x |
| dNTPs (10 mM) | 200 µM |
| Forward primer (10 µM) | 0.5 µM |
| Reverse primer (10 µM) | 0.5 µM |
| Phusion High-Fidelity DNA-Polymerase (2000 units/ml) | 0.02 units/µl |
| $H_2O$ | Add to 50 µl |

Success of the colony PCR was monitored by agarose gel electrophoresis (3.2.1.2).

#### 3.2.3.2 Mutagenesis

Site-direct mutagenesis was performed by using whole plasmid mutagenesis approaches resulting in either nicked-circular or blunt-ended linear (Q5-site directed mutagenesis kit) plasmids. For the nicked-circular plasmid method, a complementary primer pair containing the desired mutation was designed manually. Non-complementary primer pairs for Q5-site directed mutagenesis were designed according to the manufacturer`s instructions using the NEBaseChanger online tool. Plasmid amplification was performed as described in 3.2.3. The annealing temperatures were adapted according to the Tm calculator (http://tmcalculator.neb.com/) or NEBasechanger tool (http://nebasechanger.neb.com/).

### 3.2.4 Cloning

#### 3.2.4.1 Restriction digest and dephosphorylation of DNA

Restriction digest of linear or plasmid DNA was performed according the manufacturers protocol. Digestion products were purified according to 3.2.1.3. DNA-fragments digested with two individual restriction enzymes were subsequently used for ligation or stored at -20°C. Plasmids treated with one restriction enzyme were 5` dephosphorylated using Antarctic Phosphatase according to the manufacturer`s instructions prior to ligation or storage.

#### 3.2.4.2 Ligation of DNA fragments

Linearized plasmid DNA and gene inserts were mixed at a 1:1 to 1:3 molar ratio and supplemented with T4-DNA ligase in T4-Ligation Buffer or Quick-Ligation buffer. The final volume was adjusted to 10 µl. Reactions containing Quick-Ligation buffer were incubated for 20 min at RT. Normal ligation reactions containing the T4-Ligation Buffer were incubated at 15°C overnight.

### 3.2.4.3 Transformation

#### 3.2.4.3.1 Preparation of competent *E. coli* cells

Chemically competent *E. coli* cells were prepared as described (Wood, 1983). In short, 200 ml LB were inoculated with 2 ml of an *E. coli* ONC. Cells were grown to $OD_{600}$ ~ 0.6 at 37 °C, resuspended in 4 ml 1 M $MgCl_2$ and subsequently grown at 37°C for further 10 min. Cells were then incubated on ice for 1 h, pelleted at 3,500 x g for 10 min at 4 °C and resuspended in 40 ml CC solution. After another incubation step on ice for 1 h, cells were harvested, resuspended in 10 ml CC solution + 15 % glycerol and aliquoted. Competent cells were stored at -80 °C until transformation.

#### 3.2.4.3.2 Transformation of *E. coli*

Chemically competent *E. coli* cells were transformed using a heat-shock protocol. Therefore 100-200 ng plasmid DNA or 10 µl ligation reaction were mixed with 200 µl of competent cells. After an incubation step on ice for 5-10 min, cells were heat-shocked at 42°C for 45 s and subsequently chilled on ice for 2 min. Cells were recovered by adding 800 µl LB medium and incubation at 37°C for 45-60 min. Afterwards cells were harvested at 4500 rpm for 2 min at RT, plated on the corresponding selection plate and incubated overnight at 37°C.

#### 3.2.4.3.3 Transformation of *S. cerevisiae*

Transformation of *S. cerevisiae* was performed using a high efficiency version of the lithium acetate/single-stranded carrier/PEG method as described by Gietz and Schiestl et al. (Gietz and Schiestl, 2007). Briefly, 50 ml of YPD-medium were inoculated to an $OD_{600}$ of 0.15 from an overnight yeast culture and incubated for 4.5 h at 30°C. Cells were harvested by centrifugation at 3000 rpm for 5 min and washed once with25 ml sterile $H_2O$. The cell pellet was resuspended in 1 ml 0.1 M LiAc, transferred to a 1.5 ml reaction tube, pelleted by centrifugation and resuspended in 500 µl 0.1 M LiAc. Per each transformation, 50 µl of cells were pelleted and 240 µl 50 % PEG-3000, 36 µl 1 M LiAc, 10 µl single-stranded carrier DNA and 100-400 ng DNA plasmid

were added sequentially to the cells. To reach a final of 360 µl, 74-x µl of sterile $H_2O$ were added and the samples were vortexed vigorously. Afterwards the reactions were incubated at 30°C for 30 min followed by a heat-shock at 42°C for 30 min. Cells were gently pelleted at 7000 rpm for 30 sec, resuspended in 1 ml sterile $H_2O$ and 50-200 µl of cells were plated on the respective auxotrophy-selection plate. The plates were incubated at 30°C for at least 3 days.

### 3.2.5 DNA sequencing

Integrity and correctness of plasmid DNA was probed by sequencing. Samples of 20 µl at a concentration of 30-100 ng/µl were analyzed by GATC Biotech AG (Konstanz, Germany).

## 3.3 Microbiological methods

### 3.3.1 Cultivation and storage of *E. coli*

*E. coli* was cultivated at 37°C in LB-medium or LB-plates dependent on the purpose of cultivation containing the respective antibiotics. Cell growth was monitored by optical density measurements at 600 nm ($OD_{600}$). Small LB-cultures were inoculated with a single colony whereas large LB-cultures were inoculated with 1:40 (v/v) of an ONC. Auto-induction cultures were inoculated with 1:1000 (v/v) of an LB-ONC supplemented with 1% Glucose. For long-term storage *E. coli* LB-ONCs were supplemented with 30 % glycerol and stored at -80°C.

### 3.3.2 Cultivation and storage of *S. cerevisiae*

*S. cerevisiae* was cultivated in YPD or selective drop-out media dependent on the auxotrophic marker at 30°C. Cell growth was monitored by optical density measurements at 600 nm ($OD_{600}$). Long-term storage of yeast was conducted as described in 3.3.1.

## 3.4 Protein chemical methods

### 3.4.1 Protein expression in *E. coli*

All proteins used in this work were expressed in *E. coli* BL21-Codon Plus (DE3)-RIL using the pET28 expression system. For normal protein expressions in LB- or 2YT-media, cells were grown to an $OD_{600}$ of 0.8-1.0 at 37°C and induced with 1 mM IPTG. Proteins were expressed for 4-16 h at various temperatures dependent on the protein requirements. For Hsp90 and mutants expression took place at 37°C for 4 h.

GR-related constructs were produced using the auto-induction medium ZYM-5052 (Studier, 2005). Cultures were grown at 37°C for 4 h and afterwards shifted to the desired expression temperature (16-18°C) for 16-18 h. For constructs expressed in the presence of hormone (holo-forms) 500 µM Dexamethasone were added after cultivation for 1 h at expression temperature.

Isotopically-labeled proteins were expressed in minimal media. Labeled GR-LBD was induced with 0.5 mM IPTG and expressed overnight at 18°C. Labeled Hsp90-M domains were induced with 1 mM IPTG and expressed for 4 h at 37°C.

### 3.4.2 Cell harvest and disruption

After expression, *E. coli* cells were harvested by centrifugation at 10000 x g, 8°C and 15 min. Cell pellets that were not directly disrupted or cell pellets from auto-induction expressions were washed once with ice-cold PBS. Prior to the cell disruption, Protease Inhibitor Mix HP and DnaseI were added to the cell suspensions. Disruption was performed either by ultrasonication (4 x 45 s, 5 x 10 % duty cycle, 55 % output) or by a cell disruption system at 2.0 kbar. Hsp90 containing lysates were spiked with 2 mM PMSF. After disruption, lysates were cleared by centrifugation at 100 000 x g, 4°C and 35-60 min.

For Western blot analysis of GR- and Hsp90-expression levels in yeast, cells were harvested at 4500 rpm for 5 min, washed once and treated with 0.1 M NaOH for 3 min at RT. Cells were pelleted again and the supernatant discarded. The pellet was then boiled in 1 x Laemmli sample buffer for 5 min at 95°C.

### 3.4.3 Protein purification

Protein purifications were performed on Äkta FPLC systems at 4°C. Proteins retaining the $His_6$-tag were typically purified by a combination of $His_6$-affinity, anion-exchange and gel-filtration chromatography. For protein constructs containing a solubility-enhancing tag, i.e. Sumo-, Halo- and TEV cleavable $His_6$-tag, the tag was cleaved off. Therefore a strategy of $His_6$-affinity chromatography, proteolytic digest and gel-filtration chromatography was chosen. All columns were run at the manufacturer`s recommendations and pre-equilibrated prior to purification. Success of the purifications was monitored by SDS-PAGE (3.4.4). Of note, the Tau protein used in this thesis was provided by Chad Dickey.

#### 3.4.3.1 Human GR-LBD and GR-DBDLBD

Human GR-LBD and GR-DBDLBD were expressed in ZYM-5052 autoinduction medium (3.4.1) as $His_6$Halo- or $His_6$-SUMO-fusion constructs, respectively. Cells were harvested and disrupted as mentioned in 3.4.2. For GR-LBDm the purification strategy was adopted form Seitz et al. (Seitz et al., 2010). In brief, cleared GR-LBD lysates were loaded on a HisTrap FF-column equilibrated in GR-LBD disruption-buffer (disruption buffer). After loading, the column was washed with 10 CV disruption buffer. This procedure was repeated once to ensure complete binding of the $His_6$Halo- GR-LBD construct. Next, the column was washed with a gradient from 0-100 % NiA buffer and target protein was eluted with NiB buffer. $His_6$Halo-GR-LBD containing fractions were subjected to proteolytic digestion by $His_6$ tagged TEV-protease over night with simultaneous dialysis in GR-dialysis buffer. The digestion reaction was then applied to a HisTrap FF column equilibrated in GR-dialysis buffer to remove the $His_6$-tagged TEV-protease and the $His_6$Halo-tag. The FT containing the cleaved GR-LBD was collected, concentrated to 10 ml in an Amicon cell with a 10 kDa MWCO filter and applied to a Superdex 16/60 200pg gel-filtration column equilibrated in GR-SEC buffer in two runs. GR-LBD containing fractions were pooled, frozen in liquid nitrogen and stored at -80°C until further use. Purity of the protein batch was determined by SDS-PAGE (3.4.4). Hormone-free GRLBD was expressed and purified in the absence of hormone. To prevent binding of *E. coli* chaperones (GroEL or DnaK) ATP was

incorporated the disruption and NiA buffer. To increase solubility 0.2-0.5 % CHAPS were added to all buffers.

A similar purification strategy was applied for $His_6$-Sumo-GR-DBDLBD except that proteolytic digestion was performed with $His_6$-tagged Sumo-protease. To increase the protein purity an additional purification step was added. By combining features of affinity-chromatography with cation-exchange-chromatography, Heparin columns are suited best to improve purity of DNA-binding proteins. Prior to gel-filtration, the GR-DBDLBD was applied to a HiTrap Heparin HP column equilibrated in HepA buffer and eluted by a linear salt-gradient from 0-100 % HepB buffer.

| Buffer | Concentration | Component |
|---|---|---|
| Disruption buffer | 50 mM | Tris, pH 7.9 |
| | 2 M | Urea |
| | 100 mM | NaCl |
| | 5 mM | $MgCl_2$ |
| | 10 mM | Imidazole |
| | 2 mM | ß-Mercaptoethanol |
| | 50 µM | Dexamethasone |
| NiA/B buffer | 50 mM | Tris, pH 7.9 |
| | 500 mM | NaCl |
| | 10/350 mM | Imidazole |
| | 10 % (w/v) | glycerol |
| | 2 mM | ß-Mercaptoethanol |
| | 50 µM | Dexamethasone |
| GR-dialysis buffer | 50 mM | Tris, pH 7.9 |
| | 100 mM | NaCl |
| | 10 % (w/v) | Glycerol |
| | 0.5 % | CHAPS |
| | 2 mM | ß-Mercaptoethanol |
| | 50 µM | Dexamethasone |
| GR-SEC buffer | 25 mM | Tris, pH 7.9 |
| | 100 mM | NaCl |
| | 10 % (w/v) | glycerol |
| | 2 mM | DTT |
| | 50 µM | Dexamethasone |
| HepA buffer | 25 mM | Tris, pH 7.9 |
| | 125 mM | NaCl |

| | | |
|---|---|---|
| | 10 % (w/v) | glycerol |
| | 2 mM | β-Mercaptoethanol |
| | 50 µM | Dexamethasone |
| HepB buffer | 25 mM | Tris, pH 7.9 |
| | 1 M | NaCl |
| | 10 % (w/v) | glycerol |
| | 2 mM | β-Mercaptoethanol |
| | 50 µM | Dexamethasone |

### 3.4.3.2 Hsp90, Hsp70 and co-chaperones

Hsp90 (yeast and human) and its co-chaperones were expressed from pET28 with a N-terminal $His_6$-tag. As mentioned under 3.4.3, proteins with a $His_6$-tag were purified by a combination of $His_6$-affinity, anion-exchange and gel filtration chromatography. After expression in LB- or 2YT-media, cell disruption and lysate clarification (3.4.1, 3.4.2), proteins were loaded on a HisTrap FF/HP column equilibrated in NiA buffer. After loading the column was washed with 10 CV NiA and 10 CV 5 % NiB buffer before elution with 100 % NiB buffer. Fractions containing the target protein were pooled and diluted to 150 ml with ResQA buffer to dilute the salt concentration that would prevent the protein from binding the anion-exchange column. The protein was then loaded on the ResQ column equilibrated in ResQA buffer. After loading, the column was washed with 10 CV ResQA buffer and eluted using a gradient from 0-50% ResQB buffer. Protein-containing fractions were pooled, concentrated and loaded on a Superdex 16/60 200 pg gel-filtration column. Purity of the protein charge was controlled by SDS-PAGE (3.4.4) and the protein was frozen in liquid nitrogen. For wt yeast Hsp90 and human Hsp90ß, a hydroxyl apatite column was added to the purification strategy to decrease the amount of background ATPases from *E. coli.*

Human Hsp70 and yeast Ydj1 were expressed as SUMO-fusion constructs. Therefore anion-exchange chromatography was omitted. Instead, after proteolytic digest overnight by $His_6$-tagged SUMO-protease, the proteins were loaded again on a NiA equilibrated HisTrap FF column. During SUMO-cleavage also the $His_6$-tag was cleaved off, so the target proteins eluted during the flow trough. The flow through was then concentrated and loaded on a Superdex 16760 200 pg gel filtration column. To prevent binding of DnaK form *E. coli* 0.5 mM ATP were added to NiA and NiB buffers.

| Buffer | Concentration | Component |
|---|---|---|
| NiA buffer | 50 mM | NaPi pH 7.5 |
| | 500 mM | NaCl |
| | 10 mM | Imidazole |
| | 1 mM | DTT |
| NiB buffer | 50 mM | NaPi pH 7.5 |
| | 500 mM | NaCl |
| | 300 mM | Imidazole |
| | 1 mM | DTT |
| ResQA buffer | 40 mM | HEPES pH 7.5 |
| | 20 mM | KCl |
| | 1 mM | EDTA |
| | 1 mM | DTT |
| ResQB buffer | 40 mM | HEPES pH 7.5 |
| | 1 M | KCl |
| | 1 mM | EDTA |
| | 1 mM | DTT |
| SEC buffer | 40 mM | HEPES pH 7.5 |
| | 150 mM | KCl |
| | 5 mM | $MgCl_2$ |
| HatA buffer | 10 mM | KPi |
| HatB buffer | 400 mM | KPi |

### 3.4.4 Sodium dodecyl sulfate polyacrylamide gel electrophoresis (SDS-PAGE)

SDS-PAGE was performed according to Laemmli et al. in order to confirm purity of protein purifications and perform separation of crude extracts of *S. cerevisiae* for Western blotting (3.4.5) (Laemmli, 1970). Samples were supplemented with 1 x Laemmli sampling buffer and boiled for 5 min at 95°C prior to gel electrophoresis to ensure denaturation of the protein sample. The acrylamide concentration was adapted to the implementation and size of protein that was analyzed. In general, separation gels from 10-15 % acrylamide were used in this work.

| Component | 10-15 % separation gel | 5% stacking gel |
|---|---|---|
| 40 % Acrylamide | 2.5-3.75 ml | 0.625 ml |
| 4 x separation gel SDS buffer | 2.5 ml | - |
| 2 x stacking gel SDS buffer | - | 2.5 ml |
| $H_2O$ | 3.75- 5 ml | 1.875 ml |
| Σ | 10 ml | 5 ml |
| APS | 130 µl | 130 µl |
| TEMED | 6.6 µl | 6.6 µl |

The gels were developed at constant amperage of 45 mA for 45-60 min and stained according to Fairbanks et al. (Fairbanks et al., 1971). In brief, gels were incubated in prewarmed Fairbanks A solution for 5-10 min and destained using prewarmed Fairbanks D solution for 10-15 min.
The molecular weight of the analyzed proteins was estimated by comparison with the Low Range molecular weight marker.

### 3.4.5 Western blotting

Western blotting was performed to visualize Hsp90 and Hsp90 mutants from crude yeast extracts. A SDS-PAGE (3.4.4) was performed prior to the blotting procedure and included the prestained Protein Marker IV as molecular weight standard. Gels were subsequently electro-blotted on methanol-activated PVDF membranes in a semi-dry blotting apparatus for 90 min at constant amperage of 72 mA per gel. After blotting, the membranes were incubated in blocking solution for 1 h. Next, blots were incubated for 1 h with the primary antibody diluted in PBS-T supplemented with 1 % milk powder. Following three washing steps with PBS-T, blots were incubated with Peroxidase (POD)-conjugated secondary antibody for 1 h. After another three washing steps with PBS-T, protein bands were detected using the Western Bright ECL spray and ImageQuant LAS400 system according to the manufacturer`s recommendations.

### 3.4.6 Protein labeling

Proteins were labeled with fluorescent dyes for various purposes including analytical ultracentrifugation and FRET measurements. Labeling was either performed using native lysine side chains with NHS-chemistry or native/mutationally introduced cysteine residues with maleimide chemistry. The labeling procedure was adopted from the manufacturer`s protocol. For labeling of lysine residues, proteins were incubated with a 1-1.5 fold molar excess of fluorescent label in DMSO for 1 h at RT or for 3-4 h on ice. Reactions were quenched with excess of Tris and unreacted label was removed by using a PD-10 column according to the manufacturer`s recommendations. For labeling of cysteine residues, proteins were incubated with a 1.5-2 fold molar excess of fluorescent label in DMSO for 1 h at RT. Unreacted label was quenched by adding 5-fold molar excess of DTT and removed by PD-column or extensive dialysis. Double-labeled GR-LBD constructs for single-molecule measurements were incubated with a 1:1 ratio of the first label for 1.5 h and another 2 h with a 2-3 fold molar excess of the second label. Unreacted labels were again quenched by molar excess of DTT and removed by extensive dialysis. Protein concentration and degree of labeling (DOL, labeling efficiency) were determined photometrically as described in the protocol supplied by the manufacturer.

## 3.5 Spectroscopy

### 3.5.1 UV/Vis absorbance spectroscopy

Peptides and proteins absorb UV-light in solution with maxima at 190 nm and 280 nm. While the maximum at 190 nm is produced by the absorption of the peptide-bond, the aromatic side-chains of phenylalanine, tryptophan and tyrosine, and also disulfide-bonds, are responsible for the absorbance maximum at 280 nm (Knowles, 1981).

| | $\lambda_{max}$ [nm] | $\varepsilon_{max}$ [$M^{-1} cm^{-1}$] |
|---|---|---|
| tryptophan | 280 | 5700 |
| tyrosine | 274 | 1400 |
| phenylalanine | 257 | 200 |
| disulfide bond | 250 | 300 |

With $\lambda_{max}$ as the wavelength of the absorbance maximum and $\varepsilon_{max}$ as the molar extinction coefficient;

UV-absorbance of proteins was exploited in this work to determine protein concentrations by using the Lambert-Beer law (Equation 1). Absorbance was determined by recording absorbance spectra from 200-450 nm on a Varian Cary 50/100 Bio UV-VIS spectrophotometer in quartz cuvettes using adequate dilutions of the protein solution. To correct for buffer absorbance, absorbance spectra of only buffer were subtracted. The molar extinction coefficients were determined using the protparam online tool (http://web.expasy.org/protparam/) which estimates the molar extinction coefficient by summing up the extinction coefficients of the aromatic residues in the protein.

### 3.5.2 Fluorescence spectroscopy

#### 3.5.2.1 Fluorescence polarization (anisotropy)

When fluorophores are excited with linear polarized light, the emission from many samples is also polarized. The extent of polarization is described by the fluorescence polarization P or anisotropy r. The degree of polarization or anisotropy is determined by two intensities. $I_{\parallel}$ describes the fluorescence intensity when excitation and emission polarizers are oriented parallel and $I_{\perp}$ reflects the fluorescence intensity when the polarizers are oriented perpendicular. Both values together are used to calculate the anisotropy r or polarization P (Lakowicz, 2007)

$$\mathbf{P} = \frac{\mathbf{I}_{\parallel} - \mathbf{I}_{\perp}}{\mathbf{I}_{\parallel} + \mathbf{I}_{\perp}}$$

**Equation 2**

$$r = \frac{I_{\parallel} - I_{\perp}}{I_{\parallel} + 2I_{\perp}}$$

**Equation 3**

There are several phenomena affecting the polarization of the emitted light. One example is the rotational diffusion of the fluorophore during the lifetime of the excited state. As the rotational diffusion is a diffusive motion, it is dependent on the viscosity of the solvent and on the size and shape of a molecule. Small molecules in solvents with low viscosity show faster rates of rotational diffusion than rates of emission. Therefore, the emitted light is depolarized and the anisotropy is close to zero. The dependence of the polarization/anisotropy on the rotational behavior of a molecule makes it a powerful tool to study ligand-protein or protein-protein interaction, as the decay time of many fluorophores is comparable to the rotational correlation time of biomolecules. Therefore, a change in the rotational correlation time, for example by binding of a ligand to its protein receptor, alters directly the polarization or anisotropy of the emitted light (Lakowicz, 2007).

Fluorescence anisotropy measurements were performed in this work to follow binding of fluorescently labeled Dexamethasone to GR-LBD constructs, in absence and presence of various chaperone mixtures. Experiments were conducted on a Jasco Fluorescence Spectrometer FP-8600 equipped with polarizers. Measurements were performed in FP-measurement buffer (see below).

| **FP-measurement buffer** | |
|---|---|
| Concentration [mM] | Component |
| 30 | HEPES pH 7.5 |
| 150 | KCl |
| 5 | $MgCl_2$ |
| 2 | DTT |

The excitation wavelength was set to 490 nm and the emission wavelength to 520 nm. Slit sizes and detector sensitivity were adapted to the concentration of labeled species in the sample. Data fitting was performed using Origin 9.1G. Used fit functions are indicated in the respective figure legends.

### 3.5.2.2 Ensemble fluorescence resonance energy transfer (FRET) measurements

Fluorescence resonance energy transfer (FRET) or Förster resonance energy transfer is a widely used application to determine intra- and intermolecular distances as well as conformational changes within proteins. FRET occurs between a donor-fluorophore (D) and an acceptor-fluorophore (A). Prerequisite for this energy transfer is that the emission spectrum of D overlaps with the excitation spectrum of A. During FRET there is no appearance of photons as the energy is transferred by long-range dipole-dipole interactions between D and A. The FRET-efficiency is determined by the spectral overlap of D and A, the quantum yield of D, the relative orientation of and most importantly the distance between the two fluorophores (Lakowicz, 2007). The strong dependence on the distance is demonstrated in the following formula:

$$\mathbf{E} = \frac{\mathbf{R_0^6}}{\mathbf{R_0^6 + r^6}} = \mathbf{1} - \frac{\mathbf{F_{DA}}}{\mathbf{F_D}}$$

**Equation 4**

With the Förster distance $R_0$ which describes the distance between D and A at 50 % FRET-efficiency, r the distance between the fluorophores, $F_{DA}$ the donor fluorescence in the presence of the acceptor and $F_D$ the donor fluorescence in the absence of the acceptor.

There are two major applications for FRET studying proteins. On the one hand FRET can be used as “spectroscopic ruler”. By monitoring FRET-efficiencies, distances between D and A can be measured, so structural information can be acquired. On the other hand FRET is used to study protein-protein interactions and conformational changes within multi-domain proteins. In these experiments the focus is less on the exact efficiencies but more on the general occurrence of FRET when D and A are in close proximity (Lakowicz, 2007).

In this work an established yeast Hsp90 FRET system was used to monitor the effects of GR-LBD and Tau on the conformational changes in Hsp90 (Hessling et al., 2009). Therefore, yeast Hsp90 was labeled at engineered cysteine residues in the N-terminal domain or middle-domain (61C, 385C) with ATTO488-maleimide donor dye and ATTO550-maleimide acceptor dye as mentioned in 3.4.6. To follow GR-LBD binding to yeast Hsp90, GR-LBD was labeled with ATTO488-maleimide donor dye and yeast Hsp90 at an engineered cysteine residue at position 333 within the middle-domain (E333C).

Measurements were conducted either on a Horiba Fluoromax 3 Fluorescence Spectrometer or on a Jasco Fluorescence Spectrometer FP-8600 using quartz cuvettes. Temperature was set to 30°C. Excitation wavelength was set to 490 nm and emissions were recorded at 520 nm and 575 nm. Slit sizes and detector sensitivity was adapted to the used proteins. For the yeast Hsp90 FRET system, 200 nM donor and 200 nM acceptor labeled Hsp90 were mixed in HKM buffer (see below), incubated with different amount of GR-LBD constructs or Tau and closing of the dimer was followed by addition of 2 mM ATPγS. Chase experiments were performed by adding 4 µM unlabeled Hsp90 or excess of ADP to the samples. Association of GR-LBDm with Hsp90, 200 nM ATTO488-labeled GR-LBD was mixed with various amounts of ATTO550-labeled Hsp90. Nucleotides were used at a concentration of 2 mM and competition experiments were assessed by addition of excessive co-chaperone or Tau amounts.

| **HKM buffer** | |
|---|---|
| Concentration [mM] | Component |
| 40 | HEPES pH 7.5 |
| 150 | KCl |
| 5 | $MgCl_2$ |

Data processing and fitting was performed by the program Origin 9.1G and a single exponential decay equation.

### 3.5.2.3 Single molecule FRET spectroscopy

Single-molecule FRET (smFRET) experiments were performed in cooperation with Daniela Wengler and Don Lamb (Ludwig-Maximilians-Universität München, Germany). Measurements were performed on a custom-built two-color confocal microscope system based on an Eclipse TE2000 (Nikon, Tokyo, Japan) with pulsed interleaved excitation and multi-parameter fluorescence detection. GR-LBD was labeled on engineered cysteine residues at the very N- and C-terminus, or N-terminus and C638 with three different combinations of FRET dyes (ATTO532-ATTO647, ATTO488-ATTO647, ATTO488-ATTO700). Labeling was performed as described in 3.4.6. Measurements were performed in HKM buffer (3.5.2.2) using 10 pN labeled

GR-LBD, 2 mM ATP, 2-5 µM Ydj and 15-10 µM Hsp70. 50 µM Dexamethasone were added to the experiments as indicated in the respective figure.

#### 3.5.2.4 Thermal stability assay (TSA)

Thermal stability assay was performed to probe thermal stability of Hsp90 and Hsp90-mutants. The assay uses the environmentally sensitive fluorescent dye Sypro Orange. The dye shows an increase in fluorescence when bound to hydrophobic surfaces exposed during unfolding of protein structures (Lo et al., 2004). 0.2 mg/ml protein of interest were mixed with 2 µl 1:1000 (v/v) dilution of Sypro Orange to a final volume of 20 µl. HKM buffer was used for all measurements (3.5.2.2). The TSA assay was performed in an Agilent Mx3000P QPCR-System using a stepwise temperature increase program from 25 to 90.5°C (131 cycles, 0.5°C per cycle). Excitation wavelength was set to 470 nm and emission was detected at 570 nm. Data processing and analysis was performed using Origin 9.1G. The melting temperature was determined using the Boltzmann fit function.

### 3.5.3 Single molecule force spectroscopy

Single molecule force spectroscopy was performed in cooperation with Thomas Suren and Matthias Rief (Technische Universität München). Functionalized DNA-handles were coupled to GR-LBD at engineered Cysteine residues at the very N- and C-terminus by maleimide chemistry as described previously. DNA-handles were formed at RT for 30 min. Experiments were conducted on a custom-built dual-trap optical tweezers featuring a dual-beam design with back focal plane detection and one piezo mirror steered beam. Measurements were performed as mentioned previously (Jahn et al., 2014).

### 3.5.4 Circular dichroism spectroscopy

Circular dichroism spectroscopy (CD) exploits the characteristic of optically (chiral) active molecules to differentially absorb right-hand circular (RHC) and left-hand circular polarized light. Optically active elements in peptides and proteins are the peptide bond with an absorbance

between 170-260 nm (far-UV) and the aromatic amino acids phenylalanine, tyrosine and tryptophan absorbing at 250-350 nm (near-UV). Near-UV CD-spectroscopy gives important information about the tertiary structure of proteins as the chemical environment influences the absorbance characteristics of the aromatic amino acids. Far-UV CD-spectroscopy is even more important for structural biochemistry as the spectrum contains important information about the secondary structure of peptides and proteins. α-helical proteins exhibit two minima at 222 nm and 208 nm, β-sheets show a single minimum at 218 nm whereas unfolded structure give rise to a specific minimum at 195 nm (Lottspeich et al., 2012).

In this work far-UV CD-spectra and CD-based temperature transitions were recorded using 1 mm quartz cuvettes on a Jasco J715 CD-Spectrometer with a PTC343-Peltier unit. Protein concentration was set to 0.1 mg/ml and temperature to 10°C. CD-spectra were recorded from 200-260 nm with a scanning speed of 20 nm/min and, depending on the signal, with 10-15 accumulations. Buffer spectra were measured separately and subtracted from the protein spectra. Thermal transitions were recorded from 10-90°C with a data pitch of 0.2°C, a temperature slope of 20°C/h, a sensitivity of 100 mdeg, a response time of 8s and a band width of 1.0 mm.

CD-spectra data was converted to the mean residual weight ellipticity by the following formula.

$$\Theta_{MRW} = \frac{\Theta \times 100 \times M}{d \times c \times N_{aa}}$$

**Equation 5**

With $\Theta_{MRW}$ as the mean residual weight ellipticity, Θ as the measured ellipticity in [mdeg], M the molecular weight of the protein [M], d the layer thickness in [cm], c the protein concentration in [mg/ml] and $N_{aa}$ the number of amino acids;

Thermal transition data was normalized, plotted against the temperature and fitted by the Boltzmann equation to determine the melting point. All CD-data conversion, procession and fitting was performed using Origin 9.1G.

## 3.6 Analytical gel filtration

Analytical gel filtration separates proteins by their molecular weight or more precisely by their hydrodynamic volume. Proteins or protein complexes interact differentially with the porous stationary phase dependent on their hydrodynamic volume, with large proteins/complexes having shorter retention times and smaller proteins/complexes having longer retention times. This effect is explained by the observation that large complexes show less intensive interactions with the porous stationary phase, due to their large size, than small proteins or complexes (Lottspeich et al., 2012).

In this work, analytical gel filtration was performed on a Shimadzu Prominence HPLC system. GR and GR-chaperone mixtures at different concentrations were injected on a Superdex 200 Increase 10/300 GL column equilibrated in HKM buffer (3.5.2.2). The flow rate was set to 0.5 ml/min. Peaks were detected at 280 nm or 350 nm (intrinsic fluorescence). The apparent molecular mass was estimated using a calibration curve generated with Thyroglobulin (670 kDa), γ-globulin (158 kDa), Ovalbumin (44 kDa), Myoglobin (17 kDa) and Vitamin $B_{12}$ (1.35 kDa) (0). If needed, HPLC-runs were fractionated and the fractions analyzed on their protein composition by SDS-PAGE (3.4.4).

## 3.7 Analytical ultracentrifugation

Analytical ultracentrifugation (AUC) provides first-principle hydrodynamic and thermodynamic information concerning the size, shape and interactions of macromolecules. The fundamental information needed in AUC is the macromolecular concentration as a function of radial position and time. It can be used to identify and quantify species present in a solution of macromolecules.

The sedimentation process is dependent on three major forces: the centrifugal force, the friction and the buoyant force. The Svedberg equation describes the relation of these three forces (Lottspeich et al., 2012).

$$\boldsymbol{s = \frac{v}{\omega^2 r} = \frac{MD\left(1 - \bar{\nu}\rho\right)}{RT}}$$

**Equation 6**

With s as the sedimentation coefficient [S], v the observed radial velocity [m/s], ω the angular velocity of the rotor [m/s$^2$], $\omega^2 r$ the centrifugal field in [N], M the molecular weight [g/mol], $\bar{v}$ the partial specific volume [cm$^3$/g], ρ the density of the solvent [g/cm$^3$], D the diffusion coefficient [m$^2$/s], R the gas constant [8.314 J/mol K] and T the temperature in [K];

There are generally two types of experiments by which bio-macromolecules can be analyzed, sedimentation equilibrium and sedimentation velocity experiments. Sedimentation equilibrium experiments are performed at relatively low angular velocity which leads to an equilibrium of sedimentation and diffusion. Thereby, a distribution of analytes is forming within the cell which is only dependent on the molecular weight of the respective species. In sedimentation velocity experiments, a high centrifugal force is applied to the sample leading to complete sedimentation of the analyte. From the experimental data the sedimentation coefficient s, the diffusion coefficient and the molecular weight M of all species present in the sample can be determined. Therefore, an advantage of sedimentation velocity experiments is that the sample composition is studied in greater detail than in sedimentation equilibrium experiments. Here, only average sedimentation coefficients and molecular masses of all analytes present in the sample are provided (Lottspeich et al., 2012; Schuck, 2005). Sedimentation boundaries or distributions are in both cases detected by either UV-absorbance, interference or fluorescence. Thereby, the latter is the most sensitive technique which requires only very little sample amounts (Lottspeich et al., 2012).
In this work, only sedimentation velocity experiments were performed to acquire information about the size, oligomerization and binding behaviour of various proteins. Sedimentation velocity experiments of GR-LBD constructs and Tau were performed on a Beckman Optima XL-I centrifuge equipped with absorbance and interference optics. For GR-constructs GR-SEC buffer and for Tau, Tau-AUC buffer (20 mM HEPES pH 7.5, 100 mM NaCl) was used as reference. Sedimentation was monitored at 280 nm.

Interaction studies were performed on a Beckman XL-A centrifuge equipped with an AVIV fluorescence detection system. GR-LBD, Tau and co-chaperones were randomly labeled with ATTO488 on cysteine and lysine residues or the N-terminus as described in 3.4.6. Dependent on the labeling efficiencies, 400-1000 nM of fluorescently-labeled protein or Dexamethasone were used. Concentrations of Hsp90, Hsp70 and co-chaperones were 1-12 µM and nucleotides were

added at 2 mM. Experiments were performed in AUC buffer (see below). Binding of holo-GR-LBD was monitored in the presence of 50 µM Dexamethasone. Excitation wavelength was set to 488 nm and fluorescence emission was detected with a band pass filter from 505-565 nm.

| **AUC buffer** | |
|---|---|
| Concentration [mM] | Component |
| 20 | HEPES pH 7.5 |
| 20 | KCl |
| 5 | $MgCl_2$ |
| 5 | DTT |

All samples were loaded into assembled cells with quartz windows and 12-mm path length charcoal-filled epon double sector centerpieces and were centrifuged at 42 000 rpm in an eight-hole Beckman–Coulter AN-50 Ti rotor. Data analysis was performed by using SedView (Hayes and Stafford, 2010), SedFit (Schuck, 2000) and Origin 9.1G using a bi-gaussian. Viscosity, density and the partial specific volume $\bar{v}$ were calculated using the online tool SEDNTERP (Laue TM, 1992).

## 3.8 Structural methods

### 3.8.1 NMR spectroscopy

To map the Tau-Hsp90 binding interface, NMR spectroscopy was carried out. All NMR experiments and data analysis were performed by Lee Freiburger (Technische Universität München). NMR spectra were recorded on a Bruker AV900 spectrometer (Bruker Topspin 2.1, Bruker, Billerica, USA) at 25 °C. For Hsp90 binding experiments, Tau was diluted in NMR buffer (see below) containing the isotopically enriched Hsp90 component of interest (e.g. Hsp90-N, -M, -C and segmentally labeled Hsp90-NM). The protein solution was then concentrated. NMR experiments were processed using NMRPipe (Delaglio et al., 1995) and the data was analyzed using CcpNMR analysis (Vranken et al., 2005).

| NMR buffer | |
|---|---|
| Concentration | Component |
| 20 mM | Sodium phosphate, pH 6.5 |
| 200 mM | NaCl |
| 2 mM | $MgCl_2$ |
| 2 mM | DTT |
| 0.2 % | $NaN_3$ |

Chemical shift assignments were already available for Hsp90-N domain (1-210) (Dehner et al., 2003; Salek et al., 2002), Hsp90-M domain, Hsp90–C domain (277-527) (Hagn et al., 2011) and the segmentally Sortase A-ligated Hsp90-NM constructs (Lorenz et al., 2014).

### 3.8.2 Small angle x-ray scattering (SAXS)

SAXS exploits the elastic scattering of monochromatic x-rays at very low angles (0.1-10 °). The scattering pattern provides information about the radius of gyration $R_g$, the volume of hydration $V_h$, the maximal dimension $D_{max}$ and the molecular mass. In contrast to x-ray crystallography, SAXS is performed in solution and is thereby able to detect conformational changes due to interactions with other proteins or small molecules like nucleotides. Therefore, SAXS is a powerful tool to study protein interactions and is also providing structural information when computational methods are applied (Blanchet and Svergun, 2013; Lottspeich et al., 2012).
In this work, SAXS was used to analyze the conformational diversity of yeast Hsp90 and Hsp90 W300 mutants. SAXS experiments and analysis were performed by Tobias Madl (Technische Universität München). Proteins were diluted to a final concentration of 80 µM in HKM buffer (3.5.2.2). Samples were measured on an in-house Anton Paar SAXSess mc2 SAXS instrument equipped with a Kratky camera, a sealed X-ray tube source and a two-dimensional PI SCX:4300 Princeton Instruments CCD detector. The scattering patterns were recorded with a 180-min exposure time (1080 frames, each 10 seconds). All SAXS data was analyzed with ATSAS (version 2.5). The data was processed with the SAXSQuant software (version 3.9). The forward scattering, I(0), $R_g$,, $D_{max}$, desmearing and the inter-atomic distance distribution functions, P (R), were computed with the program GNOM (Svergun, 1992). To calculate the P(R)s of mixtures of ‘closed’ and ‘open’ Hsp90 conformations, the experimental P(R) of ‘open’ Hsp90 and the P(R)

back-calculated for the 'closed' form of Hsp90 complexes (PDB 2CG9), using the program Crysol (Svergun et al., 1995) were normalized and combined at different ratios.

### 3.8.3 Atomistic molecular dynamics (MD) simulations of Hsp90 and Hsp90 mutants

Molecular dynamics simulations were performed in cooperation with Qi Luo and Ville R. I. Kaila (Technische Universität München). Simulations were conducted based on full-length yeast Hsp90 dimer with ATP-$Mg^{2+}$ in the closed state, constructed based on the X-ray structure obtained from the Protein Data Bank (PDB ID: 2CG9). Missing loops were modeled using MODELLER (Sali and Blundell, 1993). Each model was solvated in a water box with 100 mM NaCl concentration. The molecular systems comprised *ca*. 300,000 atoms, and were simulated in an *NPT* ensemble at $T$=310 K and $p$=101.3 kPa. All simulations were performed using NAMD 2.9 (Phillips et al., 2005) for 200 ns, with an integration time-step of 2 fs using the CHARMM27 force field (Brooks et al., 1983). Visual Molecular Dynamics was used for analysis (Humphrey et al., 1996). For the dynamical networks analysis, Hsp90 was coarse grained into edges and nodes based on the last 150 ns MD trajectories. Amino acid residues and $Mg^{2+}$ were each represented by a single node, while the adenine ring, the ribose, and triphosphate unit of ATP, were each represented by separate nodes. Edges were defined as a node contact within 4.5 Å for at least 75% of the analyzed trajectory. The shortest force propagation pathway between nodes in the network was calculated using the Floyd-Warshall algorithm, and the dynamic network analysis was performed using the Carma software (Girard, 2014). Solvation free energy of the ATP-$Mg^{2+}$ complex in the active site of Hsp90 was calculated along the trajectory by Poisson-Boltzmann continuum electrostatic calculations using the Solinprot module of MEAD.

## 3.9 Functional assays

### 3.9.1 5`fluoro-orotic acid (FOA) shuffling of essential genes in *S. cerevisiae*

To test the viability of yeast and human Hsp90 mutants *in vivo* an plasmid shuffling assay was performed as described by Nathan and Lindquist (Nathan and Lindquist, 1995). In brief, the *S. cerevisiae* ΔPCLDα strain was used that contains a knock-out of both genomic copies of *hsp90* with a leucine selection marker. Additionally this strain carries an URA-selected plasmid coding for *hsp90* constitutively expressed under the control of the glycerinaldehyde-3-phosphate dehydrogenase gene promoter (GPD promoter). The *URA3* gene encodes for the orotidine-5`-phosphate decarboxylase that converts 5`FOA to 5`fluorouracil which interferes with DNA and RNA processing and is therefore toxic for yeast. This selective pressure leads to survival of yeast cells that have lost the *URA3* plasmid and therefore contain only the mutagenic version of the *hsp90* gene.

### 3.9.2 GR activity assay in *S. cerevisiae*

GR activity assay in *S. cerevisiae* was performed to test functionality of yeast Hsp90 mutants *in vivo* (Nathan and Lindquist, 1995). For this purpose, yeast (ΔPCLDα) were transformed with a reporter plasmid (p2A/GRGZ), carrying a GPD-controlled rat GR gene and a ß-galactosidase gene under control of a Glucocorticoid response element (GRE), and the p413 vector coding for wt *hsp90* or mutants under control of the GPD-promoter. Plasmid shuffling was performed as described in 3.9.1. Single clones were picked and grown overnight at 30°C to stationary phase. The next day, cells were diluted to an $OD_{600}$ of 0.3, induced with 10 µM Deoxycorticosterone (DOC) and incubated for 6-8 h at 30°C. After induction, $OD_{600}$ was determined and 50 µl of cells were transferred to a 96-well plate and harvested at 4500 rpm for 5 min. Supernatant was discarded, the pellet resuspended in 150 µl SDS-lysis buffer (see below) and incubated for 15 min at RT with mixing. After cell lysis, 50 µl 4mg/ml 2-nitrophenyl ß-D-galactopyranosid (OPNG) in Z buffer (see below) were added and ß-galactosidase activity was monitored at 420 nm for 30 min in a Tecan Sunrise plate reader. The absolute activities were calculated by determining the slopes of the reaction and normalized by $OD_{600}$. Data processing and fitting was performed in Origin 9.1G.

| SDS-lysis buffer | |
|---|---|
| **Concentration** | **Component** |
| 94 mM | NaPi, pH 7.5 |
| 0.1 % | SDS |

| Z buffer | |
|---|---|
| **Concentration [mM]** | **Component** |
| 100 | NaPi, pH 7.0 |
| 15 | KCl |
| 5 | $MgCl_2$ |

### 3.9.3 Regenerative ATPase assay

ATPase activities were determined using an enzyme-coupled activity assay in combination with an ATP-regenerating system. In a first step, ATP is hydrolyzed by the ATPase (Hsp90 or Hsp70) to ADP. The pyruvate kinase (PK) converts ADP to ATP under production of pyruvate from Phosphoenol-pyruvate (PEP). Pyruvate is further converted by the lactate dehydrogenase (LDH) to L-lactate under oxidation of NADH to $NAD^+$ which can be monitored by the decrease in absorbance at 340 nm. As the ATP hydrolysis is the rating limiting step in the system, the ATPase activity is directly proportional to the decrease in $A_{340}$ (Ali et al., 1993).

ATPase assays were performed on a Cary 50/100 Bio UV/Vis spectrometer at 30°C (yeast proteins) or 37°C (human proteins) in quartz cuvettes. Each reaction contained 100 µl premix (see below), 3-10 µM ATPase (yeast Hsp90, human Hsp90ß, human Hsp70), varying concentrations of client proteins (GR-LBD, Tau) and co-chaperones and was filled up with HKM buffer (3.5.2.2) to a final volume of 147 µl. The samples were temperature equilibrated for 5-10 min and the ATPase reaction started by the addition of 2 mM ATP. In case of Hsp90, background activity was determined by addition of 50 µM Radicicol

| **ATPase premix** | |
|---|---|
| Volume [µl] | Component |
| 8656 | HKM buffer |
| 240 | 100 mM PEP |
| 24 | 100 mM NADH |
| 44 | LDH |
| 12 | PK |

ATP hydrolysis rates were determined using the following formula.

$$\mathbf{k_{hyd}} = \frac{\mathbf{m}}{\mathbf{d} \times -(\boldsymbol{\varepsilon}_{\mathbf{NADH}}\mathbf{at\ 340\ nm}) \times \mathbf{c_{ATPase}}}$$

**Equation 7**

With $k_{hyd}$ the hydrolysis rate in [$min^{-1}$], m the slope in [$min^{-1}$], d the layer thickness in [cm], $\varepsilon_{NADH}$ the molar extinction coefficient of NADH at 340 nm in [$M^{-1}$ $cm^{-1}$] and $c_{ATPase}$ the concentration of the ATPase in [M];

For Hsp90 activity assays, the slope after addition of Radicicol was subtracted from the slope m to correct for background ATPase activity. Data processing, slope determination and fitting was performed using Origin 9.1G.

# 4 Results and Discussion

## 4.1 Tryptophan 300 is an important switch point for GR homeostasis in Hsp90

### 4.1.1 A Tryptophan in the middle domain of Hsp90 strongly affects GR-LBD binding to the Hsp90-MD

The Hsp90-M domain plays a crucial role for client binding and activation (Taipale et al., 2010). Mutational studies have shown that many residues within the Hsp90-M domain are important to ensure full functionality of GR *in vivo* (Bohen and Yamamoto, 1993; Nathan and Lindquist, 1995) and structural investigations have proven *in vitro* that it is the major interaction site of the GR-LBD with Hsp90 (Lorenz et al., 2014). A tryptophan residue within the MD has attracted special attention. In several publications it was shown that mutation of tryptophan 300 to alanine (W300) impairs yeast growth at 30°C, alters client activation *in vivo* and binding of co-chaperones *in vitro* (Flom et al., 2012; Hawle et al., 2006; Johnson et al., 2007; Meyer et al., 2003). Further, W300 has been implicated to play a role in the association of Hsp90 with the co-chaperone Cdc37 and the client kinase Cdk4 (Vaughan et al., 2006). Thus, the question was addressed whether this residue is directly involved in the interaction of Hsp90 with the GR-LBD.

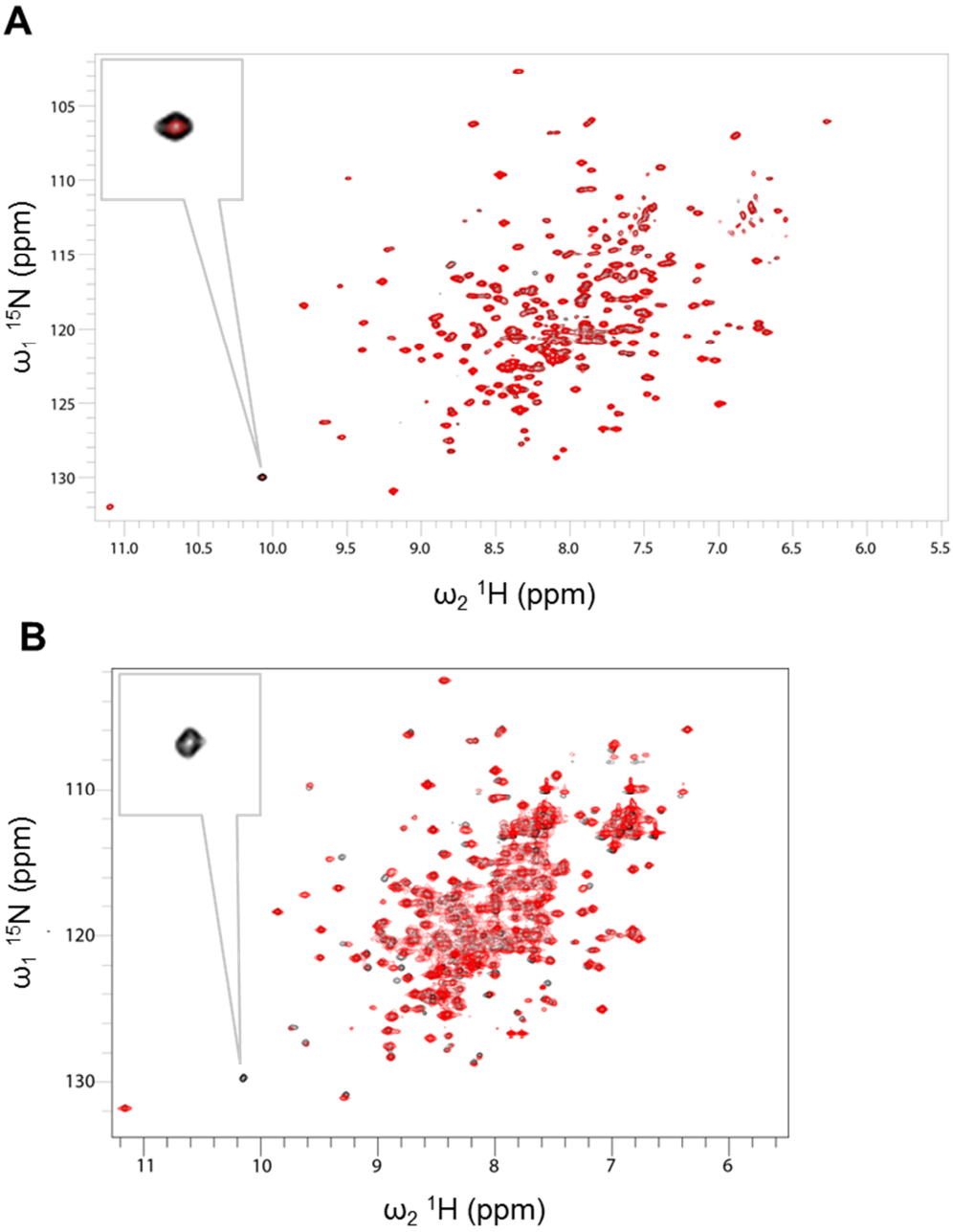


**Figure 12: NMR analysis of W300; A)** $^{1}H$, $^{15}N$ HSQC experiments for 200 µM Hsp90-MD in the presence of 250 µM GR-LDB spin labeled oxidized (black) or reduced (red); the blow-up shows the downfield shifted Trp signal of interest at greater magnification. **B)** $^{1}H$, $^{15}N$ HSQC experiments for 200 µM Hsp90-MD (black) and 200 µM Hsp90 W300A-M domain (red); the blow-up shows the downfield shifted Trp signal of interest at greater magnification. The loss of the signal in the Hsp90 W300A-M domain indicates that the Trp signal affected by the IPSL label was indeed W300. Experiments were performed in cooperation with Lee Freiburger (Technische Universität München).

**Table 4: Residues affected by the spin label**

| **Remaining signal intensity [%]** | **< 40 (strong)** | **< 60 (medium)** | **< 80 (weak)** |
|---|---|---|---|
| **Residues** | F332 | L331, L376 | F349, K449, L513 |

First, paramagnetic relaxation enhancement (PRE)-experiments using PROXYL-labeled GR-LBD and $^{15}$N-Hsp90 MD were performed to map the GR-LBD binding-site on Hsp90 in more detail and to see whether the region around W300 is significantly affected by binding of the GR-LBD. Several residues experienced PREs with a maximum of 80% signal reduction (Table 4) especially around position 330 which lies close to W300. Interestingly, also a typically downfield shifted tryptophan signal was significantly affected by the spin label (Figure 12 A). Unfortunately, tryptophan residues have not been assigned for the Hsp90-M domain. To clarify which tryptophan was affected by the binding of GR-LBD, $^{15}$N-HSQCs of wt Hsp90-M domain and Hsp90 W300A-M domain were recorded and compared (Figure 12 B). The peaks were similarly distributed in both spectra. As expected, some peaks were shifted due to the mutation of W300. The most dramatic effect of the mutation was apparently on the tryptophan signal which was significantly reduced during the PRE-experiment. As seen in Figure 12 B and in the blow-up, the signal completely disappeared from the spectrum. The loss of the tryptophan signal from the Hsp90 W300A-M domain spectra allowed to unambiguously assigning W300.

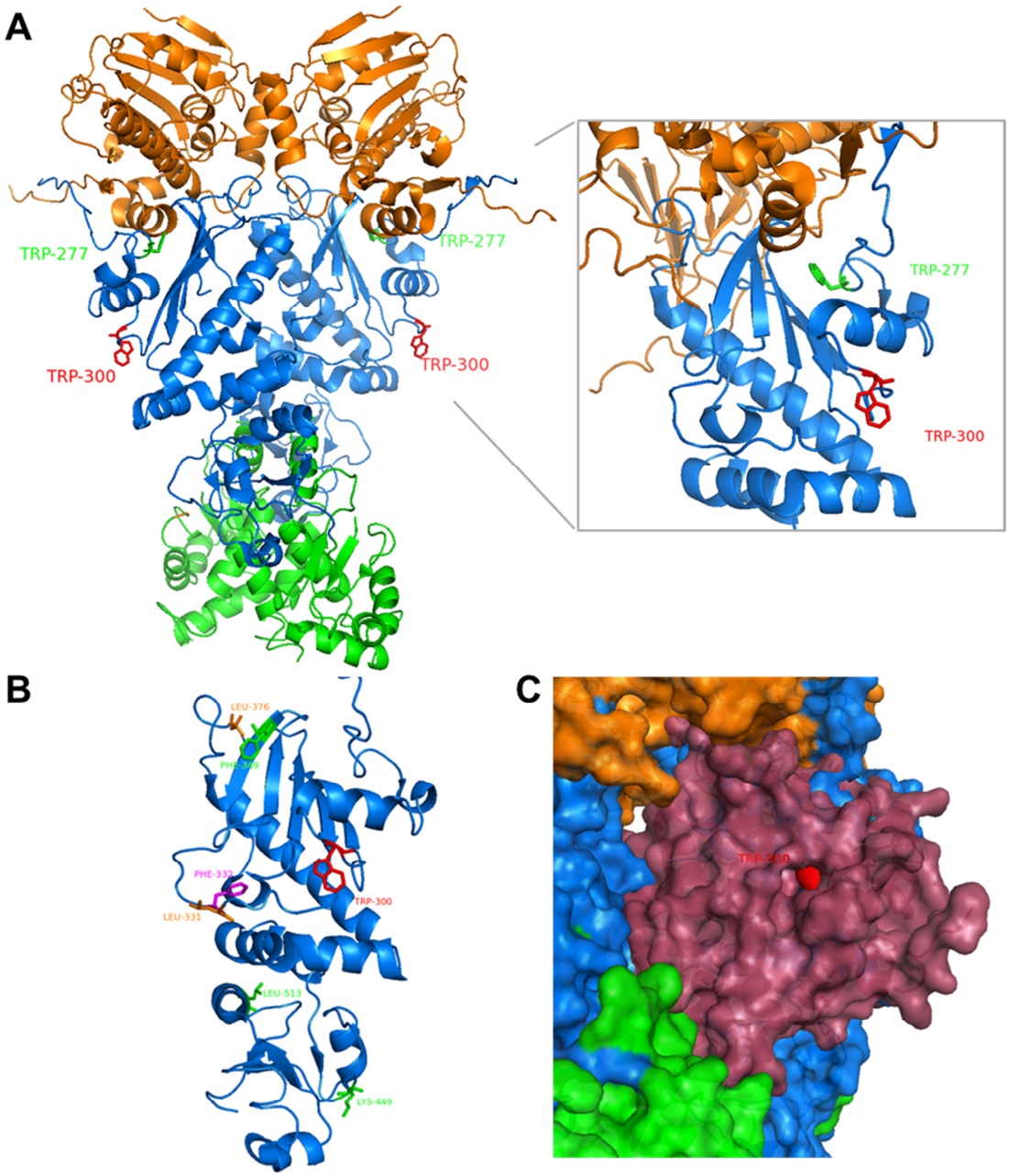


**Figure 13: Positioning of PRE-affected residues within the Hsp90 structure; A)** Crystal structure of yeast Hsp90 (PDB ID: 2CG9); Hsp90-N (1-258) is colored in orange, Hsp90-M (259-527) in blue, Hsp90-C (528-709) in green, W300 in red and W277 in green (see label); **B)** Mapping of PRE-affected residues within the Hsp90-MD; W300 is colored in red, residues showing a strong decrease in signal intensity in magenta (F332), moderately affected residues in orange (L331, L367) and weakly affected in green (F349, K449, L513); **C)** Surface representation of Hsp90 (PDB ID: 2CG9) and GR-LBD (PDB ID: 1M2Z); W300 is colored in red, Hsp90-N domain in orange, Hsp90-M in blue and GR-LBD in dark red; Docking was performed in cooperation with Tobias Madl (Technische Universität München).

These results clearly indicate that W300 plays an important role in the interaction of the GR-LBD and Hsp90 *in vitro*. Whether this is due to directly contributing to the binding or by an indirect effect is not clear. W300 is strongly affected by the spin-label, arguing for not being completely buried within the binding site. This is in line with the crystal structure of yeast Hsp90 where W300 shows an extraordinary surface exposition for Tryptophans in a mostly charged loop structure (Figure 13 A). The spin-label samples the binding surface on Hsp90 and is not able to contact residues that lie deep within the binding surface. When mapping the PRE-affected residues on the Hsp90-MD crystal structure this becomes even more obvious (Figure 13 B). Residues losing signal intensity in the presence of the spin-label are distributed all over the Hsp90-MD and are not clustered, indicating that these residues surround the actual binding patch. This indicates that W300 lies probably very close to the binding site, a view which is also supported by the positioning in a structural GR-Hsp90 model (Figure 13 C). This would support the idea that W300 positions the two Hsp90 protomers in order to form a high affinity conformation for GR.

### 4.1.2 An aromatic residue at position 300 is essential for yeast viability and effective GR-maturation

The previous results implied that W300 plays an important role in the GR-Hsp90 interplay *in vitro.* Earlier publications showed that mutation of W300 significantly affected viability and client maturation *in vivo* (Hawle et al., 2006; Meyer et al., 2003). As these studies were restricted to the alanine substitution, we were also interested in how charges at position 300 affect Hsp90 function *in vivo.* Therefore, in addition to the alanine substitution, W300 was exchanged to glutamate and lysine. Further, phenylalanine and tyrosine substitutions were made to test whether other aromatic side chains are able to rescue the mutation of W300. Additionally, the second tryptophan in the Hsp90-MD W277 was exchanged to alanine. This mutant should serve as a control that the effects observed are due to mutation of W300. Hsp90 mutants were produced, cloned into the p413-GPD vector and transformed into the yeast strain ΔPCLDα to perform shuffling experiments to replace wt Hsp90 by the respective mutants (3.9.1).

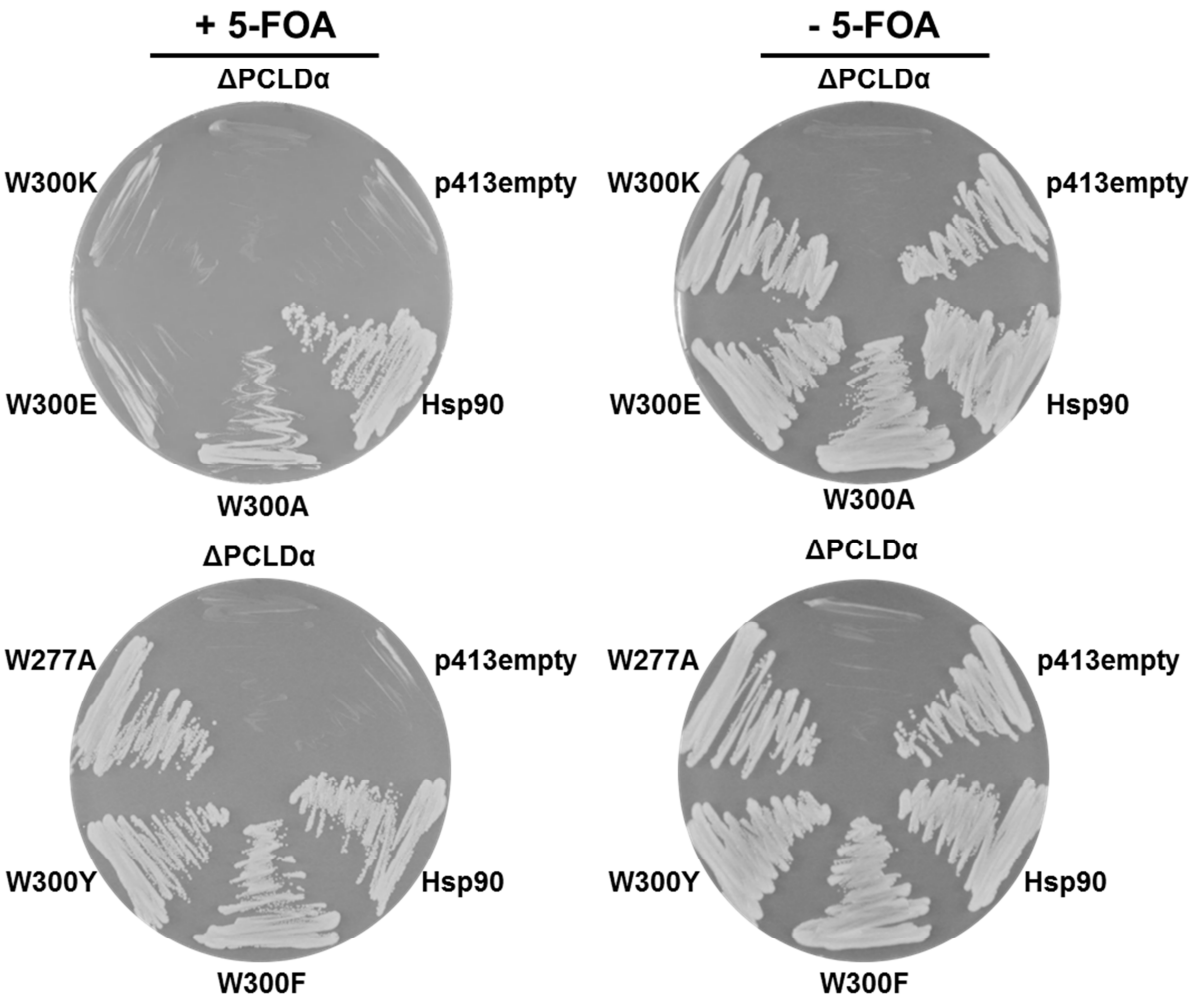


**Figure 14: Viability of yeast containing Hsp90 mutants as the sole source of Hsp90.** Yeast were plated on respective selective media +/- 5`FOA as indicated. The shuffling strain ΔPCLDα and ΔPCLDα transformed with the empty p413-GPD vector were plated as negative controls. ΔPCLDα transformed with p413-GPD containing wt Hsp90 served as positive control. Mutations in Hsp90 are as indicated.

In line with previous work, yeast containing Hsp90 W300A as the sole source of Hsp90 showed a severe growth defect at 30°C (Figure 14) (Hawle et al., 2006; Meyer et al., 2003). The colony size was significantly decreased in comparison to cells expressing wt Hsp90 and cell growth was dramatically decreased (data not shown). When W300 was substituted by charged amino acids (glutamate or lysine) the phenotype became even stronger. Yeast expressing these mutants were not viable, as no growth was detectable after several days (Figure 14). In contrast to these results, the consequences of mutating the second tryptophan within the Hsp90-MD, W277, to alanine was significantly different. Surprisingly, W277A did not show any growth defect and was fully viable

(Figure 14). W300 is strikingly solvent exposed in contrast to W277 which is buried within the structure (Figure 13 A). This is unexpected as one would suspect that perturbations in the hydrophobic core of a folded domain would interfere with the structure and function. Instead, it is the substitution of a hydrophobic tryptophan for a charged hydrophilic residue in a surface-exposed unstructured loop that abrogates the essential function of Hsp90, underlining the importance of W300. To address the importance of an aromatic residue at position 300, W300F and Y mutants of Hsp90 were generated. Indeed, those mutants were able to rescue viability in yeast implying that the general functionality of Hsp90 is dependent on the aromatic residue at this switch point position.

To gain further insights into the functionality of these Hsp90 mutants, their ability to maturate GR *in vivo* was assessed for the viable mutants (W300A/F/Y and W277A) using a previously established ß-galactosidase reporter assay (Nathan and Lindquist, 1995). The assay was performed as described in 3.9.2. Further, western blot analysis of Hsp90 expression levels was conducted (3.4.2, 3.4.5).

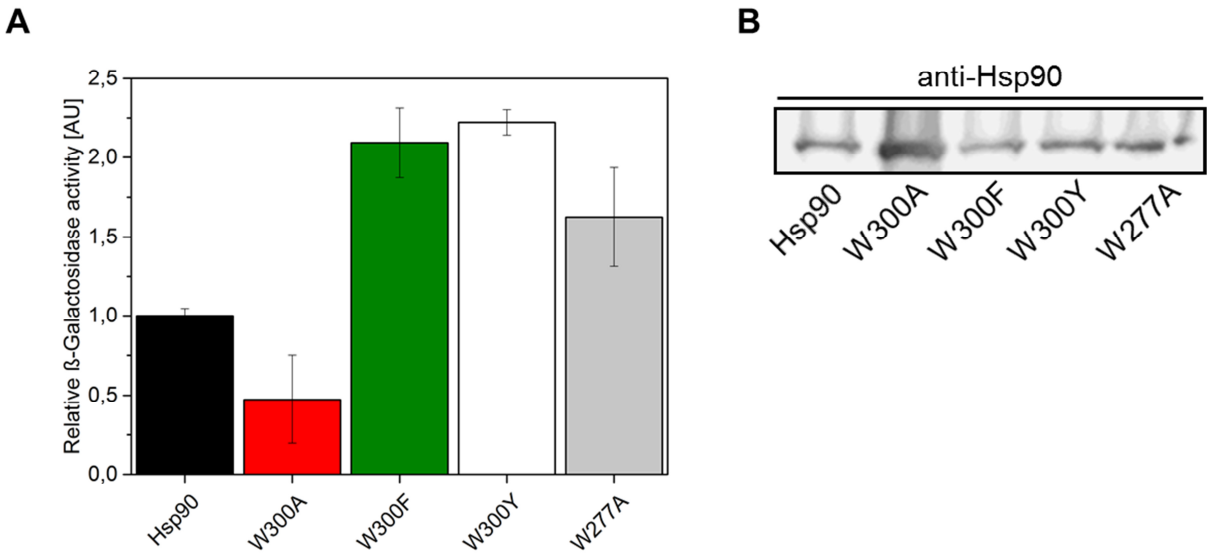


**Figure 15: GR-maturation by Hsp90 mutants *in vivo*. A)** ß-galactosidase reporter assay in yeast; Plotted are relative ß-galactosidase activities for the respective Hsp90 mutants. Activities were normalized to ß-galactosidase activity in the presence of wt Hsp90. Black bars indicate standard deviations from 3 independent measurements. **B)** Western blot analysis of Hsp90 expression levels. Western blot analysis was performed using an anti-yeast Hsp90 primary and an anti-rabbit HRP-conjugate secondary antibody.

As expected, the mutations differentially affected GR-maturation *in vivo*. The aromatic substitutions, W300F and Y, and the control substitution W277A, were sufficient to establish a fully functional GR triggering ß-galactosidase expression (Figure 15 A). In these assays, there was a two fold increase in ß-galactosidase activity in comparison to wt Hsp90, indicating that these mutants are slightly more efficient in GR-maturation. In contrast to these activating mutations, exchange of W300 to alanine led to a decrease in ß-galactosidase activity of roughly 50% in comparison to wt Hsp90 indicating reduced GR maturation (Figure 15). This result fits to previously published data, were the W300A mutation decreased the GR-dependent ß-galactosidase activity to 60 % in comparison to wt Hsp90 (Hawle et al., 2006). The reduced maturation is consistent with the W300A mutant showing a severe growth phenotype (Figure 14 A) implicating that this mutation leads to an impaired Hsp90 system that is not able to mature GR efficiently and also affects other clients like v-Src (Hawle et al., 2006). This is in line with earlier speculations about W300 being involved in the Hsp90-client interplay (Meyer et al., 2003). Western blot analysis of the Hsp90/Hsp90 mutant expression revealed a striking difference when co-expressed with GR that was induced with 10 µM DOC (Figure 15 B). None of the mutants showed significant degradation ruling out the possibility that the effects seen in the viability assay and the ß-galactosidase reporter assay were due to reduced protein levels. In contrast, there was a significant increase in the protein level of the W300A mutant in comparison to wt Hsp90 or the functional mutants W300F/Y and W277A which showed similar protein levels (Figure 15 B).
In summary, the *in vivo* analysis of Hsp90 W300, extended to charged residues and aromatic substitutions, fits the idea that W300 is an important switch point in the GR-Hsp90 interplay. Mutation of W300 to alanine leads to a severe growth defect in yeast and decreased GR-maturation. Mutation to a charged amino acid (glutamate, lysine) further impairs Hsp90 function leading to inviability. Introduction of other aromatic residues (phenylalanine, tyrosine) at position 300 and exchange of the second tryptophan in the Hsp90-M domain to alanine (W277A) leads to mutants restoring viability and capable of producing fully active GR. Interestingly those mutants exhibited an unexpected two fold increase in ß-galactosidase activity. An explanation might be that the release of the receptor from the translationally inhibitory GR-Hsp90 complex is faster. Therefore, GR is more readily in a DNA-binding competent state and able to trigger translation of target genes. This would fit to the notion that GR-chaperone complexes effectively prevent GR binding to DNA (Catelli et al., 1985; Smith and Toft, 2008).Western blot analysis of the Hsp90 expression levels showed that by increasing the Hsp90 W300A protein levels, the cell tries to

bypass the reduced chaperone power of the mutant. Whether the increase in protein is due to increased expression or a decrease in protein turn-over is so far not clear. The former is certainly more unlikely as gene expression is controlled by the GPD-promotor which should trigger expression at a constitutive high level. In the future, these results should be further verified by comparing the expression levels to a house-keeping protein like PGK to exclude generally increased protein expression in this mutant strain or inhibition of the protein turn-over by proteasomal inhibitors.

Altogether, the *in vivo* analysis implicates that an aromatic residue at position 300 is not only important for a specific client but also essential for a fully functional Hsp90 system in general. In the future, analysis of the alterations in the *in vivo* function of Hsp90 due to the mutation of W300 should be expanded to other client proteins. It would be of interest whether the accumulation of v-Src in the W300A mutant show by Hawle et al. (Hawle et al., 2006), can be reproduced and whether the other mutants, especially W300E and K, exhibit differential effects on the v-Src maturation. These results could support the idea that the switch point W300 is not GR-specific but important for clients in general.

### 4.1.3 Mutation of W300 leads to consequences in Hsp90 and the GR-chaperone interplay

#### 4.1.3.1 Hsp90 W300 mutants show altered ATPase activity and are differentially influenced by the GR-LBD

The *in vivo* analysis of the Hsp90 mutants gave important insight into the importance of an aromatic amino acid at position 300. To further investigate the role of this switch point and the functional consequences of mutations at this position *in vitro*, we purified Hsp90 W300 mutants as described in 3.4.3.2. To confirm structural integrity and stability of the Hsp90 W300 mutants a thermal stability assay (TSA) was performed (3.5.2.4).

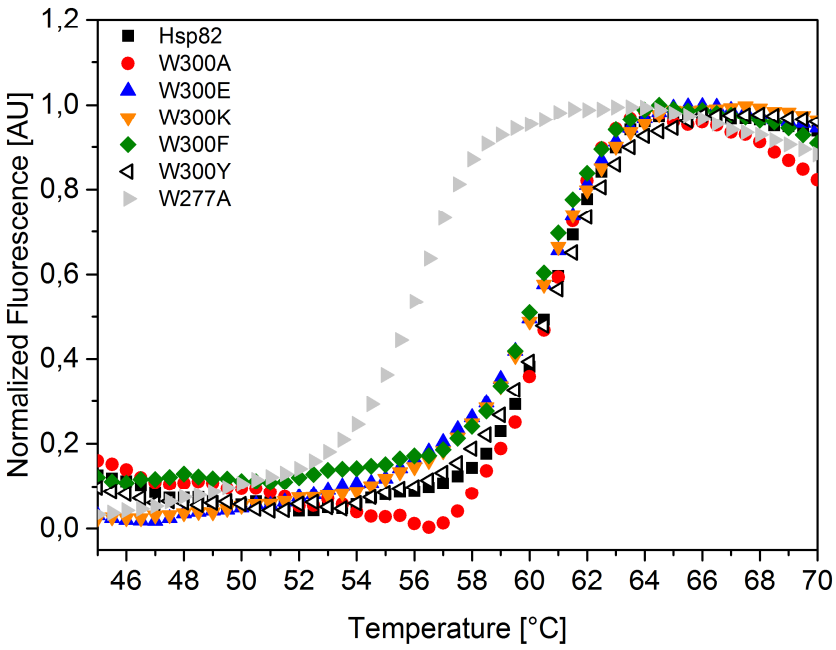


**Figure 16: Thermal stability of Hsp90 W300 mutants;** TSA assay performed with different Hsp90 W300/W277 mutants. Melting curve for wt Hsp90 is shown in black, for W300A in red, for W300E in blue, for W300K in orange, for W300F in green, for W300Y in black bordered triangles and for W277A in grey. Color code will be maintained for the mutants throughout the work. For melting temperatures see **Table 5**.

**Table 5: Melting temperatures ($T_M$) of Hsp90 mutants;** Melting temperatures were calculated using the Boltzmann fit function in Origin 9.1G.

| **Hsp90** | **wt** | **W300A** | **W300E** | **W300K** | **W300F** | **W300Y** | **W277A** |
|---|---|---|---|---|---|---|---|
| **$T_M$ [°C]** | 60.7 | 60.6 | 60.4 | 60.4 | 60.4 | 60.7 | 56.0 |

All mutants showed thermal stabilities in the TSA assay comparable to the wt protein as deduced form the virtually identical melting temperatures (Table 5). Further, the melting curves were highly comparable in terms of cooperativity indicating structural integrity and no global unfolding events due to the mutations (Figure 16). The W277A mutant was an exception to this. The mutant showed a significant reduction in the melting temperature of > 4°C indicating a significantly weaker thermal stability. These results are in line with the idea that mutation of W277 in the hydrophobic core affects the structure of the Hsp90-M domain. Still, the thermal

stability was sufficient and cooperativity of unfolding was comparable to wt Hsp90 and the other mutants implying that the mutant could be analyzed *in vitro.*

Next, ATPase activity measurements were conducted in the presence and absence of the GR-LBD (3.9.3). These experiments were planned to provide information about the influence of the mutation on Hsp90 functionality and to further examine how W300 influences the interplay between the chaperone and its client.

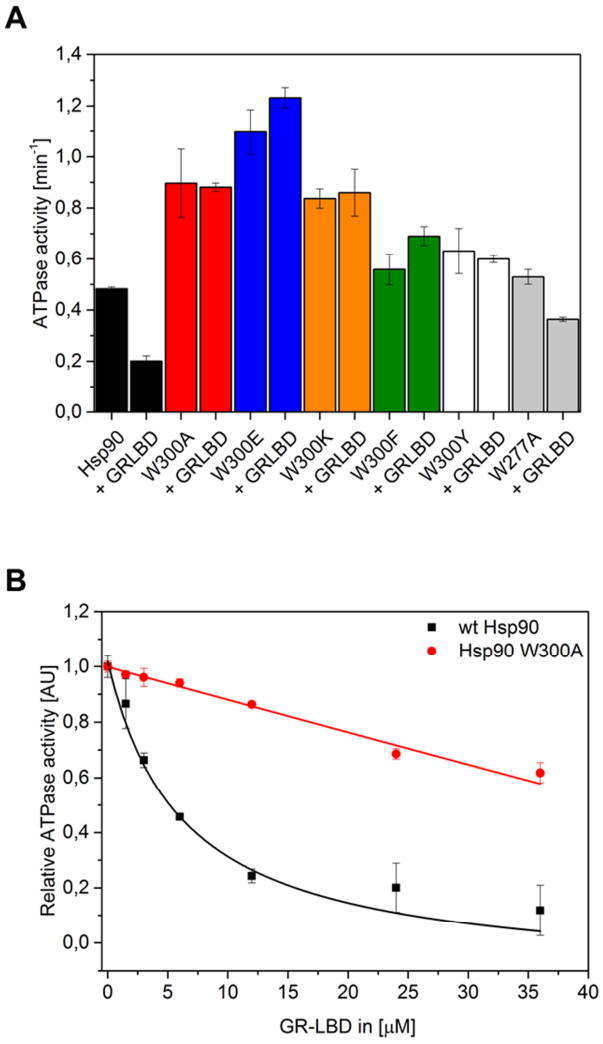


**Figure 17: ATPase activity of Hsp90 mutants in the presence and absence of GR-LBD; A)** Absolute ATPase activities of different Hsp90 mutants in the absence and presence of 6 µM GR-LBD. Color coding as mentioned in Figure 16; **B)** ATPase activity of wt Hsp90 in black and W300A in red in the presence of increasing amounts of GR-LBD; Relative ATPase activities were plotted against the GR-LBD concentration. Black and red bars indicate standard deviations from three independent measurements.

As expected, the GR-LBD decreased the ATPase activity of wt Hsp90 from 0.5 $min^{-1}$ to 0.2 $min^{-1}$, a reduction of roughly 60 %. It was shown that the GR-LBD preferentially interacts with ATP-bound Hsp90 and decelerates ATP-hydrolysis (Lorenz et al., 2014). The Hsp90 W300A/E/K mutants showed increased ATPase activity in the absence of the GR-LBD with a two-fold higher activity (Figure 17 A). The two-fold increase in activity is in line with published data for W300A (Meyer et al., 2003). W300F/Y and W277A displayed wt-like activity. Surprisingly, for none of the mutants, except W277A, an inhibitory effect of GR-LBD was observed (Figure 17 A). The ATPase activities stayed also unaffected by the presence of higher GR-LBD concentrations. As shown in Figure 17 B, the ATPase activity of wt Hsp90 was nearly completely inhibited by GR-LBD concentrations higher than 12 µM, whereas at 36 µM GR-LBD, the Hsp90 W300A ATPase activity was only reduced by about 25 %.

Two scenarios could explain the differential behavior of the W300 mutants. It is possible that W300 is directly involved in the interaction of the GR-LBD and Hsp90. This would lead to a decreased binding affinity. The GR-LBD would no longer be bound and could not inhibit Hsp90´s ATPase activity. But this is unlikely for several reasons. A simple matter of affinity could be overcome by increasing GR-LBD concentrations but even very high concentrations (> 30 µM) could not induce wt-like inhibition (Figure 17 B). Furthermore as a variety of residues is involved in GR-binding (Lorenz et al., 2014), a single point mutation may not be sufficient to lead to a severe decrease in affinity. This view is further opposed by the fact that W277A was inhibited by GR-LBD. W277 might not be directly involved in binding due to its location in the hydrophobic core but it is also positioned within the proposed GR binding patch and further leads to structural alterations in the Hsp90-MD as deduced from the thermal stability data (Figure 16), so it is more likely that this mutation would lead to a more severe decrease in affinity which was not the case. Additionally, one would suspect that an involvement in direct interaction would be differentially influenced by exchanging a large aromatic amino acid to smaller or charged residues which is also not the case as the A, E and K mutations behave identical. The more likely scenario is that W300 functions as a switch point in Hsp90 that triggers a certain conformation in the conformational cycle of the Hsp90 dimer that is on the one hand effective in GR-LBD binding and on the other hand susceptible for the inhibitory effect by GR-LBD.

Surprisingly, the aromatic substitutions which were able to rescue yeast viability and GR-maturation *in vivo,* could not rescue the inhibitory effect. This indicates that the effect is not based on a hydrophobic interaction between Hsp90 and the GR-LBD. An explanation would be

that neither the phenylalanine nor the tyrosine substituents are capable of forming the GR-specific conformation indicating that maybe a π-cation interaction is required for induction of this special conformation which is not established by W300F/Y. This interpretation is supported by the statistical analysis of π-cation interactions in structural biology, indicating that 26 % of all tryptophans are involved in such interactions (Gallivan and Dougherty, 1999). As the aromatic substitutions W300F and Y were nevertheless able to mature GR *in vivo,* the question arises of how important this GR-specific conformation really is. Throughout the last decades a picture of the GR-chaperone interplay has emerged that abandoned the idea of chaperones being solely involved in the maturation of GR but spotlights the interplay as a further dimension of GR regulation (Echeverria and Picard, 2010; Kirschke et al., 2014). In line with the interpretation of the GR *in vivo* data (4.1.2), GR is released faster from the W300F/Y mutant as GR-LBD is not able to establish its inhibitory effect on Hsp90. ATP is hydrolyzed at a normal rate which in turn leads to the release of the GR-LBD from Hsp90 (Lorenz et al., 2014). Thereby, the interaction of client and chaperone is not prolonged like in the presence of W300 which is thought to be important in the regulation of nuclear translocation of the receptor (Chen et al., 1998; Galigniana et al., 1998). Interestingly, previous studies indicated also a role of W300 in kinase binding and substitution of W300 to alanine led to significant v-Src accumulation altered v-Src maturation (Hawle et al., 2006; Vaughan et al., 2006). Thus, the specific conformation formed with the help of W300 might not solely play an essential role in establishing the regulatory effect of Hsp90 on GR. It seems possible that this special conformation is also necessary for the interplay with other clients like kinases or even clients in general. Due to the intrinsic instability of many Hsp90 clients, such information is rare. Thus, experiments using other SHR-LBDs or stabilized kinase domains (solubilized B-Raf kinase domain, Tsai et al. (2008)) might help to clarify this issue in the future.

#### 4.1.3.2 Alterations in the conformational cycle of Hsp90 W300 mutants

The ATPase activity measurements of the W300 mutants gave already insights into the functional consequences of mutating an important switch point position. To gain further information on the conformational cycle of the Hsp90 W300 mutants, we used an established FRET-system in which donor- and acceptor-labeled Hsp90 dimers allow following the closing and opening of the dimer as well as influences of co-chaperones and clients (Hessling et al., 2009; Lorenz et al., 2014).For

this, Hsp90 and Hsp90 W300 mutants were differentially labeled at an engineered cysteine residue in the Hsp90-N domain (D61C) using the FRET-donor ATTO488 and the acceptor ATTO550. Labeling was performed as described in 3.4.6. First, the formation of the FRET-heterodimer was monitored by mixing equimolar amounts of donor- and acceptor-labeled Hsp90 (Figure 18 A). As the velocity of this reaction is dependent on the closing state of the dimer, closed Hsp90 species will take longer to form a heterodimer than open dimers.

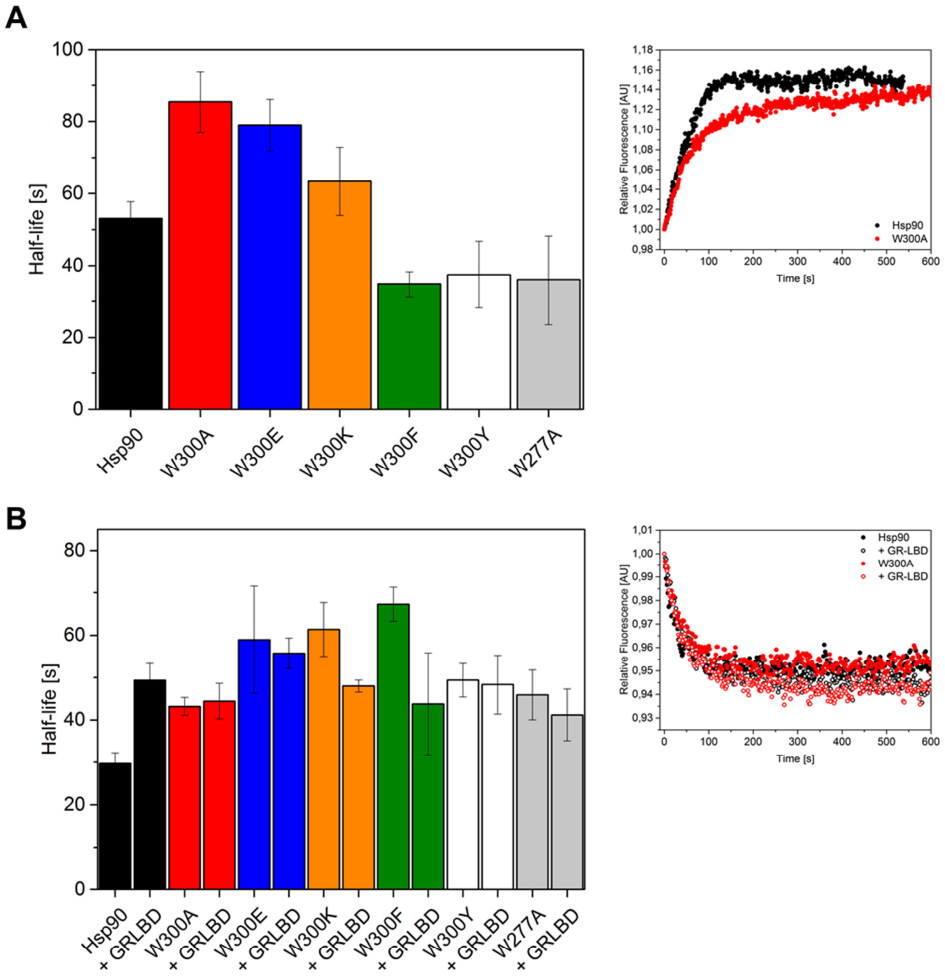


**Figure 18: Formation and stability of the open Hsp90 conformation; A)** Formation of the FRET heterodimer; Formation of the FRET heterodimer was monitored by mixing 200 nM ATTO488 donor-labeled Hsp90/Hsp90 mutant with 200 nM ATTO550 acceptor-labeled Hsp90/Hsp90 mutant. Reaction half-lives were derived from the original traces and plotted. Exemplary kinetics are shown for wt Hsp90 (black) and Hsp90 W300A (red). Black bars indicate standard deviations of three independent measurements. **B)** Chase experiments with the open Hsp90 dimer in the absence and presence of 6 µM GR-LBD. Chase experiments were started by the addition of 4 µM wt Hsp90. Reaction half-lives were derived from the original traces and plotted. Exemplary kinetics are shown for wt Hsp90

(black) and Hsp90 W300A (red) in the absence and presence of the GR-LBD (open circles). Black bars indicate standard deviations of three independent measurements.

The wt protein showed a half-life of 53 s for the formation of the FRET-heterodimer. The W300A/E mutants displayed longer half-lives for the reaction whereas those of W300K were similar to wt. The W300F/Y and W277A mutants exhibited shorter half-lives in comparison to wt Hsp90. To test the influence of the GR-LBD on the open conformation of Hsp90, chase experiments in the presence of the open Hsp90 conformation were performed (Figure 18 B). The preformed Hsp90 (mutant) FRET-heterodimer was preincubated with or without the GR-LBD in the absence of nucleotide. An excess of unlabeled Hsp90 was added to the FRET complex to induce subunit exchange in the dimer. The half-life of the subunit exchange is again dependent on the closing status of the complex. The GR-LBD could increase the half-life of the subunit exchange for wt Hsp90 from 30 s to 50 s (Figure 18B). This is consistent with the notion that the GR-LBD induces a semi-closed Hsp90 conformation and might link the two protomers also in an open conformation (Lorenz et al., 2014). The W300 mutants showed extended half-lives for the exchange in the absence of the GR-LBD, but for none of the mutants a clear difference in the half-life of the reaction could be observed in the presence of the GR-LBD (Figure 18 B).

The results suggest that the W300 mutants might display different conformation in comparison to the wt Hsp90. The increase in the half-lives of the heterodimer formation for W300A/E in the absence of the GR-LBD suggests a more closed conformation. In contrast, the decreased half-lives for W300F/Y and W277A indicate slightly more open conformations. Interestingly, the mutants remained unaffected by the presence of the GR-LBD. These results are in line with the ATPase activity data. The GR-LBD is only able to induce a semi-closed conformation in which the ATPase activity is inhibited when W300 is present. This effect requires the aromatic system of tryptophan as neither phenylalanine nor tyrosine could substitute. Surprisingly, the subunit exchange of the open Hsp90 conformation did not change in the W277A mutant in the presence of GR-LBD. In the previous experiments this mutant showed wt-like behavior. It can be speculated that changes in the Hsp90-M domain or in the inter-protomer crosstalk might lead to alterations in the kinetics of the mutant.

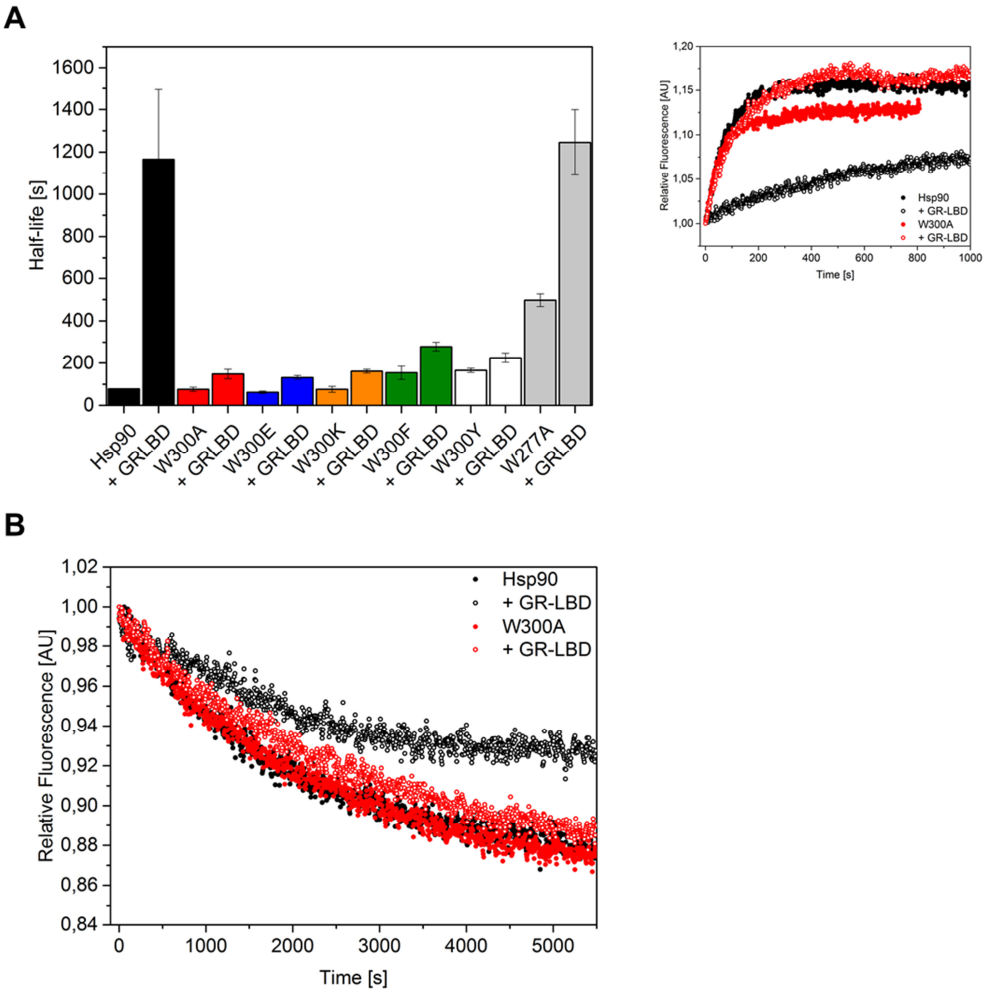


**Figure 19: Formation and stability of the closed Hsp90 conformation; A)** Closing reaction of the FRET heterodimer; Closing of the wt/mutant Hsp90 dimer was monitored after addition of 2 mM ATPγS in presence and absence of 6 µM GR-LBD. Reaction half-lives were derived from the original traces and plotted. Exemplary kinetics are shown for wt Hsp90 (black) and Hsp90 W300A (red) in the absence and presence of the GR-LBD (open circles). Black bars indicate standard deviations of three independent measurements. **B)** Chase experiments with the closed wt/W300A Hsp90 dimer in the absence and presence of 6 µM GR-LBD. Chase experiments were started by the addition of 4 µM wt Hsp90.

Next, closing kinetics in the presence of ATPγS were monitored. The closing reaction of the wt protein had a half-life of roughly 80 s. The closing kinetics were not affected by the A/E/K substitutions in the absence of the GR-LBD (Figure 19 A) indicating that the general nucleotide-induced closing reaction is not affected by the mutations. W300F/Y showed slightly and W277A moderately increased half-lives for the closing reaction supporting the idea of more opened conformations probably due to structural changes within the Hsp90-M domain structure or

alterations in the dimer crosstalk. The closing kinetics of wt Hsp90 in the presence of the GR-LBD were dramatically decelerated (Figure 19 A). A 12-fold increase in the half-life could be detected in line with previous findings (Lorenz et al., 2014). Surprisingly, all W300 mutants showed strikingly different behavior. The closing reaction was marginally affected by addition of the GR-LBD in comparison to the wt protein. The reaction half-lives exhibited a maximum two-fold increase in the presence of the GR-LBD (Figure 19 A). For example, the W300A mutant showed an increase in the half-life of the closing reaction from 75 s to 150 s when the GR-LBD was present. Only W277A showed a substantially increased half-life for the closing reaction although the relative increase was not as strong as for wt Hsp90, due to the generally slower closing kinetics of the mutant.

In a further FRET-experiment, the influence of the GR-LBD and the W300 mutations on the ATPγS-bound, closed Hsp90 dimer was investigated (Figure 19 B). By adding unlabeled Hsp90 to the closed dimer, subunit exchange was initiated. The half-life of this reaction is, similar to the open chase, a measure how stable the complexes are with open states exchanging more rapidly than closed ones. The signal amplitudes in these experiments are a good measure of how strong the reopening is. The larger the decrease in the acceptor signal, the more FRET signal is lost implying stronger reopening of the dimer. In the absence of the GR-LBD, wt Hsp90 and Hsp90 W300A showed comparable reopening as both traces displayed similar signal amplitudes (black and red circles, Figure 19 B). In the presence of the GR-LBD, the dissociation of the wt Hsp90 FRET complex is partly inhibited as deduced by a smaller decrease in the acceptor signal (black open circles, Figure 19 B). This is indicative of the presence of a stabilized, partially closed state which cannot be dissolved by the excess of unlabeled Hsp90. The W300A mutant in contrast was not sensitive to GR-LBD in the reopening. The signal amplitude of the reaction remained virtually unchanged in comparison to the measurement in the absence of GR-LBD (red open circles, Figure 19 B). Similar results were acquired for the other mutants (data not shown), except W277A, showing that the mutants are not able to form a stabilized, semi-closed conformation.

The FRET results are in good accordance with the ATPase activity data. The W300 mutants were only marginally affected in their closing kinetics which is in line with the lack of inhibition in the ATPase assay. As previously mentioned, it seems that W300 is essential to prime a GR-competent Hsp90 conformation that on the one hand efficiently binds GR and is also susceptible to GRs influence on the ATPase and conformational cycle. The absence of the aromatic indole system of tryptophan at this switch point position leads to an Hsp90 with an altered

conformational cycle that is not able to form a GR-competent conformation in which the client is able to establish its inhibitory effects on the chaperone cycle. Further, the GR-LBD is not able to prolong the chaperone-client interaction in the W300 mutants as indicated by the missing stabilization of the Hsp90 dimer in the chase experiments in the presence of ATPγS. Together, this might lead to misregulation of GR signaling in the cell as GR is not able to efficiently prolong the chaperone interaction. One might speculate that this leads to dramatic alterations in the kinetics and nature of the glucocorticoid-dependent gene response.

#### 4.1.3.3 Homologous human Hsp90ß W312 mutants are incapable of efficiently restoring hormone-binding in the GR-LBD

The preceding results showed that mutation of the switch point position W300 in yeast Hsp90 leads to limited viability of yeast, decreased GR maturation *in vivo* and significantly reduced functional influence of the GR-LBD on the ATPase activity and the conformational cycle of Hsp90. Besides the functional influence of the client on its chaperone, Hsp90 massively affects the functionality of GR. The GR-LBD is not able to bind ligands when associated with Ydj1/Hsp70 but after transfer via Hop to Hsp90 and p23, ligand-binding is recovered (Kirschke et al., 2014). In this process, Hsp90 is essential as in the absence of the chaperone very little amounts of functional GR-LBD are recovered from the Ydj1 (Hsp40)/Hsp70 complex. Thus, the assay can provide important information on how mutation of W300 affects ligand-binding recovery and therefore the functionality of Hsp90. First, the ligand-binding recovery assay was tested with yeast Hsp90. All previous experiments were performed with yeast proteins due to the lack of a human FRET system and the intrinsically low ATPase activity of human Hsp90ß which makes it difficult to measure inhibitory effects. Unfortunately hormone binding could not be efficiently restored using yeast Hsp90 and a human co-/chaperone ensemble (human Hsp70, Hop, p23) (data not shown) probably due to differential cycle kinetics or interaction profiles of yeast and human systems. Therefore, homologous hHsp90ß W312 mutants were generated. To see whether the human mutants behaved comparable to the yeast mutants, the viability of yeast expressing the mutants as the sole source of Hsp90 was tested in a 5`FOA shuffling experiment (3.9.1).

.

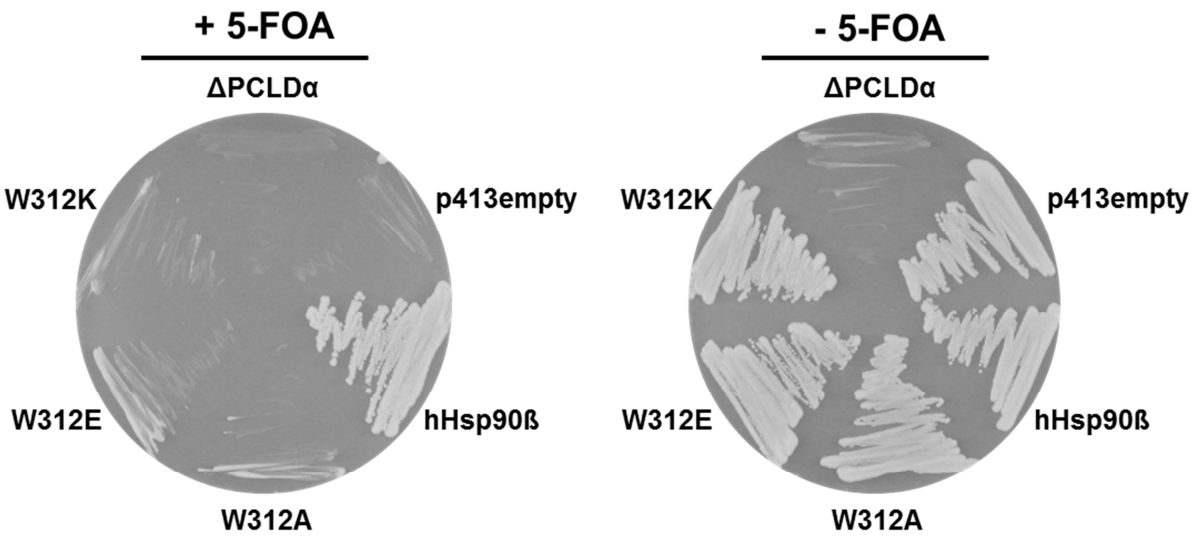


**Figure 20: Viability of yeast containing human Hsp90ß or W312 mutants as the sole source of Hsp90.** Yeast were plated on respective selective media +/- 5`FOA as indicated. The shuffling strain ΔPCLDα and ΔPCLDα transformed with the empty p413-GPD vector were plated as negative controls. ΔPCLDα transformed with p413-GPD containing wt human Hsp90ß served as positive control. Mutations in human Hsp90ß are as indicated.

The Hsp90ß W312 mutants could not rescue the absence of wt Hsp90 in the yeast, leading to the loss of viability (Figure 20). In contrast and as previously reported, wt human Hsp90ß conferred viability to *S. cerevisiae* (Wider et al., 2009).

These results fit to the viability data obtained for the yeast mutants as Hsp90 W300E/K lead to inviability and W300A showed a severe growth phenotype (Figure 14, 4.1.2).

Next, W312A/E/K mutants were purified to homogeneity (3.4.3.2) to assess thermal stability and basic functionality *in vitro* by TSA assay and ATPase activity measurements, respectively.

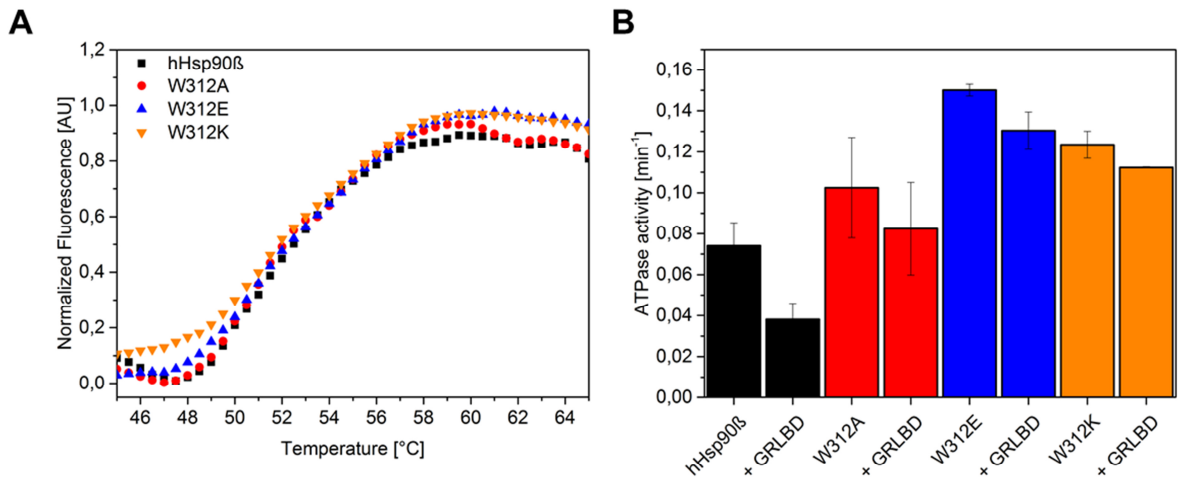


**Figure 21: Thermal stability and ATPase activity measurements of human Hsp90ß W312 mutants in the absence or the presence of the GR-LBD; A)** TSA assay of human Hsp90ß and human Hsp90ß W312 mutants. For the melting temperatures see **Table 6**. **B)** ATPase activity measurements of wt human Hsp90ß and W312 mutants in the absence and the presence of 12 µM GR-LBD; Hsp90ß is shown in black, W312A in red, W312E in blue and W312K in orange; Color coding will be maintained in the following figures.

**Table 6: Melting temperatures ($T_M$) of human Hsp90ß and human Hsp90ß W312 mutants;** Melting temperatures were calculated using the Boltzmann fit function in Origin 9.1G.

| **Human Hsp90ß** | **wt** | **W312A** | **W312E** | **W312K** |
|---|---|---|---|---|
| **$T_M$ [°C]** | 51.9 | 51.6 | 50.9 | 52.2 |

The results for the TSA assay and the ATPase activity measurements are shown in Figure 21. Melting temperatures ($T_M$) were comparable to wt Hsp90ß indicating no global changes in protein structure and stability (Table 6). As mentioned earlier, human Hsp90ß exhibited a low ATPase activity of 0.072 $min^{-1}$, in line with the literature (Figure 21) (Richter et al., 2008). Similar to the homologous yeast mutants, W312 mutants showed moderately increased ATPase activities and could not be inhibited by the presence of an excess of the GR-LBD, in contrast to the wt protein as its ATPase activity was decreased to roughly 50 % by the GR-LBD. In the experiments presented, the human mutants behaved comparable to the yeast homologues indicating that the effects seen in the yeast system are conserved in the human system. In a next step, fluorescence anisotropy based hormone-binding recovery assays were performed using the human Hsp90ß W312 mutants (3.5.2.1).

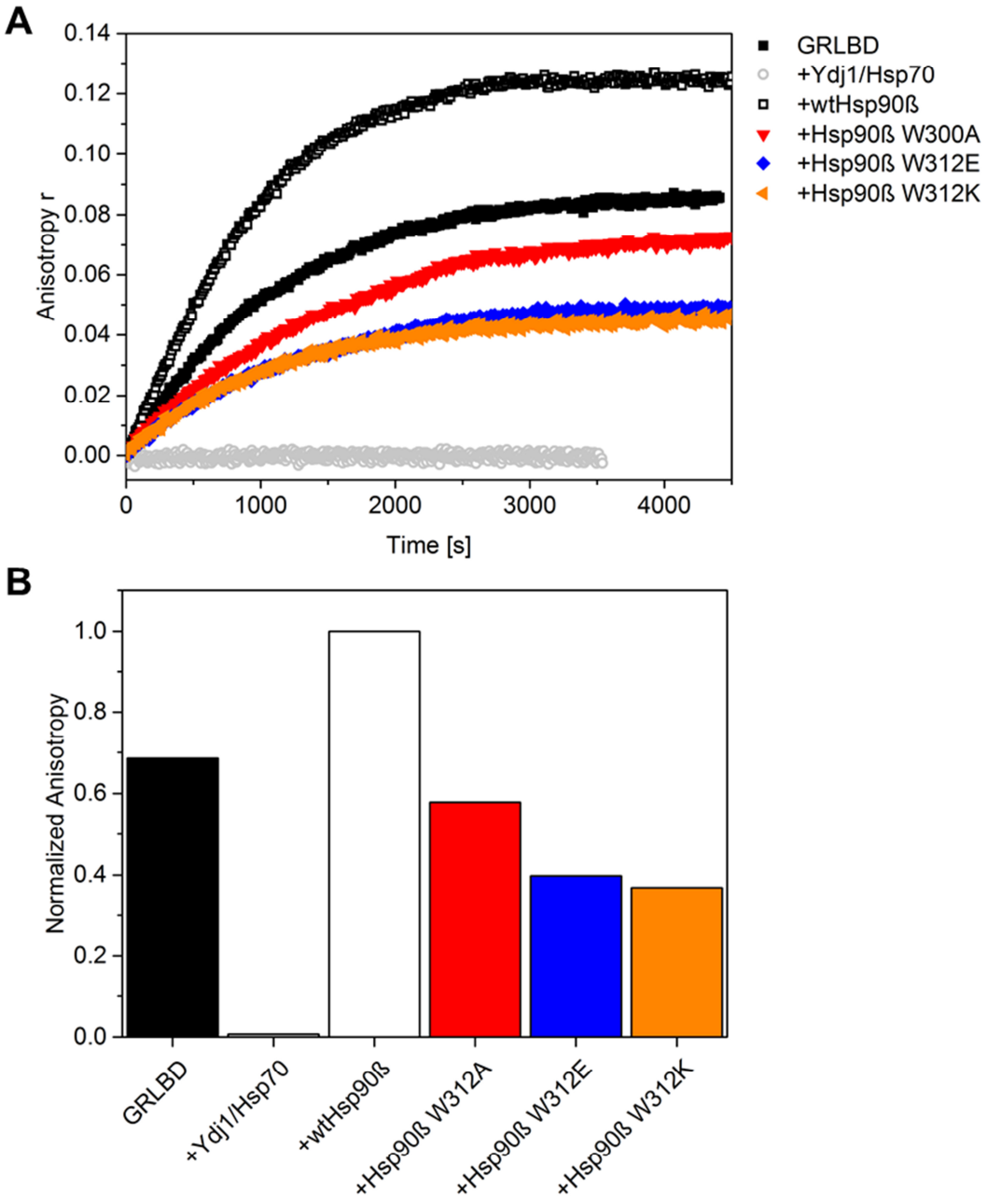


**Figure 22: Fluorescence anisotropy hormone-binding recovery measurements with human Hsp90ß W312 mutants; A)** Binding kinetics of 50 nM F-Dex and 1 µM GR-LBD in the absence of chaperones in black squares, in the presence of 2 µM Ydj1, 15 µM Hsp70 and 2 mM ATP in grey, in the presence of the full chaperone system (2 µM Ydj1, 15 µM Hsp70, 15 µM Hop, 15 µM p23, 2 mM ATP) and 15 µM wt human Hsp90ß in black open circles, in the presence of the full chaperone system and 15 µM human Hsp90ß W312A in red triangles, 15 µM human Hsp90ß W312E in blue triangles and 15 µM human Hsp90ß W312K in orange squares. Traces were fitted by a single exponential decay equation in Origin 9.1G; **B)** Normalized fluorescence anisotropy equilibrium values; Plotted are end values of the binding kinetics in **A,** normalized to the value in the presence of the full chaperone system and wt human Hsp90ß.

In line with previous studies, the GR-LBD was able to bind fluorescently labeled Dexamethasone (F-Dex) without the help of chaperones (black open squares, Figure 22 A) underlining the importance of chaperones as an additional dimension of regulation (Lorenz et al., 2014). The presence of Hsp40, Hsp70 and ATP completely abolishes ligand-binding (grey open circles, Figure 22 A) by opening of the hormone-binding cleft (Kirschke et al., 2014). Addition of Hop, p23 and wt hHsp90ß restores and also optimizes ligand-binding as more hormone is faster bound ($t_{1/2\ GR\ alone}$ = 18.4 min vs. $t_{1/2\ fullchap}$ = 14.5 min) in the presence of the full chaperone system compared to the absence of chaperones. Values appear to be in the time-scale as published for the GR-LBD F602S-Mannose binding protein fusion (Kirschke et al., 2014). Interestingly, the Hsp90ß W312 mutants could not recover ligand-binding to the same extent as wt Hsp90 (Figure 22 B). Ligand binding reached only 60 % for W312A and less than 40% in the case of W312E and K, thus, less than in the absence of any chaperones (~65 %). Additionally, hormone-binding kinetics were significantly slowed down. In the presence of the full wt chaperone system, the half-life of F-Dex binding was 14.5 min whereas in the presence of Hsp90ß W312A the half-life was increased by nearly a factor of two (24.9 min).

The hormone-binding recovery data fits very well to the previously shown data for the Hsp90 W300 mutants. Hormone-binding recovery was reduced by the W312 mutants to a similar extent as the GR-dependent ß-galactosidase response *in vivo* when only the Hsp90 W300A mutant was present. It is questionable whether both assays are fully comparable when using homologous chaperone systems *in vivo* and *in vitro,* but still a similar tendency could be observed. Further, the assay proved that the switch point position W300/312 is not only important for GR to establish its inhibitory effects on Hsp90 but also of importance for the chaperoning of GR by Hsp90. Without the important tryptophan Hsp90 is not able to efficiently restore full hormone-binding of the GR-LBD *in vitro.* As speculated earlier, this is most probably due to the incapability of the W300 mutants to present a high-affinity GR-competent conformation.

### 4.1.4 Substitution of W300 leads to impaired GR-LBD binding in a nucleotide-dependent manner

The previous paragraphs suggested from different point of views that the switch position W300 plays an important role in triggering a conformation competent for GR-LBD binding and essential for the inhibitory effect of the GR-LBD on the cycle dynamics. As the hormone-binding recovery data implicated, the tryptophan switch point is further needed to re-establish full hormone binding of GR transferred from the Hsp40/70 system implicating also a role in client chaperoning. To rule out that these effects were simply due to a direct involvement of W300 in binding, GR-LBD binding to wt Hsp90 and W300 mutants was assayed by fluorescence-coupled analytical ultracentrifugation using ATTO488 labeled GR-LBD.

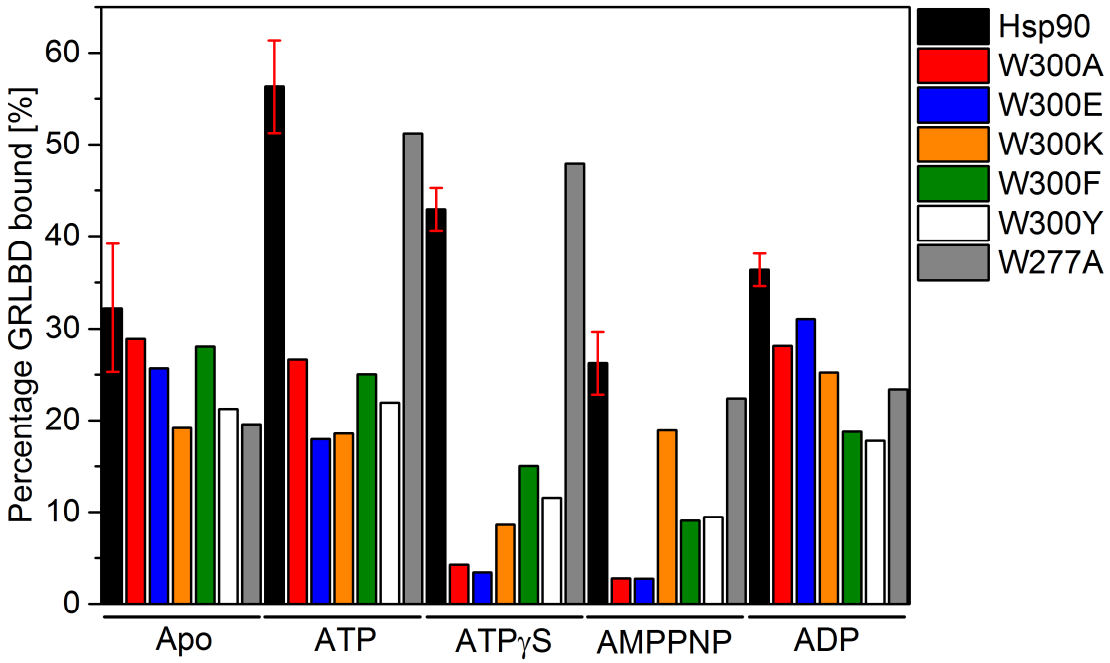


**Figure 23: AUC-analysis of GR-LBD binding to Hsp90 W300 mutants in different nucleotide states;** Bars indicate amount of labeled GR-LBD found in the Hsp90/mutant complex in the presence of 3 µM Hsp90 and indicated nucleotides at 2 mM. Color code for the different mutants is as previously used. Measurements with wt Hsp90 were performed in triplicates to rule out experimental fluctuations. Red error bars indicate standard deviations from three independent measurements. Data analysis was performed using SedFit 14.1 and Origin 9.1G.

In the absence of nucleotide (apo-state), only slight changes were found in the bound GR-LBD fraction. At a concentration of 3 µM, roughly 33 % of the labeled GR-LBD was found to be associated with Hsp90, comparable to previously published results (Figure 23) (Lorenz et al., 2014). The Hsp90 mutants W300A/E and F showed similar amounts of the GR-LBD bound within the range of deviation. W300K/Y and W277A associated with slightly decreased amounts of the GR-LBD. As none of the mutants displayed a severe GR-LBD binding defect in the open apo Hsp90-conformation it can be excluded that the effects observed for the W300 mutants in the other assays are simply due to a direct involvement of W300 in the interaction. As ATP significantly increases the affinity of Hsp90 for the GR-LBD by inducing a semi-closed conformation (Lorenz et al., 2014), the W300 mutants were investigated in this respect. As expected for wt Hsp90 ATP resulted in a strong decrease in the bound GR-LBD fraction (Figure 23). Except for Hsp90 W277A, which showed a wt-like increase in the affinity, the W300 mutants did not increase the affinity but instead the fraction of the bound GR-LBD remained on the apo state level. The lack in response to nucleotide became even more pronounced, especially for W300A and E, in the presence of ATPγS as well as the non-hydrolysable analogue 5'–adenylyl-ß,γ-imido-diphosphate (AMP-PNP). It is known that these nucleotides induce fully closed conformations in Hsp90 (Hessling et al., 2009; Lorenz et al., 2014). Here we found only 5 % or less GR-LBD bound to the Hsp90 W300 A and E mutants. The other mutants (W300K/F/Y) exhibited decreased affinities in the presence of ATPγS and AMP-PNP although not as strong as A and E. In comparison, 45 % of the labeled GR-LBD was bound by wt Hsp90 in the presence of ATPγS. Again, only W277A showed wt-like nucleotide-dependency. As the presence of ADP leads to an open conformation in Hsp90 resulting in a decrease in the affinity for GR, ATP hydrolysis has been implicated to be essential for GR release from Hsp90 (Lorenz et al., 2014). The decrease in affinity was seen again for wt Hsp90 as the amount of the bound GR-LBD was reduced to 36 % (Figure 23). The mutants W300F and Y showed the strongest reduction in GR binding in the presence of ADP in comparison to the wt protein with only 18 % of the GR-LBD associated. The other mutants exhibited only mild changes in the GR binding affinity displaying wt-like complex formation (Figure 23).

As the hormone-binding recovery experiments were performed using human Hsp90ß W312 mutants, the binding of GR-LBD was further assayed to wt human Hsp90ß and the W312E mutant. The binding experiments were again conducted in the presence of different nucleotides to ensure that the effects seen for the yeast system were conserved.

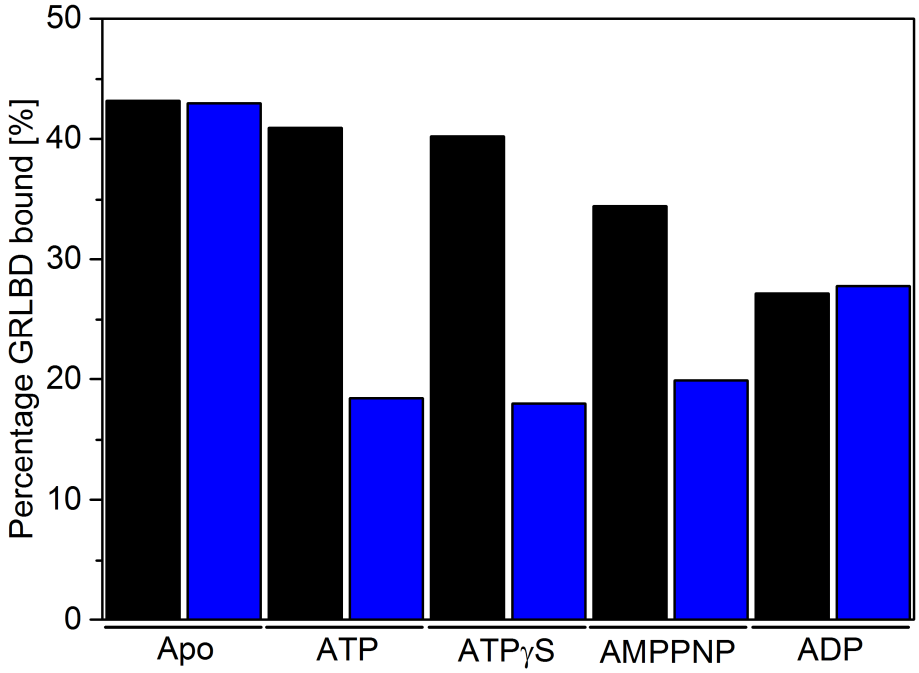


**Figure 24: AUC-analysis of GR-LBD binding to the human Hsp90 W312E mutant in different nucleotide states;** Bars indicate amount of labeled GR-LBD found in the Hsp90/mutant complex in the presence of 3 µM Hsp90 and indicated nucleotides at 2 mM. Black bars indicate bound GR-LBD fraction in the presence of human Hsp90ß and blue bars in the presence of the human Hsp90ß W312E mutant. Data analysis was performed using SedFit 14.1 and Origin 9.1G.

In the absence of any nucleotide, wt Hsp90ß and W312E bound equal amounts of GR-LBD similar to the yeast system (Figure 24). The presence of ATP, ATPyS and AMP-PNP did not significantly change the Hsp90-associated GR-LBD fraction for the wt protein but again led to a decrease in binding of 50 % in the case of W312E (Figure 24). Comparable to the results with the yeast proteins, ADP reduced the affinity of both wt Hsp90ß and W312E similarly by about 20 % (Figure 24).

The results of the binding experiments demonstrate that the effects seen in ATPase, FRET and hormone-binding recovery are not due to a missing direct interaction with W300. Instead they point to the importance of W300 in inducing a GR-LBD binding competent conformation in Hsp90. Substitutions of this important switch point seem to lead to certain Hsp90 conformations during the Hsp90 cycle that are decreased in their affinity for the GR-LBD, are not susceptible for the effects of the client on its ATPase cycle and further are not capable of effectively chaperoning the GR. These conformations are presumably more closed than the wt protein as the

effects are enhanced in presence of ATPγS and AMP-PNP. This interpretation is further supported by the binding of the GR-LBD to wt human Hsp90ß and W312E. Association was not as nucleotide-dependent as seen for the yeast system. This is in line with the literature as addition of ATPγS did not significantly change the global shape of the conformational ensemble of human Hsp90 in SAXS experiments implying that the structural changes in the human system are not as strong as for yeast Hsp90 (Karagöz et al., 2014). Nevertheless, addition of ATP or ATP-analogues led to a significant decrease in affinity of the W312E mutant implying that the speculative closed conformation is also of importance in the human system. The idea is especially illustrated by comparing the ATPase results and the GR-LBD binding data in the presence of ATP. Although there was a significant decrease in the GR-LBD binding in the presence of ATP in comparison to wt yeast and human Hsp90, still some GR-LBD remained associated with Hsp90. One would suspect that the bound GR-LBD is still inhibiting Hsp90 but the ATPase results draw a different picture. As seen in Figure 17 and Figure 21, the W300/312 mutants were completely unaffected in their ATPase activity underlining the importance of the tryptophan in establishing the influence of GR on Hsp90.

It is necessary to mention that wt-like GR-Hsp90 interplay could not be rescued by other aromatic residues at position 300. In terms of the influence on Hsp90 and GR-binding, the W300F and Y mutations behaved similarly to the other tested mutants. This implies that the aromatic system of tryptophan is essential to establish the effects and that other functionalities like small uncharged, charged or even other aromatic residues cannot substitute at this position. As mentioned earlier, this suggests that a π-cation interaction might be important within Hsp90 monomer or the dimer in forming a GR-competent conformation. In the future, it would be of interest to determine if this conformation is GR-specific or if it is also used by other client proteins and is therefore a general feature of Hsp90. The published results concerning v-Src maturation by W300A speak in favor of an involvement of W300 also for kinase clients (Hawle et al., 2006). Further, in a recent EM structure of the Hsp90-Cdc37-Cdk4, W300 lies in close proximity to the kinase client which was bound in a closed conformation supporting the idea that W300 is also important in kinase chaperoning (Verba et al., 2016). Of note, the W300F and Y showed the strongest decrease in affinity in the presence of ADP which fits to the speculations made in the context of the GR maturation *in vivo* and ATPase activity. It is possible that GR is matured by these mutants but as the release is faster, due to the lack of ATPase inhibition, and

more efficient as more GR-LBD is released from Hsp90 in the presence of ADP, this might lead to misregulation in the Hsp90-dependent trafficking of GR.

### 4.1.5 Hsp90 W300 mutants show altered sensitivity to co-chaperones

In the previous paragraphs it was shown that mutation of W300 leads to alterations in the inhibitory effect of GR-LBD on Hsp90 and on the interaction of the client with its chaperone. As several co-chaperones are known to be important for establishing a hormone-binding competent conformation in GR (Pratt and Toft, 1997), it was investigated next whether these co-chaperones (Sti1, Sba1, Cpr6) were still able to establish their characteristic effects on the ATPase activity of Hsp90 W300 mutants. Further, as Aha1 and GR-LBD use overlapping binding sites on Hsp90, the stimulatory effect of Aha1 on the Hsp90 W300 mutants was also evaluated.

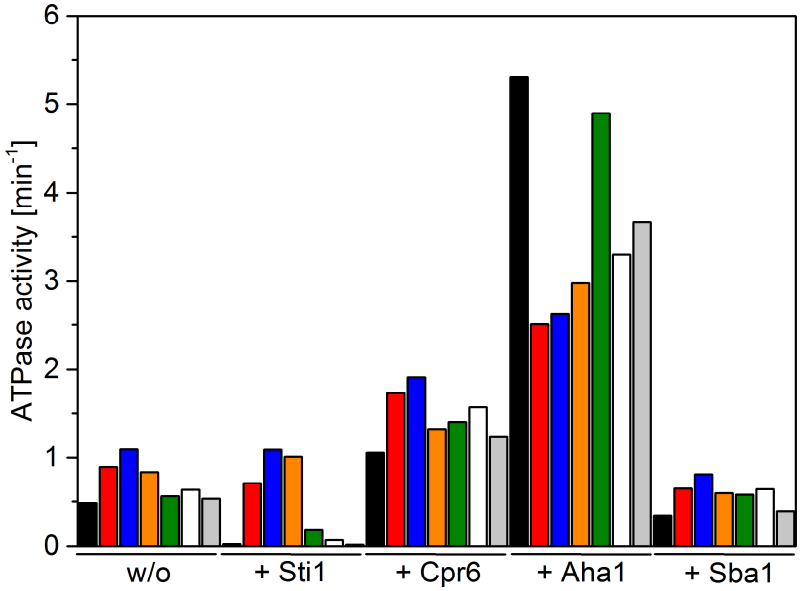


**Figure 25: Hsp90 W300 ATPase activities in the presence of different co-chaperones;** ATPase activities in the absence of co-chaperones (w/o), in the presence of 6 µM Sti1 (+ Sti1), 6 µM Cpr6 (+ Cpr6), 3 µM Aha1 and 9 µM Sba1. Color code as previously used.

The co-chaperone Sti1 is known to inhibit the ATPase activity of Hsp90 (Prodromou et al., 1999; Richter et al., 2003). An excess of Sti1virtually inhibited the ATPase activity of wt Hsp90,

W300F and Y and W277A whereas the W300A/E/K mutants were unaffected by the presence of the co-chaperone (Figure 25). The presence of Cpr6 in Hsp90 co-chaperone complexes leads to slight stimulation of the ATPase activity (Li et al., 2013; Prodromou et al., 1999). Indeed, Cpr6 stimulated wt Hsp90 and all tested mutants by a factor of two (Figure 25). Another known stimulator of the Hsp90 ATPase activity is Aha1 (Panaretou et al., 2002). In the ATPase assay, Aha1 was able to induce an 11-fold increase in the wt ATPase activity. W300F and Y, as well as W277A were slightly less efficiently stimulated (8-10-fold), whereas the W300A/E/K mutants were significantly less activated by a factor of three which is in line with previously published data for W300A (Figure 25) (Hawle et al., 2006). The co-chaperone p23/Sba1 is able to inhibit Hsp90`s ATPase activity (Panaretou et al., 2002; Richter et al., 2004). Indeed, p23/Sba1 could reduce the ATPase activity of wt Hsp90 and all mutants to 50 % in comparison to the activity in the absence of the co-chaperone (Figure 25).

The ATPase activity data showed that there were significant alterations in the modulation of Hsp90 by co-chaperones due to the mutations. Whereas the mutants similar to the wt (W300F/Y and W277A) reacted comparable to wt Hsp90, the W300A/E/K mutants showed not inhibition by Sti1 and weakened stimulation by Aha1. To find out whether this was due to altered interaction of the co-chaperones with the mutants, analytical ultracentrifugation (AUC) coupled to fluorescence detection using labeled co-chaperones was applied to study the binding behavior of the mutants.

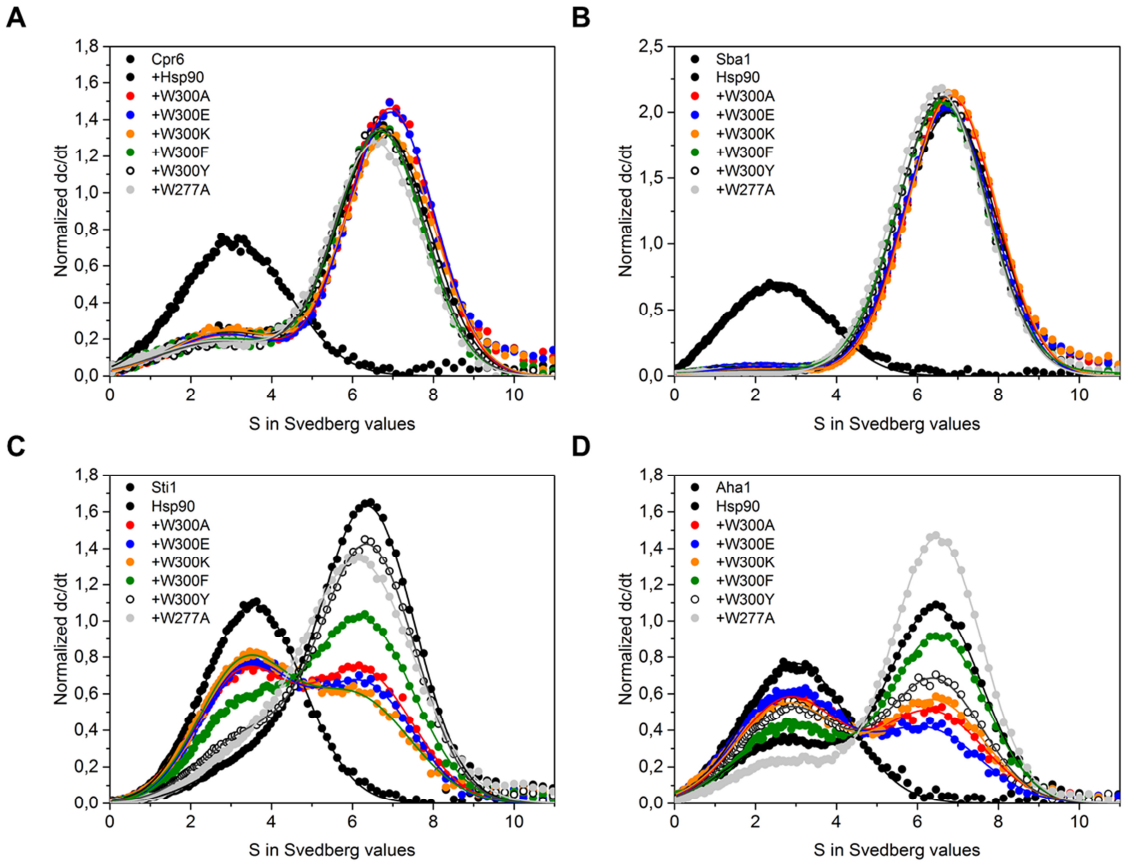


**Figure 26: Analysis of co-chaperone binding to the Hsp90 W300 mutants by AUC; A)** 1 µM ATTO488-labeled Cpr6 was incubated with 6 µM wt Hsp90 or mutant in the presence of 2 mM ATPγS. **B)** 400 nM FAM-labeled Sba1 was incubated with 6 µM wt Hsp90 or mutant in the presence of 2 mM ATPγS. **C)** 400 nM ATTO488-labeled Sti1was incubated with 6 µM wt Hsp90 or mutant in the presence of 2 mM ATPγS. **D)** 400 nM ATTO488-labeled Aha1 was incubated with 6 µM wt Hsp90 or mutant in the presence of 2 mM ATPγS. Mutant color code as used previously; Data analysis was performed using SedView 1.1 and Origin 9.1G.

Figure 26 A shows the results of the binding experiment for Cpr6. Cpr6 alone sedimented with a S-value of 3 S (black curve, Figure 26 A), whereas in complex with Hsp90 and in the presence of 2 mM ATPγS most of the labeled Cpr6 was bound in a complex with an S-value of 6.8 S (black curve, Figure 26 A). As depicted in Figure 26 A, Cpr6 formed a complex with all of the mutants as in each sample a peak at 6.8 S could be detected. The amplitude of the unbound species allows a rough estimation of the amount of free labeled species in solution and therefore can be used as an indication for changes in the affinity. Importantly, there was no change in the affinity for Cpr6 due to the mutations as the amount of unbound Cpr6 stayed constant for each mutant.

The results for p23/Sba1 draw a similar picture (Figure 26 B). Labeled p23/Sba1 sedimented with an S-value of 2.5 S, but when in complex with Hsp90 the S-value shifted to 6.8 S (black curves,

Figure 26 B). p23/Sba1 formed the same complex with all of the mutants and also the affinity was not altered due to the mutations as deduced from the amplitude of the free Sba1 species.
As expected, binding of Sti1 and Aha1 to the Hsp90 W300 mutants was affected. Unbound Sti1 sedimented with an S-value of 3.5 S, whereas the S-value shifted to 6.8 S (black curves, Figure 26 C) when bound to Hsp90. All of the mutants bound to Sti1 as shown by the presence of a species at 6.8 S but there were significant alterations in the affinities. The mutants W300Y, W277A bound Sti1 like wt, but there was a slight reduction in the proportion of bound Sti1 detectable for W300F. An even stronger decrease in affinity was found for the Hsp90 W300A/E/K mutants. Significantly less Sti1 was found in the Hsp90 complex as the amplitude of the free species at 3.5 S was clearly increased compared to wt Hsp90 (Figure 26 C). Labeled Aha1 alone sedimented with an S-value of 3 S and with 6.8 S when bound to Hsp90 (black curves, Figure 26 D). Again, all mutants formed a complex at 6.8 S similar to wt Hsp90 but with changes in the affinities. Hsp90 W300F and W277A bound similar amounts of Aha1 like wt Hsp90 whereas W300A/E/K and Y interacted with Aha1 less efficiently as an increase in the amplitude of the free species at 3 S was detected (Figure 26 D).
The results of the AUC-binding analysis fit to the data of the ATPase activities in the presence of the co-chaperones (Figure 25). Whereas all mutants bound Cpr6 and p23/Sba1 with similar affinities, the interaction with Sti1 and Aha1 was altered. Especially the W300A/E/K mutants that showed practically no ATPase inhibition by Sti1 interacted with lower affinity. Further, the same mutants were less efficiently stimulated by Aha1 and bound less Aha1 in the AUC experiment. The measured data is in excellent agreement with binding and ATPase activity data for W300A from the literature. It was found in several publications that binding of W300A to Aha1 and Sti1 was altered whereas the interaction with Sba1 and Cpr6 remained mostly unchanged. Also the stimulatory effect of Aha1 on Hsp90 W300A was identified to be slightly weaker (Hawle et al., 2006; Johnson et al., 2007).
The data presented concerning co-chaperone effects on the ATPase activity and co-chaperone binding to the Hsp90 W300 mutants expands the importance of the switch point position W300. Not only the interplay with one of Hsp90s most stringent clients, the GR, is altered by mutations at this position but also the cooperation with co-chaperones is disturbed. The reason for changes in the affinity and modulation are not clear, but as W300 lies close to the binding sites of Aha1 and Sti1 in the Hsp90-M domain, changes in the interaction site might play a role. This is probably not due to a direct effect of Sti1 and Aha1 interacting with W300 as both binding site do

not significantly overlap (Johnson et al., 2007; Meyer et al., 2004; Schmid et al., 2012). It is more likely that the mutations affect the Hsp90-M domain structure and the dimer conformation resulting in a lower affine binding surface. Sti1 is here of special importance as it connects the Hsp70 cycle to the Hsp90 cycle (Chen and Smith, 1998). Mutation of W300 leads to a decreased affinity for Sti1 and in turn to a reduced inhibition of Hsp90s ATPase activity. By changing these parameters, the transfer and reactivation of hormone-binding by GR to the Hsp90 system might be less efficient leading to less functional GR similar to the absence of Sti1(Morishima et al., 2000a). The hormone-binding recovery data is also in line with these findings as the W312A/E/K mutants decreased the rate of hormone re-binding by GR-LBD (Figure 22). Of note, the binding of yeast Hsp90 to Sti1 and human Hsp90ß to Hop has been found to be highly comparable enabling extrapolation of the observed effects in the yeast system to the human system (Rohl et al., 2015a). This suggests that the deficient chaperoning of these mutants is not solely based on the missing GR- or client-specific conformation but is further linked to the altered interaction with Sti1/Hop which plays an important role in the transfer of GR to Hsp90. Absence of Hop in the hormone-binding recovery assay and a Sti1 *S. cerevisiae* deletion strain showed significant reduction in hormone binding and GR response, respectively (Kirschke et al., 2014) (P. Sahasrabudhe, personal communication). Also other client proteins might be affected by the altered Sti1 and Aha1 interaction. For example, protein kinases depend on Sti1/Hop in the transfer from Hsp70 to Hsp90 and Aha1 is thought to be important for v-Src maturation under stress conditions (Caplan et al., 2007; Lotz et al., 2003). The data therefore strengthens the role of W300 as a crucial switch position. It seems that this position is not only important for inducing a GR-specific conformation in Hsp90 but also for co-chaperone binding and maintenance of their function and modulating effects.

### 4.1.6 Hsp90 W300 mutants present altered conformations to the client

To acquire structural information on the consequences of mutating W300 in Hsp90, SAXS measurements with W300A/E and K were performed in the absence of nucleotide and in the presence of ATP and ATPγS. Thereby, it was of special interest whether the mutation of W300 results in altered Hsp90 conformations that would lead to differential binding of the GR-LBD and thus a modulated influence of the client on its chaperone. Measurements, data analysis and figure

preparation were performed in collaboration with Tobias Madl (Technische Universität München)

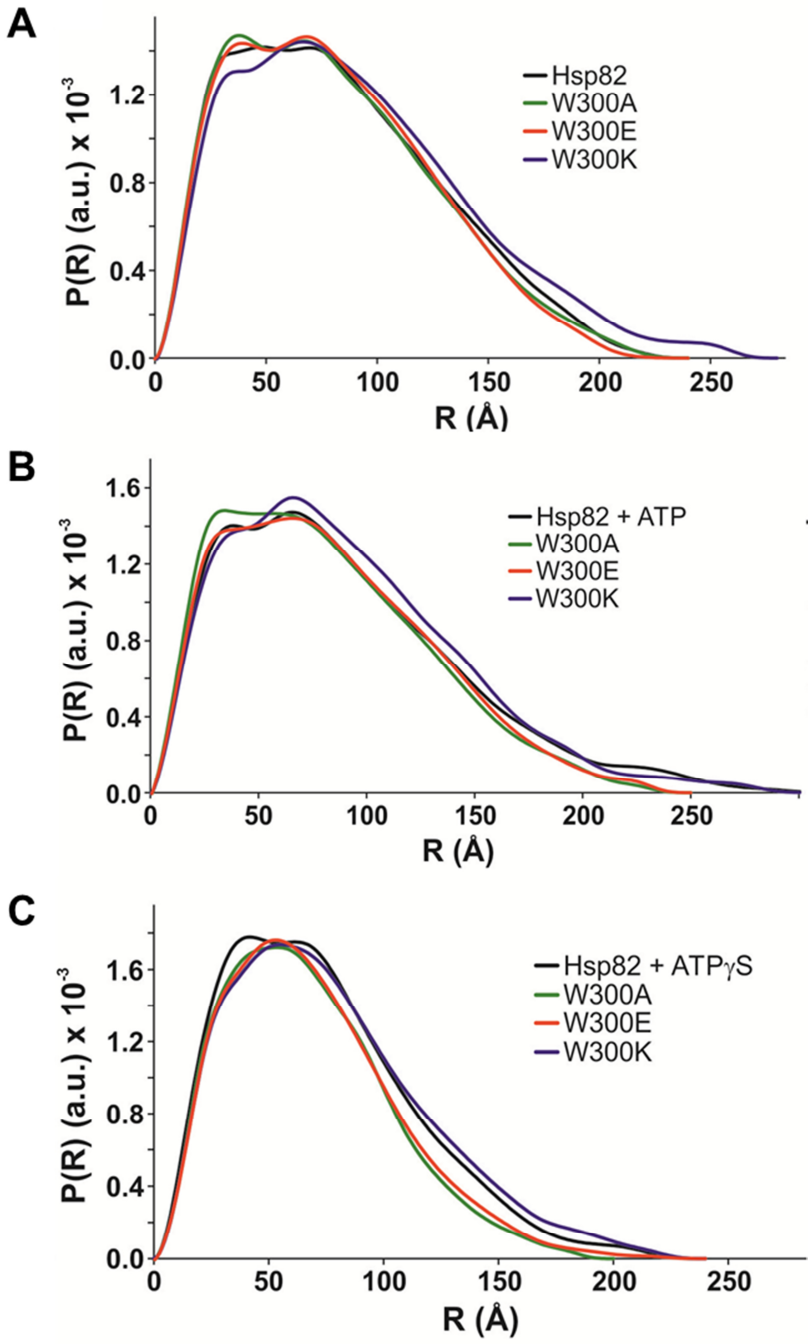


**Figure 27: Pair-distance distributions of Hsp90 and Hsp90 W300 mutants measured by SAXS in the absence and the presence of different nucleotides;** P (R) distributions of Hsp90 in black, Hsp90 W300A in green, Hsp90 W300E in red and Hsp90 W300K in blue, **A)** in the absence of nucleotide, **B)** in the presence of 2 mM ATP and **C)**

in the presence of 2 mM ATPγS; Measurements, data analysis and figure preparation were performed in cooperation with Tobias Madl (Technische Universität München).

The SAXS measurements revealed intriguing differences in the Hsp90 conformations due to the mutation of W300. In the absence of nucleotide, wt Hsp90, W300A and E exhibited similar conformations as deduced from the $R_g$ and $D_{max}$ of the proteins with the W300A and E mutants being slightly more compact. Surprisingly, W300K showed in the absence of nucleotide a more elongated conformation in comparison to the wt protein (Figure 27 A). Addition of ATP led to stronger compaction in the W300A and E mutants than in wt Hsp90 (~ 5 % more closed). Although both proteins showed increased compaction, the P (R) distributions were significantly different at shorter distances which might reflect slightly different conformations (Figure 27 B). W300K displayed a similar conformation like the wt protein in presence of ATP but with larger differences at shorter distances suggesting a conformation that differs from the wt protein (Figure 27 B). The measurements in the presence of ATPγS amplified the effects seen for ATP (Figure 27 C). Hsp90 W300A and E were significantly more closed than wt Hsp90 with the wt protein being 20-30 % in the closed conformation and W300A/E being 50 % in the closed conformation. Similar to the measurements in the presence of ATP, W300K was in a similar conformation like the wt Hsp90 with slight differences in the short distances of the P (R) distribution implying alterations in the conformation.

The SAXS data could provide important experimental evidence for the speculations made in the context of the previous experiments. Mutation of W300 to alanine and glutamate led to a significant increase in the compaction of the Hsp90 conformations. This increase was most prominent in the presence of ATPγS inducing ~ 20-30 % more compaction than in comparison to the wt protein. The SAXS measurements are in great accordance with the AUC binding data. The increase in the compaction for W300A and E seems to lead to an Hsp90 conformation that is not as competent in GR-LBD binding as the conformation formed by the wt protein (Figure 23). Further, these conformations are not susceptible to the inhibitory influence of the GR on the Hsp90 cycle dynamics as shown by ATPase and FRET measurements (Figure 17, Figure 18, Figure 19). Interestingly, already ~ 5 % more closing of W300 A and E in the presence of ATP seem to be sufficient to produce a significant alteration in the Hsp90-GR interplay as presence of ATP led to a significant reduction in GR-LBD binding and the effect on the ATPase activity of Hsp90 W300. Surprisingly, the Hsp90 W300K mutant did not exhibit increased compaction in comparison to the wt protein. In contrast, W300K seemed to be slightly more elongated than wt

Hsp90 and showed conformations that differed from the wt in the presence of nucleotides. Still, W300K showed, similar to W300A and E, reduced GR-LBD binding and inhibition of the conformational cycle. These results indicate that an increase in compaction does not exclusively alter the interaction of Hsp90 with its client. It seems that also more elongated or generally altered conformations are inefficient in binding of the GR-LBD and also less receptive to the influence of the GR-LBD on the cycle dynamics. One might speculate that the alterations in the Hsp90 conformations due to the mutation of W300 might lead also to changes in the interaction with Hsp90 co-chaperones and other client proteins. For example, as Sti1/Hop was shown to bind preferentially to an open Hsp90 conformation (Richter et al., 2003), the altered conformations result in decreased Sti1 binding and inhibition of the ATPase activity (Figure 25, Figure 26). Further, the recent EM complex of Hsp90, Cdc37 and the kinase Cdk4 showed Hsp90 in a very specialized conformation clamping around the partially unfolded kinase, stabilizing kinase N- and C-lobe via interactions with the Hsp90-M domain (Verba et al., 2016). It is tempting to suspect that alterations in the conformations by mutating W300 might result also in a differential interaction of Hsp90 with kinase clients. This idea is supported by data showing that the Hsp90 W300A mutant exhibited significantly different vSrc activation *in vivo* (Hawle et al., 2006). Altogether, the SAXS measurements refined the picture of how W300 is important for the Hsp90 client interplay. By driving GR or client-competent conformations in Hsp90, high affinity binding of the client to Hsp90 is promoted to a conformation that is, in the case of the GR-LBD, susceptible to the influence of the client on the Hsp90 chaperone cycle.

### 4.1.7 Atomistic molecular dynamics (MD) simulations of the Hsp90 W300 mutants

The SAXS data unambiguously proved that mutation of the switch point position W300 lead to Hsp90 mutants with an altered conformational cycle showing significantly stronger closing especially for W300A and E in the presence of ATP and ATPγS explaining the changes in the Hsp90-GR interplay. SAXS gives important information about global changes in the conformational ensemble of Hsp90 but to gain a more atomistic picture about the consequences of mutating W300, atomistic MD simulations of Hsp90 were conducted with *in silico* mutated W300A/E/K constructs. The calculations were performed in cooperation with Qi Luo and Ville R. I. Kaila (Technische Universität München) as described in 3.8.3.

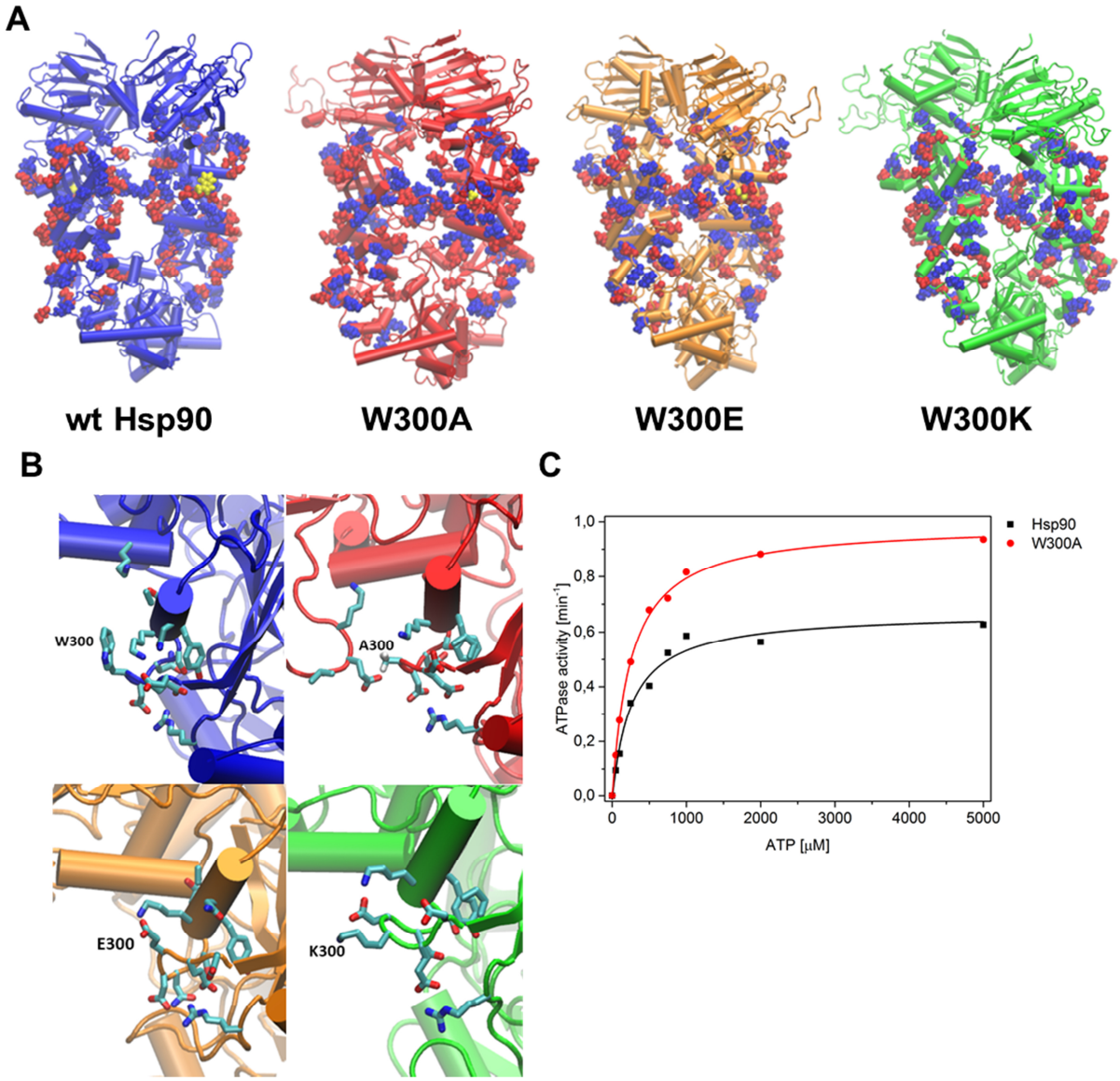


**Figure 28: Atomistic molecular dynamics simulations of the Hsp90 W300 mutants and ATP-affinity determination of the Hsp90 W300A mutant; A)** Cartoon representation of wt Hsp90 and W300 mutants with the charged residues of the Hsp90-M domian shown as VdW-representations in red for negative charges and blue for positive charges; From left to right: wt Hsp90 in blue, W300A in red, W300E in orange and W300K in green; **B)** Blow-ups of the mutation sites within one Hsp90 chain; Residues within 7 Å are shown in stick representations. Wt Hsp90 is shown in blue, W300A in red, W300E in orange and W300K in green; **C)** ATP-affinity determination of wtHsp90 and Hsp90 W300A by ATPase activity measurements. Fit of the wt Hsp90 data is shown in black and for Hsp90 W300A in red; Data was fitted according to Michaelis-Menten kinetics by Origin 9.1G; *in silico* dynamics simulations were performed in cooperation with Qi Luo and Ville R. I. Kaila (Technische Universität München).

During the 200 ns MD trajectories, all tested Hsp90 W300 mutants underwent significant conformational changes leading to more compact global structures in comparison to the wt protein (Figure 28 A). In line with the presented SAXS data, the calculated $R_g$ was found to be

significantly smaller in comparison to the wt protein (data not shown). The structural compaction was mainly driven by increased interactions between the two Hsp90 monomers. A closer look at the atomistic consequences of the mutations gave a possible explanation for this compaction. In the wt Hsp90, W300 formed a transient π-cation interaction with K294 that lies directly above the tryptophan. This transient interaction was found to be important to stabilize the structure of the Hsp90-M domain as mutations lead to an altered interaction pattern of the W300 loop and Hsp90-MD structure. In the presence of an alanine and especially glutamate (W300A/E), the negatively charged loop associated significantly stronger with the surrounding positive charges (Figure 28 C). Mutations to lysine (W300K) conversely led to a stronger repulsion between K300 and K294 (Figure 28 C). Remarkably, the observed effects propagated also to the Hsp90-N and –C domain (Figure 28 A). Changes in the latter increased the disorder in the dimerization interface of the four helix-bundle compared to the wt protein. The mutation-induced conformational changes in the Hsp90-N domain seemed to favor N-terminal dimerization. As increased N-terminal dimerization has been shown to increase the affinity for ATP and ATP hydrolysis (Pullen and Bolon, 2011), Poisson-Boltzmann (PB) continuum electrostatic calculations were performed (data not shown). The electrostatic solvation-free energies implicated that ATP binds much stronger to all W300 mutants. Unfortunately, the experimental data could only partly support the theoretical calculations (Figure 17, Figure 28 C). As shown earlier, the Hsp90 W300 mutants indeed exhibited increased ATPase activities but no significant change in the $K_M$ for ATP could be observed between wt Hsp90 and Hsp90 W300A ($K_M$ (wt Hsp90) = 255.5 μM vs. $K_M$ (W300A) = 247. μM).

Altogether, the MD simulations are in line with the experimental data and interpretations. The overall conformational compaction of the W300A and E mutants seen by SAXS was supported by the calculations. Further the *in silico* approach could provide reasons for this compaction. W300 in wt Hsp90 forms an essential transient π-cation interaction with K294 preventing the negatively charged loop from too close contacts with the surrounding positive charges. This force propagation leads to the correct positioning of the Hsp90-M domain and may contribute to the overall conformation. For W300K it seems to be more complicated. The SAXS data of the W300K mutant did not exhibit a significant more closure of the dimer but indicated a different conformation. Thus, the seen effects in the molecular dynamics simulation might not result in a more closed conformation but nevertheless lead to a conformation that significantly affects the Hsp90-GR interplay. As speculated in the previous sections, the π-cation interaction seems to be

of special importance in providing a high affinity client binding conformation. In the case of GR it allows the client to modulate Hsp90 on the one hand and on the other hand the stimulation of hormone binding. In the absence of W300, the negatively charged loop forms an interaction pattern leading to differential interaction pattern in the Hsp90 protomer and finally to a more closed Hsp90. The more closed or generally altered conformations seem to be unfavorable also for the binding of co-chaperones like Sti1 which binds to a predominantly open conformation (Richter et al., 2003).

### 4.1.8 Summary and conclusion

In the previous paragraphs the importance of the switch point W300 in Hsp90 was analyzed. Paramagnetic relaxation enhancement NMR experiments identified a single tryptophan residue to be influenced by the presence of the GR-LBD. Mutation of this residue to alanine led to complete loss of the signal in the $^{15}$N-HSQC spectrum of the Hsp90-M domain implying W300 to be affected by the GR-LBD. 5`FOA shuffling in *S. cerevisiae* identified W300 to be crucial for viability as the alanine mutant displayed a severe growth defect and E and K substitutions were inviable. Interestingly the W300F and Y mutants could rescue viability. Further, monitoring of GR-maturation *in vivo* underlined the importance of W300. The W300A mutant significantly reduced the GR-response in yeast and its protein levels were increased. *In vitro* analysis of the GR-Hsp90 interplay showed that the W300 mutants could not be inhibited in their ATPase activity by GR-LBD and also the conformational dynamics were no longer influenced. The GR-LBD was further not able to induce a stabilized semi-closed conformation in Hsp90. Not only the influence of the GR-LBD on Hsp90 was altered by mutations in W300 but the homologous human W312 mutants showed also a decreased ability to induce hormone binding to the GR-LBD. Analysis of the GR-LBD binding to the Hsp90 mutants revealed that instead of an increased affinity for GR-LBD in the presence of ATP observed for the wt, the affinity was significantly reduced. Closed conformations of Hsp90 were strongest affected with severely reduced binding. Further, the influence of co-chaperones was altered in the mutants. The inhibitory effect of Sti1 and the stimulation by Aha1 were affected mostly.

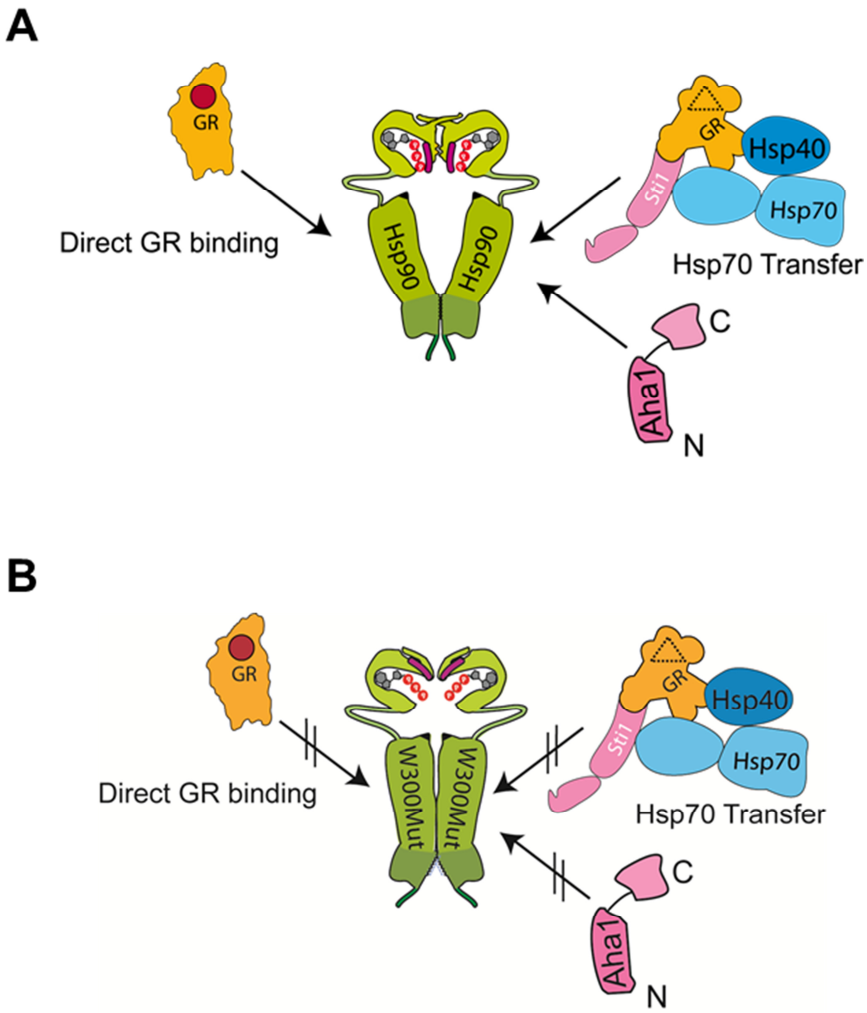


**Figure 29: Stronger closing of the Hsp90 W300 mutants leads to conformations insensitive for GR and co-chaperones. A)** By forming a semi-closed conformation in the presence of the GR-LBD, the client is bound with high affinity and able to modulate the Hsp90 chaperone cycle. Binding of and regulation by the co-chaperone Sti1 is possible, ensuring efficient transfer of the GR-LBD form the Hsp70- to the Hsp90-system. Importantly, binding and full activation of Hsp90 by Aha1 is also possible. **B)** By forming significantly altered conformations, the Hsp90 W300 mutants show altered binding of the GR-LBD and become also insensitive to the inhibitory effects of GR on the conformational cycle dynamics. Further, the mutants show reduced induction of hormone-binding recovery which is explained on the one hand by reduced binding and on the other also by decreased affinity for Sti1/Hop which is important for transfer from the Hsp70 system. Altered Aha1 binding might also affect the dynamics of the Hsp90 chaperone cycle and client proteins depending on Aha1 in their maturation.

Binding analysis by AUC could show that this was probably due to decreased affinities for the co-chaperones. SAXS analysis of the conformational ensemble of the mutants showed significantly more closed conformations of the W300A and E mutants and generally altered conformations for W300K. *In silico* MD simulations supported the SAXS data and further provided atomistic information on the underlying mechanisms. By forming a transient π-cation

interaction with a close lysine residue, W300 primes Hsp90 for a high affinity GR-competent conformation. This conformation is of special importance as it enables GR to modulate its own chaperoning by influencing Hsp90. By inhibiting the ATP hydrolysis and preventing release from Hsp90, GR prolongs the interaction with its chaperone, guaranteeing a regulated Hsp90-dependent nuclear translocation. It is not clear whether the significance of this special conformation can be transferred to other SHRs, client families like kinases or even to Hsp90 clients in general. Further client analyses *in vitro* are indispensable to clarify this aspect but results from literature already suggest an involvement of W300 in v-Src maturation (Hawle et al., 2006). The structure of the Hsp90-Cdc37-Cdk4 complex might further support the idea of an involvement of W300 in kinase chaperoning. In the complex, W300 lies close to the kinase binding patch and might participate directly or indirectly in the kinase binding (Verba et al., 2016). Importantly, the described conformation is further required for efficient transfer of GR from the Hsp70-system to Hsp90 via Sti1/Hop and stimulation of hormone binding. The results implicate that inefficient transfer of GR to the Hsp90 W300 mutants is based on the loss of the high-affinity GR binding conformation and on decreased Sti1/Hop binding. Importantly, the transfer was not completely abolished, however the bound the GR was not able to modulate the Hsp90 cycle suggesting rapid release of the client from Hsp90. Interestingly, it has been previously shown that Hsp90-dependent nuclear translocation is abolished by Geldanamycin and that diffusion-controlled translocation is inefficient (Galigniana et al., 1998). Additionally, hormone-binding and association of GR-LBD to Hsp90 was observed to be reduced in the presence of Radicicol (Kirschke et al., 2014; Lorenz et al., 2014). Thus, lack of this very special conformation controlled by W300 might lead to a similar mis-regulation of GR like in the presence of Hsp90 inhibitors resulting in an uncontrolled GC-dependent gene response with unknown consequences for the cell.

Several switch point position have been described in the literature to alter the conformational cycle of Hsp90 and client binding or maturation. The bulk of these switch points are phosphorylation sites (T22, Y24, S379, S485, S602, S604) and thus Hsp90 function has been thought to be regulated by kinases and phosphatases (Mollapour et al., 2010; Mollapour et al., 2011; Soroka et al., 2012). A recently accepted publication suggested also several residues to be indispensable for Hsp90 function as they affect the timing of the conformational changes (Δ8, R380) (Zierer et al., 2016 accepted).

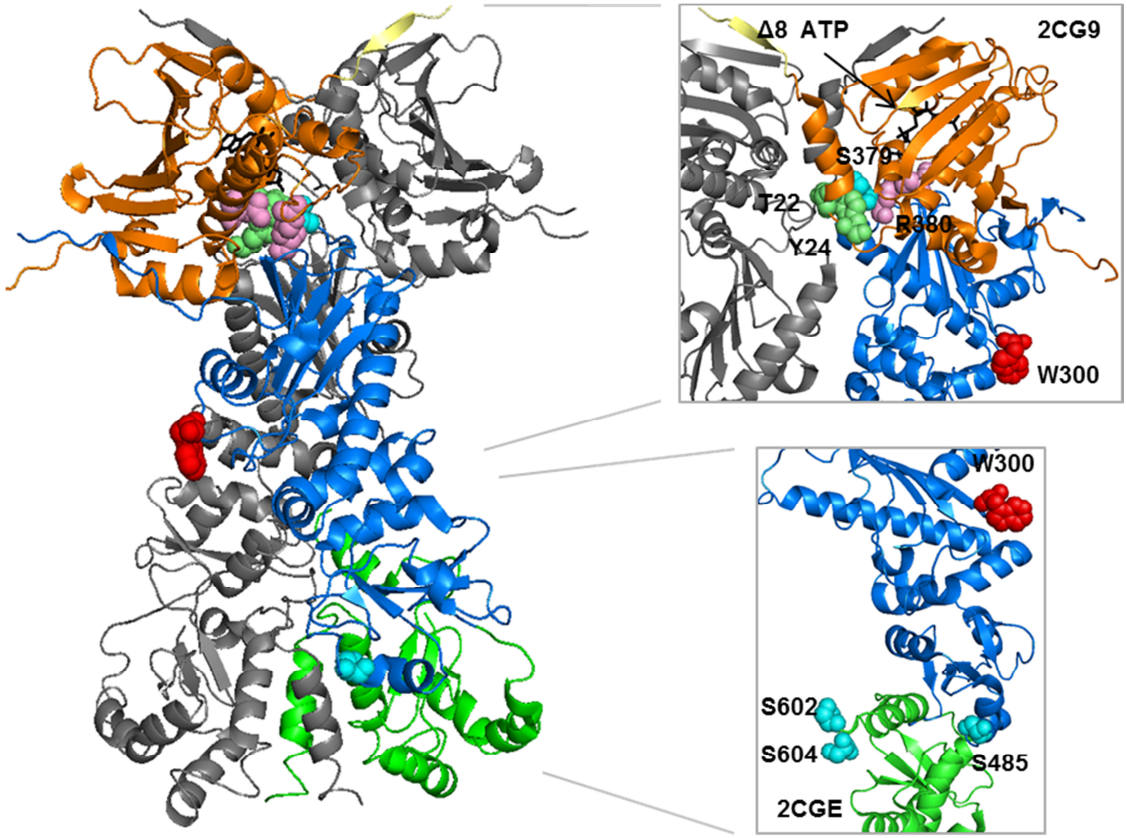


**Figure 30: Mapping of the switch point positions in Hsp90;** Switch point positions were mapped on the crystal structure of Hsp90 (PDB ID: 2CG9) and Hsp90-MC (PDB ID: 2CGE). T22 and Y24 (Mollapour et al., 2010; Mollapour et al., 2011) are colored in lime. S379, S485, S602 and S604 (Soroka et al., 2012) are colored in cyan. S602 and S604 are not resolved in the full-length crystal structure and are therefore mapped on the Hsp90-MC structure. R380 is shown in pink and the first eight N-terminal residues (Δ8) in yellow (Zierer et al., 2016 accepted). W300 is colored in red. Boxes show blow-ups from the closed Hsp90 (2CG9) and the 90-MC construct (2CGE).

Most of the switch points cluster in the N-terminal and the middle domain, especially in the N-M interface involving the hydrophobic loop around R380 from Hsp90-M which has been shown to be essential for stabilization of a hydrolysis competent state (Figure 30) (Cunningham et al., 2012). Changes in the charge pattern due to phosphorylation or mutation have been observed to differential affect N-terminal dimerization and ATPase activity. Phsopho-mimicking mutants in this region seem to generally reduce N-terminal dimerization and ATPase activity resulting also in decreased client maturation (Mollapour et al., 2010; Soroka et al., 2012). Other mutants like R380A or the Δ8 construct, lacking the first eight amino acids that perform the strand exchange in the closed conformation, exhibit dramatically different effects on the ATPase activity with the R380A mutant significantly decreasing and the Δ8 mutant showing a two fold increase in ATP

hydrolysis. Interestingly, both mutants did not confer viability to yeast as the sole source of Hsp90. It was observed that R380A is trapped in the closed I state and is deficient in transiting to the hydrolysis competent closed II state. In contrast, the Δ8 construct readily transited to the close II state in the presence of ATP but the authors could not observe reopening of this mutant. Interestingly, the Δ8 mutant showed significantly reduced GR-LBD binding in the presence of ATP. Thus, the authors speculated that functional timing of conformational transitions is essential (Zierer et al., 2016 accepted). Phosphorylation/phospho-mimetic mutations of the switch points in the C-terminal domain (S602, S604) or in close proximity of Hsp90-C (S485) seemed to have more long-range structural consequences than the positions located in Hsp90-N or the N-M interface. Interestingly, the S485E mutation positioned close to Hsp90-C (Figure 30) led to decreased N-terminal dimerization, compaction in the presence of AMP-PNP and GR-maturation. The S602E and S604E induced structural changes altering inter-domain communication, Aha1 binding but left GR-maturation unaffected (Soroka et al., 2012).

The positioning of W300 in comparison to the above mentioned switch points is significantly different. Whereas most of the known switch points are within the Hsp90 structure in close proximity to domain interfaces, W300 is highly surface exposed in the Hsp90-M domain (Figure 30). Nevertheless, it seems that both types of switch points manage to induce a special Hsp90 conformation in similar manner. In case of the phosphorylation sites, introduction of negative charge leads changes in the local interaction pattern resulting in the desired local and/or long range conformational changes. W300 might work similar by promoting formation of its special conformation by a local π-cation interaction. However there is a significant difference in the regulatory requirements. The phosphorylation-dependent switch points seem to be transiently favorable for the cell and therefore are dynamically controlled by kinases, phosphatases and differential co-chaperone influence. In contrast, W300 displays a constant feature of Hsp90 implicating that W300 is important for the general function of Hsp90. This supports the idea that W300 and the induced conformation might be also essential for other client proteins. In this regard, W300 seems to be equally important to crucial constant switch points like R380 or the ß-strand formed by the first 8 amino acids. Similar to these features of Hsp90, W300 might trigger an important client-competent conformation at a certain time point. Like for R380A or Δ8, mutations in W300 lead to altered conformations deranging the cycle timing resulting in dysfunctional Hsp90 (Zierer et al., 2016 accepted). Thus, the results on W300 support the idea that correct conformational timing of Hsp90 is essential for its function in the cell.

## 4.2 Comparison of Hsp90-client complexes

Hsp90 shows a vast variety of different client proteins ranging from the well-known protein kinases, transcription factors (SHRs, p53) and E3 ligases to other unrelated proteins like the microtubule-binding protein Tau. Tau is an exception from the large group of Hsp90 clients as it does not show any readily formed secondary structure (Mayer and Le Breton, 2015). Literature has shown that Tau interacts with Hsp90 using its MT-binding repeat. The modelled binding region consists of large hydrophobic and positively charged residues that are largely scattered indicating a rather unspecific binding motif. Binding to Hsp90 has been shown to be ATP-independent (only ATPγS was used) and involving large parts of the Hsp90-N but also –M domain. Binding analysis was performed by NMR of isoleucine-labeled full-length Hsp90 in combination with SAXS. Thereby, the study provided mostly information about the indirect binding patch of Tau as isoleucines are usually not surface exposed. It was further speculated that the binding sites of Tau and the GR-LBD largely overlap and that binding of most co-chaperones to an Hsp90-Tau complex is possible (Karagöz et al., 2014; Mayer and Le Breton, 2015). Due to the lack of a comprehensive Tau binding site on Hsp90, missing information on the influence of Tau on Hsp90 (ATPase, conformational cycle kinetics) and the absence of co-chaperone binding data, the present study was intended to provide further details of the Tau-Hsp90 interplay. By comparing the data with reproduced results for the GR-LBD, the work should further help in understanding how Hsp90 handles different client proteins and whether they influence Hsp90 differentially.

### 4.2.1 Tau, an intrinsically disordered monomeric Hsp90 client

The previous paragraph mentioned that Tau in contrast to other client proteins is intrinsically disordered. To prove that this was also the case with the protein provided by Chad Dickey (University of South Florida, Tampa) and used in this study, CD spectroscopy was performed (3.5.4). The GR-LBD in the presence of its hormone Dexamethasone was included in the analysis for structural comparison.

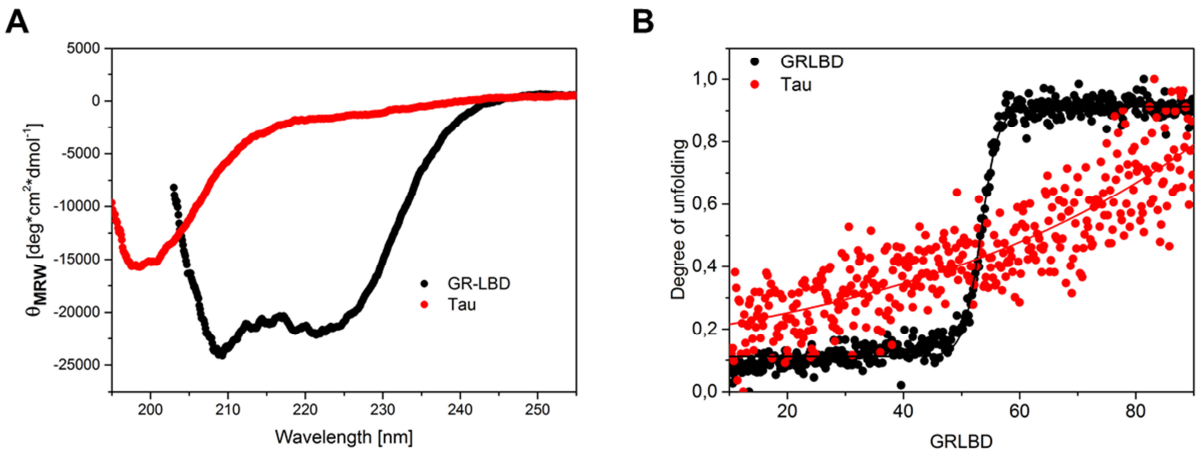


**Figure 31: Secondary structure analysis of Tau and the GR-LBD; A)** Far-UV CD spectra of the GR-LBD in the presence of 10 µM Dexamethasone in black and Tau in red; **B)** Thermal unfolding of the GR-LBD in the presence of 10 µM Dexamethasone in black and Tau in red followed by CD spectroscopy; Data was analyzed using the Boltzmann equation in Origin 9.1G.

The results of the secondary structure analysis are shown in Figure 31. As expected and in line with the literature, the GR-LBD displayed an α-helical spectrum containing typical minima at 222 nm and 208 nm (Lorenz et al., 2014). The far-UV spectrum of Tau exhibited only one minimum at 200 nm indicative for an unordered structure (Venyaminov et al., 1993). The GR-LBD unfolded in a cooperative manner in the thermal transition with an apparent melting temperature $T_M$ of 53.3°C whereas Tau did not show cooperative unfolding in line with the absence of secondary structure (Figure 31 B). It is known that the Tau microtubule binding region tends to promote aggregation and that Tau aggregates lead to Alzheimer disease (Haass and Selkoe, 2007). As it was essential to determine the oligomeric state of Tau *in vitro*, the quaternary structure was tested by analytical ultracentrifugation coupled to UV-detection. Again, the GR-LBD was simultaneously analyzed for comparison.

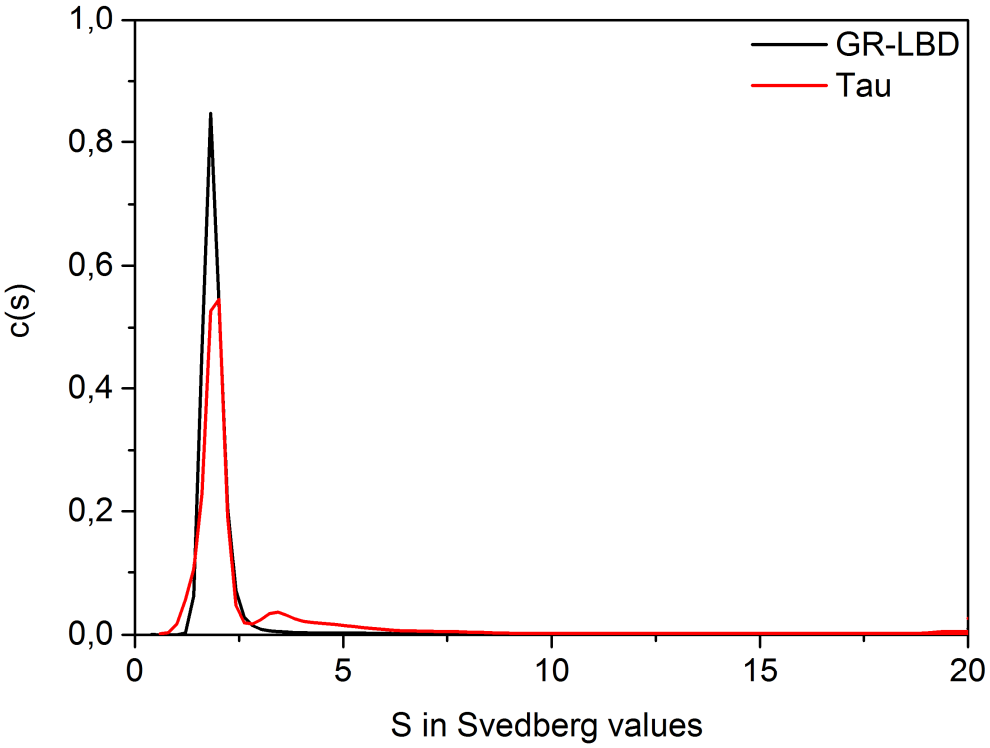


**Figure 32: Analysis of the oligomeric state of GR-LBD and Tau in solution.** c (S) distributions of 7 µM GR-LBD in the presence of 50 µM Dexamethasone in black and 30 µM Tau in red at 20°C; Data analysis was performed using SedFit 14.1.

As previously shown, the GR-LBD in the presence of Dexamethasone sedimented at 2.7 S and was thus monomeric (Lorenz et al., 2014). Data analysis using SedFit 14.1 indicated a monomer content of > 95 %. Tau sedimented with an S-value of 2 S and was also mainly monomeric with > 75 % but there was a significant proportion of smaller oligomers (< 20 %) present in the sample (Figure 32). As the size distribution was relatively broad, the oligomeric species could not be defined further. Unstructured proteins are often prone to proteolytic digestion during purification, therefore it might well be that the undefined oligomers are formed by truncated Tau molecules consisting of the aggregation-prone microtubule binding region (Yu et al., 2012). Nevertheless, AUC in combination with the CD analysis indicated that both proteins were stable at the performed assay temperatures and predominantly monomeric. The predominantly monomeric nature of Tau is in line with the literature where unphosphorylated Tau was shown to not readily aggregate *in vitro* (Luna-Muñoz et al., 2007).

### 4.2.2 Tau and GR-LBD differ significantly in their binding to Hsp90

#### 4.2.2.1 Nucleotide-dependent Hsp90 association

Recent literature implicated that binding of Tau and GR-LBD might differ greatly in their nucleotide-dependent binding to Hsp90 (Karagöz et al., 2014; Lorenz et al., 2014). To test this, binding of Tau to Hsp90 was monitored using human Hsp90ß in the presence and the absence of ATPγS in a fluorescence-based assay, whereas GR-LBD binding to Hsp90 was monitored using yeast Hsp90 but with all available nucleotides (ATP, ATPγS, AMP-PNP, ADP) by analytical ultracentrifugation. As different assay conditions and proteins might lead to incomparable results, the binding assays were repeated side-by side in a consistent experimental setup. Binding of ATTO488-labeled Tau and GR-LBD to yeast Hsp90 and human Hsp90ß in the presence of various nucleotides (ATP, ATPγS, AMP-PNP, ADP) was assayed by analytical ultracentrifugation coupled to fluorescence detection (3.7). Tau was labeled by NHS chemistry to prevent any interference of the label with binding to Hsp90 as the two cysteines in Tau (isoform D) (C264, C233) are located in the proposed Hsp90-binding site. Preliminary experiments (data not shown) and the literature indicated a higher $K_D$ for binding of Tau to Hsp90 than for the GR-LBD (Karagöz et al., 2014). Therefore, the Hsp90 concentration in the Tau binding experiments was increased to 6 μM to ensure reliable complex detection.

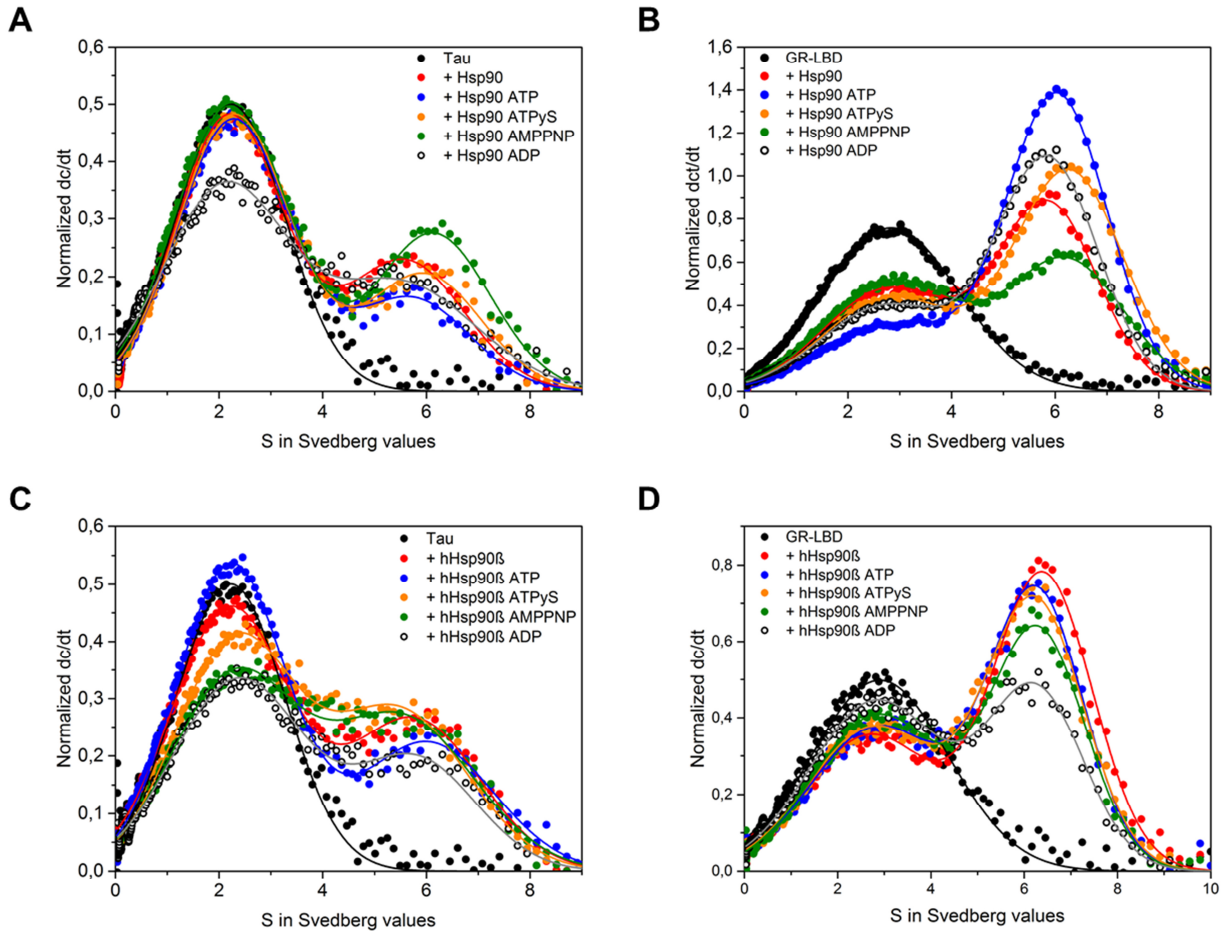


**Figure 33: Comparison of the nucleotide-dependent binding of Tau and the GR-LBD to yeast Hsp90 and human Hsp90ß; A)** Binding of 400 nM ATTO488 labeled Tau to 6 µM yeast Hsp90 in the presence of different nucleotides. Tau in the absence of Hsp90 and nucleotide in black, with of apo-Hsp90 in red, ATP-bound Hsp90 in blue, ATPγS-bound Hsp90 in orange, AMP-PNP-bound Hsp90 in green and ADP-bound Hsp90 in black open circles; **B)** Binding of 400 nM ATTO488 labeled GR-LBD to 3 µM yeast Hsp90 in the presence of different nucleotides. Color code for the different nucleotides as indicated in **A**. **C)** Binding of 400 nM ATTO488 labeled Tau to 6 µM human Hsp90ß in the presence of different nucleotides. Color code for the different nucleotides as indicated in **A**; **D)** Binding of 400 nM ATTO488 labeled GR-LBD to 3 µM human Hsp90ß in the presence of different nucleotides. Color code for the different nucleotides as indicated in **A**; Data processing and analysis was performed using SedView 1.1 and Origin 9.1G.

In line with the AUC results from the previous section (Figure 32, 4.2.1), fluorescently labeled Tau sedimented with an S value of roughly 2 S and GR-LBD with 2.7 S (Figure 33 A, B, C and D, black curves). When in complex with yeast Hsp90, Tau sedimented around 5.7 S in the presence of ATP, ADP or in the absence of nucleotide (Figure 33 A red, blue and orange curve) and around 6 S with ATPyS or AMP-PNP. The increase in the S value is consistent with a closed Hsp90 dimer indicating that the closing reaction is possible when Tau was bound to Hsp90.

Interestingly, no strong nucleotide dependency of binding was observed. All conditions, except in the presence of ADP, where seemingly more Tau was bound (Figure 33 A, black open circles), showed the same amounts of Tau associated in the complex as deduced from the amplitude of the free species. Further, the amount bound was in general less than in the GR-LBD binding experiment (Figure 33 B), confirming a weaker affinity for Hsp90 of Tau in comparison to the GR-LBD. Consistent with results from previous sections (Figure 23, 4.1.4) and the literature, GR-LBD binding to yeast Hsp90 was again strongly nucleotide-dependent (Lorenz et al., 2014). Binding was most efficient in the presence of ATP whereas tightly closed Hsp90 conformations in the presence of AMP-PNP were less populated (Figure 33 B, blue and green curve). Results of binding experiments in the presence of human Hsp90ß were comparable to the yeast system (Figure 33 C and D). Fluorescently labeled Tau bound Hsp90ß similarly independent of nucleotides as indicated by a shift in the S value from 2 S to 5.7-6 S. ATPγS and AMP-PNP could not induce a further shift in the S value of the Tau-Hsp90ß complex implying significantly less closing of the human Hsp90 dimer (Figure 33, orange and green curve). Binding of the GR-LBD to Hsp90ß was not as nucleotide-dependent as for the yeast system due to less closed Hsp90 states in the human system but still the ATP-bound Hsp90 was the preferred conformation by the GR-LBD, (Figure 33 D) consistent with previous results (Figure 24).

The amplitude of the free Tau was significantly decreased in the presence of ADP-bound yeast Hsp90, AMP-PNP- and ADP-bound human Hsp90ß, indicating higher affinity for Tau (Figure 33 A and B). More detailed analysis of the data using SedFit 14.1 and titration experiments using increasing concentrations of Hsp90 in the presence of ADP unfortunately did not support these observations (data not shown). Further, the experiments revealed that the affinity of the labeled Tau was not in the published range of a $K_D$ of 5 µM (Karagöz et al., 2014) indicating that labeling of Tau, also at lysine residues, may lead to a significantly decreased affinity for Hsp90. To rule out alterations in Tau binding to Hsp90 due to the labeling, competition experiments using unlabeled Tau should be performed in the future. Nevertheless, the binding results implicated that binding of Tau to yeast Hsp90 or human Hsp90ß is in contrast to binding of the GR-LBD, not strongly nucleotide dependent. The nucleotides tested did not decrease or significantly increase binding of Tau to Hsp90, indicating that Tau is not as conformationally sensitive in its binding as GR. To confirm these observations and to eliminate alterations in the binding due to labeling of Tau, binding experiments were reproduced using labeled yeast Hsp90. Further Tau binding to the Hsp90 W300A mutant was assessed to confirm the conformational insensitivity of Tau binding.

The previous section had shown that this mutant was significantly more closed in the presence of ATPγS leading to a strong decrease in the ability to bind the GR-LBD (4.1.4).

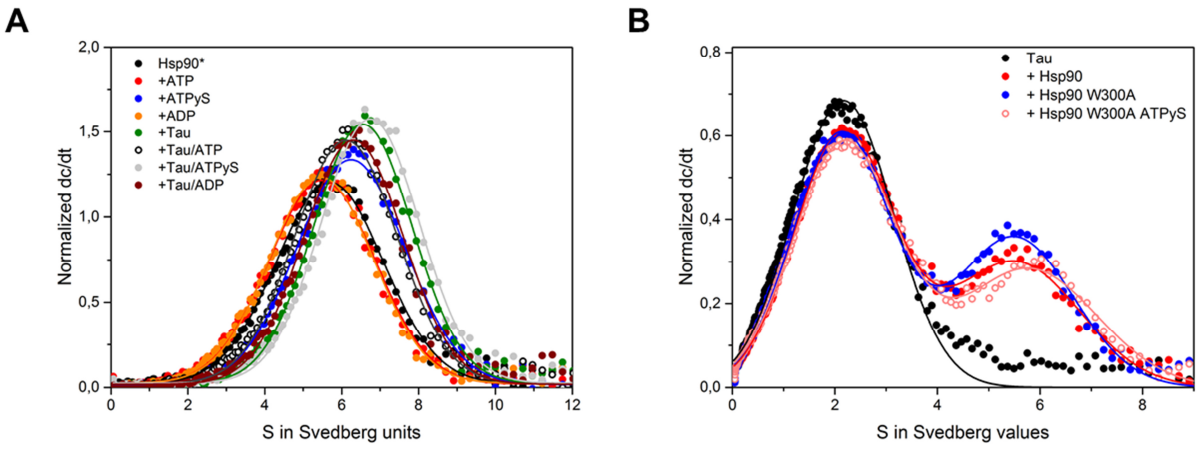


**Figure 34: Binding of Tau to labeled Hsp90 and the Hsp90 W300A mutant. A)** Sedimentation analysis of 400 nM ATTO488 labeled Hsp90 (Hsp90 D61C) to 3 µM Tau in the absence or the presence of 2 mM nucleotide. Hsp90 alone is shown in black, Hsp90 with ATP in red, Hsp90 with ATPγS in blue, Hsp90 with ADP in orange, with Tau in green, with Tau and ATP in black open circles, with Tau and ATPγS in grey and with Tau and ADP in brown; **B)** Binding of Tau to the Hsp90 W300A mutant; Sedimentation analysis of 400 nM ATTO488 labeled Tau with 6 µM Hsp90 or mutant is shown. Tau alone in black, with Hsp90 in red, with Hsp90 W300A in blue and with Hsp90 W300A plus ATPγS in rose; Data analysis was performed using SedView 1.1 and Origin 9.1G.

Labeled Hsp90 alone sedimented with an S value of 5.9 S. ATPγS induced a shift to 6.1 S in contrast to ATP or ADP, in line with a higher degree of compaction in the presence of the slowly hydrolyzing nucleotide analogue (Figure 34 A). The presence of Tau led to a shift in the S value of labeled Hsp90 from 5.9 S to 6.7 S, both in the absence of nucleotide and the presence of ATPγS (Figure 34 A, grey and green curve). In contrast, Tau shifted the S value to only 6.2 S when ATP or ADP was present (Figure 34 A, black open circles and brown curve). Tau binding to the Hsp90 W300A mutant is shown in Figure 34 B. In the absence of nucleotide Tau formed similar complexes with wt Hsp90 and W300A with an S value of 5.8 S. In contrast to the results with the GR-LBD (Figure 23), addition of ATPγS did not change the amount of complex formed as deduced from the unbound Tau species (Figure 34 B, blue vs. rose curve).

The experiments using labeled Hsp90 were able to confirm the previous results with regard to general nucleotide dependency of Tau binding. As expected, no significant difference in the binding in the presence of different nucleotides could be observed. Further, the results are in good accordance with the results from literature. In a fluorescence-based assay, binding of Tau to

Hsp90ß was not altered by the presence of ATPγS (Karagöz et al., 2014). Moreover, the data indicates that in the presence of ATP/ADP, Tau binds to an open Hsp90 conformation and Tau on its own might induce a slightly more closed conformation in Hsp90 as addition of ATPγS in the presence of Tau did not lead to a further shift in comparison to only Hsp90 and Tau. The results concerning the W300A mutant supported the idea of a conformationally insensitive binding of Tau to Hsp90. The GR-LBD was highly sensitive to the presence of ATPγS in its binding to W300A. Tau in contrast did not change its interaction with W300A in the presence of the nucleotide showing a reduced sensitivity in binding to different Hsp90 conformations.

In general, Tau and GR seem to belong to two different groups of clients concerning their nucleotide-dependent association with Hsp90. One part of the client family seems to prefer specific conformations of Hsp90 as they bind to Hsp90 with highest affinity only in the presence of certain nucleotides. It has been described that a fragment of the staphylococcal nuclease, Δ131Δ, is bound with highest affinity to *E. coli* Hsp90 in the presence of AMP-PNP indicating preference for a hydrolysis-competent closed II conformation (Street et al., 2011). In recent work, it was shown that the Cdk4 kinase associates with Hsp90 and its co-chaperone Cdc37 in a special complex resulting in the partial unfolding of the kinase client. Interestingly, the authors found ATP-like density in the nucleotide-binding pocket of Hsp90 and speculated that ATP or ADP plus stabilizing molybdate might be bound by Hsp90 when associated with Hsp90 (Verba et al., 2016). Similarly, early studies showed that immuno-precipitated SHR-Hsp90 complexes were also stabilized by the presence of molybdate (Scherrer et al., 1990). These results indicate that also the association of kinases might be dependent on an ATP-induced conformation similar to the GR-LBD. As simultaneous association of Cdc37 to Hsp90 is a prerequisite for kinase binding, this is further in line with the notion that Cdc37 inhibits ATP hydrolysis when bound to Hsp90, thus stabilizing an ATP-induced conformation (Gaiser et al., 2010; Siligardi et al., 2004). Binding to a special nucleotide-induced conformation favors also the idea that release of these clients might be triggered by ATP-hydrolysis (Grenert et al., 1999; Lorenz et al., 2014; Obermann et al., 1998; Panaretou et al., 1998) Interestingly, all three clients (Δ131Δ, Cdk4, GR) belong to different client classes and show no significant structural similarities as Δ131Δ is unfolded, Cdk4 partially unfolded and the GR-LBD fully folded when associated with Hsp90 indicating that structurally different clients might be bound by similar nucleotide-dependent conformations but maybe at different position. The other part of the Hsp90-clients like Tau seems to associate with Hsp90 independent of nucleotide and certain conformations. It has been

previously shown that also the transcription-factor p53 binds to Hsp90 independent of nucleotide (Hagn et al., 2011). It is to date unclear how the release of these client proteins is controlled. It might be speculated that co-chaperones promote the exit of the nucleotide-independently bound client.

#### 4.2.2.2 Tau and the GR-LBD do not compete for binding sites on Hsp90

The previous section described that binding of Tau to Hsp90 (yeast and human) is not sensitive to conformational changes in the Hsp90 dimer as Tau was bound in the presence of every tested nucleotide and no selectivity for any nucleotide condition could be observed. These results differed greatly from the obtained results for the GR-LBD and as literature implied binding of Tau to the Hsp90-N and -M domains, it was of interest to compare the GR-LBD results with binding of Tau to the individual domains (Hsp90-N, -M and –C) and segmentally labeled Hsp90-NM constructs by NMR (Karagöz et al., 2014; Lorenz et al., 2014). Experiments were performed in cooperation with Lee Freiburger and Michael Sattler (Technische Universität München).

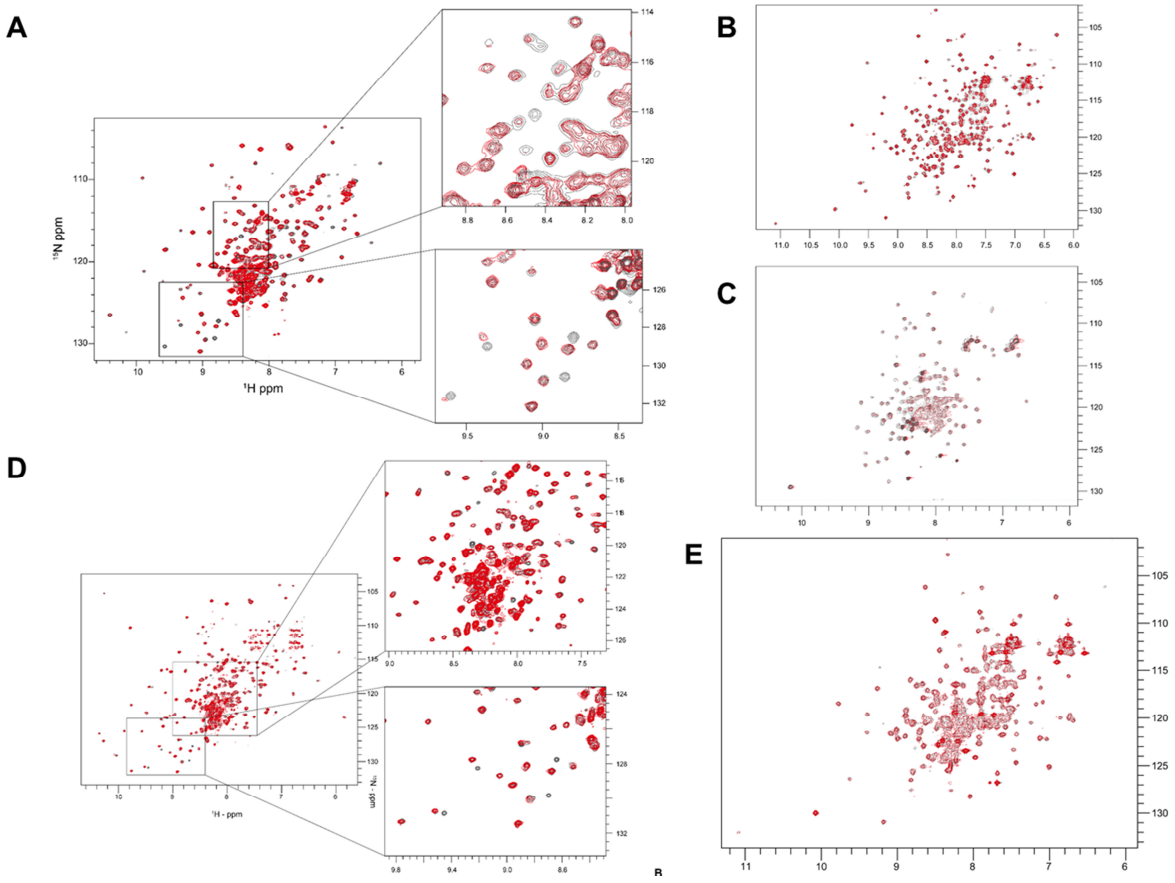


**Figure 35: NMR experiments using individual and segmentally labeled Hsp90 domains. A)** Overlay of $^{1}$H-$^{15}$N HSQC spectra of Hsp90-N (gray) and in the presence of Tau (red). Insets show enlarged views of the spectra where major changes in the chemical shift and intensities of the signals occur. **B)** Overlay of $^{1}$H-$^{15}$N HSQC spectra of isolated Hsp90-M (gray) and in the presence of Tau (red). **C)** Overlay $^{1}$H-$^{15}$N HSQC spectra of isolated C domain (gray) and in the presence of Tau (red). **D)** Overlay of $^{1}$H-$^{15}$N HSQC spectra of Hsp90-N*M (gray) and in the presence of Tau (red). Insets show enlarged views of the spectra where major changes in the chemical shift and intensities of the signals occur. **E)** Overlay of $^{1}$H-$^{15}$N HSQC spectra of Hsp90-NM* (gray) and in the presence of Tau (red). Data acquisition, analysis and figure preparation was performed in cooperation by Lee Freiburger, Abraham Lopez and Michael Sattler (Technische Universität München).

The results of the NMR analysis are presented in Figure 35. The overall spectra similarity between the free and bound states suggests that the binding of Tau did not induce large conformational rearrangements in the individual domains similar to the binding of the GR-LBD (Figure 35 A, B, C) (Lorenz et al., 2014). However, experiments using the isolated N-terminal domain of Hsp90 demonstrated that a select set of signals showed significant chemical shift perturbations (CSPs) and/or severe line broadening upon the addition of Tau (Figure 35 A, blow-ups). Surprisingly, in both the individual Hsp90-M and –C domain no significant CSPs or intensity changes could be observed indicating that the major site of interaction is located in the

Hsp90-N domain (Figure 35 B, C). Interestingly, addition of AMP-PNP to the isolated Hsp90-N domain did not produce strong changes in the CSP pattern as similar regions in Hsp90-N were affected compared to the absence of nucleotide (data not shown). Binding of Tau to the segmentally labeled Hsp90-N*M domain (Hsp90-N labeled) induced even greater effects in Hsp90-N with the addition of several new peaks experiencing CSPs and intensity changes (Figure 35 D). In contrast, the Hsp90-NM* domain (Hsp90-M labeled) was less affected by the binding of Tau. Nevertheless, in contrast to the isolated Hsp90-M domain, a small set of residues experienced CSP and/or intensity changes in the presence of Tau (Figure 35 E). To compare the binding sites in greater detail, the Tau data was mapped onto the Hsp90 crystal structure (PDB ID: 2CG9) together with the results for Tau and GR-LBD from the literature (Figure 36) (Karagöz et al., 2014; Lorenz et al., 2014).

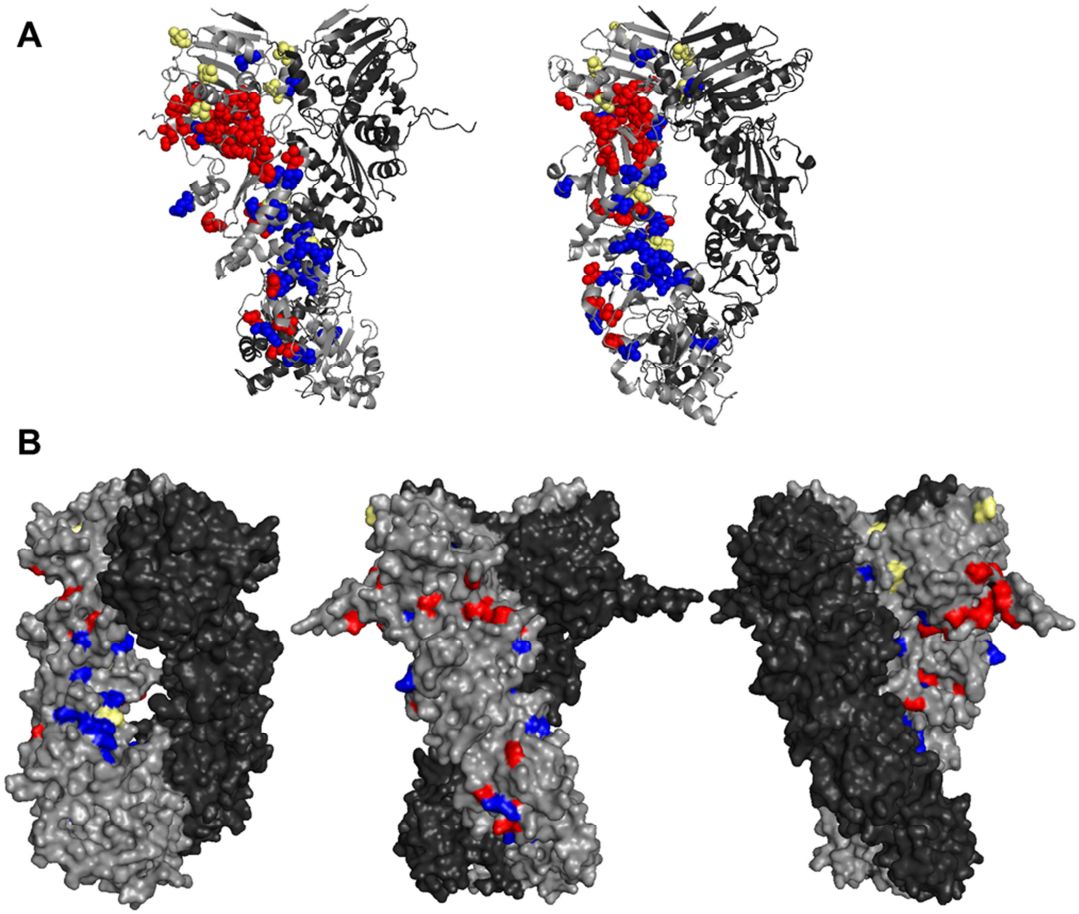


**Figure 36: Mapping of the residues in closed Hsp90 (PDB ID: 2CG9) showing strong CSPs upon the binding of Tau.** Residues from the binding experiments in **Figure 35** experiencing min. two fold increases in CSPs above the

average are shown in red. CSPs introduced in Hsp90 by the addition of the GR-LBD are shown in blue (Lorenz et al., 2014). Isoleucines affected by the binding of Tau in human Hsp90ß were mapped to the homologous yeast residues and are shown in yellow (Karagöz et al., 2014). **A)** Respective residues were mapped in the cartoon-representation of the closed Hsp90. **B)** Surface-representation of the closed Hsp90 and the residues experiencing signal changes due to the binding of Tau or the GR-LBD.

Residues exhibiting strong CSPs upon binding of Tau to Hsp90 clustered mainly to the lower outside part of the Hsp90-N-domain (residues 31-71 and residues 186-211) and to the N-M interface (residues 364-388) (Figure 36 A). Additionally, the affected residues in Hsp90-M were spread over the complete domain without forming specific clusters but were located mostly on the outside part (Figure 36 A). Importantly, the residues experiencing major CSPs were located to similar regions as the observed isoleucine residues by Karagöz and co-workers but were more surface-exposed probably due to the hydrophobic nature of isoleucines (Figure 36 A, yellow residues) (Karagöz et al., 2014). Further, significantly more affected residues were located in the Hsp90-N domain in contrast to previous reports, whereas fewer residues were identified in the Hsp90-M domain. Thus, the data suggests the Hsp90-N domain as the major site of interaction. Interestingly, it was speculated that the binding sites for GR and Tau might significantly overlap on Hsp90 as GR-LBD binding was also described to affect the Hsp90-N and -M domain (Karagoz and Rudiger, 2015; Lorenz et al., 2014; Mayer and Le Breton, 2015). The mapping of the Tau and GR-LBD binding sites using the identical Hsp90 domain constructs conferred a significantly different picture. As shown in Figure 36 A and B, the GR-LBD binding site is mostly located on the inside of the Hsp90 dimer within the cleft formed by the two protomers and additional contacts are formed with Hsp90-N and –C. In contrast, Tau seems to be wrapped around the Hsp90-N domain and extending its binding surface to Hsp90-M along the outside parts of the protomer arm. Thus, in contrast to speculations in the literature, the binding surface proposed here shows significantly less overlap with the GR-LBD binding surface.

To rule out further speculations of overlapping interaction sites and competitive binding of the GR-LBD and Tau, a FRET system between Hsp90 and the GR-LBD was established. Yeast Hsp90 was labeled with ATTO550 at an engineered Cysteine residue at position 333. This position was chosen as a PRE-experiment (Figure 12) had shown strong signal reduction in the region surrounding E333 and further E333C was successfully used in an intramolecular Hsp90 FRET system established by Hessling and co-workers (Hessling et al., 2009). Randomly labeled GR-LBD with ATTO488 was used as the FRET donor. As GR-LBD labeling was mainly

occuring at position C638 (Lorenz et al., 2014), which was also used in the PRE experiment, this setup should yield a FRET system for monitoring GR-LBD binding to Hsp90.

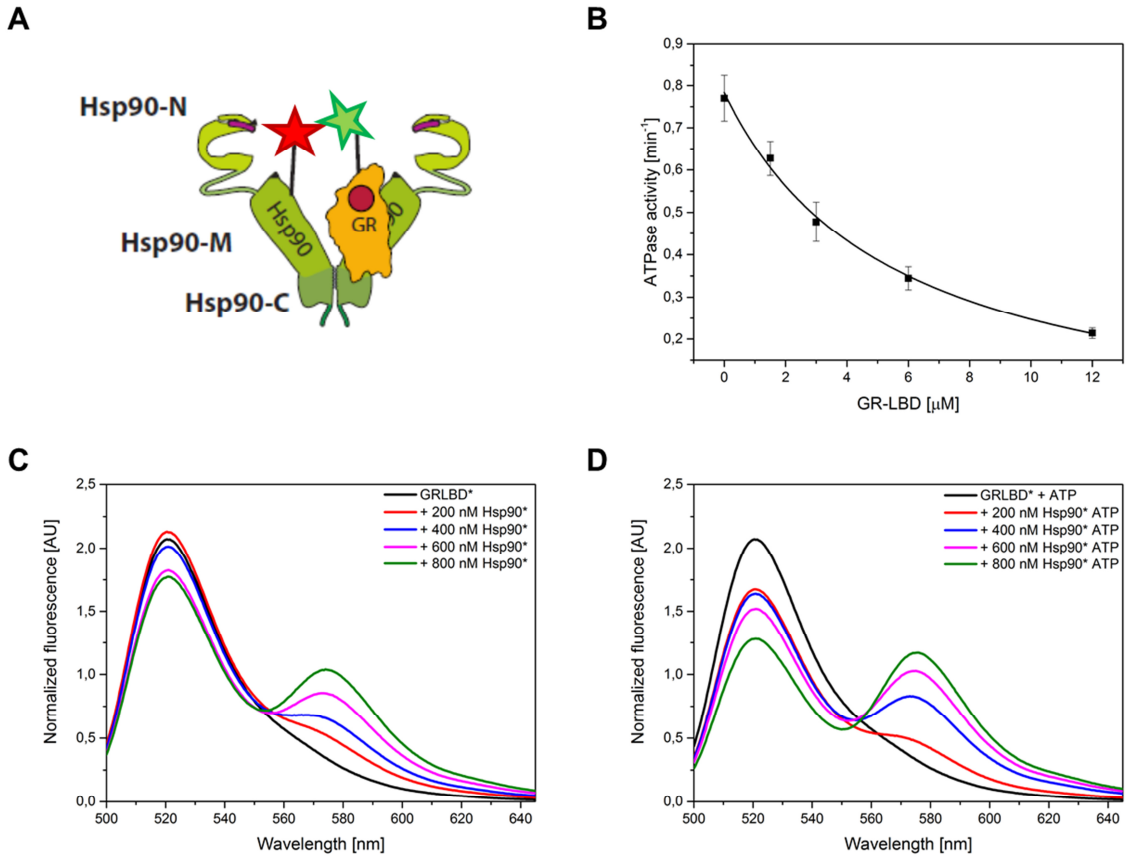


**Figure 37: A FRET system using ATTO488 labeled GR-LBD and ATTO550 labeled Hsp90. A)** The GR-LBD-Hsp90 FRET system; **B)** ATPase assay of Hsp90 E333C with increasing concentrations of GR-LBD; **C and D)** FRET spectra were excited at 490 nm and recorded from 500 to 645 nm with 200 nM FRET donor (ATTO488 GR-LBD) and increasing concentrations of FRET acceptor (ATTO550 Hsp90) in **C)** in the absence of nucleotide and in **D)** in the presence of 2 mM ATP.

Prior to FRET experiments, the Hsp90 E333C mutant was tested on its interaction with the GR-LBD to rule out alterations due to the mutation of E333. The ATPase activity of Hsp90 E333C was assayed in the presence of increasing concentrations of the GR-LBD. Hsp90 E333C could be efficiently inhibited by the GR-LBD with an apparent $K_I$ of 5.5 µM which is highly similar to wt Hsp90 ($K_I$ = 6.3 µM) (Figure 37 B and Figure 17 B) indicating no influence of the mutation on the GR-LBD interaction. Initial FRET spectra with increasing amounts of acceptor ATTO550 Hsp90 displayed increasing FRET signals with a maximum at 575 nm. This effect was even

stronger in the presence of ATP consistent with the notion that ATP increases the affinity of GR-LBD for Hsp90 (Figure 37 C and D).

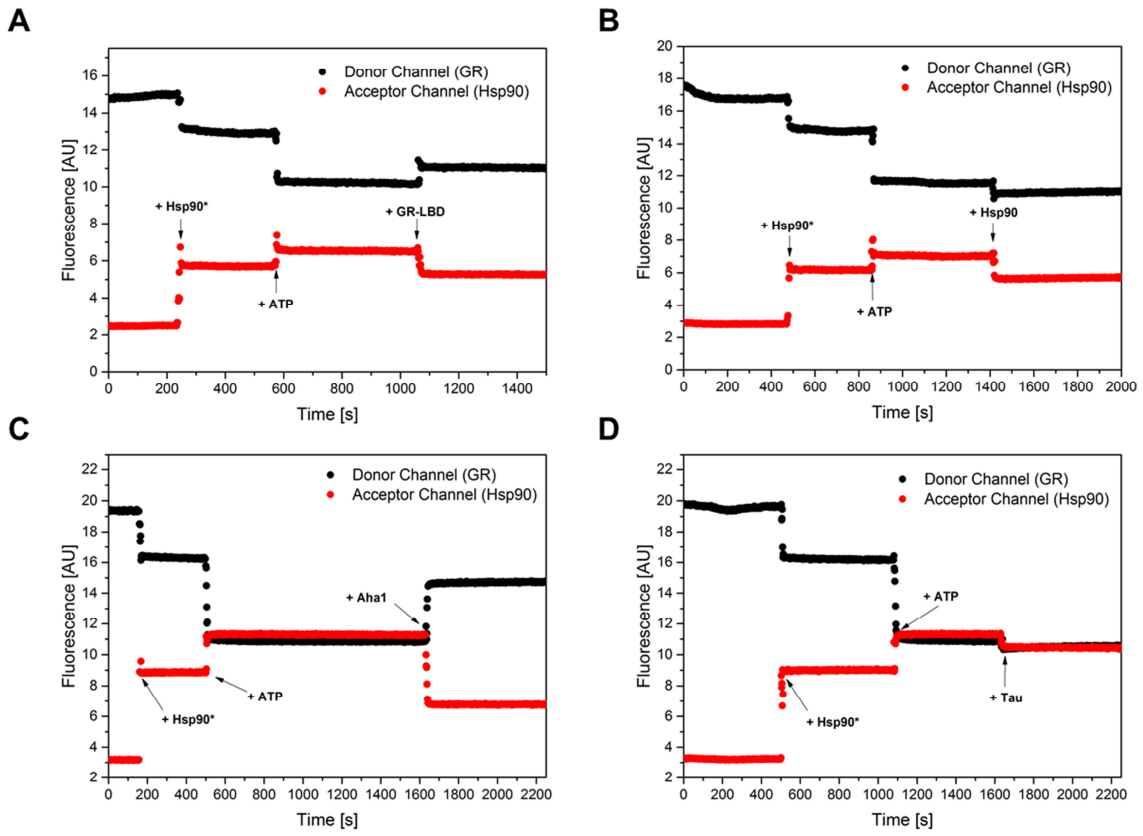


**Figure 38: FRET kinetics with the GR-LBD and Hsp90; A)** 200 nM ATTO488 labeled GR-LBD were incubated with 1 µM ATTO550 labeled Hsp90, 2 mM ATP and FRET signal was dissolved by the addition of 5 µM unlabeled GR-LBD. **B)** 200 nM ATTO488 labeled GR-LBD were incubated with 1 µM ATTO550 labeled Hsp90, 2 mM ATP and FRET signal was dissolved by the addition of 10 µM unlabeled Hsp90. **C)** 200 nM ATTO488 labeled GR-LBD were incubated with 1 µM ATTO550 labeled Hsp90, 2 mM ATP and FRET signal was dissolved by the addition of 10 µM unlabeled Aha1. **D)** 200 nM ATTO488 labeled GR-LBD were incubated with 1 µM ATTO550 labeled Hsp90, 2 mM ATP and 10 µM Tau was added subsequently. Arrows indicated time point of the addition of the respective component. Fluorescence at 520 nm (donor channel) is shown in black and fluorescence at 575 nm (acceptor channel) is shown in red.

To further confirm the functionality of the FRET system, several control kinetics were recorded. Addition of labeled Hsp90 led to a rapid increase in the acceptor channel intensity. The FRET signal was further increased by the addition of ATP, in line with the FRET spectra (Figure 38). All kinetics were beyond the resolution of manual mixing, so only final intensity changes could be detected. Addition of unlabeled GR-LBD or Hsp90 led to a partial or complete dissolution of

the FRET signal as deduced from the rapid loss of the intensity of the acceptor signal (Figure 38 A and B). As Aha1 possesses a highly overlapping binding site with the GR-LBD, it was also incorporated in the analysis (Lorenz et al., 2014). Excess of Aha1 effectively dissolved the FRET signal suggesting highly similar binding patches and competition for binding sites on Hsp90 (Figure 38 C). Together, the results implicated a functional FRET system which was able to detect competition for the GR-LBD binding site. Therefore, excess of unlabeled Tau (50 x) was added to a preformed GR-LBD-Hsp90-ATP complex (Figure 38 D). There was a slight decrease in the acceptor fluorescence detectable, but significantly less than, for example, in the kinetics with Aha1, indicating no competition for the binding sites on Hsp90 of the GR-LBD and Tau. To further support the results of the GR-LBD-Hsp90 FRET system, AUC coupled to fluorescence detection with labeled GR-LBD, Hsp90 and Tau was performed.

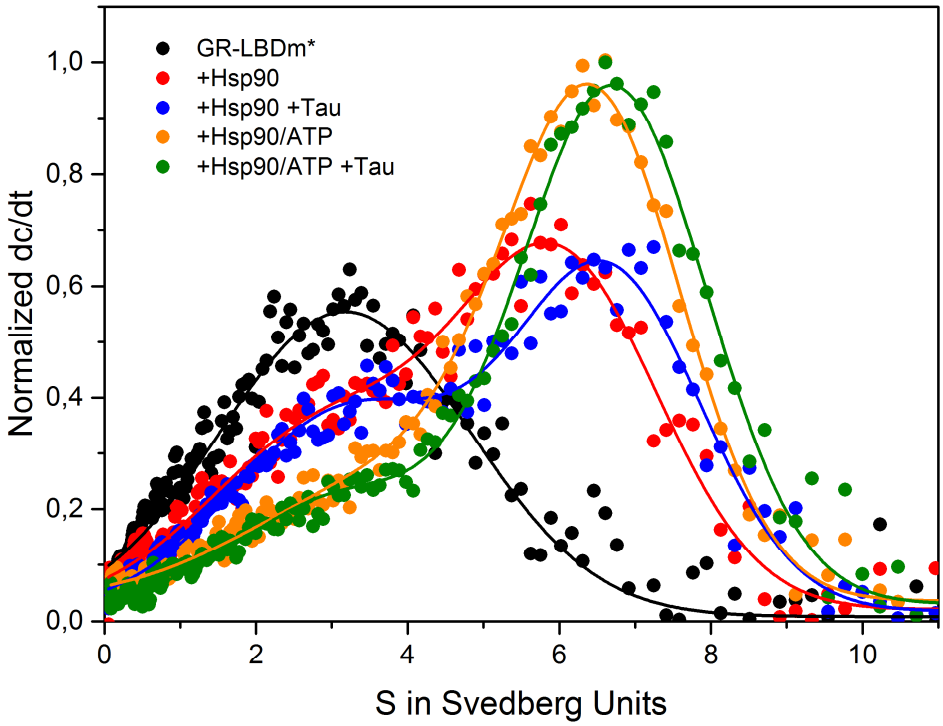


**Figure 39: AUC sedimentation analysis of labeled GR-LBD in the presence of Hsp90 and Tau;** 400 nM ATTO488 labeled GR-LBD alone in black, together with 3 µM Hsp90 in red, with 3 uM Hsp90 and 10 µM Tau in blue, with 3 µM Hsp90 and 2 mM ATP in orange and with 3µM Hsp90, 10 µM Tau and 2 mM ATP in green; Data analysis was performed with SedView 1.1 and Origin 9.1G.

When in complex with apo-Hsp90, the GR-LBD experienced a shift in the S value from 2.7 S to 5.9 S. Addition of 10 µM Tau increased the S value to 6.4 S indicative for additional binding of Tau to the GR-Hsp90 complex. No GR-LBD was released by the binding of Tau, as the amplitude in the free GR-LBD species at 2.7 S did not increase (Figure 39, red and blue curve). The results displayed a similar tendency in the presence of ATP (Figure 39, orange and green curve). As mentioned earlier, ATP increased the affinity of Hsp90 for the GR-LBD leading to a decrease in the amplitude of the free GR-LBD. Addition of an excess of Tau again did not release the GR-LBD from the complex but induced a further shift in the S value of the complex to 6.9 S indicative for additional Tau binding to the complex.

The detailed analysis and comparison of the Tau and GR-LBD binding sites on Hsp90 by combining NMR CSPs, FRET and AUC data draw a slightly different picture than what was speculated in literature. The NMR data for Tau from Karagöz and co-workers was obtained using isoleucine-labeled full length Hsp90ß (Karagöz et al., 2014). It can be speculated that the extensive modelling approach based on the isoleucine shifts used by Karagöz et al. might result in a different binding surface by stronger weighting of the isoleucine residues. These are mostly on the inside of the structure and may therefore be more indirectly affected by slight changes in the domain structure of Hsp90 upon binding of Tau. Thus, the binding surface suggested seems to be slightly different form the actual one. The presented NMR data consists of observed CSPs of all assigned residues incorporating effects originating mostly on the direct interaction of residues in Hsp90 with Tau. Mapping of the data suggests that the binding site for Tau is mainly located on the outside parts of the Hsp90-N domain with contributions from Hsp90-M. The overlap in the binding sites seems to be less pronounced as the GR-LBD predominantly binds to the inside parts of the Hsp90-M domain. The speculations of overlapping binding sites were further called into question by a GR-LBD-Hsp90 FRET system and AUC sedimentation velocity analysis which eliminate the idea of competition but show simultaneous binding of Tau and GR-LBD to Hsp90. It would be legitimate to criticize the use of yeast Hsp90 but AUC binding experiments suggest similar binding of Tau to yeast Hsp90 and human Hsp90ß (Figure 33).

When comparing the mostly N-terminal binding site of Tau and the MD-based binding of the GR-LBD with other Hsp90 clients, it seems that clients studied occupy different binding sites on Hsp90. For the tumor-suppressor p53 the binding site on Hsp90 has been mapped to be predominantly located to the Hsp90-C domain with some contributions from Hsp90-N and –M

indicating a significantly different binding site in comparison to Tau and the GR-LBD (Figure 6) (Hagn et al., 2011).

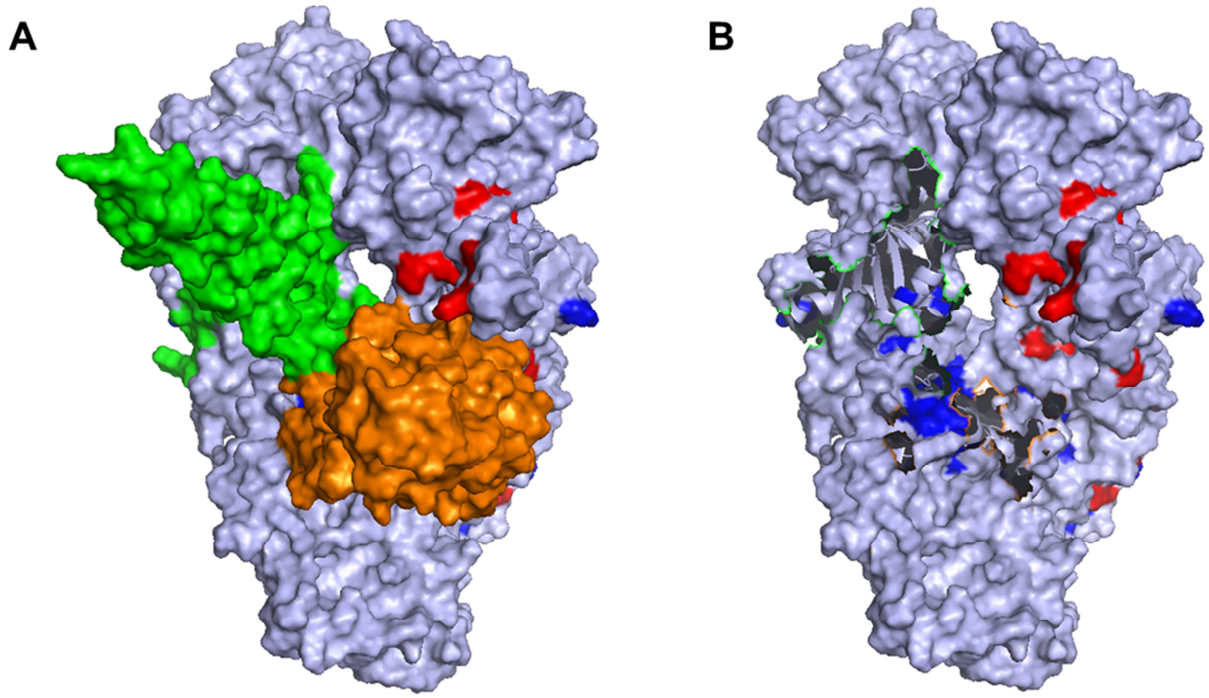


**Figure 40: Mapping of the Tau and GR-LBD binding sites on the structure of the Hsp90-Cdc37-Cdk4 complex (PDB ID: 5FWK).** Hsp90 is shown in grey, the Cdc37 N-terminal domain in green, the Cdk4 C-lobe in orange, the major CSPs induced by the binding of Tau in red and by the binding of the GR-LBD in blue; **A)** Surface-representation in the presence of the Cdc37 N-terminal domain and Cdk4 C-lobe; **B)** Same surface-representation as in **A** in the absence of the Cdc37 N-terminal domain and the Cdk4 C-lobe; The CSPs from yeast Hsp90 were transferred to the homologous human Hsp90ß residues.

A recent cryo-EM structure of Hsp90 in complex with its kinase client Cdk4 and its co-chaperone Cdc37 suggested that the partially unfolded kinase binds mainly to the Hsp90-M domain (Verba et al., 2016). The proposed site seems to be mainly different from the presented Tau binding patch but it might show some overlap on the outside parts of the N-M interface (Figure 40 A). Interestingly, the binding sites for Cdk4 together with Cdc37 seem to significantly overlap with the GR-LBD binding site on the Hsp90-M domain (Verba et al., 2016). Presence of the Cdc37 N-terminal domain and the Cdk4 C-lobe largely occupies the proposed GR-LBD binding site on the inside cleft of the Hsp90 dimer (Figure 40 B). Unfortunately, as the authors did not provide the exact residues involved in the kinase/Cdc37 binding, the mentioned overlap in the binding sites is of pure speculation. Thus, further analyses are required to clarify this question. An earlier EM

structure of Hsp90 and Cdk4 implicated a significantly different binding site for Cdk4 implicating stronger overlap with the Tau binding site (Vaughan et al., 2006). Due to the low resolution of the complex, this binding site is probably not correct and thus might be excluded from the comparison. Of note, SAXS data for the fragment of the staphylococcal nuclease, Δ131Δ, indicated also a binding site in the Hsp90-M domain in *E. coli* (Hsp90) but it is questionable how relevant this model client binding site is in comparison to binding sites on eukaryotic Hsp90s (Street et al., 2011). Altogether, it seems that besides different nucleotide-dependency of binding, different clients might also bind to varying sites on Hsp90. Although being mainly different, an involvement of the Hsp90-M domain is suggested in most of the cases. It might be speculated that by binding to different conformations and patches, Hsp90 clients could differentially regulate the Hsp90 chaperone cycle.

### 4.2.3 Structurally unrelated client proteins differentially influence Hsp90

As analyzed in detail earlier in this work and shown in the literature, the GR-LBD has a significant effect on the ATPase activity and the cycle kinetics of Hsp90 implying a direct involvement of the GR-LBD in fine-tuning the chaperone cycle for its needs (4.1) (Lorenz et al., 2014). Previous paragraphs proved that Tau behaved considerably different from GR-LBD in terms of nucleotide dependency of binding and general binding site on Hsp90 as the two clients did not compete for binding to Hsp90. Given that Tau and GR-LBD also displayed extensive differences concerning structural features (4.2.1), it seemed likely that both clients influence Hsp90 differentially according to their requirements.

To analyze this in greater detail, ATPase activity measurements of Hsp90 were conducted with increasing Tau concentrations. The GR-LBD was added to the analysis and served as a control.

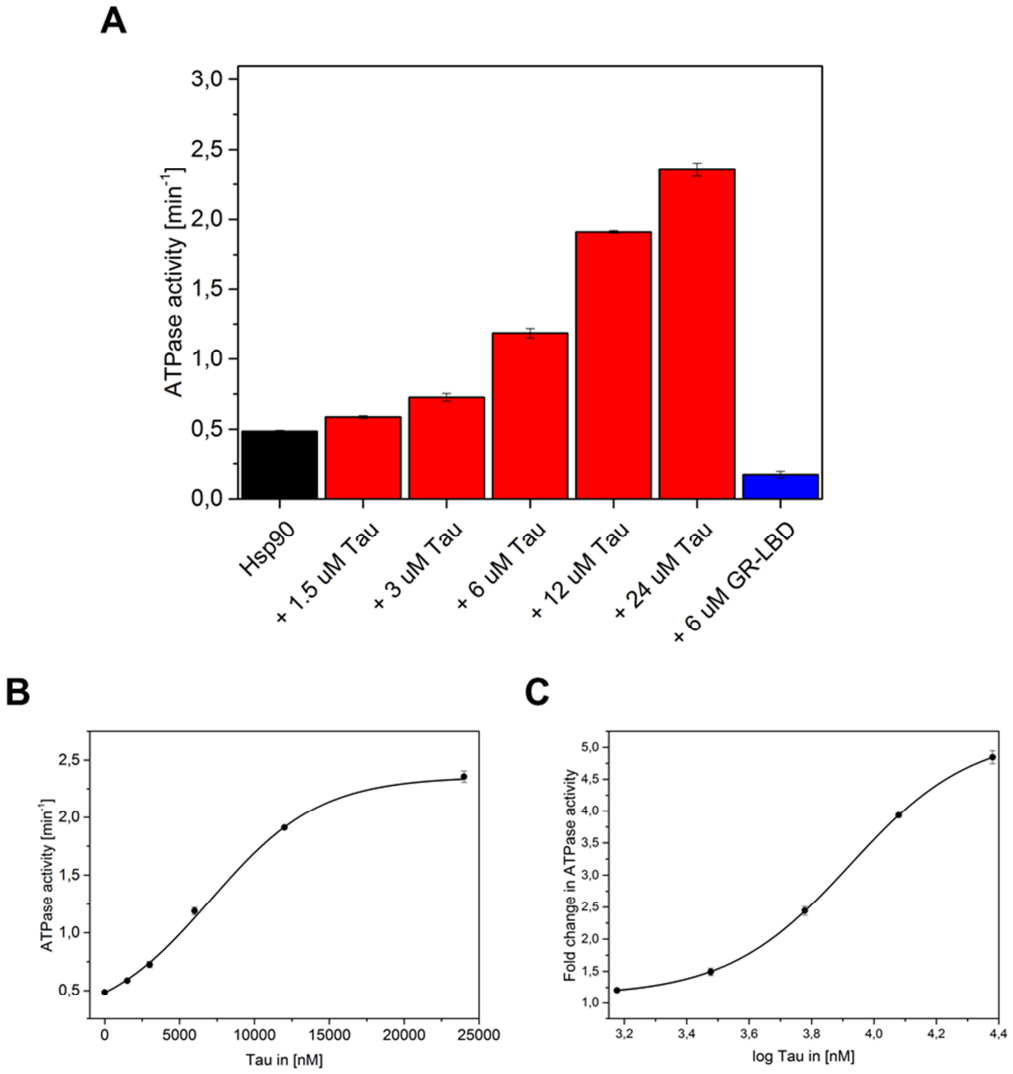


**Figure 41: ATPase activity measurements with Hsp90 in the presence of Tau and the GR-LBD; A)** ATPase activities of Hsp90 in black in the absence of Tau/GR-LBD, in red with increasing Tau concentrations as indicated and in blue with 6 µM GR-LBD. **B) and C)** ATPase activity data in the presence of Tau fitted to a dose response relationship by Origin 9.1G; Plotted were fold changes in ATPase activity against the Tau concentration in **B)** or the logarithm of the respective Tau concentration in **C)**;

Absolute ATPase activities of Hsp90 in the presence of various Tau concentrations are plotted in Figure 41 A. Surprisingly, increasing amounts of Tau could significantly stimulate the ATPase activity of Hsp90. The effect saturated at a Tau concentration of 24 µM where a five-fold stimulation in the ATPase activity from 0.5 min $^{-1}$ to 2.5 min $^{-1}$ was observed (Figure 41 A). The GR-LBD was added as control and inhibited the ATPase activity of Hsp90 by roughly 50 %, as shown previously (Figure 17) (Lorenz et al., 2014). Interestingly, the stimulation data could not

be fitted to a single site binding hyperbola. Instead, data fitted best to a sigmoidal dose response model (Figure 41 B and C) with an $EC_{50}$ of 8.3 µM which fits to the published binding constant of 5 µM (Karagöz et al., 2014).

The ATPase results suggested that the ATPase activity of Hsp90 was stimulated by Tau in a concentration-dependent manner. It has been speculated in the literature that the conformational rearrangements after ATP binding and prior to ATP hydrolysis are the rate-limiting steps in the Hsp90 cycle (Richter et al., 2008; Weikl et al., 2000). Therefore it was of interest whether Tau had an influence on the closing kinetics of Hsp90 thereby accelerating the cycle. To test this notion, Hsp90 FRET closing kinetics were recorded upon addition of ATPγS. As the ATPase activity measurements indicated a saturating effect at a concentration of 24 µM Tau, this concentration was chosen for further measurements.

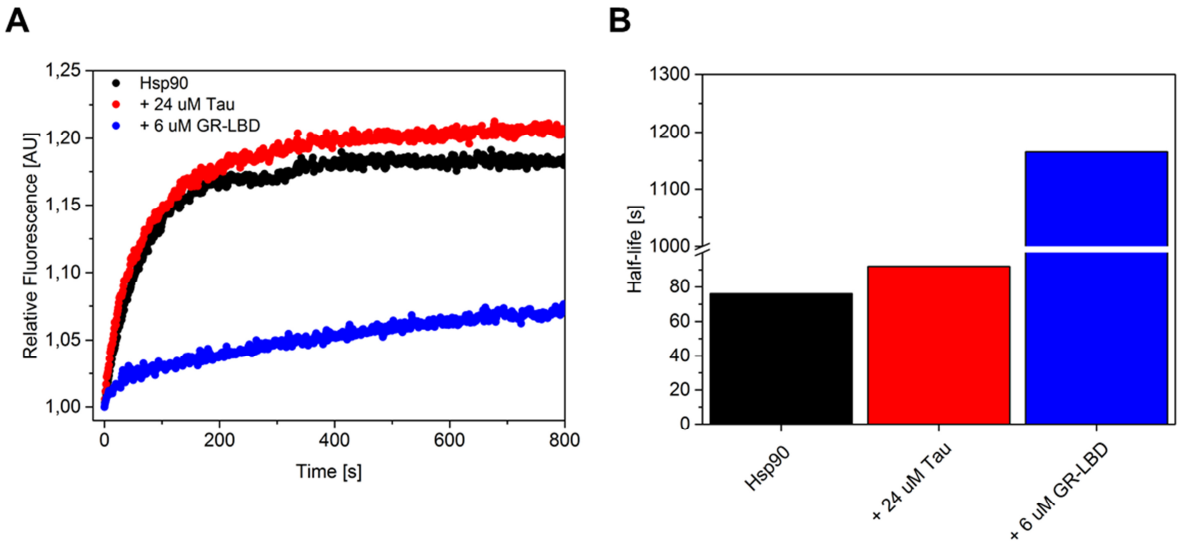


**Figure 42: Hsp90 closing kinetics in the presence of Tau and the GR-LBD. A)** FRET closing kinetics upon the addition of 2 mM ATPγS in the absence of client in black, in the presence of 24 µM Tau in red and in the presence of 6 µM GR-LBD in blue; **B)** Half-lives of the closing reactions upon addition of ATPγS;

FRET kinetics in the presence of Tau did not display significant alterations in the closing reaction in comparison to the absence of Tau (Figure 42 A). The half-life of the closure was weakly affected increasing from 76 s to 92 s which might also be within the range of variation (Figure 42 B). Various concentrations (3-36 µM) were tested but no change in the kinetics could be observed (data not shown). As expected, the GR-LBD considerably slowed down the closing kinetics with a 15 fold increase in the half-life of the reaction consistent with previous results

(Lorenz et al., 2014). These unexpected results indicate that the acceleration of the closing reaction was not the molecular basis for the increased ATPase activity in the presence of Tau, in contrast to the GR-LBD which inhibits the cycle by slowing down the closing reaction.

As the major site of interaction was found to be located in the Hsp90-N domain and the N-M interface, the increase in ATPase activity by Tau might be promoted by increased N-terminal dimerization of the Hsp90 protomers. Enhanced N-terminal dimerization has been implicated to play a role in increasing ATP affinity and ATPase activity (Pullen and Bolon, 2011). To test this idea, further Hsp90 FRET measurements were conducted. In open and closed subunit exchange measurements, the preformed FRET Hsp90 heterodimer was preincubated with or without ATPγS and the respective client protein. The subunit exchange was induced upon addition of excess of unlabeled Hsp90. As mentioned in 4.1.3.2, elongated half-lives in the exchange kinetics indicate enhanced dimerization and stronger closing of the Hsp90 dimer.

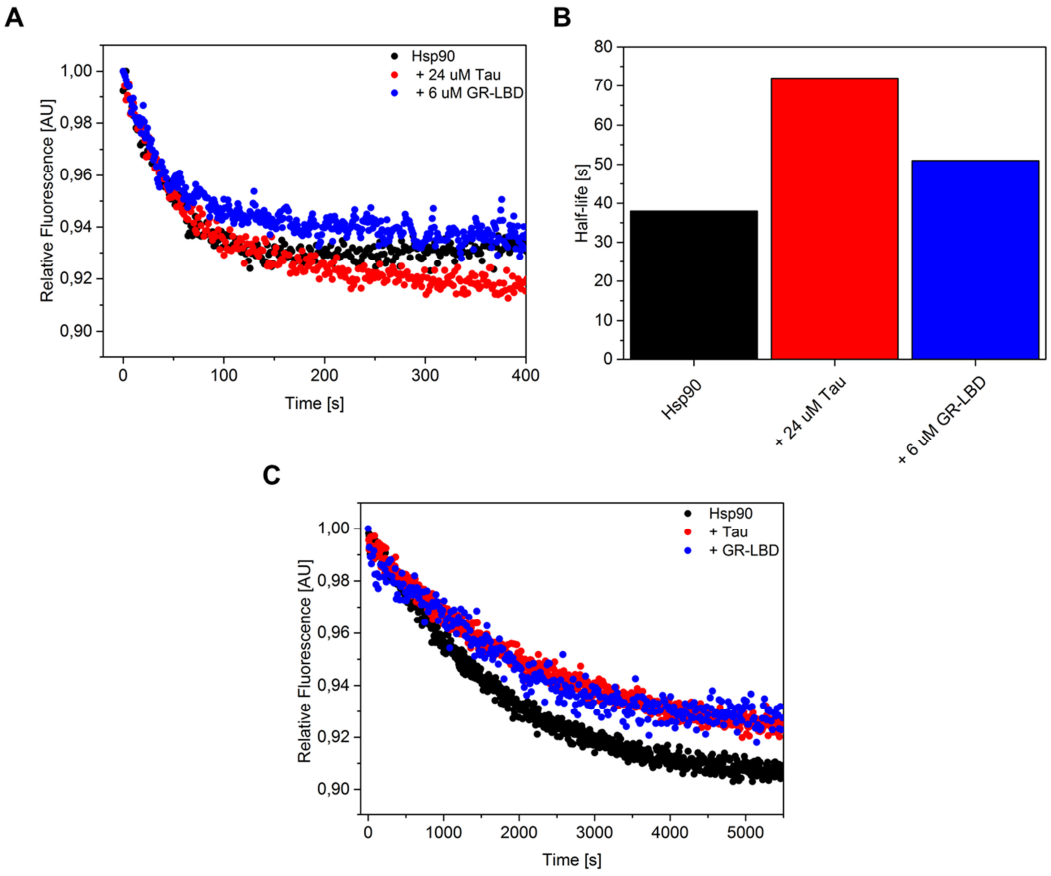


**Figure 43: Subunit exchange Hsp90 FRET measurements in the presence of Tau and the GR-LBD; A)** Subunit exchange kinetics of the open Hsp90 in the absence of client in black, in the presence of 24 µM Tau in red and in the presence of 6 µM GR-LBD in blue; Kinetics were induced by the addition of 4 µM unlabeled Hsp90. **B)** Comparison

of the half-lives for the open chases in the absence or presence of 24 µM Tau or 6 µM GR-LBD. **C)** Subunit exchange kinetics of the closed Hsp90 in the presence of 2 mM ATPγS. In black in the absence of client, in red in the presence of Tau and in blue in the presence of the GR-LBD;

First, subunit exchange kinetics were recorded in the absence of nucleotides (Figure 43 A). Interestingly, 24 µM Tau significantly increased the half-life of the subunit exchange of the open conformation by a factor of two from 38 s to 72 s (Figure 43 B). As shown earlier, also the GR-LBD was able to prolong the half-life, although not as strong as Tau. Next, closed subunit exchange measurements were conducted. The signal amplitude in these experiments is of special importance. Stronger decrease in the acceptor signal indicates more subunit exchange implying that the subunits exchange more readily. In contrast, less decrease in the acceptor signal indicates that Hsp90 dimers are more closed, thereby the exchange is hindered. The signal amplitude in the presence of Tau was indeed smaller than in the absence of client indicative of a stabilized closed Hsp90 dimer (Figure 43 C). This effect was similar to the presence of the GR-LBD in line with earlier findings that the GR-LBD also stabilizes the closed conformation (Lorenz et al., 2014). Together, the subunit exchange results were indicative for an enhanced N-terminal dimerization in line with the increase in ATPase activity in presence of Tau. Interestingly, the stabilization of the closed Hsp90 dimer results in different consequences for the Hsp90 cycle. By linking the two protomers, the GR-LBD stabilizes the dimer but also hinders reopening leading to a reduced ATPase activity. Tau in contrast, probably does not link the protomers, but simply increases N-terminal dimerization by binding to the Hsp90-N domain. Thereby, Tau does not influence reopening of the dimer, resulting in stimulation of the ATPase activity.

Pullen and co-workers observed that not only the ATPase activity was increased upon enhanced dimerization of Hsp90, but also the apparent ATP affinity (Pullen and Bolon, 2011). Thus, the ATP affinity of Hsp90 in the presence of increasing Tau concentrations was probed by ATPase activity measurements.

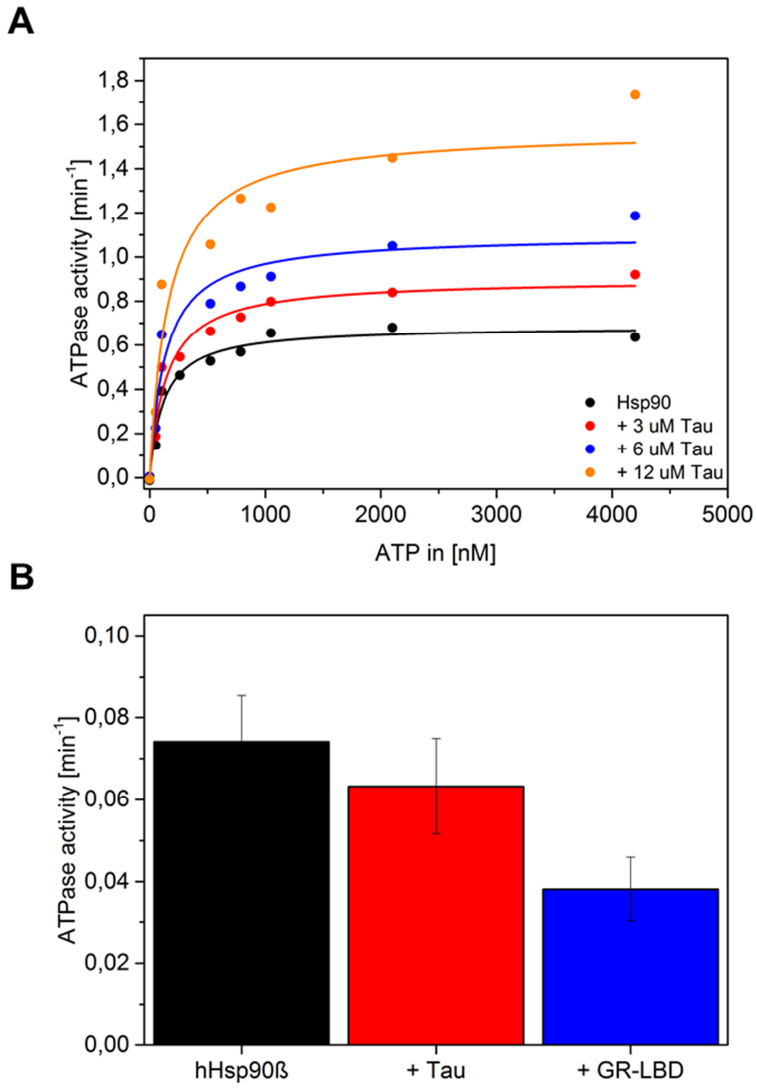


**Figure 44: ATP affinity of Hsp90 in the presence of different Tau concentrations and ATPase activity measurements of human Hsp90ß in the presence of Tau and the GR-LBD; A)** ATP affinity of Hsp90 in the presence of different Tau concentrations was determined by ATPase activity measurements. Data in the absence of Tau is shown in black, with 3 µM Tau in red, with 6 µM Tau in blue and 12 µM Tau in orange; Data was fitted according to Michaelis-Menten kinetics in Origin 9.1G. **B)** ATPase activity of human Hsp90ß in the presence of 12 µM Tau in red and 12 µM GR-LBD in blue;

Results of the measurements are shown in (Figure 44 A). In the absence of Tau, the apparent $K_M$ for ATP was determined to be 120 µM. The $K_M$ is moderately lower than previously published and reported in 4.1.7 probably due to a different purification and ATP batches (Pullen and Bolon, 2011). Increasing Tau concentrations promoted the ATPase activity of Hsp90 but did not induce

a significant increase in the affinity of Hsp90 for ATP as the apparent $K_M$ values did not significantly change (Table 7).

**Table 7: Apparent $K_M$ values of Hsp90 for ATP in the presence of increasing Tau concentrations;**

| Tau in [µM] | Apparent $K_M$ [µM] |
|---|---|
| 0 | 120 ± 25 |
| 3 | 143 ± 30 |
| 6 | 135 ± 46 |
| 12 | 159 ± 61 |

Although the ATP affinity measurements could not further support the idea that enhanced dimerization in the presence of Tau correlates with a significant change in the affinity for ATP, the subunit exchange data and ATPase measurements still supported the idea. To ensure that the provided results could be transferred to the human Hsp90 system, the ATPase activity of human Hsp90ß was assayed in the presence of Tau. The ATPase activity of Hsp90ß alone was found to be 0.072 $min^{-1}$ in line with the literature (Richter et al., 2008). Unfortunately, no increase in the ATPase activity upon addition of Tau could be observed for human Hsp90ß. The values remained within the range of variation (Figure 44). The GR-LBD significantly decreased the ATPase activity of human Hsp90ß to ~ 50 % as expected and thus ruled out problems with the assay.

Taken together, interestingly, Tau conferred considerably different effects on the Hsp90 system than the GR-LBD. The ATPase activity measurements in the presence of increasing Tau concentrations indicated a stimulatory effect of Tau. The recorded data did not fit to a single-site binding model but displayed a homo-cooperative behavior indicating that binding of two Tau molecules to the Hsp90 dimer is required to establish the stimulatory effect. As the binding curve had a sigmoidal shape, positive cooperativity of the binding was implicated. The Hsp90 dimer has in principle two available binding sites for Tau. Thus, the positive cooperativity suggests that binding of one Tau molecule seems to increase the affinity and stimulate binding of a second Tau molecule. In the future, SAXS measurements or HPLC analysis could help to support this idea and help in determining the binding stoichiometry of Tau to Hsp90. The stimulatory property of Tau is in strong contrast to the inhibitory effect of the GR-LBD on the ATPase activity. Inhibition data of the GR-LBD fitted to a single-site binding model indicating that one GR-LBD

molecule is enough to establish the effect (Lorenz et al., 2014). The differential characteristics of Tau and GR-LBD were also reflected in the influence on the conformational cycle of Hsp90. Whereas the GR-LBD dramatically slows down the closing kinetics by forming a semi-open conformation, Tau leaves the reaction unaffected. Instead, Tau showed a significantly stronger effect on stabilizing an enhanced N-terminal dimerized Hsp90 conformation in the absence and presence of nucleotide. By promoting this conformation, it seems that Tau is able to stimulate the ATPase activity. The NMR data provides an experimental basis for these observations. Binding of Tau to the Hsp90-N domain and the N-M interface might induce local conformational changes that promote N-terminal dimerization but leave the closing reaction unaffected. An explanation would be that Tau binding induces changes in the N-terminal dimerization interface strengthening the interaction of the two protomers. These Tau-induced structural changes seem to have to occur in both protomers to establish the full effect. Thereby, the induced changes in one arm facilitate Tau binding and conformational changes in the other, resulting in a positively cooperative behavior. This is supported by findings in literature where increased N-terminal dimerization was shown to positively affect the ATPase activity of Hsp90 (Pullen and Bolon, 2011; Richter et al., 2002). This idea is further backed by the AUC sedimentation analysis in Figure 34 A. Here, no additional shift to a higher S value could be observed upon the addition of ATPγS when Tau was already bound to Hsp90 supporting the idea of an enhanced N-terminally closed conformation of Hsp90 introduced by Tau. Interestingly, the ATP affinity of Hsp90 in the presence of Tau was not affected suggesting that the stimulation is solely based on the enhanced dimerization.

Both Tau and the GR-LBD stabilized the Hsp90 dimer in the presence of ATPγS. This seems to appear as a common feature but the two clients differ significantly in their effects on the ATPase activity and thereby in the Hsp90 re-opening. The GR-LBD inhibits ATPase, stabilizes a special Hsp90 conformation and prolongs thereby its interaction with Hsp90. By binding to the inside cleft of the Hsp90 dimer, the GR-LBD effectively links the protomers thereby hindering the re-opening. Tau in contrast presumably does not directly link the two protomers as its binding site is mainly located to the outside of the Hsp90 molecule. By binding to Hsp90-N and the N-M interface in one Hsp90 arm, Tau might stimulate a conformation that indirectly facilitates N-terminal dimerization but does not affect the ADP-dependent re-opening of the dimer. Thus, an increased ATPase activity can be achieved. In the presence of ATPγS, ATP hydrolysis and therefore reopening is hindered and might lead to the stabilization of the dimer resulting in a

similar effect of Tau and the GR-LBD on the closed Hsp90. To support this idea, FRET subunit exchange kinetics in the presence of ATP should be measured in the future.

Surprisingly, the stimulatory effect of Tau on the ATPase activity of yeast Hsp90 could not be reproduced in the human system. It is difficult to find reasons for this discrepancy but it might go hand in hand with the generally more open conformations and reduced tendency to form a closed conformation of the human Hsp90 (Karagöz et al., 2014; Richter et al., 2008). It is possible that human Hsp90ß is not as susceptible to the enhancement of dimerization introduced by Tau as the yeast homologue due to the generally decreased tendency to for an N-terminal dimerized state in the absence of cross-linker (Southworth and Agard, 2008). The reported findings are in line with SAXS studies of Tau and human Hsp90ß where no influence on the general Hsp90 conformation was found (Karagöz et al., 2014). It can be speculated that co-chaperones like Aha1 might synergistically work with Tau in the human system, helping to promote the influence of the client on its chaperone.

Of note, data concerning the influence of clients on the chaperone cycle except for the GR-LBD is rare. The tumor-suppressor p53 has been shown to leave the ATPase activity of yeast Hsp90 unaffected but might act synergistically together with Aha1 in stimulating Hsp90 (Hagn et al., 2011). Further analyses with different client classes are required to determine whether the presented effects for Tau and reported for the GR-LBD and p53 on Hsp90 are conserved for other clients and whether they correlate with similar preferences for certain Hsp90 conformations and binding sites on Hsp90. In the context of Tau, especially simultaneous binding of Hsp90-dependent kinases like the Src-family might be of interest as phosphorylation has been shown to significantly affect Tau function and propensity to aggregate (Fontaine et al., 2015).

### 4.2.4 Tau and the GR-LBD form different Hsp90 co-chaperone complexes

Co-chaperones form an additional level in the interplay of Hsp90 with its client proteins. It was observed that the GR-LBD allowed only a restricted set of Hsp90 co-chaperones to simultaneously associate with the client chaperone complex. Thus, it was of interest to investigate whether Tau also exhibits certain preferences when in complex with Hsp90 in terms of co-chaperone binding. To get an idea of the complexes, AUC sedimentation velocity analysis using labeled Tau, Hsp90 and different co-chaperones was performed.

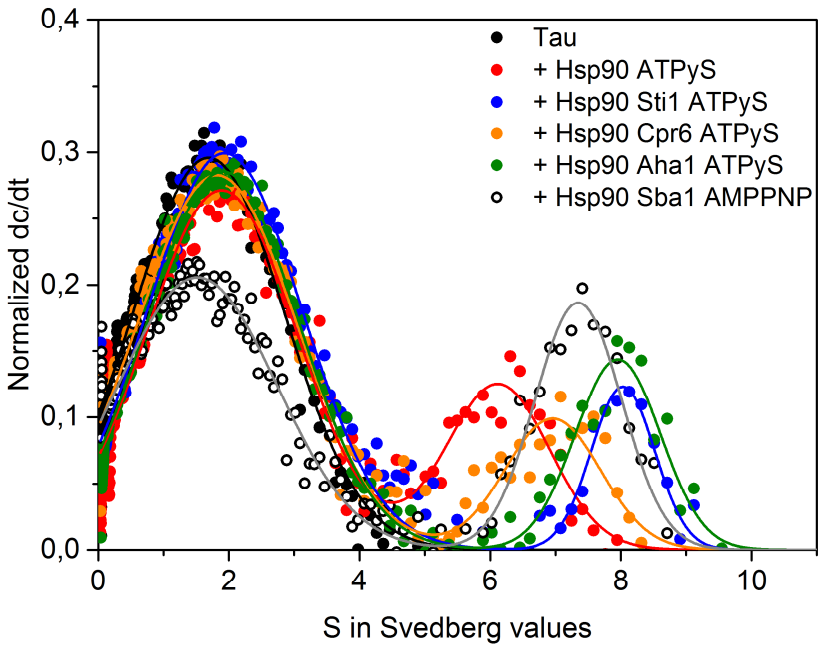


**Figure 45: AUC sedimentation velocity experiments of the Tau-Hsp90 complex together with different co-chaperones.** 400 nM ATTO488 labeled Tau (in black), was incubated with 6 µM Hsp90 (in red) and 6 µM Sti1 (blue curve), 6 µM Cpr6, 6µM Aha1 or 6 µM Sba1 in the presence of 2 mM ATPγS or AMP-PNP; Data analysis was performed using SedView 1.1 and Origin 9.1G.

The co-chaperone binding experiment is presented in Figure 45. Labeled Tau alone sedimented with an S value of roughly 2 S (black curve) but when in complex with Hsp90 and ATPγS, the S value shifted to 6 S (red curve). Interestingly, addition of Sti1 led to a further shift to 8.2 S, Cpr6 to 7 S, Aha1 to 8 S and Sba1 to 7.5 S indicating ternary complex formation in the presence of all tested co-chaperones. It seems that Sba1 might have increased the affinity of Tau for the Hsp90 complex as depicted from the amplitude of the free Tau species at 2 S but all others did not significantly in- or decrease the amount of bound Tau. It should be noted that due to a general decrease in the affinity of labeled Tau for Hsp90, as mentioned previously (Figure 33), quantitative statements should be handled carefully.

Similar to the preceding paragraphs, Tau displayed also significant differences in the co-chaperone binding to the Hsp90-client complex in comparison to the GR-LBD. It was shown that the affinity of the GR-LBD to Hsp90 is significantly decreased when Sti1 is present, presumably by induction of an open Hsp90 conformation. The PPIase Cpr6 displaces Sti1 from Hsp90, increases the affinity for the GR-LBD and promotes cycle kinetics. Sba1 then binds to a late

Hsp90-GR-LBD complex further prolonging the client chaperone interaction (Lorenz et al., 2014). Importantly, Aha1 could not be found to form a complex with Hsp90 when the GR-LBD was present, due to competition for the binding site (Figure 38) (Lorenz et al., 2014). The present data for Tau implicates no such preferences, in line with speculations in the literature (Mayer and Le Breton, 2015). Tau formed complexes with each of the tested co-chaperones and none of the chaperones significantly altered binding of Tau. The literature provides very little information about the influence of Hsp90 co-chaperones of Tau *in vitro* but *in vivo* knock-down or knock-out experiments have proven that co-chaperones regulate Tau protein levels. Knock-down of Sti1/Hop and the PPIase FKBP52 have been found to increase Tau levels in the cell whereas knock-down of Aha1 or knock-out of p23 lead to reduced Tau levels (Blair et al., 2013; Blair et al., 2014; Dickey et al., 2007; Jinwal et al., 2013b). Whether the co-chaperones affect Tau cycling *in vitro* similarly has to be investigated in further detail but the presented data implicates that the Tau affecting complexes *in vivo* also exist *in vitro.* Importantly, in this study, complexes were formed with the yeast homologues of the respective co-chaperones but preliminary data (data not shown) suggested that ternary complex formation of Tau, Hsp90 and the human PPIases (FKBP51, FKBP52 and Cyp40) is possible, similar to Cpr6 binding. This might indicate that the results for the yeast homologues can be transferred to the human system but further analyses are required. Additionally, the co-chaperone binding analysis to Tau-Hsp90 complexes should be extended to Cdc37 and PP5. Both Cdc37 and PP5 up- or downregulation has been shown in the literature to differentially affect Tau clearance and phosphorylation (Blair et al., 2014). Cdc37 would be of special interest in combination with an Hsp9-client kinase as this could provide detailed insights into the processes leading to Tau phosphorylation.

*In vitro* defined co-chaperone sets have not yet been defined for other Hsp90 clients than GR. It has been shown in the literature that p53 simultaneously stimulates the ATPase activity of Hsp90 with Aha1 (Hagn et al., 2011). Further, kinase clients require the kinase-specific co-chaperone and regulation of kinase activity is controlled by the phosphatase PP5 (Vaughan et al., 2008). Nevertheless, other possible combinations and their functional consequences remain largely uncharted territory. Further analyses could help in understanding whether client proteins also indirectly affect the Hsp90 cycle by differential co-chaperone binding besides their direct influence.

### 4.2.5 Summary and conclusion

The previous paragraphs provided information of how structurally unrelated Hsp90 clients differentially associate with and influence Hsp90 concerning functional consequences and co-chaperone binding. Sedimentation analysis and CD spectroscopy proved that Tau is a natively unfolded, monomeric Hsp90 client *in vitro*. Binding experiments using fluorescently labeled Tau indicated that Tau binds to yeast and human Hsp90 independent of the present nucleotide. NMR results using labeled isolated Hsp90-N, -M and -C domains and segmentally labeled Hsp90-NM constructs indicated that the binding site of Tau is mainly located in the Hsp90-N domain with some contributions from the Hsp90-M domain. A GR-Hsp90 FRET system and AUC sedimentation analysis demonstrated that the GR-LBD and Tau do not compete for the same binding site on Hsp90 but simultaneous association of the clients was possible. Therefore the presented data ruled out speculations from the literature that the GR-LBD and Tau binding sites overlap extensively. Analysis of the functional consequences of Tau binding to Hsp90 revealed that Tau surprisingly stimulates the ATPase activity of yeast Hsp90 in a cooperative way presumably by promoting enhanced N-terminal dimerization leaving the general closing rate and ATP affinity unaffected. Unfortunately, the stimulating effect of Tau on Hsp90 could not be reproduced for human Hsp90 probably due to the altered sensitivity of the human system to influences on the conformational ensemble. Co-chaperone binding to the Tau-Hsp90 complex revealed that, in contrast to the GR-LBD, Tau did not have any co-chaperone preferences. All tested co-chaperones could simultaneously bind and did not change the interaction of Tau and Hsp90.

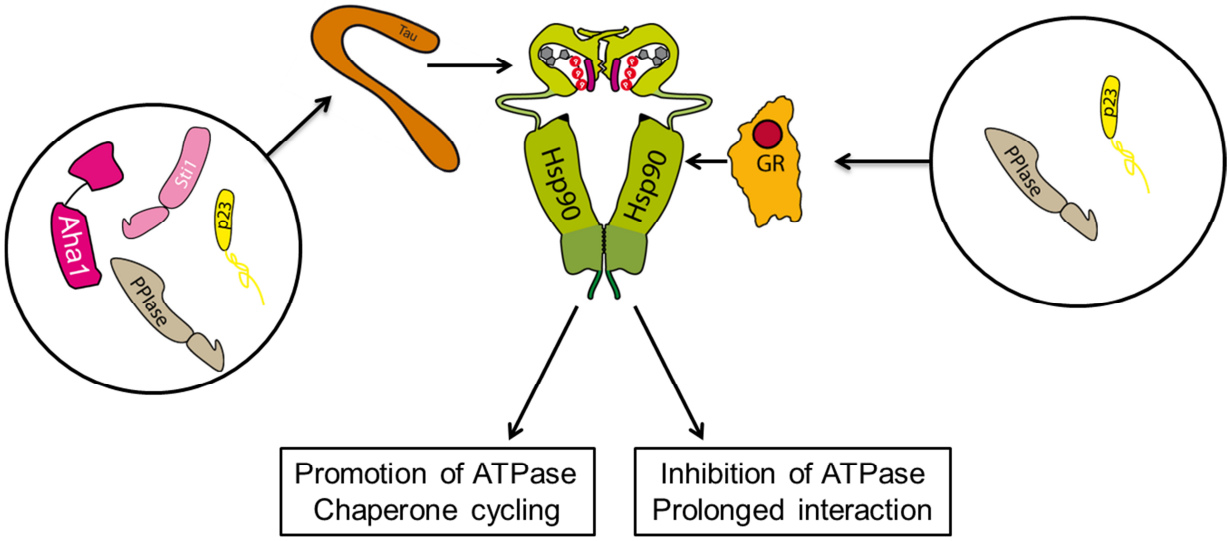


**Figure 46: Differential control of the Hsp90 chaperone cycle by structurally unrelated client proteins;** The well-folded GR-LBD preferentially binds to a semi-closed Hsp90 with a binding site mainly located within the Hsp90-M domain. By stabilization of this conformation and recruitment of a special subset of co-chaperones, the GR-LBD inhibits the ATPase activity and the cycle kinetics resulting in a prolonged interaction of the client with its chaperone. In contrast, the major interaction site of the natively unfolded Tau is located in the Hsp90-N domain. Binding of Tau leads to enhanced N-terminal dimerization of the Hsp90 dimer resulting in an increased ATPase activity promoting cycle kinetics. Further, Tau does not show preferential co-chaperone association ensuring full Hsp90 cycling.

The presented data suggests that the structurally unrelated clients Tau and GR differentially fine-tune the Hsp90 chaperone cycle depending on their requirements (Figure 46). The GR-LBD on the one hand is well-folded and is dependent on Hsp90 in regulating its action via induction of hormone binding and an Hsp90-dependent nuclear import. Thus, the GR-LBD ´wants´ to retain the association with Hsp90 and does that by binding to the dimer cleft, actively stabilizing a client-competent Hsp90 conformation in which the cycle kinetics are slowed down, thereby preventing client release. Tau on the other hand is significantly different in its structural features. Being natively unfolded, it might take a different line. In contrast to the GR-LBD, Tau binds mainly to Hsp90-N and stimulates the ATPase activity by increasing N-terminal dimerization, thereby promoting actively its chaperone cycling. Further, Tau stays bound to Hsp90 independent of the nucleotide conditions which supports the idea of steady chaperoning as it is not released during the different cycle steps. Thus it might not be the chaperone that recognizes the requirements of the client but the client tunes the chaperone according to its needs. The idea of the client tuning the Hsp90 chaperone cycle is supported by the presented binding data and

results from the literature (Hagn et al., 2011; Street et al., 2011). In contrast to previous speculations (Karagoz and Rudiger, 2015; Mayer and Le Breton, 2015), Tau and the GR-LBD seem to have significantly different binding sites on Hsp90. Thus, by binding to specialized binding surfaces in a certain Hsp90 conformation, the clients might be able to confer their influences on the chaperone. Other client binding data is rare, but the staphylococcal nuclease fragment Δ131Δ has been shown to bind to *E. coli* Hsp90 at the inner MD face with some contributions from the N-terminal domain (Street et al., 2011). Interestingly, both Tau and the model substrate Δ131Δ show a similar intrinsically disordered structure but it seems that they do not bind to the same surface on Hsp90. This might implicate that both clients have different requirements on Hsp90 and thus bind to different binding patches. This view is supported by the notion that Tau binds in a nucleotide-independent manner and that Δ131Δ prefers a closed Hsp90 conformation (Karagöz et al., 2014; Street et al., 2011). Another example is the tumor-suppressor p53. It seems that this client also has a specific binding site as it binds predominantly to the Hsp90-C domain and therefore might claim different requirements than the other client proteins (Hagn et al., 2011). Recent structural data on the kinase client Cdk4 indicate that also kinases seem to bind to specialized binding surfaces in Hsp90-M in a presumably ATP-bound Hsp90 conformation (Verba et al., 2016).

The idea of client-specific tuning of the Hsp90 cycle is further supported by the differential binding of co-chaperones to Hsp90-GR or Hsp90-Tau complexes. Whereas the GR-LBD exhibits a restricted set of co-chaperones built to support its demands on Hsp90 to prolong the interaction, Tau does not display certain preferences. This might meet the requirements of a natively unfolded client. By allowing the binding of Aha1, the two proteins might work synergistically in promoting the cycling by Hsp90. It is of speculation whether this is beneficial for Tau in the cell, but studies have shown that inhibition of Hsp90 by ATPase affecting inhibitors lead to rapid degradation of Tau (Blair et al., 2014; Dickey et al., 2007; Luo et al., 2007). Thus steady association and cycling of Tau by Hsp90 might prevent fast degradation in the cell. This idea is supported by the observation that the knock-down of Aha1, which also drives the cycle kinetics, results in rapid Tau degradation.

Altogether, the comparison of two structurally unrelated Hsp90 clients results in a differentiated picture of how Hsp90 acts on client proteins. In general, it seems that Hsp90 provides on the first hand stabilization of intrinsically instable clients by simply associating with them (Boczek et al., 2015; Taipale et al., 2012).On the other hand, it is the client that skillfully uses and dictates the

additional features of Hsp90, like chaperone cycling or recruitment of co-chaperones, to benefit from the Hsp90 interplay. This hypothesis would also provide an explanation how Hsp90 manages to chaperone its large cohort of structurally unrelated clients. It is not the chaperone that adjusts the client but the client that adapts the chaperone for its needs. Certainly, further *in vitro* analyses with client proteins from other classes like kinases or E3-ligases are required to expand this picture.

## 4.3 GR-LBD associates with Hsp40 and Hsp70 in a unique complex

Prior to the binding to Hsp90, GR is associated with Hsp70 and Hsp40 (Smith and Toft, 2008). Recent literature has shown that in this early complex of the GR-maturation cycle, the GR-LBD is not able to bind its ligand Dexamethasone (Kirschke et al., 2014). The authors explained their observations by partial opening of the ligand binding site in the GR-LBD by Hsp40 and Hsp70. Ligand binding could be fully recovered only by a chaperone system, consisting of Hop, Hsp90 and p23 (Kirschke et al., 2014). So far, literature has failed to provide detailed information about the nature of the GR-LBD-Hsp40/Hsp70 complex except that ATP is required for stable complex formation (Kirschke et al., 2014; Morgner et al., 2015). Therefore, this part of the present work was initiated to shed further light on this unique inhibitory complex.

### 4.3.1 Formation of the GR-LBD-Hsp40/Hsp70 complex

Results from the literature have shown that a MBP-fusion construct of the GR-LBD was only able to stably interact with Hsp70 in the presence of Hsp40 (Ydj1) and ATP (Kirschke et al., 2014). To reproduce the published data with a more native-like construct missing the stabilizing MBP-fusion and to acquire more information about the nature of GR-LBD binding to Hsp70, AUC sedimentation velocity experiments were performed using fluorescently labeled GR-LBD and different chaperone combinations.

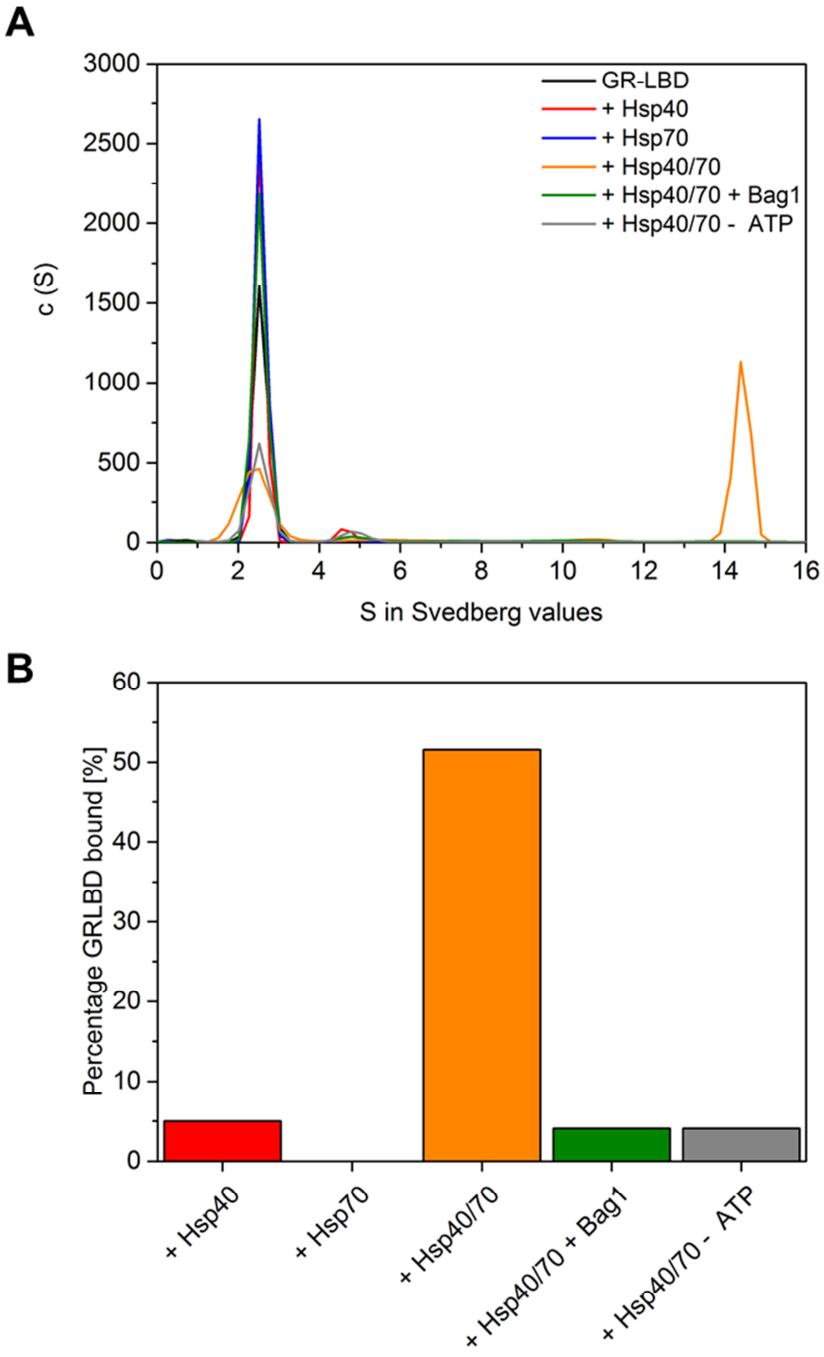


**Figure 47: The GR-LBD binds to Hsp40 and Hsp70 forming a unique complex. A)** c (S) distributions of 400 nM ATTO488 labeled GR-LBD alone in black, with 2µM Hsp40 and 2 mM ATP in red, with 6 µM Hsp70 and 2 mM ATP in blue, with 2 µM Hsp40, 6 µM Hsp70 and 2 mM ATP in orange, with 2 µM Hsp40, 6 µM Hsp70, 6 µM Bag1 and 2 mM ATP in green and with 2 µM Hsp40 and 6 µM Hsp70 in the absence of ATP in grey; **B)** Quantification of the bound GR-LBD fraction; columns indicated the percentage of labeled GR-LBD found in complex in the respective sample; Color code was maintained from **A)**; Data analysis was performed using SedFit 14.1 and Origin 9.1G.

The results of the sedimentation velocity experiment are shown in Figure 47. Similar to previously performed experiments, labeled GR-LBD sedimented with an S value of 2.7 S (black curve). Surprisingly, the addition of Hsp40 led to the appearance of a weakly populated species at 4.7 S (red curve) with an calculated apparent molecular mass of ~ 70 kDa, implying the presence of a stable GR-LBD-Hsp40 complex. The presence of Hsp70 alone did not trigger complex formation (blue curve), but Hsp40, Hsp70 and ATP promoted a dramatic shift in the S value of the GR-LBD from 2.7 S to 14.4 S (orange curve). The molecular mass of this complex was determined to be ~ 450 kDa, dependent on the estimated frictional ratio of the complex. As expected, the presence of the Hsp70 nucleotide exchange factor Bag1 or the absence of ATP prevented formation of the large 14 S complex but small quantities of the 4.7 S complex could be detected again (green and grey curves). Of note, similar results could be obtained using the longer construct GR-DBDLBD, consisting of the DNA binding domain, the hinge region and the ligand binding domain of GR (data not shown). Detailed quantification of the binding proportions revealed that the presence of Hsp40, Hsp70 and ATP significantly increased binding of the GR-LBD to the complex to roughly 50 % of bound GR-LBD at 2 µM Hsp40 and 6 µM Hsp70. The presence of only Hsp40, Bag1 or the absence of ATP reduced the fraction of the bound GR-LBD dramatically leaving 5 % of the GR-LBD associated with Hsp40. The literature indicated that efficient complex formation was only possible in the presence of ATP (Kirschke et al., 2014). To test this and whether the stable association of the GR-LBD with Hsp40 and Hsp70 was dependent on the formation of the large 14.4 S complex, an AUC sedimentation velocity experiment in the presence of different nucleotides was performed.

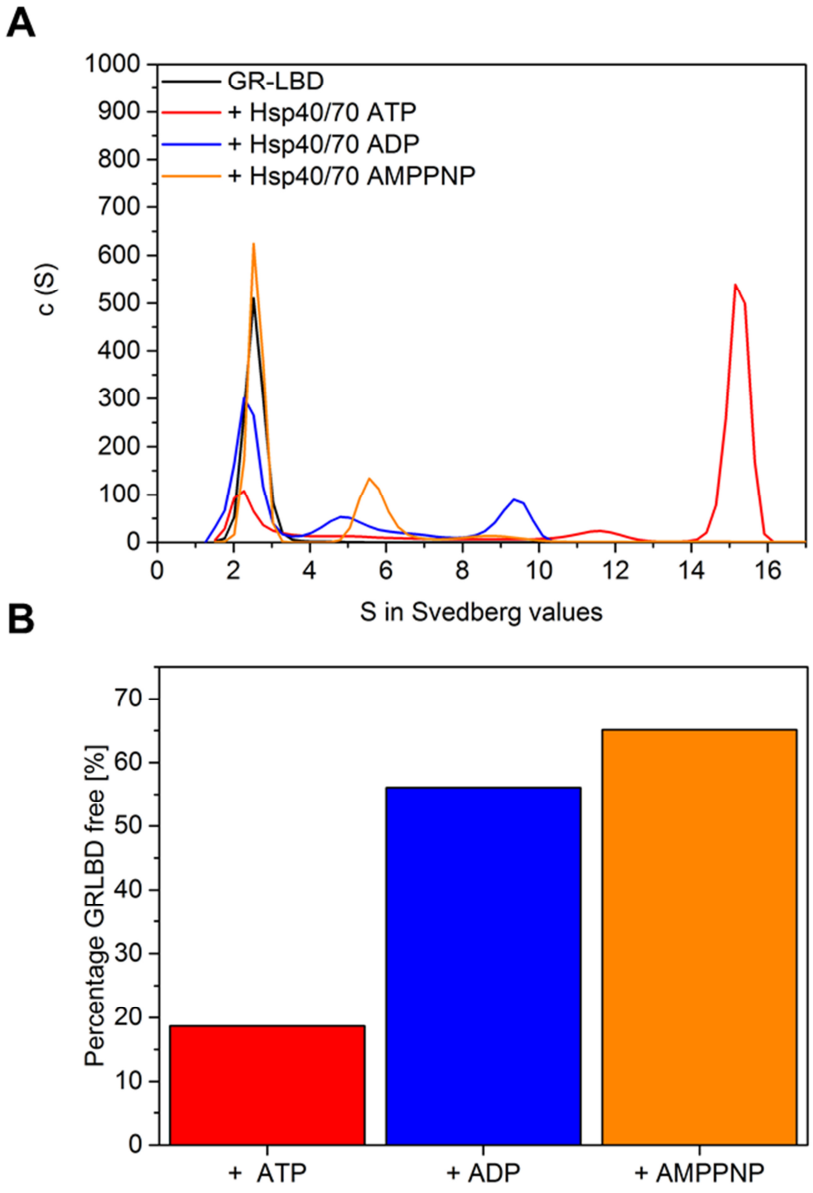


**Figure 48: AUC sedimentation analysis of the GR-LBD, Hsp40 and Hsp70 in the presence of different nucleotides; A)** c (S) distributions of 400 nM ATTO488 labeled GR-LBD alone in black, together with 2 µM Hsp40, 6 µM Hsp70 and 2 mM ATP in red, with Hsp40/Hsp70 and 2 mM ADP in blue and 2 mM AMP-PNP in orange; **B)** Quantification of the unbound GR-LBD fractions; columns indicate the amount of free GR-LBD found in the respective samples; Data analysis was performed using SedFit 14.1 and Origin 9.1G.

The sedimentation profiles in the presence of ADP and AMP-PNP were significantly altered in contrast to ATP (Figure 48 A). The GR-LBD alone sedimented at 2.7 S whereas in complex with Hsp40, Hsp70 and ATP, a species at 14-15 S could be observed, indicating formation of the large

GR-LBD-Hsp40/Hsp70 complex (black and red curve). The complex completely disappeared in the presence of ADP and AMP-PNP. ADP led to formation of an intermediate species at 9.3 S and the presumable GR-LBD-Hsp40 complex at 4.7 S (blue curve). With AMP-PNP an even smaller complex was formed at 5.8 S (orange curve). Quantification of the sedimentation velocity data implicated that efficient complex formation was only possible in the presence of ATP (Figure 48 B). In the presence of ADP or AMP-PNP ~ 60 % of the GR-LBD were unbound but the presence of ATP reduced this fraction significantly to 18 %, indicating a dramatic increase in the affinity of the GR-LBD.

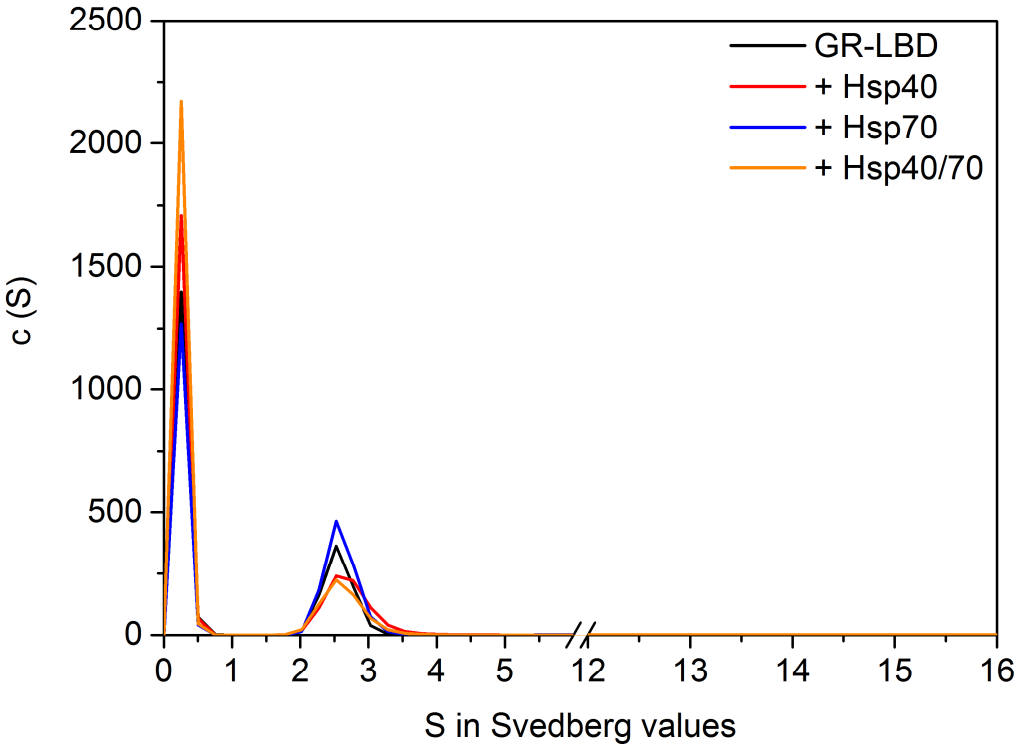


**Figure 49: Sedimentation velocity analysis of the apo GR-LBD in the presence of fluorescently labeled Dexamethasone, Hsp40 and Hsp70;** c(S) distributions of 400 nM F-Dex in the presence of 1 µM apo GR-LBD in black, with 2 µM Hsp40 and 2 mM ATP in red, with 6 µM Hsp70 and 2 mM ATP in blue and with 2 µM Hsp40, 6 µM Hsp70 and 2 mM ATP in orange; Data was analyzed using SedFit 14.1 and Origin 9.1G.

To investigate the hormone binding in the found Hsp40 and Hsp40/70 complexes in the presence of ATP, AUC sedimentation analysis was conducted using fluorescently-labeled Dexamethasone (Figure 49). Incubation of 400 nM F-Dex and 1 µM apo GR-LBD resulted in sedimentation profile containing a very small species at 0.2 S and a larger species at 2.7 S. The larger species

displayed exactly the same S value as covalently labeled GR-LBD indicating that this species was the F-Dex bound GR-LBD. Thus, the species at 0.2 S was produced by unbound F-Dex (black curve). Addition of Hsp40, Hsp70 or both in the presence of ATP did not induce a further shift in the S value of the F-Dex bound GR-LBD (red, blue and orange curves). Neither the 4.7 S nor the 14.4 S complexes appeared in the sedimentation profiles in contrast to the experiments using covalently labeled GR-LBD (Figure 47), proving that the GR-LBD is not able to bind hormone in an Hsp40/Hsp70 complex but also, surprisingly, indicating that GR-LBD is not able to bind its ligand when associated with Hsp40.

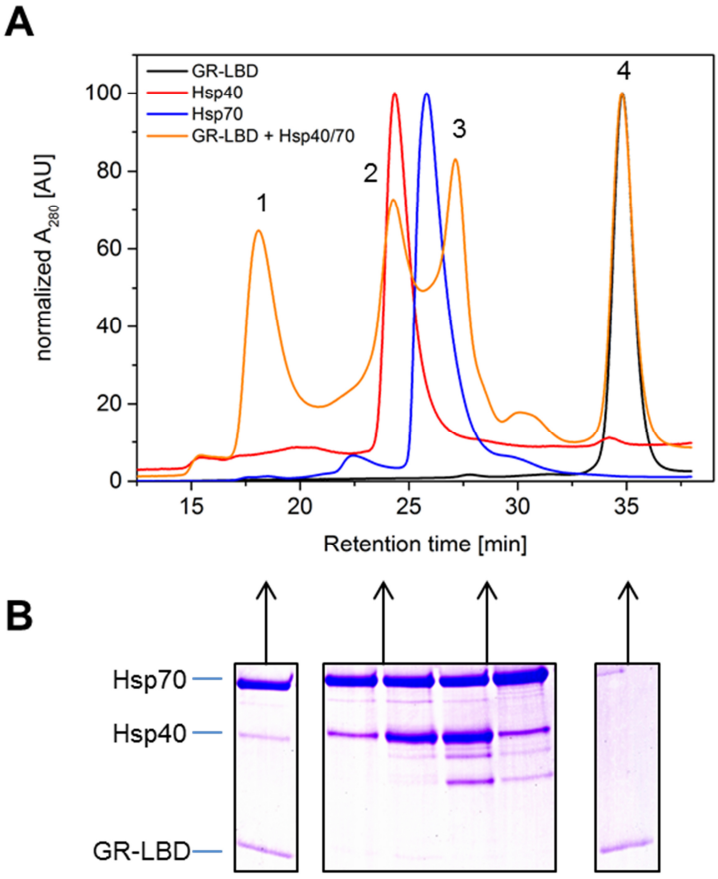


**Figure 50: HPLC analysis of the GR-LBD Hsp40/Hsp70 complex; A)** HPLC retention profiles detected by absorbance at 280 nm using single components and the preformed GR-LBD Hsp40/Hsp70 complex. 5 µM apo GR-LBD in black, 5 µM Hsp40 in red, 12 µM Hsp70 in blue and a combination of 5 µM apo GR-LBD, 5 µM Hsp40 and 12 µM Hsp70 in orange. Samples contained 2 mM ATP. Numbers indicate eluted peaks in chronological order. Absorbance data was normalized. **B)** SDS-PAGE of the peak fractions. The analyzed peaks are indicated by the respective arrows. Data analysis was performed using Origin 9.1G.

To confirm the presence of the GR-LBD-Hsp40/Hsp70 complex using a complementary analytical method, gel filtration chromatography was performed (Figure 50). The GR-LBD alone eluted after 35 min, Hsp40 alone after 24 min and Hsp70 alone after 26 min (black, red and blue curves). When a preformed GR-LBD-Hsp40/Hsp70 complex in the presence of ATP was loaded onto the column, four separate peaks could be observed with retention times of 18.2 min (peak 1), 24.3 min (peak 2), 27.2 min (peak 3) and 35 min (peak 4), respectively. To acquire information about the protein composition of these peaks, the chromatography run was fractionated and the fractions of interest were loaded on a 12.5 % SDS-PAGE. The SDS-PAGE analysis indicated the presence of Hsp70, Hsp40 and the GR-LBD in peak 1 proving the presence of all three proteins in a very large complex. In peaks 2 and 3 only Hsp70 and Hsp40 were present whereas peak 4 contained mainly the GR-LBD. Unfortunately, molecular mass determination by using a calibration curve was not successful, as the molecular mass of the single components did not provide reliable results. Thus, molecular mass determination by HPLC was abandoned.

Detailed analysis of the GR-LBD-Hsp40/Hsp70 complex by AUC and SEC-HPLC provided important information about the nature of the unique inhibitory complex. The experiments shown could support the previously published data as the GR-LBD could stably associate only in the presence of Hsp40, Hsp70 and ATP and hormone binding to the GR-LBD was not possible in this complex (Kirschke et al., 2014). The presence of ADP or AMP-PNP did not induce formation a high affinity complex but led to the formation of smaller complexes with lower affinities for the GR-LBD. Interestingly, small amounts of a stable complex consisting of the GR-LBD and Hsp40 independent of nucleotide and Hsp70 could be detected in the AUC sedimentation velocity experiment. Data analysis suggested a molecular weight of around 70 kDa indicative for a 1:1 stoichiometry of the GR-LBD-Hsp40 complex. Surprisingly, the GR-LBD could not bind its ligand in this complex indicating an important role of Hsp40 independent from Hsp70 in prevention of ligand binding. So far, it has only been described in the literature that Hsp40 together with Hsp70 prevents hormone binding to the GR-LBD in an ATP-dependent manner (Kirschke et al., 2014). Unfortunately, SEC HPLC failed to detect this species probably due to the small quantity of the complex present in the sample. Complex formation with Hsp40 might be in line with earlier findings although the provided information in the literature is contradictory. Morgner and co-workers also observed interaction of the GR-LBD with Hsp40 independent of nucleotides by native MS but text and figures mention different stoichiometries (text 1:1, figure 2:1 Hsp40:GR-LBD) (Morgner et al., 2015). The presented GR-LBD-

Hsp40/Hsp70 complex here is significantly different from what was previously shown. It was suggested by native MS data that the GR-LBD interacts with Hsp70 in 1:1 ratio without Hsp40 (Morgner et al., 2015). In contrast, the same authors presented pull-down experiments in an earlier work indicating the presence of Hsp70 and Hsp40 when pulling on MBP-GR-LBD (Kirschke et al., 2014). The data presented here suggests that the GR-LBD associates with Hsp40 and Hsp70 forming large complexes. AUC showed that the presence of the GR-LBD, Hsp40 and Hsp70 led to formation of a specific complex at 14.4 S. Further, SEC-HPLC in combination with SDS-PAGE revealed that the GR-LBD was found in the very same peak fraction as Hsp70 and Hsp40 suggesting ternary complex formation. It is difficult to deduce a complex stoichiometry from the presented data. AUC suggested a molecular mass of ~ 450 kDa. Molecular mass determination by AUC is very sensitive to the shape of the analyzed complex. As no further information about the shape of the complex is known, the calculated molecular weight should be handled with care. Rough estimation of the intensities of the protein bands on the SDS-PAGE suggested that there was significantly more Hsp70 present in the complex than GR-LBD and Hsp40. In combination with the calculated molecular mass of 450 kDa from the sedimentation velocity data, this might suggest a stoichiometry of 2:1:1 ($Hsp70_4$ : $Hsp40_2$ : $GR\text{-}LBD_2$). As this is in stark contrast to the partially contradictory published data, further information about this interesting complex is indispensable. Interestingly, a similar complex has been described by Sun et al. for DNJ-13 and Hsc70 in the absence of substrate in the *C. elegans* system indicating a general importance of this complex in the function of Hsp70 (Sun et al., 2012). Structural approaches like electron microscopy or SAXS might be able to shed further light on the nature of the complex and help to elucidate the exact complex stoichiometry presence of Hsp40 and conformation of the substrate protein.

### 4.3.2 Complex formation prevents Hormone-binding but leaves ATPase activity of Hsp70 unaffected

The previous section described that the GR-LBD is bound by Hsp40/Hsp70 in a unique large complex. It was previously described that in this complex, the GR-LBD MBP-fusion protein was unable to bind its ligand Dexamethasone and that ligand release was accelerated (Kirschke et al., 2014). To check this notion, fluorescence anisotropy-based ligand binding assays were performed

using the GR-LBD purified in the absence of stabilizing Dexamethasone lacking a solubility enhancing tag (apo GR-LBD).

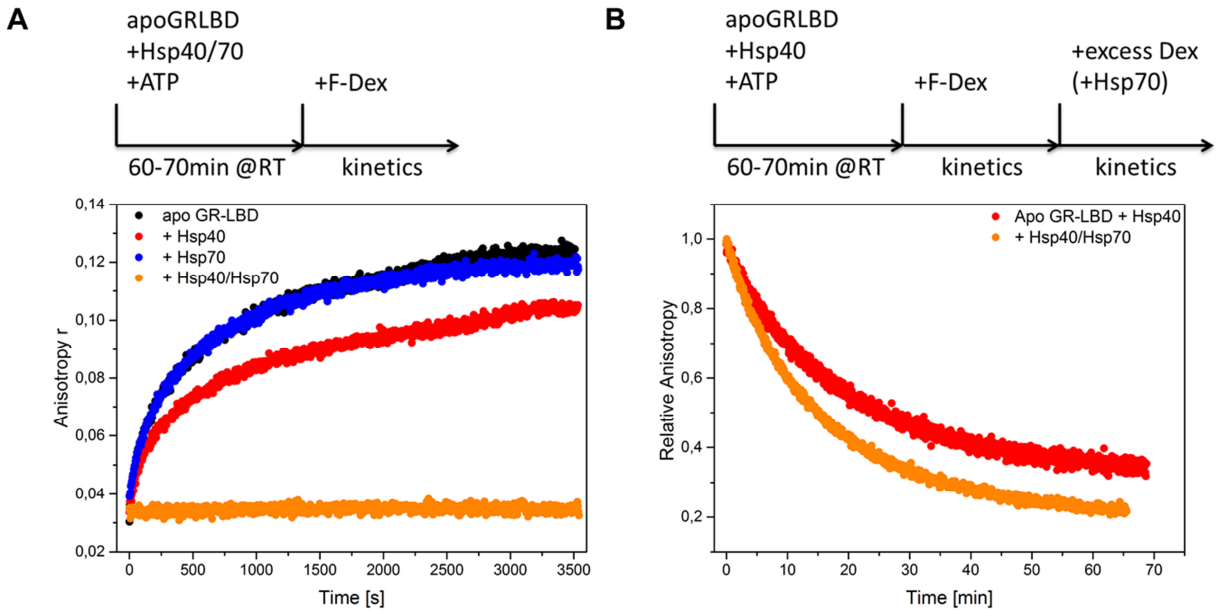


**Figure 51: Hormone binding experiments with the apo GR-LBD and different Hsp40/Hsp70 combinations; A)** Binding of 100 nM F-Dex to 1 µM apo GR-LBD in black, with 2 µM Hsp40 and 2 mM ATP in red, with 12 µM Hsp70 and 2 mM ATP in blue and with 2 µM Hsp40, 12 µM Hsp70 and 2 mM ATP in orange; **B)** Homone release kinetics; 1 µM apo GR-LBD together with 2 µM Hsp40, 2 mM ATP and 200 nM F-Dex were chased with an 100 µM excess of unlabeled Dex in the absence (red curve) or presence of 12 µM Hsp70 (orange curve); Data analysis was performed using Origin 9.1G.

Figure 50 A summarizes the results of the hormone-binding experiments to the apo GR-LBD. The apo GR-LBD was incubated without chaperones, with Hsp40, Hsp70 or both in the presence of ATP for 60-70 min at RT, prior to the addition of fluorescently labeled F-Dex and recording of the binding kinetics. The apo GR-LBD was able to bind the hormone without the help of any chaperone (black curve). Hsp70 alone did not induce significant changes in the hormone binding kinetics (blue curves). Hsp40 alone moderately reduced the anisotropy value which is in line with the previous observations by AUC that Hsp40 alone is able to reduce the hormone-binding competent fraction of the GR-LBD (red curve). Both chaperones together, completely prevented F-Dex binding to the GR-LBD (orange curve). The effect of Hsp40 and Hsp70 on hormone release was assayed by chase experiments using excess of unlabeled Dex. The apo GR-LBD was incubated with Hsp40 and ATP for 60-70 min. F-Dex was subsequently added and hormone was allowed to bind. Hormone release was induced by the addition of excess Dex in the absence or

presence of Hsp70. The kinetics revealed a moderate increase in the release rate in the presence of Hsp70 from 0.053 $min^{-1}$ to 0.064 $min^{-1}$.

As expected, the observed effects for the apo GR-LBD with solubility enhancing tag were in good accordance with the previously published data. Hormone binding to the GR-LBD was observed on a similar time-scale and the inhibitory effect of Hsp40 and Hsp70 could be nicely reproduced. Hormone release rates were not as strongly affected by the presence of Hsp70 as shown by Kirschke and co-workers. The authors observed a two fold increase in the release rate (k (w/o Hsp70) = 0.029 $min^{-1}$ vs. k (Hsp70) = 0.066 $min^{-1}$) (Kirschke et al., 2014). The rate of hormone release in the presented data was only 1.2 fold increased by Hsp70, indicating that the effect on the release of hormone from the GR-LBD that was purified in the complete absence of hormone might be weaker. An explanation for this could be that the apo GR-LBD structure is affected in a way leading to a generally enhanced hormone release. This is in line with the increased exchange rate in the absence of Hsp70 in comparison to the published data. Nevertheless, the presented data suggests that the inhibitory effect of Hsp40 and Hsp70 seems to hold true also for a GR-LBD construct that is closer to the native GR protein. Surprisingly, Hsp40 alone moderately affected hormone-binding to GR-LBD which is in line with the AUC experiments in the presence of F-Dex (Figure 49) which supports the idea of Hsp40 independently affecting hormone binding to the GR-LBD. As this effect has not been previously described, certainly more experimental data is required to draw further conclusions and therefore current models should be handled with care. In future experiments, concentration-dependent binding of Hsp40 to GR-LBD or the concentration dependency of Hsp40 on the prevention of hormone binding should be investigated to support the presented data.

So far the data here and published in the literature focused on the effects of Hsp40 and Hsp70 on the GR-LBD but it remained unclear how Hsp70 is affected in this unique complex. To get further information about the influence of the GR-LBD and Hsp40 on Hsp70, ATPase activity measurements of Hsp70 were performed in the presence of the GR-LBD and Hsp40 (Figure 52).

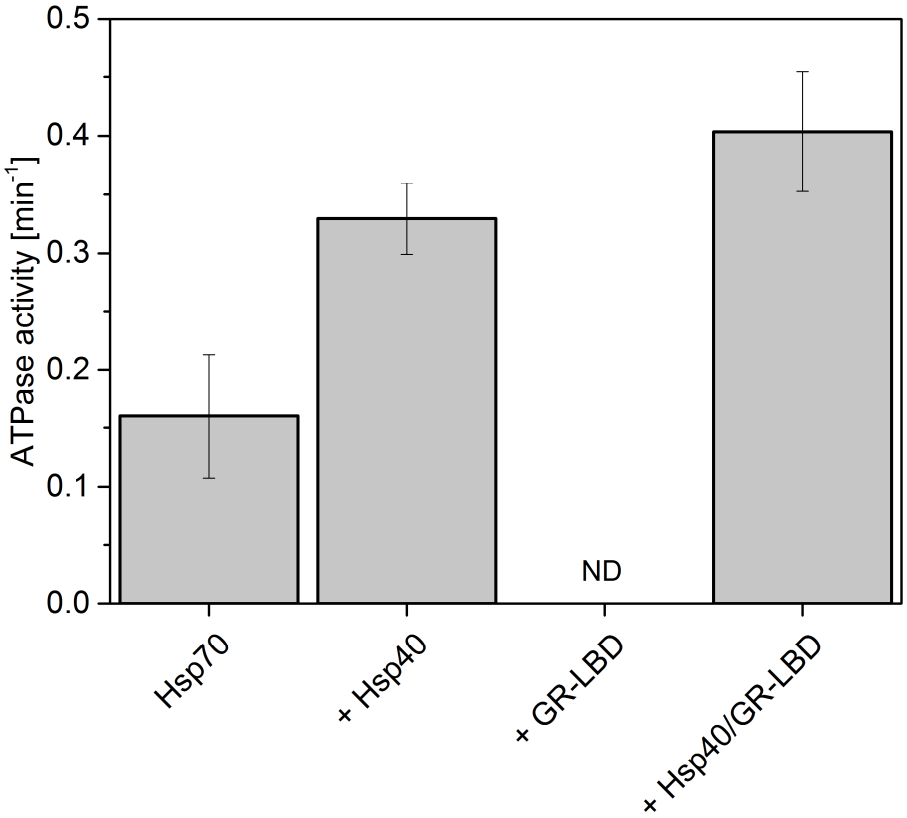


**Figure 52: ATPase activity of Hsp70 in the presence of Hsp40 and GR-LBD;** Columns show absolute ATPase activities of 4 µM Hsp70 in the respective combinations. 2 µM of GR-LBD and 2 µM of Hsp40 were added to the respective samples. ATPase activity in the presence of only GR-LBD could not be determined due to severe thermal aggregation of the apo GR-LBD (ND). Data analysis was performed using Origin 9.1G.

In the absence of additional factors, Hsp70 exhibited a ATPase activity of 0.15 $min^{-1}$, similar to previously published values for human Hsp70, Hsp40 was able to stimulate the ATPase by a factor of two (Schlecht et al., 2013; Tsai and Douglas, 1996). The ATPase activity in the presence of only apo GR-LBD could not be determined due to severe aggregation of the apo GR-LBD. Combination of all three factors resulted in an ATPase activity similar to the activity in the presence of only Hsp40 indicating no further effect of the GR-LBD on the ATPase or the stimulatory effect of Hsp40. Interestingly, the GR-LBD did not aggregate in the presence of Hsp40 implying that when bound to the complex, self-association is prevented.

The ATPase activity measurements supported previous speculations that ATP hydrolysis is important for the binding of the GR-LBD to the Hsp40/Hsp70 complex as AMP-PNP and ADP failed to form a high affinity complex (Figure 48) (Kirschke et al., 2014) indicating that the

conformational changes occurring upon ATP hydrolysis are a prerequisite for GR-LBD binding. Of note, the GR-LBD did not further stimulate ATP hydrolysis of Hsp70. This is in strong contrast to the classical picture of substrate peptides increasing the ATPase activity of Hsp70 (Fan et al., 2003). Although the GR-LBD is probably partially unfolded when bound by Hsp70 (Kirschke et al., 2014), this client might act differentially on Hsp70 due to a different binding mode than a small peptide substrate. This idea is supported by results from the literature where peptide- and protein-substrates haven been shown to differentially influence the Hsp70 ER-homologue BiP (Mayer et al., 2003).

### 4.3.3 Influence of co-/chaperone binding to the GR-LBD Hsp40/Hsp70 complex

#### 4.3.3.1 Hormone-binding recovery by the complete chaperone system

The previous sections suggested that the GR-LBD is bound by Hsp40 and Hsp70 in a unique inhibitory complex. The presented results indicated a significantly different complex than previously published. It was shown in the literature that the full chaperone system of Hop, Hsp90ß and p23 is required to restore the full hormone binding activity by the GR-LBD MBP-fusion construct (Kirschke et al., 2014). Although the preceding results implied that the apo GR-LBD used here behaved highly similar to the MBP-fusion protein, hormone binding recovery was assayed using the complete chaperone system. In contrast to the literature, the analysis was extended by assessing the influence of Hop and p23 in the absence of Hsp90ß.

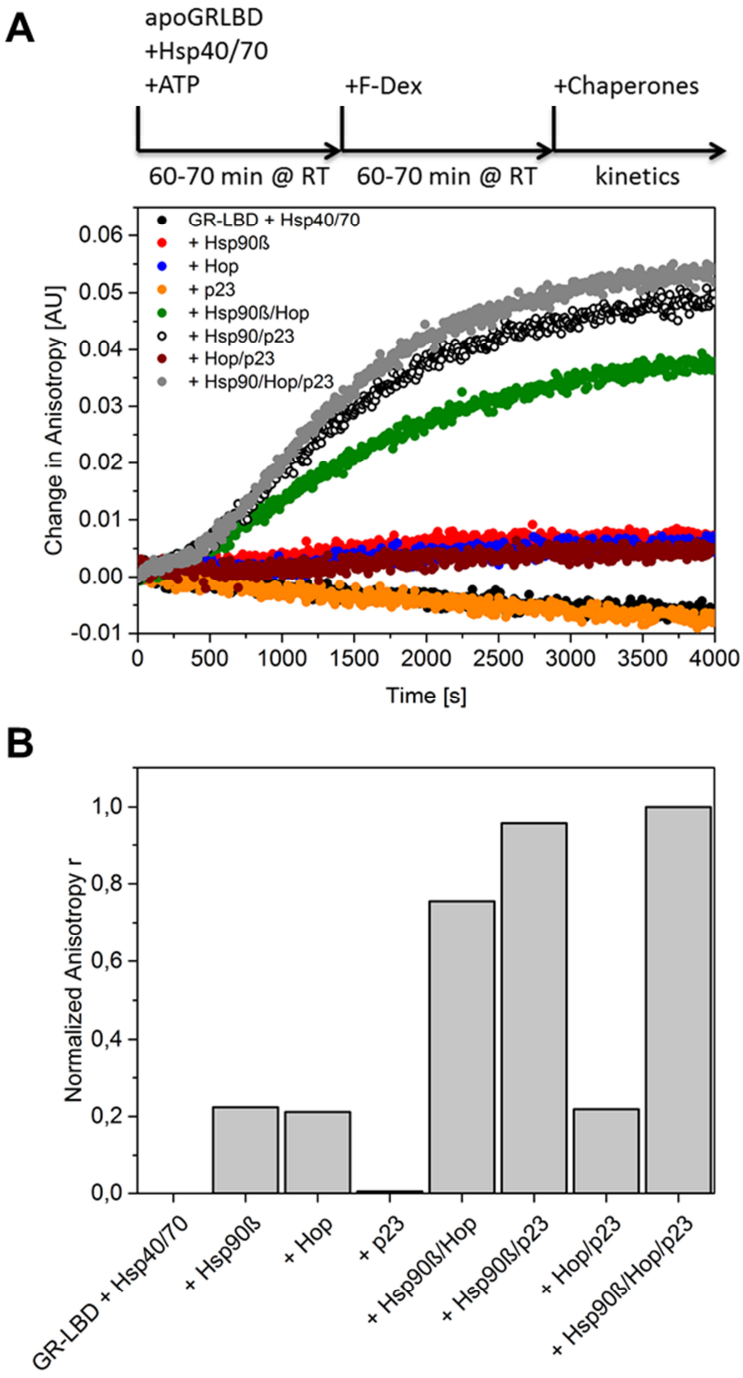


**Figure 53: Hormone binding recovery of the GR-LBD from Hsp40/Hsp70 complexes in the presence of different chaperone combinations. A)** Hormone binding recovery kinetics of 1 µM apo GR-LBD in the presence of 100 nM F-Dex, 2 µM Hsp40 and 12 µM Hsp70 in black, chase kinetic including 12 µM Hsp90ß in red, including 12 µM Hop in blue, including 12 µM p23 in orange, including 12 µM Hop and Hsp90ß in green, including 12 µM Hsp90ß and p23 in black open circles, including 12 µM Hop and p23 in brown and including 12 µM Hop, Hsp90ß and p23 in grey; All kinetics were measured in the presence of 2 mM ATP. Relative changes in the anisotropy signal were plotted. **B)** Normalized anisotropy equilibrium values from chase kinetics in **A)**. Equilibrium end values were

normalized to the end value in the presence of the full chaperone system. Data analysis was performed using Origin 9.1G.

The hormone binding recovery of the GR-LBD from Hsp40/Hsp70 complexes was assayed performing chase kinetics. First, the apo GR-LBD was incubated for 60-70 min at RT with Hsp40 and Hsp70 in the presence of 2 mM ATP to ensure the formation of the inhibitory complex. In a second step, F-Dex was added to the complexes and incubation was continued for another 60-70 min at RT. Finally, hormone binding kinetics were induced by the addition of different chaperone mixtures and recorded (Figure 53 A). The results revealed the importance of different co-/chaperone combinations in the efficient hormone-binding recovery (Figure 53 A and B). As expected, in the presence of Hsp40 and Hsp70, no hormone binding was detectable (black curve) and also the presence of only p23 did not induce significant hormone binding recovery (orange curve). Interestingly, Hop and Hsp90ß alone, as well as the combination of Hop and p23, were similarly able to induce slight hormone binding (red, blue and brown curve). The combinations containing Hsp90ß and Hop or p23 were able to induce significant hormone binding with the Hsp90-p23 combination being slightly more efficient (black open circles and green curve). The combination of all three chaperones was, expectedly, most efficient in hormone-binding recovery (grey curve) of the GR-LBD originating from the Hsp40/Hsp70 complex. By plotting the anisotropy equilibrium values, the mentioned effects became more evident (Figure 53 B).

The results with the apo GR-LBD are in good accordance with results from literature using the GR-LBD MBP-fusion construct (Kirschke et al., 2014). The full chaperone set was also most efficient in inducing hormone binding whereas differences between the full chaperone system and the binary combinations of Hsp90ß and Hop or p23, respectively appear to be less significant. Interestingly, Hop on its own could induce hormone binding similar to Hsp90ß alone whereas p23 was not able to promote any hormone binding. The slight increase in hormone binding in the Hop/p23 combination can therefore be attributed to Hop. The results suggest that Hop might act independently on the GR-LBD-Hsp40/Hsp70 complex beyond passively linking the chaperone cycles of Hsp70 and Hsp90.

#### 4.3.3.2 Hop alters the interaction of the GR-LBD with Hsp40 and Hsp70

The previous section indicated that Hop might act independently on the GR-LBD-Hsp40/Hsp70 complex as addition of Hop alone was able to stimulate partial hormone binding. Thus, the

effects of Hop regarding GR-LBD-Hsp40/Hsp70 complex formation and hormone binding ability in the complexes were tested by AUC sedimentation velocity experiments using labeled GR-LBD or F-Dex. Further the influence of Hop on the ATPase activity in the Hsp70-complex was assayed.

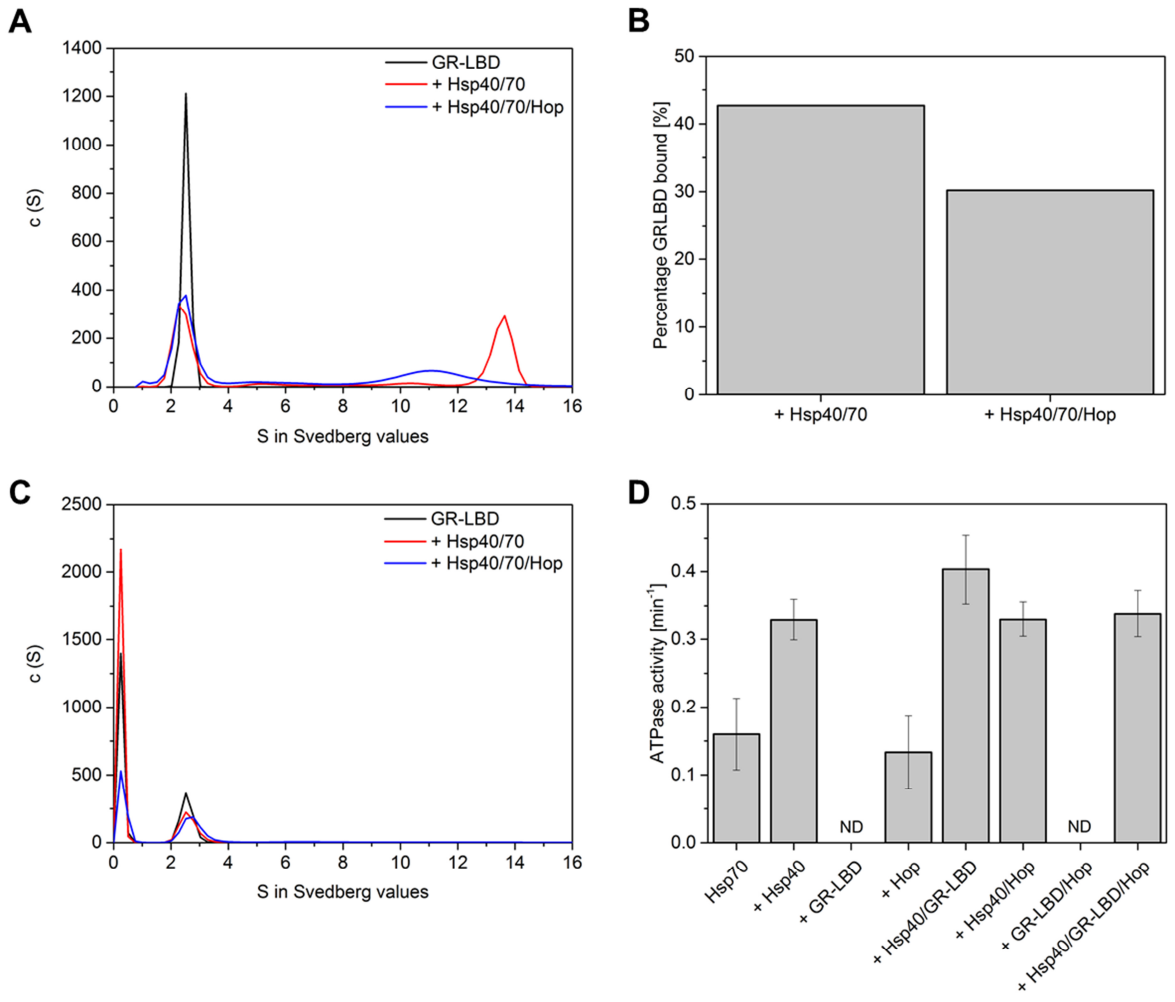


**Figure 54: Influence of Hop on the GR-LBD-Hsp40/Hsp70 complex; A)** c (S) distribution of 400 nM ATTO488 labeled GR-LBD in black, together with 2 µM Hsp40, 6 µM Hsp70 and 2 mM ATP in red and upon the addition of 6 µM Hop in blue; **B)** Quantification of the bound GR-LBD species from the c (S) distributions in **A)**; **C)** c (S) distributions of 400 nM F-Dex in the presence of 1 µM apo GR-LBD in black, together with 2 µM Hsp40, 6 µM Hsp70 and 2 mM ATP in red and upon addition of 6 µM Hop in blue; Data analysis was performed using SedFit 14.1. **D)** ATPase activities of Hsp70 in the presence of different Hsp40, Hop and GR-LBD combinations; Samples including GR-LBD in the absence of Hsp40 showed significant aggregation and ATPase activities could therefore not be determined (ND). Shown are mean values and error bars of three independent measurements. Data analysis was performed using Origin 9.1G.

First, AUC sedimentation velocity experiments using labeled GR-LBD in the presence of Hsp40, Hsp70 and were performed (Figure 57 A). The GR-LBD alone sedimented at 2.7 S but when in complex with Hsp40 and Hsp70, the S value was dramatically increased to ~ 14 S, in line with previous results (Figure 47). Surprisingly, the addition of Hop to the GR-LBD-Hsp40/Hsp70 led to the disassembly of the 14 S complex and in the formation of a new, broad species at ~ 11 S (Figure 54 A). Further, the addition of Hop significantly decreased the amount of the complex-bound GR-LBD (Figure 54 B). In the absence of Hop, more than 40 % of GR-LBD was bound in the Hsp40/Hsp70 complexes, whereas in the presence of Hop the species was reduced to below 30 %. The GR-LBD alone bound fluorescently labeled Dexamethasone as deduced from the species appearing at 2.7 S in addition to the free F-Dex species at 0.2 S (Figure 54 C, black curve). Interestingly, the GR-LBD was not able to bind F-Dex in the new broad species at 11 S in the presence of Hop, similar to the species at 14 S in the absence of Hop, as no peaks at 11 S and 14 S were detected (Figure 54 C, red and blue curves). ATPase activities were not significantly affected by the presence of Hop. Hsp70 alone displayed again an ATPase activity of 0.15 $min^{-1}$ and addition of Hsp40 led to a two fold increase, as shown previously (Figure 52 D). The presence of Hop alone or in combination with Hsp40 and/or GR-LBD did not induce any changes in the ATPase activities. Of note, the presence of the apo GR-LBD in the absence of Hsp40 resulted again in significant aggregation of the GR-LBD. Thus, ATPase activities could not be determined.

The data concerning the influence of Hop on the GR-LBD-Hsp40/Hsp70 complex support the idea that Hop on its own modulates GR-LBD binding to Hsp40 and Hsp70. Surprisingly, Hop disassembled the GR-LBD-Hsp40/Hsp70 14 S complex leading to the formation of a new species around 11 S. Thus, it is obvious that binding of Hop to the complex altered the stoichiometry. As the peak in the c (S) distribution appeared to be very broad it seems that this was not a single species, but might represent a heterogeneous population. It has been shown in literature that Hop binds preferentially to ADP-bound Hsp70 and that Hsp40 stimulates Hop binding by ATP conversion (Hernandez et al., 2002; Johnson et al., 1998). These observations might provide reasons for the change in complex stoichiometry when Hop is present. One might reason that binding of Hop induces a conformational change in Hsp70 resulting in the ADP-bound conformation leading to disassembly of the GR-LBD-Hsp40/Hsp70 complex. It can be speculated that this change is necessary for the formation of the client transfer complex with Hsp90 as the transfer might not be possible from the initial GR-LBD-Hsp40/Hsp70 complex.

Further analyses are required to investigate the precise processes occurring upon Hop binding to the GR-LBD-Hsp40/Hsp70 complex, but recent results implicated that Hsp40 is not present in the Hsp70-Hsp90 transfer complex (Alvira et al., 2014). These results might implicate the release of Hsp40 from the complex upon binding of Hop. Of note, the presence of Hop moderately decreased the affinity of the GR-LBD in the Hsp40/Hsp70 complex as the fraction of bound GR-LBD was decreased. The released fraction might be able to bind hormone and contribute to the increase in hormone binding as seen in Figure 53. The Hop-induced decrease in the affinity might also play a role in the client transfer process. By lowering the affinity of the GR-LBD for the Hsp40/Hsp70 complex, it might be more favorable for GR to move to the Hsp90-p23 complex resulting in client transfer from the Hsp70 to the Hsp90 system. This idea is further supported by the literature. When Hop is bound only to Hsp90, the conversion of Hsp90 to the p23-bound form is blocked resulting in a low affinity for GR in the Hsp90-Sti1/Hop complex (Johnson et al., 1998; Lorenz et al., 2014). This is not the case when Hop is associated with Hsp70 and Hsp90 (Hernandez et al., 2002). Thus, the conformational transition of Hsp90 to a highly affine conformation for GR is possible in the transfer complex. Presenting this special conformation might promote subsequent client transfer. The ATPase activity measurements further support this idea as ATP hydrolysis is possible in every complex promoting the entry of Hop and progression of the transfer process. In the future, it is necessary to acquire more information on the changes in stoichiometry upon entry of Hop. SAXS, electron microscopy data or GR-Hsp70/Hsp40 FRET systems could be helpful in shedding further light on the processes leading to disassembly of the GR-LBD-Hsp40/Hsp70 complex and entry of Hop. Further it would be of interest which Hop domains are involved and whether the switch of Hsp70 from TPR1 to TPR2B controlled by Hsp90 plays a role in these processes (Rohl et al., 2015b). Therefore, the usage of Hop domain constructs could be of interest in the future.

### 4.3.4 Establishing single-molecule FRET and force spectroscopy systems for the GR-LBD

It was shown in the previous paragraphs that upon binding to Hsp40 and Hsp70, the GR-LBD loses its ability to bind hormone. Recently performed HDX analysis suggested local conformational changes in the hormone binding site induced by Hsp70 to be responsible for this

effect (Kirschke et al., 2014). As the provided information was limited and it was of interest to study the influence of other co-/chaperones on the GR-LBD in greater detail in the future (Hop, Hsp90, p23), a single molecule GR-LBD system was developed. For this purpose, GR-LBD constructs applicable for single molecule FRET and force spectroscopy measurements were designed containing either two genetically introduced cysteines at the N- and C-terminus or only one at the N-terminus for labeling with different FRET dye pairs or DNA-handles (Figure 55, Figure 56 A).

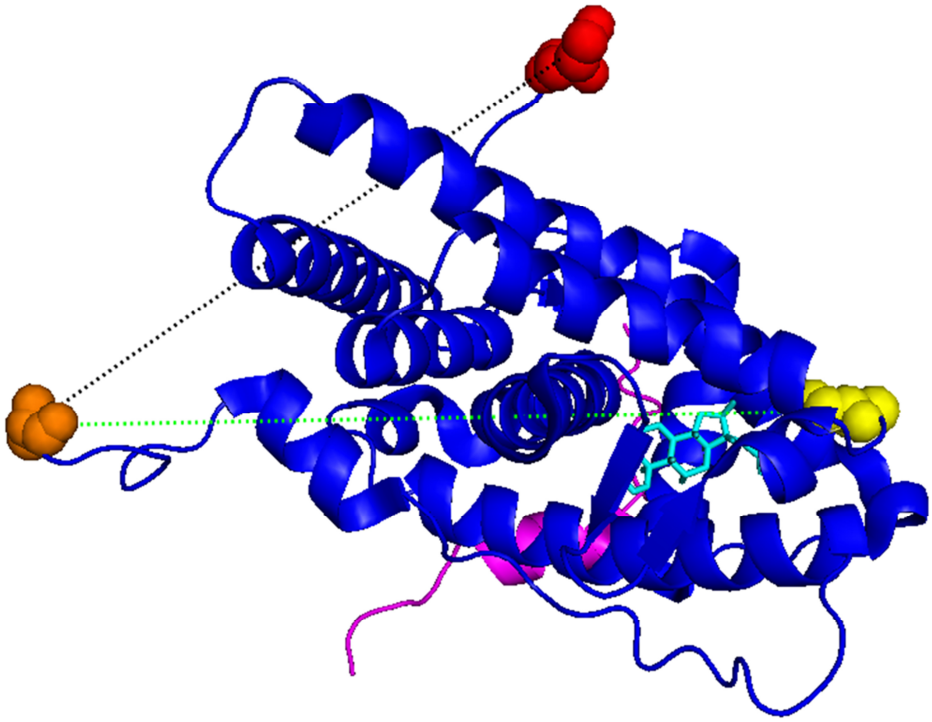

**Figure 55: Positions and distances of labeling positions in the single-molecule GR-LBD constructs;** The GR-LBD (PDB ID: 1M2Z) is shown in blue with the transcriptional co-activator peptide derived from Tif-2 in magenta and bound Dexamethasone in cyan. The N-terminal alanine is colored in orange, the C-terminal Lysine in red and C638 in yellow. The distance between N- and C-terminus is represented by a black dashed line (46.9 Å) and between N-terminus and C638 by a green dashed line (58.1 Å).

It was previously shown that the GR-LBD can be specifically labeled at C638 (Lorenz et al., 2014). Thus, for the construct containing cysteines at the N- and C-terminus, C638 was exchanged to aspartate (smGR-LBD) to ensure specific labeling only at the termini. In the construct containing only an N-terminal cysteine, C638 was retained for labeling (NC-GR-LBD). By using the smGR-LBD construct, general influences on the GR-LBD fold could be probed

whereas the NC-GR-LBD should be especially useful for monitoring conformational changes due to hormone binding/release as C638 is positioned in a helix close to the hormone binding site (Figure 55). Of note, cysteine residues at the N- and C-terminus were embedded within a neutral hydrophobic and a lysine (NC: ACK, CC: LCK) to increase labeling rates.

### 4.3.4.1 Basic characterization of different single-molecule constructs

The two single-molecule constructs were expressed in *E. coli* and purified to homogeneity in the presence of Dexamethasone to increase the stability of the constructs (Lorenz et al., 2014). Prior to performing the single molecule measurements, the constructs were characterized concerning general structural integrity, stability and oligomerization. The standard GR-LBD construct was included for comparison to ensure that the single-molecule constructs behaved similarly.

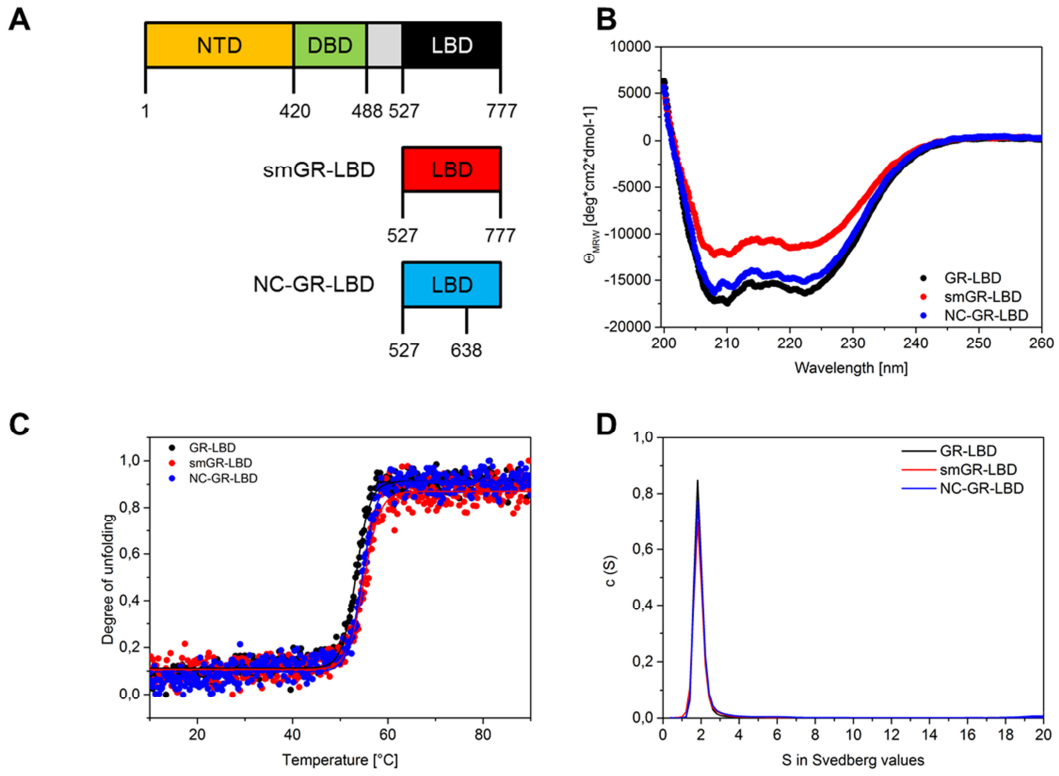


**Figure 56: Basic characterization of single molecule GR-LBD constructs; A)** Domain architecture of the GR and the single molecule GR-LBD constructs; N-terminal domain of the GR is colored in yellow (NTD), the DNA-binding domain (DBD) in green, the hinge-region in grey and the LBD in black; Numbers indicate domain boarders; The smGR-LBD is shown in red and the NC-GR-LBD in blue; Numbers indicate the position of the introduced

cysteine residues for labelling; **B)** Far-UV CD-spectra of 0.1 mg/ml GR-LBD constructs in the presence of 10 µM Dexamethasone; GR-LBD is shown in black, smGR-LBD in red and NC-GR-LBD in blue; The color code was maintained for the following figures; **C)** Thermal unfolding of different GR-LBD constructs monitored by CD spectroscopy; **D)** Absorbance AUC sedimentation velocity experiments using different GR-LBD constructs; Data analysis was performed using SedFit 14.1 and Origin 9.1G;

In the presence of Dexamethasone, the two single-molecule constructs displayed highly α-helical spectra, similar to the standard GR-LBD construct typical for SHR LBDs (Figure 56 B) (Wurtz et al., 1996), although the smGR-LBD showed slightly decreased signal intensities. Thermal unfolding monitored by CD spectroscopy produced highly cooperative transitions with melting temperatures of around 55°C for all three constructs (Figure 56 C). AUC sedimentation velocity analysis coupled to absorbance detection proved that the two constructs were monomeric and sedimented with an identical S value of 2.7 S like the standard GR-LBD construct (Figure 56 D). Altogether, the basic structural and oligomerization analysis could not detect significant differences in comparison to the standard GR-LBD construct proving the suitability for further experiments. As the single-molecule measurements were intended to investigate the structural consequences of chaperone binding to the GR-LBD, it was necessary to analyze the binding of the designed constructs to the two major chaperones of interest, Hsp90 and Hsp70.

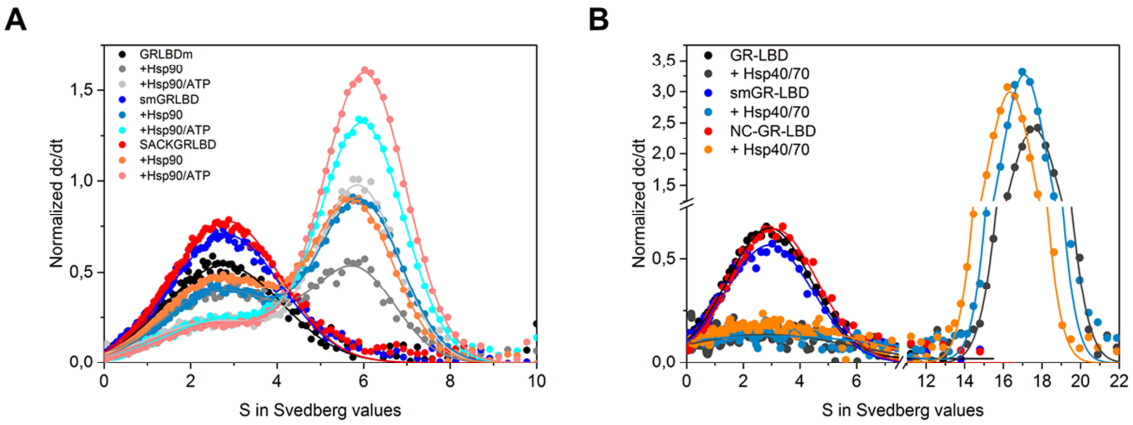


**Figure 57: Binding analysis of the single-molecule GR-LBD constructs to Hsp90 and Hsp70; A)** Binding of different GR-LBD constructs to Hsp90; 400 nM ATTO488 labeled GR-LBD or single molecule constructs were analyzed alone or together with 3 µM Hsp90 in the presence of absence of 2 mM ATP; **B)** Binding of different GR-LBD constructs to Hsp40/Hsp70; 400 nM ATTO488 labeled GR-LBD or single-molecule constructs were analyzed alone or together with 2 µM Hsp40, 6 µM Hsp70 and 2 mM ATP; Data was analyzed using SedView 1.1 and Origin 9.1G.

The binding of the two single-molecule constructs was assayed using AUC coupled to fluorescence-detection and labeled GR-LBD constructs. Both labeled single-molecule GR-LBD

constructs sedimented alone with an S value of 2.7 S identical to the standard GR-LBD construct. Addition of Hsp90 led to the known shift to 6 S, indicating complex formation for all used constructs (Figure 57 A). When ATP was incorporated in the analysis, both single-molecule GR-LBD constructs displayed an increase in the affinity for Hsp90 as deduced from the decrease in the amplitude of the free GR-LBD species at 2.7 S, similar to the standard GR-LBD construct. Association with Hsp70 presented a similar picture (Figure 57 B). In the presence of Hsp40, Hsp70 and ATP all tested constructs formed a large complex around 15 S indicating similar complex formation also with Hsp70. The experiments suggested that the single-molecule constructs bound the most important chaperones Hsp90 and Hsp70 identical to the usually used GR-LBD construct. In a last step, the influence of the single molecule constructs on Hsp90 was assayed by ATPase activity and FRET measurements.

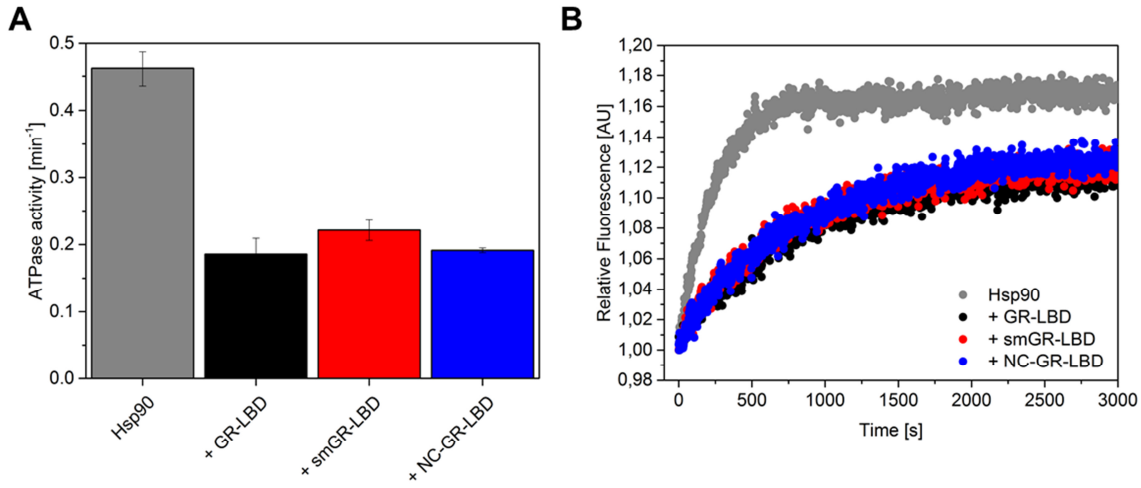


**Figure 58: Functional influence of different GR-LBD constructs on Hsp90; A)** ATPase activity measurements of 3 µM Hsp90 in the absence of client in grey, in the presence of 6 µM of the standard GR-LBD construct in black, 6 µM of the smGR-LBD in red and 6 µM NC-GR-LBD in blue; **B)** ATPγS induced closing kinetics of Hsp90 in the presence of different single-molecule GR-LBD constructs; Same color code as in **A)** was used. Data analysis was performed using Origin 9.1G.

The ATPase activity of Hsp90 was clearly inhibited by ~ 50 % in the presence of the standard GR-LBD or the single molecule constructs (Figure 58 A). In line with the ATPase measurements, ATPγS-induced closing kinetics of the Hsp90 dimer were significantly decelerated by the GR-LBD and the single-molecule LBDs (Figure 58 B). The results indicated that the introduced mutations did not significantly alter the inhibitory properties of the GR-LBD on the Hsp90 cycle kinetics (Figure 58).

Altogether, the basic characterization of the single-molecule GR-LBD constructs proved that the designed constructs behaved highly similar concerning general folding, oligomerization, interaction with and influence on chaperones suggesting high suitability to assess the influence of chaperones on the structure of GR-LBD in single-molecule FRET and force spectroscopy measurements.

#### 4.3.4.2 Single-molecule FRET measurements

Since the basic characterization of the single-molecule constructs did not indicate any changes in the LBD in comparison to the standard GR-LBD construct, initial single-molecule (sm) FRET experiments of the constructs alone and in the presence of Hsp40/Hsp70 were conducted. To this end, single-molecule construct were differentially labeled at the introduced cysteine residues using ATTO532 and ATTO647 maleimide as described in 3.4.6. The FRET pair ATTO532-647 has a Förster radius of 60 Å and was considered to be suitable for monitoring conformational changes within the GR-LBD between N- and C-terminus (46.9 Å) and between the N-terminus and C638D (58.1 Å) (Figure 55). The smFRET measurements, data analysis and figure preparation were conducted in cooperation with Daniela Wengler and Don Lamb at the Ludwig-Maximilians-Universität München.

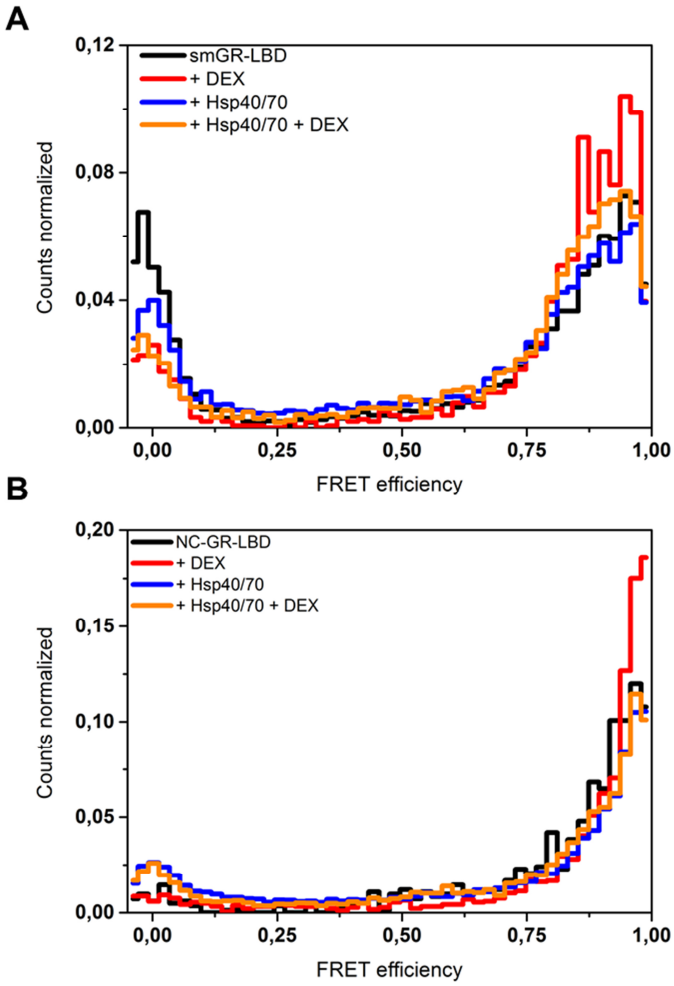


**Figure 59: Single-molecule FRET experiments with the smGR-LBD and the NC-GR-LBD in the presence of Hsp40 and Hsp70; A)** SmFRET distributions of smGR-LBD alone in black, with 50 µM Dexamethasone in red, with 2 µM Hsp40 and 12 µM Hsp70 in the presence of 2 mM ATP in blue and with 2 µM Hsp40, 12 µM Hsp70, 2 mM ATP and 5 µM Dexamethasone in orange; **B)** SmFRET distributions of NC-GR-LBD alone in black, with 50 µM Dexamethasone in red, with 2 µM Hsp40 and 12 µM Hsp70 in the presence of 2 mM ATP in blue and with 2 µm Hsp40, 12 µM Hsp70, 2 mM ATP and 5 µM Dexamethasone in orange; SmFRET measurements, data analysis and figure preparation were performed in cooperation with Daniela Wengler and Don Lamb (Ludwig-Maximilians-Universität München).

Figure 59 A illustrates the recorded data for the smGR-LBD construct labeled with ATTO532 and ATTO647. Two distinct FRET species were detected in the FRET distributions of all tested combinations. One species exhibited a very high FRET efficiency of ~ 0.9 representing the folded GR-LBD with the dyes being in close proximity (46.9 Å) whereas the other species showed very low FRET efficiencies of ~ 0 indicating the presence of 3-5 % of unfolded GR-LBD. This observation was supported by the fact that addition of 50 µM Dexamethasone

significantly decreased the low-FRET species (red distribution) and increased the high-FRET species, respectively. This is in line with the notion that excess of hormone increases the stability of the GR-LBD leading to an increase in the fraction of stably folded GR-LBD. Interestingly, addition of Hsp40, Hsp70 and ATP in the presence and absence of Dexamethasone did not induce any intermediate FRET species. Also the low- and high-FRET species remained largely unaffected although the high-FRET species was less increased than in the presence of only Dexamethasone probably due to decreased hormone binding in the Hsp40/Hsp70 complex. As no intermediate FRET population appeared upon addition of Hsp40/Hsp70, the results suggested no large conformational changes in the GR-LBD upon binding to Hsp40/Hsp70.

As previously mentioned, the smGR-LBD construct was designed to monitor large conformational changes in the GR-LBD but as the literature showed that binding of Hsp40/Hsp70 mainly affects the ligand binding site (Kirschke et al., 2014), smFRET experiments were also performed with the NC-GR-LBD construct labeled with ATTO532 and ATTO647. Due to the positioning of the C638 close to the hormone binding site (Figure 55), larger differences in the FRET efficiencies were expected in the free and bound GR-LBD. Unfortunately, the smFRET measurements in (Figure 59 B) showed no significant differences in the FRET populations in comparison to the smGR-LBD construct. Again, a very low-FRET (FRET efficiency ~ 0) and a very high-FRET species (FRET efficiency ~ 0.9) were observed, but no intermediate population appeared upon addition of Hsp40, Hsp70 and ATP (blue and orange populations). Only an increase in the high-FRET population by addition of Dex was again detected, consistent with the idea of an increase in the folded GR population in the presence of hormone (red distribution). To rule out that small conformational changes were not observed due to the relatively large Förster radius of 60 Å of the chosen FRET pair, other dye pairs with shorter radii were assessed ( ATTO488-647 $R_0$ = 51 Å, ATTO488-700 $R_0$ = 44 Å), but no significant improvement of the data was achieved (data not shown).

Altogether, the smFRET measurements did not provide additional information on the effects of Hsp40/Hsp70 on the GR-LBD. In the future, further labeling positions or incooperation of the N-terminal DNA-binding domain of the GR could be assessed to produce data with higher information content. Additionally, smFRET measurements using Hsp90, co-chaperones or the full chaperone system respectively should be conducted and might provide important information about the structural consequences of chaperone binding and cycling on the GR-LBD.

### 4.3.4.3 Unfolding the GR-LBD by force

In addition to the smFRET measurements, initial single-molecule force spectroscopy measurements were performed using the smGR-LBD construct and a custom-built dual-trap optical tweezer system (3.5.3). The initial measurements should provide information about the general functionality of the system and preliminary results concerning the influence of chaperone binding to the GR-LBD. Measurements were performed in cooperation with Thomas Suren and Matthias Rief at the Technische Universität München.

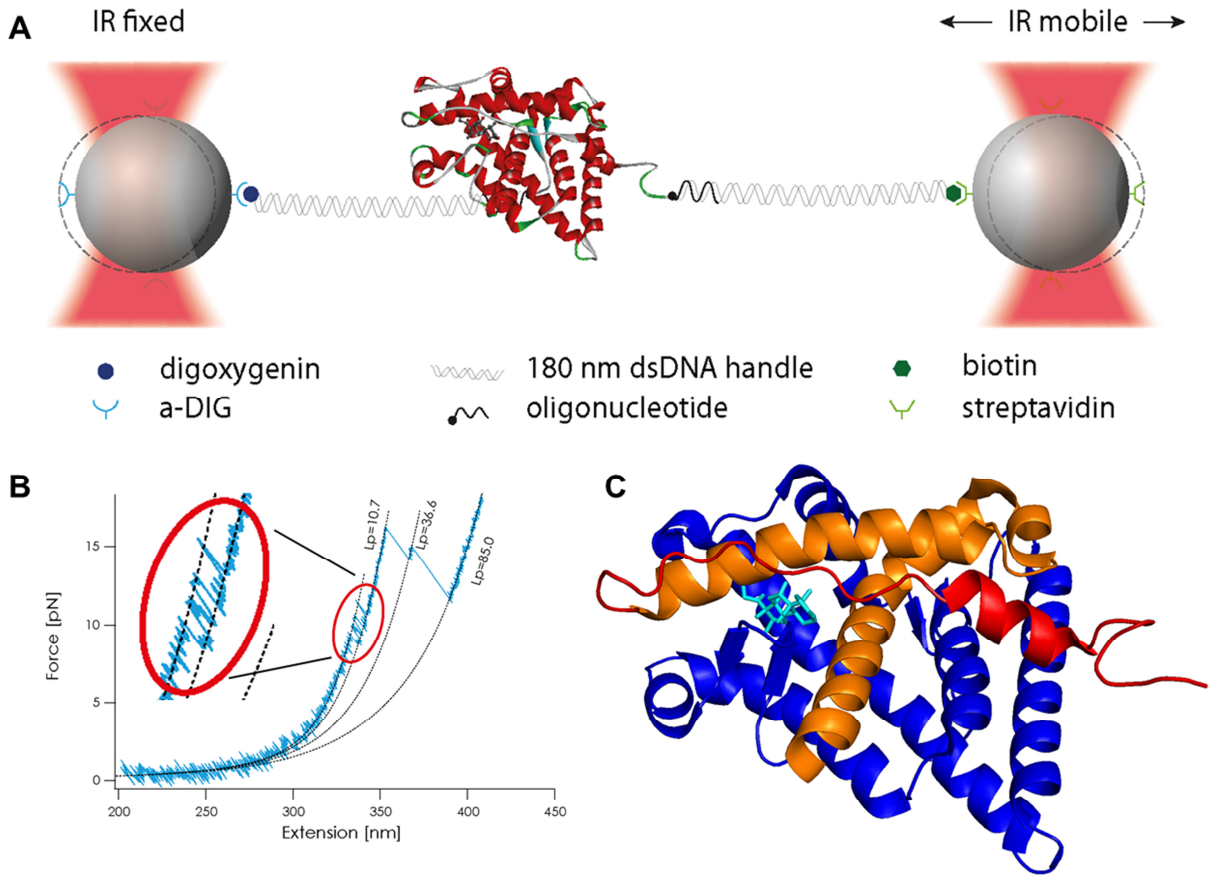


**Figure 60: Unfolding the GR-LBD by force; A)** Schematic representation of the experimental setup for monitoring GR-LBD unfolding by force. The GR-LBD (PDB ID: 1M2Z) is linked via maleimide chemistry to DNA-oligonucleotides that are hybridized with DNA-handles. DNA-handles are marked with digoxygenin or biotin, binding to anti-digoxygenin or Streptavidin coated silica beads that are held in optical traps. By moving one bead away from the other force is applied to the GR-LBD leading to (partial) unfolding. **B)** Exemplary force-extension trace of the GR-LBD; the unfolding trace shows successive unfolding in three steps. Unfolding fits to a worm-like chain model and average contour length gains for each step are indicated. Inset shows "flipping" of the first unfolding step at a force of ~ 10 pN. **C)** Mapping of the assumed unfolding steps onto the GR-LBD structure (PDB ID: 1m2z); First unfolding step with a corresponding contour length gain of 10.7 nm (positions 523-554) is shown in

red, the second unfolding with a corresponding contour length gain of 25.9 nm (positions 555-617) in orange, the remaining structure of the GR-LBD in blue and the bound ligand Dexamethasone in cyan; Measurements, data analysis and figure preparation was performed in cooperation with Thomas Suren and Matthias Rief (Technische Universität München).

Figure 60 A shows a schematic representation of the experimental setup. In brief, the smGR-LBD construct containing cysteine residues at the N- and C-terminus were labeled with maleimide functionalized DNA-oligonucleotides and subsequently hybridized with digoxygenin- or biotin-functionalized DNA-handles. The handles were then non-covalently linked to anti-digoxygenin or streptavidin functionalized silica beads held by the optical trap generating the functional setup. Unfolding of the GR-LBD was assessed in force–extension experiments by moving the silica beads apart at constant speed (10 nm/s) (Figure 60 B). Interestingly, the GR-LBD unfolded in three steps. An initial small unfolding step corresponding to a gain in contour length of 10.6 nm, a second large unfolding event with a gain in contour length of 25.9 nm and a final unfolding event resulting in the completely unfolded GR-LBD with a contour length of 85 nm. Assigning the contour lengths to possible structural elements in the crystal structure of the GR-LBD (PDB ID: 1M2Z) revealed that the first unfolding event with a contour length increase of ~ 10 nm fits to helix 1 and a linker part (colored in red, Figure 60 C) whereas the second unfolding event with a gain in the contour length of ~ 25 nm could match to unfolding of helices 3-5 (colored in orange). The final step might then correspond to unfolding of the remaining structure (colored in blue). Interestingly, the first step, assigned to helix 1 and a linker part, did not directly unfold but instead showed significant “flipping” indicative for un- and refolding of this structural segment when force was applied (inset, Figure 60 B). As this part was in close proximity of the hormone-binding pocket it was assumed that this flipping might indicate opening and closing of the lid over ligand binding site. To generate a more detailed picture of these processes, time-resolved force experiments were conducted.

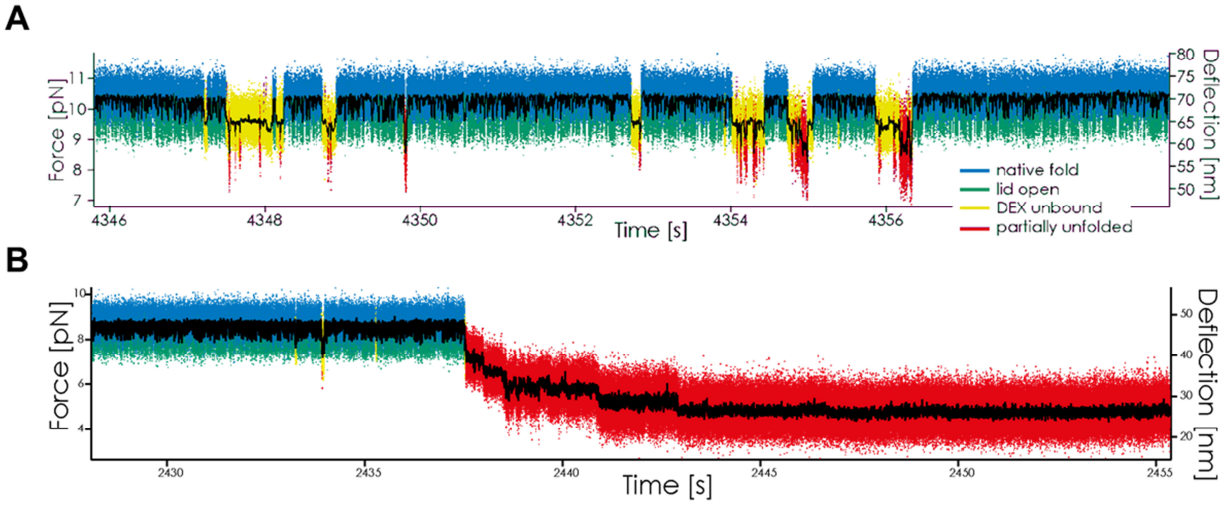


**Figure 61: Time-resolved force experiments of the GR-LBD; A)** Kinetics of the GR-LBD alone; the native GR-LBD fold is stable at around ~ 10 pN (blue shading) and "flipping" of the lid segment (green shading) possibly leads to release of Dexamethasone resulting in an apo-state of the GR-LBD (yellow shading) stable at ~ 9.5 pN. From the apo-state the GR-LBD potentially transits to a partially unfolded state (red shading). **B)** Kinetics in the presence of 2 µM Hsp40, 8 µM Hsp70 and 2 mM ATP**.** After initial "flipping" of the N-terminus (blue and green shading), the GR-LBD transits and stays in an unfolded state stable at ~ 4.5 pN. Measurements, data analysis and figure preparation was performed in cooperation with Thomas Suren and Matthias Rief (Technische Universität München).

The time-resolved force experiment of the GR-LBD alone is illustrated in Figure 61 A. Similar to the force-extension experiments, the kinetics displayed a native GR-LBD fold which was stable around 10 pN (blue shading) and additional "flipping" of the structural part that was assigned to the lid over the hormone binding site consisting of helix 1 and a linker part (green shading) indicating opening of the lid. From this lid-open fold it seemed that the GR-LBD could transit to another fold that was stable at 9.5 pN (yellow shading). Additional kinetic measurements indicated that the dwell-time of the GR-LBD in this second state is strongly dependent of the Dexamethasone concentration. High Dex concentrations shortened the dwell times whereas low concentrations prolonged the lifetime of this fold (data not shown, personal communication Thomas Suren). This highly suggests that this fold was indeed the hormone-free apo-state of the GR-LBD induced by opening of the lid segment over the ligand binding pocket. Interestingly, the seemingly destabilized GR-LBD could transit further form the apo-state to another fold stable around 8.5 pN which might reflect partial unfolding (red shading). This seems plausible as loss of the hormone results in drastic destabilization of the GR-LBD (Bledsoe et al., 2002; Lorenz et al., 2014; Seitz et al., 2010).

The initial measurements of the GR-LBD in isolation looked promising as hormone release and GR-LBD unfolding could be nicely detected. Therefore, the influence of Hsp40, Hsp70 and ATP on the GR-LBD fold was tested in a further experiment (Figure 61 B). The kinetics started similar to the GR-LBD in isolation with closing and opening of the lid over the ligand binding site, but after initial flipping, the GR-LBD completely unfolded (red shading) to a linear polypeptide chain and no refolding could be detected.

It is questionable whether the GR completely unfolds *in vivo* but the data suggest that Hsp40 and Hsp70 have a strong destabilizing influence on the general stability of the GR-LBD structure. The complete unfolding is probably a result of the applied force in the experiments shown here. Interestingly, previous studies using HDX MS showed that Hsp40 and Hsp70 lead to partial unfolding of the hormone binding site of the GR-LBD and more precisely mainly by acting on helix 1 and 3 (Kirschke et al., 2014) which were also found to unfold upon application of force in the presented results. Together, the data draws a detailed picture of how Hsp40 and Hsp70 act on the GR-LBD. It can be speculated that by promoting a lid-open GR fold, Hsp40 and Hsp70 induce hormone release from GR resulting in an instable structure. This structure is in turn stabilized by binding to the chaperones, thereby preventing aggregation/degradation of the receptor. Interestingly, the chaperones seem to use the intrinsic unfolding pathway of the GR-LBD as flipping of helix 1, opening of the ligand binding site, release of hormone and subsequent unfolding of helix 3 occurs also in the absence of chaperones when force is applied to the substrate. Further measurements including different co-/chaperone combinations are required as the established system provides the possibility to directly detect effects on the folding of the GR-LBD on the single molecule level.

### 4.3.5 Summary and conclusion

The previous sections provided a detailed analysis of the interaction of the GR-LBD with Hsp40, Hsp70 and other co-/chaperones. AUC sedimentation velocity experiments indicated stable complex formation of the GR-LBD with Hsp40 and Hsp70 only in the presence of ATP in a large 14-15 S complex. The experiments suggested further direct interaction of Hsp40 with the GR-LBD at a 1:1 ratio in a complex were the GR-LBD is not able to bind its ligand, similar to the situation in the Hsp40/Hsp70 complex. In contrast to the literature (Morgner et al., 2015), SEC HPLC combined with SDS-PAGE analysis indicated ternary complex formation of the GR-LBD,

Hsp40 and Hsp70 in a very large complex, in line with the AUC results. The results indicated a significantly different complex stoichiometry than published although more details are required to draw safe conclusions. Analysis of the functional consequences of complex formation with Hsp40 and Hsp70 could support findings in literature that ligand binding to the GR-LBD in the presence of Hsp40 and Hsp70 was prevented and hormone release facilitated (Kirschke et al., 2014). ATPase activity measurements of Hsp70 proved that ATP hydrolysis occurred in the complex but no significant stimulation by the substrate could be found in line with the literature (Mayer et al., 2003). Hormone-binding recovery by fluorescence anisotropy measurements implied that the full chaperone system is required to restore full affinity of the GR-LBD for ligands but that also Hop alone could stimulate slight reactivation. Further analysis revealed that Hop binding to the GR-LBD-Hsp40/Hsp70 complex altered the complex stoichiometry and decreased the affinity for the GR-LBD. In the Hop-induced complex, the GR-LBD was not able to bind hormone and also the ATPase activity of Hsp70 was not affected. To gain further insights into the GR-LBD chaperone interplay, a single-molecule GR-LBD system suitable for smFRET and single-molecule force spectroscopy was successfully developed. The required cysteine mutants of GR-LBD displayed similar behavior as the standard construct concerning general structure, oligomerization, interaction with chaperones and influence on Hsp90. Unfortunately, smFRET measurements did not provide any further information on the GR-LBD chaperone interplay. Single-molecule force spectroscopy in contrast revealed interesting insights into the folding of the GR-LBD. The GR-LBD unfolded in three consecutive steps with an initial opening of helix 1 possibly leading to the release of the hormone, further destabilizing the fold and resulting in complete unfolding. In the presence of Hsp40, Hsp70 and ATP, unfolding of the GR-LBD was increased leading to complete collapse of the GR-LBD structure.

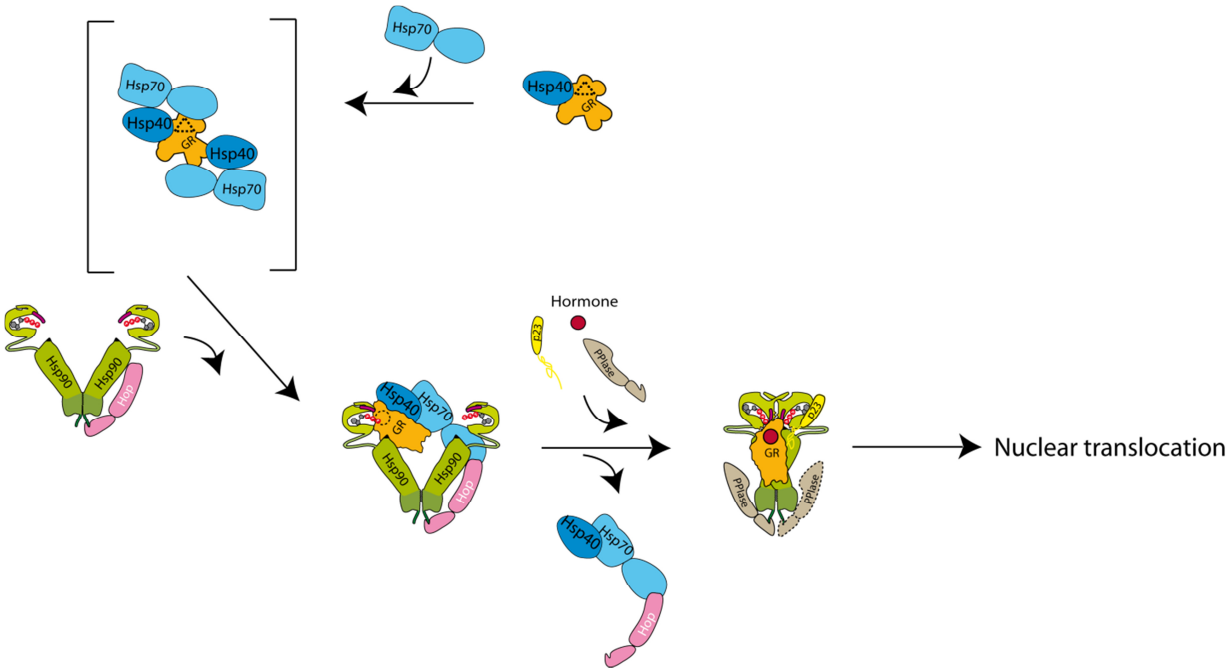


**Figure 62: The complex interplay of the GR-LBD with chaperones;** Recycled or newly synthesized GR is primarily bound by Hsp40 and transferred to the Hsp70 system by forming a large GR-Hsp40/Hsp70 complex of unclear stoichiometry (indicated by brackets) in an ATP-dependent manner. During these processes, the GR is unable to bind its hormone. In a next step, Hop in complex with Hsp90 is introduced. By binding to the GR-Hsp40/Hsp70 complex, the stoichiometry is altered leading to a decrease in the affinity of GR for Hsp40/Hsp70. This in turn promotes transfer to Hsp90 which presents a more affine binding site. The transfer is further stimulated by release of Hop/Hsp40/Hsp70 through PPIases and p23 by promoting further closing of Hsp90 and thereby increasing its affinity for GR. During this process, GR will bind its hormone and the complex consisting of GR, Hsp90, p23 and a PPIase like FKBP52 will be translocated to the nucleus via interaction with dynein and microtubules in an Hsp90-dependent manner.

Altogether, the presented results provide further insights into the complex interplay of the GR-LBD with chaperones (Figure 62). It seems that the original idea of how GR is maturated or regulated by chaperones is true in general, although the molecular details of the interactions are more complicated than assumed. Pratt, Smith and Toft speculated already in the early 1990s that GR is bound by Hsp40 in a first step which directs the client to the Hsp70 machinery (Smith and Toft, 2008). This seems to be true as data presented here, and also shown by others, indicated a direct interaction of the GR-LBD and Hsp40 and that complex formation with Hsp70 required Hsp40 together with ATP (Kirschke et al., 2014; Morgner et al., 2015). Surprisingly, the data implied that the GR-LBD is not able to bind hormone also in a 1:1 GR-LBD-Hsp40 complex which has not been previously described. It might be speculated that Hsp40 is necessary for initial inhibition of hormone binding thereby preventing direct hormone re-binding of GR and subsequent exit from the regulatory chaperone interplay. Additionally, small conformational

changes introduced in GR by Hsp40 could prime the substrate for transfer to Hsp70. This idea is supported by the observed Hsp40-dependency in complex formation. When the client is loaded on Hsp70 in an ATP-dependent fashion both proteins might act in concert to prevent ligand binding to the GR-LBD. This idea is supported by investigations on the Hsp40 homologue from *E. coli*, DnaJ. In the *E. coli* client $\sigma^{32}$, DnaJ binds to a site close to the DnaK binding surface and promotes conformational changes $\sigma^{32}$ (Rodriguez et al., 2008). The authors speculated that this might help in loading of the substrate to DnaK. The molecular details of the Hsp70-complex are contradictory. Whereas Morgner and co-workers suggested a 1:1 GR-LBD-Hsp70 complex (Morgner et al., 2015), the presented data implicate formation of a large complex consisting of the GR-LBD, Hsp40 and Hsp70 with a stoichiometry that remains to be elucidated. Consistently, hormone binding in the Hsp40/Hsp70 complex is prevented by local unfolding of the hormone binding site that results in a general instability of the GR-LBD and an Hsp70-dependent prevention of its aggregation. The presented single-molecule force experiments in combination with HDX MS data from the literature (Kirschke et al., 2014) indicate that by promoting and stabilizing a conformation of the GR-LBD, in which Helix 1 and 3 are partially unfolded, the chaperones prevent hormone binding. This is due to a generally destabilized fold of the GR-LBD which requires chaperones to preclude aggregation. This idea is supported by the findings that the GR-LBD released from Hsp70 is aggregation-prone (Kirschke et al., 2014) and application of force leads to complete unfolding of the LBD in the experiments presented. However, the question how Hsp70 binds the GR-LBD remains unanswered. The presented ATPase activity results indicate that the Hsp70 ATPase activity is not stimulated by binding of the GR-LBD in contrast to peptide substrates (Bertelsen et al., 2009; Mapa et al., 2010). This suggests a slightly different binding mode in which GR is recognized in a more native conformation similar to DnaK`s binding to $\sigma^{32}$ (Rodriguez et al., 2008). The classical GR maturation cycle describes Hop to convey the transfer from the Hsp70 to the Hsp90 system although molecular details remained elusive (Kosano et al., 1998; Pratt and Dittmar, 1998; Rohl et al., 2015b). The data shown here depict possibilities how the transfer process could take place. Binding of Hop together with Hsp90 to the GR-Hsp40/Hsp70 complex might trigger a conformational change in Hsp70 leading to changes in the complex stoichiometry ultimately decreasing the affinity of GR for the Hsp70 complex. This decrease results in the exit from the Hsp40/Hsp70 complex and transfer to Hsp90. Active priming of the Hsp40/Hsp70 complex might be required as transfer to Hsp90 from the initial 14 S complex might not be efficiently possible. This active role of Hop might contradict

the general concept of being a passive linker, but speaks in favor of a recent structural study investigating the role of Hop in the Hsp70-Hsp90-GR-LBD transfer complex (Alvira et al., 2014). In this study, conformational changes in Hop have been suggested to trigger substrate transfer from Hsp70 to Hsp90. Further, similar to the presented idea of Hop actively priming Hsp70 for transfer, a role of Hop in priming Hsp90 for substrate transfer has been proposed (Kirschke et al., 2014). Together, it seems that Hop is not a passive linker but participates actively in the client transfer process. As soon as the GR is bound by Hsp90, hormone binding is reconstituted although the molecular details of this process remain elusive. The transfer is supported by the entry of p23 and PPIases which promote the release of Hop/Hsp70/Hsp40 by driving a closed Hsp90 conformation which is highly affine for the GR (Kirschke et al., 2014; Li et al., 2013; Lorenz et al., 2014). It was speculated that ATP-hydrolysis of Hsp90 plays a role in this context but as both the GR-LBD and p23 inhibit the ATPase activity and ATP hydrolysis promotes GR release from Hsp90, further information on this is required (Kirschke et al., 2014; Lorenz et al., 2014; Richter et al., 2004). Additionally, a role of Hsp90 as NEF for Hsp70 and therefore in actively triggering Hsp70 release has been suggested but experimental evidence is lacking (Kirschke et al., 2014). In complex with Hsp90, p23 and an additional large PPIases like FKBP51, the GR might finally be translocated to the nucleus in an Hsp90-dependent manner by the dynein-microtubule system (Galigniana et al., 2001; Galigniana et al., 1998).

# 5 Summary

The present work was focused on exploring the prerequisites for the influence of the GR-LBD on the conformational cycle of Hsp90, a side-by-side characterization of the Hsp90 interplay with two structurally unrelated Hsp90 clients and the processes preceding the transfer of the GR-LBD to the Hsp90 system.

Analysis of the Hsp90 W300 mutant by NMR implicated that this special residue is significantly affected by GR-LBD binding to Hsp90. *In vivo* Hsp90 shuffling experiments and GR activity assays suggested that exchange of W300 negatively affects yeast viability and GR maturation. Hsp90 ATPase activity measurements and FRET experiments showed that the inhibitory effect of the GR-LBD on Hsp90 could not be induced in the W300 mutants. Hormone-binding recovery using the homologous human mutants proved that the mutation of this special tryptophan significantly reduced the ability of Hsp90 to restore hormone binding. The nucleotide-dependent binding of the GR-LBD to the Hsp90 W300 mutant was negatively affected, especially in the presence of non- or slowly hydrolysable ATP analogs and the mutants showed also modified co-chaperone binding. SAXS data in combination with molecular dynamics simulation led to the conclusion that by forming an important transient π-cation interaction, W300 is essential to form a conformation of Hsp90 that ensures on the one hand high-affinity binding of the GR-LBD and on the other hand susceptibility to the inhibitory influence of the GR-LBD. The absence of the tryptophan and thus the lacking π-cation interaction resulted in more closed or altered the Hsp90 conformations that bound the GR-LBD with lower affinity and could not be influenced by the GR-LBD. It can be speculated that W300 is therefore crucial for a correct Hsp90-client interplay and thus also for GR regulation in the cell.

The side-by-side characterization of the Hsp90 interaction with Tau and the GR-LBD revealed significantly different characteristics. AUC sedimentation velocity experiments showed that Tau, in contrast to the GR-LBD, bound to Hsp90 independent of the nucleotide present. NMR experiments using labeled Hsp90 domains and segmentally labeled Hsp90 constructs suggested a binding site for Tau mainly located in the Hsp90-N domain with some contacts in the Hsp90-M domain. In contrast to the speculations of overlapping binding sites in the literature (Karagoz and Rudiger, 2015; Mayer and Le Breton, 2015), FRET and AUC experiments proved that Tau and the GR-LBD could simultaneously bind to Hsp90 and do not compete for the binding sites. Tau

showed a significantly different influence on the Hsp90 chaperone cycle than the GR-LBD as it stimulated the ATPase activity of Hsp90 in cooperative manner implicating binding of two molecules to establish the effect. Stimulation was presumably achieved by inducing a more closed conformation in which general closing, re-opening and ATP affinity remained unaffected. Testing co-chaperone binding to the Hsp90-Tau complex suggested that binding of several co-chaperones was possible, including Aha1 which did not bind to the Hsp90-GR complex in earlier studies (Lorenz et al., 2014). Altogether the results implicated that different clients might differentially influence the Hsp90 chaperone cycle according to their requirements. While the GR-LBD slows down the cycle to prevent release and ensure Hsp90-dependent nuclear translocation, Tau might promote steady cycling to prevent its rapid degradation. Thereby it might be supported by co-chaperones like Aha1.

The characterization of the GR-LBD-Hsp40/Hsp70 complex provided exciting new insights into the processes preceding transfer to the Hsp90 system. Interestingly, the GR-LBD formed a complex with Hsp40 at a 1:1 stoichiometry independent of nucleotide. In support of earlier studies (Kirschke et al., 2014), the GR-LBD associated with Hsp40 and Hsp70 only in the presence of ATP. Surprisingly the three components formed a very large complex around 14 S. Hormone binding to GR-LBD was neither possible in the GR-LBD-Hsp40 nor in the ternary complex. In contrast to previous results (Morgner et al., 2015), the SEC-HPLC results supported the idea that the GR-LBD did form a ternary complex of unknown stoichiometry with Hsp70 and Hsp40 which could not be shown before. In this complex, the inhibitory effects of Hsp70 on hormone binding could be confirmed using an apo GR-LBD without solubility-enhancing tag and further it could be shown that the ATPase activity remains unaffected by the presence of the GR-LBD. Further, hormone binding experiments identified a special role of Hop as the co-chaperone could stimulate slight hormone rebinding also in the absence of Hsp90. AUC experiments suggested that Hop alters the complex stoichiometry in the GR-LBD Hsp40/Hsp70 complex and moderately decreases the affinity of GR-LBD for the complex. This process could form an important step in the client transfer. By lowering the affinity for Hsp70, Hop triggers the transfer of GR to the higher affine Hsp90-p23 complex. Importantly, single-molecule GR-LBD constructs could be created and the conservation of the effects concerning Hsp70 and Hsp90 binding as well as the influences on the Hsp90 chaperone cycle was proven. Single-molecule FRET experiments did not provide further information, but single-molecule force spectroscopy suggested that the GR-LBD unfolds in three distinct steps when force is applied. Thereby, the first unfolding step

seemed to involve helix 1 possibly facilitating hormone release, followed by unfolding of large parts of the hormone-binding pocket resulting in subsequent collapse of the complete structure. In the presence of Hsp40, Hsp70 and ATP unfolding of the GR-LBD was increased leading to complete break-up of the GR-LBD structure.

Altogether, the present thesis could provide detailed and new insights into the interplay of Hsp90 with different client proteins. The results refined the picture of how the GR-LBD influences the conformational cycle of Hsp90 and might help to establish a new model of the Hsp90 client interplay in which clients adapt Hsp90 according to their special requirements. Further, an exciting new GR-LBD-Hsp40/Hsp70 complex could be identified and the role of Hop in the client transfer process was refined. Together with the established single-molecule systems, this project part has potential to address various new aspects in the future.

# Summary

# 6 Abbreviations

| | |
|---|---|
| µl | Microliter |
| µM | Micromolar |
| A | Ampere |
| Å | Angström |
| aa | Amino acid |
| AD | Alzheimer's disease |
| ADP | Adenosindiphosphate |
| AMP-PNP | 5'–Adenylyl-ß,γ-imido-diphosphate |
| AR | Androgen receptor |
| ATP | Adenosintriphosphate |
| ATPγS | Adenosine-5'-(γ-thio)-triphosphate |
| AUC | Analytical ultracentrifugation |
| BAG domain | Bcl-2 associated athanogene domain |
| CC | C-terminal cysteine |
| CD | Circular dichroism |
| CSP | Chemical shift pertubations |
| CV | Column volume |
| *D. rerio* | *Danio rerio* |
| Dex | Dexamethasone |
| $D_{max}$ | Maximum dimension |
| DNA | Deoxyribonucleic acid |
| *E. coli* | *Escherichia coli* |
| EM | Electron microscopy |
| ER | Estrogen receptor |
| *et al.* | And others |
| F-Dex | Dexamethasone Fluorescein |
| FPLC | Fast protein liquid chromatography |
| FRET | Fluorescence Resonance Energy Transfer |
| g | Gram |
| GC | Glucocorticoids |
| GHKL | Gyrase, Hsp90, Histidine Kinase, MutL |
| GR | Glucocorticoid receptor |
| GR-DBD-LBD | GR-DBD-LBD-F602S/A605V/V702A/E705G/M752T |
| GRE | Glucocorticoid transcriptional response element |
| GR-LBD | Ligand binding domain of the glucocorticoid receptor, GR-LBD-F602S/A605V/V702A/E705G/M752T |

| | |
|---|---|
| GR-NTD | N-terminal domain of the glucocorticoid receptor |
| h | Hour |
| HDX MS | Hydrogen deuterium exchange mass spectrometry |
| *H. sapiens* | *Homo sapiens* |
| HPLC | High-performance liquid chromatography |
| Hsp | Heat shock protein |
| Hsp40 | Ydj1 |
| Hsp90-C | C-terminal domain of Hsp90 |
| Hsp90-M | Middle domain of Hsp90 |
| Hsp90-N | N-terminal domain of Hsp90 |
| $IC_{50}$ | half maximal inhibitory concentration |
| K | Potassium |
| $K_D$ | Dissociation constant |
| kDa | Kilo Dalton |
| $K_i$ | Inhibition constant |
| l | Liter |
| M | Molar |
| Mg | Magnesium |
| mg/ml | Milligram per milliliter |
| MIF | Mifepristone |
| min | Minute |
| ml | Milliliter |
| MR | Mineralocorticoid receptor |
| MS | Mass spectrometry |
| MT | Microtubule |
| MW | Molecular mass |
| NBD | Nucleotide binding domain |
| NC | N-terminal cysteine |
| NC-GR-LBD | Single-molecule GR-LBD construct containing an N-terminal cysteine, retaining C638; |
| NEF | Nucleotide exchange factor |
| NLS | Nuclear localization sequence |
| nm | Nanometer |
| nM | Nanomolar |
| NMR | Nuclear magnetic resonance |
| NTD | N-terminal domain |
| $OD_{600}$ | Optical density at 600 nm |
| ONC | Overnight culture |
| P(R) | Inter-atomic distance distribution function |
| p.a. | *pro analysi* |

| | |
|---|---|
| PCR | Polymerase chain reaction |
| POD | Peroxidase |
| PPIase | Peptidyl prolyl isomerase |
| PR | Progesterone receptor |
| PTM | Post-translational modification |
| $R_g$ | Radius of gyration |
| RLL | Reticulocyte lysate |
| rpm | Revolutions per minute |
| RT | Room temperature |
| s | Second |
| *S. cerevisiae* | *Saccharomyces cerevisiae* |
| SAXS | Small-angle X-ray scattering |
| SBD | Substrate binding domain |
| SDS-PAGE | Sodium dodecyl sulfate polyacrylamide gel electrophoresis |
| SEC | Size-exclusion chromatography |
| SHR | Steroid hormone receptor |
| smGR-LBD | Single-molecule GR-LBD construct containing cysteines at the N- and C-terminus with additional C638D mutation |
| sHsp | Small heat shock protein |
| TPR | Tetratricopeptide repeat domain |
| UV | Ultraviolet |
| V | Volt |
| VdW | Van-der-Waals |
| v/v | Volume per volume |
| w/v | Weight per volume |
| *wt* | Wild type |
| x g | multiple of the acceleration of gravity |

# Abbreviations

# 7 References

Acevedo, M.L., and Kraus, W.L. (2004). Transcriptional activation by nuclear receptors. Essays in biochemistry *40*, 73-88.
Ali, J.A., Jackson, A.P., Howells, A.J., and Maxwell, A. (1993). The 43-kilodalton N-terminal fragment of the DNA gyrase B protein hydrolyzes ATP and binds coumarin drugs. Biochemistry *32*, 2717-2724.
Ali, M.M., Roe, S.M., Vaughan, C.K., Meyer, P., Panaretou, B., Piper, P.W., Prodromou, C., and Pearl, L.H. (2006). Crystal structure of an Hsp90-nucleotide-p23/Sba1 closed chaperone complex. Nature *440*, 1013-1017.
Alvira, S., Cuéllar, J., Röhl, A., Yamamoto, S., Itoh, H., Alfonso, C., Rivas, G., Buchner, J., and Valpuesta, J.M. (2014). Structural characterization of the substrate transfer mechanism in Hsp70/Hsp90 folding machinery mediated by Hop. Nature communications *5*.
Anfinsen, C.B., Haber, E., Sela, M., and White, F.H., Jr. (1961). The kinetics of formation of native ribonuclease during oxidation of the reduced polypeptide chain. Proceedings of the National Academy of Sciences of the United States of America *47*, 1309-1314.
Augustinack, J.C., Schneider, A., Mandelkow, E.M., and Hyman, B.T. (2002). Specific tau phosphorylation sites correlate with severity of neuronal cytopathology in Alzheimer's disease. Acta Neuropathologica *103*, 26-35.
Barent, R.L., Nair, S.C., Carr, D.C., Ruan, Y., Rimerman, R.A., Fulton, J., Zhang, Y., and Smith, D.F. (1998). Analysis of FKBP51/FKBP52 chimeras and mutants for Hsp90 binding and association with progesterone receptor complexes. Molecular endocrinology *12*, 342-354.
Bertelsen, E.B., Chang, L., Gestwicki, J.E., and Zuiderweg, E.R. (2009). Solution conformation of wild-type E. coli Hsp70 (DnaK) chaperone complexed with ADP and substrate. Proceedings of the National Academy of Sciences of the United States of America *106*, 8471-8476.
Blair, L.J., Nordhues, B.A., Hill, S.E., Scaglione, K.M., O'Leary, J.C., 3rd, Fontaine, S.N., Breydo, L., Zhang, B., Li, P., Wang, L.*, et al.* (2013). Accelerated neurodegeneration through chaperone-mediated oligomerization of tau. J Clin Invest *123*, 4158-4169.
Blair, L.J., Sabbagh, J.J., and Dickey, C.A. (2014). Targeting Hsp90 and its co-chaperones to treat Alzheimer's disease. Expert opinion on therapeutic targets *18*, 1219-1232.
Blanchet, C.E., and Svergun, D.I. (2013). Small-angle X-ray scattering on biological macromolecules and nanocomposites in solution. Annual review of physical chemistry *64*, 37-54.
Bledsoe, R.K., Montana, V.G., Stanley, T.B., Delves, C.J., Apolito, C.J., McKee, D.D., Consler, T.G., Parks, D.J., Stewart, E.L., Willson, T.M.*, et al.* (2002). Crystal structure of the glucocorticoid receptor ligand binding domain reveals a novel mode of receptor dimerization and coactivator recognition. Cell *110*, 93-105.
Boczek, E.E., Reefschlager, L.G., Dehling, M., Struller, T.J., Hausler, E., Seidl, A., Kaila, V.R., and Buchner, J. (2015). Conformational processing of oncogenic v-Src kinase by the molecular chaperone Hsp90. Proceedings of the National Academy of Sciences of the United States of America *112*, E3189-3198.
Bohen, S.P., and Yamamoto, K.R. (1993). Isolation of Hsp90 mutants by screening for decreased steroid receptor function. Proceedings of the National Academy of Sciences of the United States of America *90*, 11424-11428.

Bramblett, G.T., Goedert, M., Jakes, R., Merrick, S.E., Trojanowski, J.Q., and Lee, V.M.Y. (1993). Abnormal tau phosphorylation at Ser396 in alzheimer's disease recapitulates development and contributes to reduced microtubule binding. Neuron *10*, 1089-1099.

Breuzard, G., Hubert, P., Nouar, R., De Bessa, T., Devred, F., Barbier, P., Sturgis, J.N., and Peyrot, V. (2013). Molecular mechanisms of Tau binding to microtubules and its role in microtubule dynamics in live cells. Journal of Cell Science *126*, 2810-2819.

Brooks, B.R., Bruccoleri, R.E., Olafson, B.D., States, D.J., Swaminathan, S., and Karplus, M. (1983). CHARMM: A program for macromolecular energy, minimization, and dynamics calculations. Journal of Computational Chemistry *4*, 187-217.

Brunden, K.R., Trojanowski, J.Q., and Lee, V.M.Y. (2009). Advances in tau-focused drug discovery for Alzheimer's disease and related tauopathies. Nat Rev Drug Discov *8*, 783-793.

Buchner, J. (1999). Hsp90 & Co. – a holding for folding. Trends in Biochemical Sciences *24*, 136-141.

Bukau, B., and Horwich, A.L. (1998). The Hsp70 and Hsp60 chaperone machines. Cell *92*, 351-366.

Bunker, J.M., Wilson, L., Jordan, M.A., and Feinstein, S.C. (2004). Modulation of microtubule dynamics by tau in living cells: Implications for development and neurodegeneration. Molecular Biology of the Cell *15*, 2720-2728.

Burke, L.J., and Baniahmad, A. (2000). Co-repressors 2000. FASEB journal : official publication of the Federation of American Societies for Experimental Biology *14*, 1876-1888.

Caplan, A.J., Mandal, A.K., and Theodoraki, M.A. (2007). Molecular chaperones and protein kinase quality control. Trends in cell biology *17*, 87-92.

Catelli, M.G., Binart, N., Jung-Testas, I., Renoir, J.M., Baulieu, E.E., Feramisco, J.R., and Welch, W.J. (1985). The common 90-kd protein component of non-transformed '8S' steroid receptors is a heat-shock protein. EMBO J *4*, 3131-3135.

Chen, S., and Smith, D.F. (1998). Hop as an Adaptor in the Heat Shock Protein 70 (Hsp70) and Hsp90 Chaperone Machinery. Journal of Biological Chemistry *273*, 35194-35200.

Chen, S., Sullivan, W.P., Toft, D.O., and Smith, D.F. (1998). Differential interactions of p23 and the TPR-containing proteins Hop, Cyp40, FKBP52 and FKBP51 with Hsp90 mutants. Cell Stress Chaperones *3*, 118-129.

Choi, M.C., Raviv, U., Miller, H.P., Gaylord, M.R., Kiris, E., Ventimiglia, D., Needleman, D.J., Kim, M.W., Wilson, L., Feinstein, S.C*., et al.* (2009). Human microtubule-associated-protein tau regulates the number of protofilaments in microtubules: A synchrotron X-ray scattering study. Biophysical Journal *97*, 519-527.

Chrousos, G.P. (2004). The glucocorticoid receptor gene, longevity, and the complex disorders of Western societies. Am J Med *117*, 204-207.

Clark, P.L. (2004). Protein folding in the cell: reshaping the folding funnel. Trends Biochem Sci *29*, 527-534.

Crowther, R.A., Olesen, O.F., Smith, M.J., Jakes, R., and Goedert, M. (1994). Assembly of Alzheimer-like filaments from full-length tau protein. FEBS letters *337*, 135-138.

Cunningham, C.N., Krukenberg, K.A., and Agard, D.A. (2008). Intra- and intermonomer interactions are required to synergistically facilitate ATP hydrolysis in Hsp90. J Biol Chem *283*, 21170-21178.

Cunningham, C.N., Southworth, D.R., Krukenberg, K.A., and Agard, D.A. (2012). The conserved arginine 380 of Hsp90 is not a catalytic residue, but stabilizes the closed conformation required for ATP hydrolysis. Protein science : a publication of the Protein Society *21*, 1162-1171.

Dehner, A., Furrer, J., Richter, K., Schuster, I., Buchner, J., and Kessler, H. (2003). NMR chemical shift perturbation study of the N-terminal domain of Hsp90 upon binding of ADP, AMP-PNP, geldanamycin, and radicicol. Chembiochem : a European journal of chemical biology *4*, 870-877.

Delaglio, F., Grzesiek, S., Vuister, G.W., Zhu, G., Pfeifer, J., and Bax, A. (1995). NMRPipe: a multidimensional spectral processing system based on UNIX pipes. Journal of biomolecular NMR *6*, 277-293.

Dickey, C.A., Dunmore, J., Lu, B., Wang, J.W., Lee, W.C., Kamal, A., Burrows, F., Eckman, C., Hutton, M., and Petrucelli, L. (2006). HSP induction mediates selective clearance of tau phosphorylated at proline-directed Ser/Thr sites but not KXGS (MARK) sites. FASEB Journal *20*, 753-755.

Dickey, C.A., Eriksen, J., Kamal, A., Burrows, F., Kasibhatla, S., Eckman, C.B., Hutton, M., and Petrucelli, L. (2005). Development of a high throughput drug screening assay for the detection of changes in tau levels - Proof of concept with HSP90 inhibitors. Current Alzheimer Research *2*, 231-238.

Dickey, C.A., Kamal, A., Lundgren, K., Klosak, N., Bailey, R.M., Dunmore, J., Ash, P., Shoraka, S., Zlatkovic, J., Eckman, C.B.*, et al.* (2007). The high-affinity HSP90-CHIP complex recognizes and selectively degrades phosphorylated tau client proteins. Journal of Clinical Investigation *117*, 648-658.

Dittmar, K.D., Demady, D.R., Stancato, L.F., Krishna, P., and Pratt, W.B. (1997). Folding of the glucocorticoid receptor by the heat shock protein (hsp) 90-based chaperone machinery. The role of p23 is to stabilize receptor.hsp90 heterocomplexes formed by hsp90.p60.hsp70. J Biol Chem *272*, 21213-21220.

Dobson, C.M., Šali, A., and Karplus, M. (1998). Protein Folding: A Perspective from Theory and Experiment. Angewandte Chemie International Edition *37*, 868-893.

Dolai, S., Shi, W., Corbo, C., Sun, C., Averick, S., Obeysekera, D., Farid, M., Alonso, A., Banerjee, P., and Raja, K. (2011). "Clicked" sugar.curcumin conjugate: Modulator of amyloid-βand tau peptide aggregation at ultralow concentrations. ACS Chemical Neuroscience *2*, 694-699.

Dolan, P.J., and Johnson, G.V.W. (2010). The role of tau kinases in Alzheimer's disease. Current Opinion in Drug Discovery and Development *13*, 595-603.

Dollins, D.E., Warren, J.J., Immormino, R.M., and Gewirth, D.T. (2007). Structures of GRP94-nucleotide complexes reveal mechanistic differences between the hsp90 chaperones. Molecular cell *28*, 41-56.

Dou, F., Netzer, W.J., Tanemura, K., Li, F., Hartl, F.U., Takashima, A., Gouras, G.K., Greengard, P., and Xu, H. (2003). Chaperones increase association of tau protein with microtubules. Proceedings of the National Academy of Sciences of the United States of America *100*, 721-726.

Duma, D., Jewell, C.M., and Cidlowski, J.A. (2006). Multiple glucocorticoid receptor isoforms and mechanisms of post-translational modification. Journal of Steroid Biochemistry and Molecular Biology *102*, 11-21.

Echeverria, P.C., Mazaira, G., Erlejman, A., Gomez-Sanchez, C., Piwien Pilipuk, G., and Galigniana, M.D. (2009). Nuclear import of the glucocorticoid receptor-hsp90 complex through the nuclear pore complex is mediated by its interaction with Nup62 and importin beta. Molecular and cellular biology *29*, 4788-4797.

Echeverria, P.C., and Picard, D. (2010). Molecular chaperones, essential partners of steroid hormone receptors for activity and mobility. Biochimica et Biophysica Acta (BBA) - Molecular Cell Research *1803*, 641-649.
Echtenkamp, F.J., Zelin, E., Oxelmark, E., Woo, J.I., Andrews, B.J., Garabedian, M., and Freeman, B.C. (2011). Global functional map of the p23 molecular chaperone reveals an extensive cellular network. Molecular cell *43*, 229-241.
Eckert, K., Saliou, J.M., Monlezun, L., Vigouroux, A., Atmane, N., Caillat, C., Quevillon-Cheruel, S., Madiona, K., Nicaise, M., Lazereg, S.*, et al.* (2010). The Pih1-Tah1 cochaperone complex inhibits Hsp90 molecular chaperone ATPase activity. J Biol Chem *285*, 31304-31312.
Ellis, R.J., and Minton, A.P. (2006). Protein aggregation in crowded environments. Biological chemistry *387*, 485-497.
Fairbanks, G., Steck, T.L., and Wallach, D.F. (1971). Electrophoretic analysis of the major polypeptides of the human erythrocyte membrane. Biochemistry *10*, 2606-2617.
Falsone, S.F., Leptihn, S., Osterauer, A., Haslbeck, M., and Buchner, J. (2004). Oncogenic mutations reduce the stability of SRC kinase. Journal of molecular biology *344*, 281-291.
Fan, C.-Y., Lee, S., and Cyr, D.M. (2003). Mechanisms for regulation of Hsp70 function by Hsp40. Cell Stress & Chaperones *8*, 309-316.
Fang, L., Ricketson, D., Getubig, L., and Darimont, B. (2006). Unliganded and hormone-bound glucocorticoid receptors interact with distinct hydrophobic sites in the Hsp90 C-terminal domain. Proceedings of the National Academy of Sciences of the United States of America *103*, 18487-18492.
Fink, A.L. (2005). Natively unfolded proteins. Curr Opin Struct Biol *15*, 35-41.
Flom, G.A., Langner, E., and Johnson, J.L. (2012). Identification of an Hsp90 mutation that selectively disrupts cAMP/PKA signaling in Saccharomyces cerevisiae. Curr Genet *58*, 149-163.
Fontaine, S.N., Sabbagh, J.J., Baker, J., Martinez-Licha, C.R., Darling, A., and Dickey, C.A. (2015). Cellular factors modulating the mechanism of tau protein aggregation. Cellular and molecular life sciences : CMLS *72*, 1863-1879.
Freedman, N.D., and Yamamoto, K.R. (2004). Importin 7 and importin alpha/importin beta are nuclear import receptors for the glucocorticoid receptor. Mol Biol Cell *15*, 2276-2286.
Freeman, B.C., and Yamamoto, K.R. (2002). Disassembly of transcriptional regulatory complexes by molecular chaperones. Science *296*, 2232-2235.
Frydman, J. (2001). Folding of newly translated proteins in vivo: the role of molecular chaperones. Annual review of biochemistry *70*, 603-647.
Gaiser, A.M., Kretzschmar, A., and Richter, K. (2010). Cdc37-Hsp90 complexes are responsive to nucleotide-induced conformational changes and binding of further cofactors. J Biol Chem *285*, 40921-40932.
Galigniana, M.D., Harrell, J.M., Housley, P.R., Patterson, C., Fisher, S.K., and Pratt, W.B. (2004). Retrograde transport of the glucocorticoid receptor in neurites requires dynamic assembly of complexes with the protein chaperone hsp90 and is linked to the CHIP component of the machinery for proteasomal degradation. Brain Res Mol Brain Res *123*, 27-36.
Galigniana, M.D., Harrell, J.M., Murphy, P.J., Chinkers, M., Radanyi, C., Renoir, J.M., Zhang, M., and Pratt, W.B. (2002). Binding of hsp90-associated immunophilins to cytoplasmic dynein: direct binding and in vivo evidence that the peptidylprolyl isomerase domain is a dynein interaction domain. Biochemistry *41*, 13602-13610.
Galigniana, M.D., Radanyi, C., Renoir, J.M., Housley, P.R., and Pratt, W.B. (2001). Evidence that the peptidylprolyl isomerase domain of the hsp90-binding immunophilin FKBP52 is

involved in both dynein interaction and glucocorticoid receptor movement to the nucleus. J Biol Chem *276*, 14884-14889.
Galigniana, M.D., Scruggs, J.L., Herrington, J., Welsh, M.J., Carter-Su, C., Housley, P.R., and Pratt, W.B. (1998). Heat Shock Protein 90-Dependent (Geldanamycin-Inhibited) Movement of the Glucocorticoid Receptor through the Cytoplasm to the Nucleus Requires Intact Cytoskeleton. Molecular Endocrinology *12*, 1903-1913.
Gallivan, J.P., and Dougherty, D.A. (1999). Cation-π interactions in structural biology. Proceedings of the National Academy of Sciences *96*, 9459-9464.
Garnier, C., Barbier, P., Gilli, R., Lopez, C., Peyrot, V., and Briand, C. (1998). Heat-shock protein 90 (hsp90) binds in vitro to tubulin dimer and inhibits microtubule formation. Biochemical and biophysical research communications *250*, 414-419.
Gärtner, U., Janke, C., Holzer, M., Vanmechelen, E., and Arendt, T. (1998). Postmortem changes in the phosphorylation state of tau-protein in the rat brain. Neurobiology of Aging *19*, 535-543.
Gershenson, A., and Gierasch, L.M. (2011). Protein folding in the cell: challenges and progress. Curr Opin Struct Biol *21*, 32-41.
Gietz, R.D., and Schiestl, R.H. (2007). High-efficiency yeast transformation using the LiAc/SS carrier DNA/PEG method. Nat Protocols *2*, 31-34.
Girard, J.M. (2014). CARMA: Software for Continuous Affect Rating and Media Annotation. Journal of Open Research Software. Journal of open research software *2*.
Goode, B.L., Denis, P.E., Panda, D., Radeke, M.J., Miller, H.P., Wilson, L., and Feinstein, S.C. (1997). Functional interactions between the proline-rich and repeat regions of tau enhance microtubule binding and assembly. Molecular Biology of the Cell *8*, 353-365.
Grad, I., and Picard, D. (2007). The glucocorticoid responses are shaped by molecular chaperones. Molecular and cellular endocrinology *275*, 2-12.
Graf, C., Stankiewicz, M., Kramer, G., and Mayer, M.P. (2009). Spatially and kinetically resolved changes in the conformational dynamics of the Hsp90 chaperone machine. EMBO J *28*, 602-613.
Grenert, J.P., Johnson, B.D., and Toft, D.O. (1999). The importance of ATP binding and hydrolysis by hsp90 in formation and function of protein heterocomplexes. J Biol Chem *274*, 17525-17533.
Grenert, J.P., Sullivan, W.P., Fadden, P., Haystead, T.A., Clark, J., Mimnaugh, E., Krutzsch, H., Ochel, H.J., Schulte, T.W., Sausville, E.*, et al.* (1997). The amino-terminal domain of heat shock protein 90 (hsp90) that binds geldanamycin is an ATP/ADP switch domain that regulates hsp90 conformation. The Journal of biological chemistry *272*, 23843-23850.
Grundke-Iqbal, I., Iqbal, K., and Tung, Y.C. (1986). Abnormal phosphorylation of the microtubule-associated protein τ (tau) in Alzheimer cytoskeletal pathology. Proceedings of the National Academy of Sciences of the United States of America *83*, 44913-44917.
Haass, C., and Selkoe, D.J. (2007). Soluble protein oligomers in neurodegeneration: lessons from the Alzheimer's amyloid beta-peptide. Nat Rev Mol Cell Biol *8*, 101-112.
Hagn, F., Lagleder, S., Retzlaff, M., Rohrberg, J., Demmer, O., Richter, K., Buchner, J., and Kessler, H. (2011). Structural analysis of the interaction between Hsp90 and the tumor suppressor protein p53. Nature structural & molecular biology *18*, 1086-1093.
Hainzl, O., Lapina, M.C., Buchner, J., and Richter, K. (2009). The charged linker region is an important regulator of Hsp90 function. J Biol Chem *284*, 22559-22567.
Han, D., and Paudel, H.K. (2009). FTDP-17 missense mutations site-specifically inhibit as well as promote dephosphorylation of microtubule-associated protein tau by protein phosphatases of HEK-293 cell extract. Neurochemistry international *54*, 14-27.

Hanger, D.P., Hughes, K., Woodgett, J.R., Brion, J.P., and Anderton, B.H. (1992). Glycogen synthase kinase-3 induces Alzheimer's disease-like phosphorylation of tau: Generation of paired helical filament epitopes and neuronal localisation of the kinase. Neuroscience Letters *147*, 58-62.
Harris, S.F., Shiau, A.K., and Agard, D.A. (2004). The crystal structure of the carboxy-terminal dimerization domain of htpG, the Escherichia coli Hsp90, reveals a potential substrate binding site. Structure *12*, 1087-1097.
Haslbeck, M., Franzmann, T., Weinfurtner, D., and Buchner, J. (2005). Some like it hot: the structure and function of small heat-shock proteins. Nature structural & molecular biology *12*, 842-846.
Hawle, P., Siepmann, M., Harst, A., Siderius, M., Reusch, H.P., and Obermann, W.M. (2006). The middle domain of Hsp90 acts as a discriminator between different types of client proteins. Molecular and cellular biology *26*, 8385-8395.
Hayes, D.B., and Stafford, W.F. (2010). SEDVIEW, real-time sedimentation analysis. Macromol Biosci *10*, 731-735.
Hernandez, M.P., Sullivan, W.P., and Toft, D.O. (2002). The assembly and intermolecular properties of the hsp70-Hop-hsp90 molecular chaperone complex. J Biol Chem *277*, 38294-38304.
Hessling, M., Richter, K., and Buchner, J. (2009). Dissection of the ATP-induced conformational cycle of the molecular chaperone Hsp90. Nature structural & molecular biology *16*, 287-293.
Horlein, A.J., Naar, A.M., Heinzel, T., Torchia, J., Gloss, B., Kurokawa, R., Ryan, A., Kamei, Y., Soderstrom, M., Glass, C.K.*, et al.* (1995). Ligand-independent repression by the thyroid hormone receptor mediated by a nuclear receptor co-repressor. Nature *377*, 397-404.
Huai, Q., Wang, H., Liu, Y., Kim, H.Y., Toft, D., and Ke, H. (2005). Structures of the N-terminal and middle domains of E. coli Hsp90 and conformation changes upon ADP binding. Structure *13*, 579-590.
Hudson, W.H., Youn, C., and Ortlund, E.A. (2013). The structural basis of direct glucocorticoid-mediated transrepression. Nature structural & molecular biology *20*, 53-58.
Humphrey, W., Dalke, A., and Schulten, K. (1996). VMD: Visual molecular dynamics. Journal of Molecular Graphics *14*, 33-38.
Jahn, M., Rehn, A., Pelz, B., Hellenkamp, B., Richter, K., Rief, M., Buchner, J., and Hugel, T. (2014). The charged linker of the molecular chaperone Hsp90 modulates domain contacts and biological function. Proceedings of the National Academy of Sciences of the United States of America *111*, 17881-17886.
Jeganathan, S., Von Bergen, M., Brutlach, H., Steinhoff, H.J., and Mandelkow, E. (2006). Global hairpin folding of tau in solution. Biochemistry *45*, 2283-2293.
Jinwal, U.K., Akoury, E., Abisambra, J.F., O'Leary Iii, J.C., Thompson, A.D., Blair, L.J., Jin, Y., Bacon, J., Nordhues, B.A., Cockman, M.*, et al.* (2013a). Imbalance of Hsp70 family variants fosters tau accumulation. FASEB Journal *27*, 1450-1459.
Jinwal, U.K., Koren, J., 3rd, and Dickey, C.A. (2013b). Reconstructing the Hsp90/Tau Machine. Curr Enzym Inhib *9*, 41-45.
Jinwal, U.K., O'Leary Iii, J.C., Borysov, S.I., Jones, J.R., Li, Q., Koren Iii, J., Abisambra, J.F., Vestal, G.D., Lawson, L.Y., Johnson, A.G.*, et al.* (2010). Hsc70 rapidly engages tau after microtubule destabilization. Journal of Biological Chemistry *285*, 16798-16805.
John, S., Sabo, P.J., Thurman, R.E., Sung, M.H., Biddie, S.C., Johnson, T.A., Hager, G.L., and Stamatoyannopoulos, J.A. (2011). Chromatin accessibility pre-determines glucocorticoid receptor binding patterns. Nature genetics *43*, 264-268.

Johnson, B.D., Schumacher, R.J., Ross, E.D., and Toft, D.O. (1998). Hop modulates Hsp70/Hsp90 interactions in protein folding. J Biol Chem *273*, 3679-3686.
Johnson, J.L. (2012). Evolution and function of diverse Hsp90 homologs and cochaperone proteins. Biochimica et biophysica acta *1823*, 607-613.
Johnson, J.L., Halas, A., and Flom, G. (2007). Nucleotide-dependent interaction of Saccharomyces cerevisiae Hsp90 with the cochaperone proteins Sti1, Cpr6, and Sba1. Molecular and cellular biology *27*, 768-776.
Johnson, J.L., and Toft, D.O. (1995). Binding of p23 and hsp90 during assembly with the progesterone receptor. Molecular endocrinology (Baltimore, Md) *9*, 670-678.
Kadota, Y., Amigues, B., Ducassou, L., Madaoui, H., Ochsenbein, F., Guerois, R., and Shirasu, K. (2008). Structural and functional analysis of SGT1-HSP90 core complex required for innate immunity in plants. EMBO reports *9*, 1209-1215.
Kadota, Y., Shirasu, K., and Guerois, R. (2010). NLR sensors meet at the SGT1-HSP90 crossroad. Trends Biochem Sci *35*, 199-207.
Kampinga, H.H., and Craig, E.A. (2010). The HSP70 chaperone machinery: J proteins as drivers of functional specificity. Nat Rev Mol Cell Biol *11*, 579-592.
Karagöz, G.E., Duarte, Afonso M.S., Akoury, E., Ippel, H., Biernat, J., Morán Luengo, T., Radli, M., Didenko, T., Nordhues, Bryce A., Veprintsev, Dmitry B.*, et al.* (2014). Hsp90-Tau Complex Reveals Molecular Basis for Specificity in Chaperone Action. Cell *156*, 963-974.
Karagoz, G.E., and Rudiger, S.G. (2015). Hsp90 interaction with clients. Trends Biochem Sci *40*, 117-125.
Kauppi, B., Jakob, C., Färnegårdh, M., Yang, J., Ahola, H., Alarcon, M., Calles, K., Engström, O., Harlan, J., Muchmore, S.*, et al.* (2003). The three-dimensional structures of antagonistic and agonistic forms of the glucocorticoid receptor ligand-binding domain: RU-486 induces a transconformation that leads to active antagonism. Journal of Biological Chemistry *278*, 22748-22754.
Khan, S.H., Awasthi, S., Guo, C., Goswami, D., Ling, J., Griffin, P.R., Simons, S.S., Jr., and Kumar, R. (2012). Binding of the N-terminal region of coactivator TIF2 to the intrinsically disordered AF1 domain of the glucocorticoid receptor is accompanied by conformational reorganizations. J Biol Chem *287*, 44546-44560.
Kim, Y.E., Hipp, M.S., Bracher, A., Hayer-Hartl, M., and Hartl, F.U. (2013). Molecular chaperone functions in protein folding and proteostasis. Annual review of biochemistry *82*, 323-355.
Kirschke, E., Goswami, D., Southworth, D., Griffin, P.R., and Agard, D.A. (2014). Glucocorticoid receptor function regulated by coordinated action of the Hsp90 and Hsp70 chaperone cycles. Cell *157*, 1685-1697.
Knowles, P.F. (1981). Biophysical chemistry: Part II 'Techniques for the study of biological structure and function': By CR Cantor and PR Schimmel. pp 503. WH Freeman and Co, Oxford. 1980. £20.70/£10.60 (paperback) ISBN 0-7167-1189-3/0-7167-1190-7 (paperback). Biochemical Education *9*, 157-157.
Kosano, H., Stensgard, B., Charlesworth, M.C., McMahon, N., and Toft, D. (1998). The assembly of progesterone receptor-hsp90 complexes using purified proteins. J Biol Chem *273*, 32973-32979.
Koulov, A.V., LaPointe, P., Lu, B., Razvi, A., Coppinger, J., Dong, M.Q., Matteson, J., Laister, R., Arrowsmith, C., Yates, J.R., 3rd*, et al.* (2010). Biological and structural basis for Aha1 regulation of Hsp90 ATPase activity in maintaining proteostasis in the human disease cystic fibrosis. Mol Biol Cell *21*, 871-884.

Krukenberg, K.A., Forster, F., Rice, L.M., Sali, A., and Agard, D.A. (2008). Multiple conformations of E. coli Hsp90 in solution: insights into the conformational dynamics of Hsp90. Structure *16*, 755-765.
Kumar, R., and Thompson, E.B. (2012). Folding of the glucocorticoid receptor N-terminal transactivation function: dynamics and regulation. Molecular and cellular endocrinology *348*, 450-456.
Kundrat, L., and Regan, L. (2010). Balance between folding and degradation for Hsp90-dependent client proteins: a key role for CHIP. Biochemistry *49*, 7428-7438.
Kuwajima, K. (1989). The molten globule state as a clue for understanding the folding and cooperativity of globular-protein structure. Proteins *6*, 87-103.
Laemmli, U.K. (1970). Cleavage of structural proteins during the assembly of the head of bacteriophage T4. Nature *227*, 680-685.
Lakowicz, J.R. (2007). Principles of Fluorescence Spectroscopy (Springer US).
Laue TM, S.B., Ridgeway TM, Pelletier SL (1992). Computer-Aided Interpretation of Analytical Sedimentation Data For Proteins. In: Harding SE, Rowe AJ, Horton JC, editors Analytical Ultracentrifugation in Biochemistry and Polymer Science Royal Society of Chemistry; Cambridge, UK, pp. 90–125.
Lavery, L.A., Partridge, J.R., Ramelot, T.A., Elnatan, D., Kennedy, M.A., and Agard, D.A. (2014). Structural asymmetry in the closed state of mitochondrial Hsp90 (TRAP1) supports a two-step ATP hydrolysis mechanism. Molecular cell *53*, 330-343.
Lee, C.-T., Graf, C., Mayer, F.J., Richter, S.M., and Mayer, M.P. (2012). Dynamics of the regulation of Hsp90 by the co-chaperone Sti1. EMBO J *31*, 1518-1528.
Lemon, B., and Tjian, R. (2000). Orchestrated response: a symphony of transcription factors for gene control. Genes & development *14*, 2551-2569.
Levinthal, C. (1968). Are there pathways for protein folding? Journal De Chimie Physique Et De Physico-Chimie Biologique *65*, 44-45.
Li, J., Richter, K., and Buchner, J. (2011). Mixed Hsp90-cochaperone complexes are important for the progression of the reaction cycle. Nature structural & molecular biology *18*, 61-66.
Li, J., Richter, K., Reinstein, J., and Buchner, J. (2013). Integration of the accelerator Aha1 in the Hsp90 co-chaperone cycle. Nature structural & molecular biology *20*, 326-331.
Lo, M.C., Aulabaugh, A., Jin, G., Cowling, R., Bard, J., Malamas, M., and Ellestad, G. (2004). Evaluation of fluorescence-based thermal shift assays for hit identification in drug discovery. Anal Biochem *332*, 153-159.
Lorenz, O.R., Freiburger, L., Rutz, D.A., Krause, M., Zierer, B.K., Alvira, S., Cuellar, J., Valpuesta, J.M., Madl, T., Sattler, M.*, et al.* (2014). Modulation of the Hsp90 chaperone cycle by a stringent client protein. Molecular cell *53*, 941-953.
Lottspeich, F., Engels, J.W., and Solodkoff, Z.L. (2012). Bioanalytik (Spektrum Akademischer Verlag).
Lotz, G.P., Lin, H., Harst, A., and Obermann, W.M.J. (2003). Aha1 Binds to the Middle Domain of Hsp90, Contributes to Client Protein Activation, and Stimulates the ATPase Activity of the Molecular Chaperone. Journal of Biological Chemistry *278*, 17228-17235.
Luna-Muñoz, J., Chávez-Macías, L., García-Sierra, F., and Mena, R. (2007). Earliest stages of tau conformational changes are related to the appearance of a sequence of specific phospho-dependent tau epitopes in Alzheimer's disease. Journal of Alzheimer's Disease *12*, 365-375.
Luo, W., Dou, F., Rodina, A., Chip, S., Kim, J., Zhao, Q., Moulick, K., Aguirre, J., Wu, N., Greengard, P.*, et al.* (2007). Roles of heat-shock protein 90 in maintaining and facilitating the

neurodegenerative phenotype in tauopathies. Proceedings of the National Academy of Sciences of the United States of America *104*, 9511-9516.
Mapa, K., Sikor, M., Kudryavtsev, V., Waegemann, K., Kalinin, S., Seidel, C.A., Neupert, W., Lamb, D.C., and Mokranjac, D. (2010). The conformational dynamics of the mitochondrial Hsp70 chaperone. Molecular cell *38*, 89-100.
Mayer, M., Reinstein, J., and Buchner, J. (2003). Modulation of the ATPase Cycle of BiP by Peptides and Proteins. Journal of molecular biology *330*, 137-144.
Mayer, M.P. (2010). Gymnastics of molecular chaperones. Molecular cell *39*, 321-331.
Mayer, M.P., and Bukau, B. (2005). Hsp70 chaperones: cellular functions and molecular mechanism. Cellular and molecular life sciences : CMLS *62*, 670-684.
Mayer, M.P., and Le Breton, L. (2015). Hsp90: breaking the symmetry. Molecular cell *58*, 8-20.
Mayer, M.P., Schroder, H., Rudiger, S., Paal, K., Laufen, T., and Bukau, B. (2000). Multistep mechanism of substrate binding determines chaperone activity of Hsp70. Nat Struct Biol *7*, 586-593.
McClellan, A.J., Tam, S., Kaganovich, D., and Frydman, J. (2005). Protein quality control: chaperones culling corrupt conformations. Nature cell biology *7*, 736-741.
McGuffee, S.R., and Elcock, A.H. (2006). Atomically detailed simulations of concentrated protein solutions: the effects of salt, pH, point mutations, and protein concentration in simulations of 1000-molecule systems. J Am Chem Soc *128*, 12098-12110.
McKay, L.I., and Cidlowski, J.A. (1999). Molecular control of immune/inflammatory responses: interactions between nuclear factor-kappa B and steroid receptor-signaling pathways. Endocr Rev *20*, 435-459.
McLaughlin, S.H., Sobott, F., Yao, Z.P., Zhang, W., Nielsen, P.R., Grossmann, J.G., Laue, E.D., Robinson, C.V., and Jackson, S.E. (2006). The co-chaperone p23 arrests the Hsp90 ATPase cycle to trap client proteins. Journal of molecular biology *356*, 746-758.
Meyer, P., Prodromou, C., Hu, B., Vaughan, C., Roe, S.M., Panaretou, B., Piper, P.W., and Pearl, L.H. (2003). Structural and functional analysis of the middle segment of hsp90: implications for ATP hydrolysis and client protein and cochaperone interactions. Molecular cell *11*, 647-658.
Meyer, P., Prodromou, C., Liao, C., Hu, B., Mark Roe, S., Vaughan, C.K., Vlasic, I., Panaretou, B., Piper, P.W., and Pearl, L.H. (2004). Structural basis for recruitment of the ATPase activator Aha1 to the Hsp90 chaperone machinery. The EMBO Journal *23*, 511-519.
Mickler, M., Hessling, M., Ratzke, C., Buchner, J., and Hugel, T. (2009). The large conformational changes of Hsp90 are only weakly coupled to ATP hydrolysis. Nature structural & molecular biology *16*, 281-286.
Moehren, U., Eckey, M., and Baniahmad, A. (2004). Gene repression by nuclear hormone receptors. Essays in biochemistry *40*, 89-104.
Mollapour, M., Tsutsumi, S., Donnelly, A.C., Beebe, K., Tokita, M.J., Lee, M.J., Lee, S., Morra, G., Bourboulia, D., Scroggins, B.T.*, et al.* (2010). Swe1Wee1-dependent tyrosine phosphorylation of Hsp90 regulates distinct facets of chaperone function. Molecular cell *37*, 333-343.
Mollapour, M., Tsutsumi, S., Truman, A.W., Xu, W., Vaughan, C.K., Beebe, K., Konstantinova, A., Vourganti, S., Panaretou, B., Piper, P.W.*, et al.* (2011). Threonine 22 phosphorylation attenuates Hsp90 interaction with cochaperones and affects its chaperone activity. Molecular cell *41*, 672-681.
Morgner, N., Schmidt, C., Beilsten-Edmands, V., Ebong, I.-o., Patel, Nisha A., Clerico, Eugenia M., Kirschke, E., Daturpalli, S., Jackson, Sophie E., Agard, D.*, et al.* (2015). Hsp70

Forms Antiparallel Dimers Stabilized by Post-translational Modifications to Position Clients for Transfer to Hsp90. Cell Reports *11*, 759-769.
Morishima, Y., Kanelakis, K.C., Silverstein, A.M., Dittmar, K.D., Estrada, L., and Pratt, W.B. (2000a). The Hsp organizer protein hop enhances the rate of but is not essential for glucocorticoid receptor folding by the multiprotein Hsp90-based chaperone system. J Biol Chem *275*, 6894-6900.
Morishima, Y., Murphy, P.J., Li, D.P., Sanchez, E.R., and Pratt, W.B. (2000b). Stepwise assembly of a glucocorticoid receptor.hsp90 heterocomplex resolves two sequential ATP-dependent events involving first hsp70 and then hsp90 in opening of the steroid binding pocket. J Biol Chem *275*, 18054-18060.
Mukrasch, M.D., Bibow, S., Korukottu, J., Jeganathan, S., Biernat, J., Griesinger, C., Mandelkow, E., and Zweckstetter, M. (2009). Structural polymorphism of 441-residue Tau at single residue resolution. PLoS biology *7*, 0399-0414.
Mukrasch, M.D., Biernat, J., Von Bergen, M., Griesinger, C., Mandelkow, E., and Zweckstetter, M. (2005). Sites of tau important for aggregation populate β-structure and bind to microtubules and polyanions. Journal of Biological Chemistry *280*, 24978-24986.
Mumberg, D., Muller, R., and Funk, M. (1995). Yeast vectors for the controlled expression of heterologous proteins in different genetic backgrounds. Gene *156*, 119-122.
Nagy, L., Kao, H.Y., Love, J.D., Li, C., Banayo, E., Gooch, J.T., Krishna, V., Chatterjee, K., Evans, R.M., and Schwabe, J.W. (1999). Mechanism of corepressor binding and release from nuclear hormone receptors. Genes & development *13*, 3209-3216.
Nathan, D.F., and Lindquist, S. (1995). Mutational analysis of Hsp90 function: interactions with a steroid receptor and a protein kinase. Molecular and cellular biology *15*, 3917-3925.
Neumann, M., Diekmann, S., Bertsch, U., Vanmassenhove, B., Bogerts, B., and Kretzschmar, H.A. (2005). Novel G335V mutation in the tau gene associated with early onset familial frontotemporal dementia. Neurogenetics *6*, 91-95.
Nicolaides, N.C., Galata, Z., Kino, T., Chrousos, G.P., and Charmandari, E. (2010). The human glucocorticoid receptor: Molecular basis of biologic function. Steroids *75*, 1-12.
Obermann, W.M., Sondermann, H., Russo, A.A., Pavletich, N.P., and Hartl, F.U. (1998). In vivo function of Hsp90 is dependent on ATP binding and ATP hydrolysis. The Journal of cell biology *143*, 901-910.
Panaretou, B., Prodromou, C., Roe, S.M., O'Brien, R., Ladbury, J.E., Piper, P.W., and Pearl, L.H. (1998). ATP binding and hydrolysis are essential to the function of the Hsp90 molecular chaperone in vivo. The EMBO journal *17*, 4829-4836.
Panaretou, B., Siligardi, G., Meyer, P., Maloney, A., Sullivan, J.K., Singh, S., Millson, S.H., Clarke, P.A., Naaby-Hansen, S., Stein, R.*, et al.* (2002). Activation of the ATPase Activity of Hsp90 by the Stress-Regulated Cochaperone Aha1. Molecular cell *10*, 1307-1318.
Park, S.J., Borin, B.N., Martinez-Yamout, M.A., and Dyson, H.J. (2011). The client protein p53 adopts a molten globule-like state in the presence of Hsp90. Nature structural & molecular biology *18*, 537-541.
Pearl, L.H. (2016). Review: The HSP90 molecular chaperone—an enigmatic ATPase. Biopolymers *105*, 594-607.
Pearl, L.H., and Prodromou, C. (2006). Structure and mechanism of the Hsp90 molecular chaperone machinery. Annual review of biochemistry *75*, 271-294.
Peterson, D.W., Zhou, H., Dahlquist, F.W., and Lew, J. (2008). A soluble oligomer of tau associated with fiber formation analyzed by NMR. Biochemistry *47*, 7393-7404.

Phillips, J.C., Braun, R., Wang, W., Gumbart, J., Tajkhorshid, E., Villa, E., Chipot, C., Skeel, R.D., Kale, L., and Schulten, K. (2005). Scalable molecular dynamics with NAMD. J Comput Chem *26*, 1781-1802.
Picard, D., Khursheed, B., Garabedian, M.J., Fortin, M.G., Lindquist, S., and Yamamoto, K.R. (1990). Reduced levels of hsp90 compromise steroid receptor action in vivo. Nature *348*, 166-168.
Picard, D., and Yamamoto, K.R. (1987). Two signals mediate hormone-dependent nuclear localization of the glucocorticoid receptor. EMBO Journal *6*, 3333-3340.
Pirkl, F., and Buchner, J. (2001). Functional analysis of the Hsp90-associated human peptidyl prolyl cis/trans isomerases FKBP51, FKBP52 and Cyp40. Journal of molecular biology *308*, 795-806.
Poppek, D., Keck, S., Ermak, G., Jung, T., Stolzing, A., Ullrich, O., Davies, K.J.A., and Grune, T. (2006). Phosphorylation inhibits turnover of the tau protein by the proteasome: Influence of RCAN1 and oxidative stress. Biochemical Journal *400*, 511-520.
Pratt, W.B., and Dittmar, K.D. (1998). Studies with Purified Chaperones Advance the Understanding of the Mechanism of Glucocorticoid Receptor-hsp90 Heterocomplex Assembly. Trends in endocrinology and metabolism: TEM *9*, 244-252.
Pratt, W.B., Galigniana, M.D., Morishima, Y., and Murphy, P.J. (2004). Role of molecular chaperones in steroid receptor action. Essays in biochemistry *40*, 41-58.
Pratt, W.B., and Toft, D.O. (1997). Steroid receptor interactions with heat shock protein and immunophilin chaperones. Endocr Rev *18*, 306-360.
Preuss, U., Biernat, J., Mandelkow, E.M., and Mandelkow, E. (1997). The 'jaws' model of tau-microtubule interaction examined in CHO cells. Journal of Cell Science *110*, 789-800.
Prodromou, C. (2012). The 'active life' of Hsp90 complexes. Biochimica et biophysica acta *1823*, 614-623.
Prodromou, C., Siligardi, G., O'Brien, R., Woolfson, D.N., Regan, L., Panaretou, B., Ladbury, J.E., Piper, P.W., and Pearl, L.H. (1999). Regulation of Hsp90 ATPase activity by tetratricopeptide repeat (TPR)-domain co-chaperones. EMBO J *18*, 754-762.
Pullen, L., and Bolon, D.N. (2011). Enforced N-domain proximity stimulates Hsp90 ATPase activity and is compatible with function in vivo. J Biol Chem *286*, 11091-11098.
Ratajczak, T., Hlaing, J., Brockway, M.J., and Hahnel, R. (1990). Isolation of untransformed bovine estrogen receptor without molybdate stabilization. J Steroid Biochem *35*, 543-553.
Ratzke, C., Mickler, M., Hellenkamp, B., Buchner, J., and Hugel, T. (2010). Dynamics of heat shock protein 90 C-terminal dimerization is an important part of its conformational cycle. Proceedings of the National Academy of Sciences of the United States of America *107*, 16101-16106.
Retzlaff, M., Hagn, F., Mitschke, L., Hessling, M., Gugel, F., Kessler, H., Richter, K., and Buchner, J. (2010). Asymmetric activation of the hsp90 dimer by its cochaperone aha1. Molecular cell *37*, 344-354.
Reynolds, P.D., Ruan, Y., Smith, D.F., and Scammell, J.G. (1999). Glucocorticoid resistance in the squirrel monkey is associated with overexpression of the immunophilin FKBP51. J Clin Endocrinol Metab *84*, 663-669.
Richter, K., Haslbeck, M., and Buchner, J. (2010). The heat shock response: life on the verge of death. Molecular cell *40*, 253-266.
Richter, K., Muschler, P., Hainzl, O., Reinstein, J., and Buchner, J. (2003). Sti1 is a non-competitive inhibitor of the Hsp90 ATPase. Binding prevents the N-terminal dimerization reaction during the atpase cycle. J Biol Chem *278*, 10328-10333.

Richter, K., Reinstein, J., and Buchner, J. (2002). N-terminal residues regulate the catalytic efficiency of the Hsp90 ATPase cycle. J Biol Chem *277*, 44905-44910.
Richter, K., Soroka, J., Skalniak, L., Leskovar, A., Hessling, M., Reinstein, J., and Buchner, J. (2008). Conserved conformational changes in the ATPase cycle of human Hsp90. J Biol Chem *283*, 17757-17765.
Richter, K., Walter, S., and Buchner, J. (2004). The Co-chaperone Sba1 connects the ATPase reaction of Hsp90 to the progression of the chaperone cycle. Journal of molecular biology *342*, 1403-1413.
Riggs, D.L., Roberts, P.J., Chirillo, S.C., Cheung-Flynn, J., Prapapanich, V., Ratajczak, T., Gaber, R., Picard, D., and Smith, D.F. (2003). The Hsp90-binding peptidylprolyl isomerase FKBP52 potentiates glucocorticoid signaling in vivo. EMBO J *22*, 1158-1167.
Rodriguez, F., Arsène-Ploetze, F., Rist, W., Rüdiger, S., Schneider-Mergener, J., Mayer, M.P., and Bukau, B. (2008). Molecular Basis for Regulation of the Heat Shock Transcription Factor σ32 by the DnaK and DnaJ Chaperones. Molecular cell *32*, 347-358.
Roe, S.M., Ali, M.M., Meyer, P., Vaughan, C.K., Panaretou, B., Piper, P.W., Prodromou, C., and Pearl, L.H. (2004). The Mechanism of Hsp90 regulation by the protein kinase-specific cochaperone p50(cdc37). Cell *116*, 87-98.
Rohl, A., Rohrberg, J., and Buchner, J. (2013). The chaperone Hsp90: changing partners for demanding clients. Trends Biochem Sci *38*, 253-262.
Rohl, A., Tippel, F., Bender, E., Schmid, A.B., Richter, K., Madl, T., and Buchner, J. (2015a). Hop/Sti1 phosphorylation inhibits its co-chaperone function. EMBO reports *16*, 240-249.
Rohl, A., Wengler, D., Madl, T., Lagleder, S., Tippel, F., Herrmann, M., Hendrix, J., Richter, K., Hack, G., Schmid, A.B.*, et al.* (2015b). Hsp90 regulates the dynamics of its cochaperone Sti1 and the transfer of Hsp70 between modules. Nature communications *6*, 6655.
Rudiger, S., Freund, S.M., Veprintsev, D.B., and Fersht, A.R. (2002). CRINEPT-TROSY NMR reveals p53 core domain bound in an unfolded form to the chaperone Hsp90. Proceedings of the National Academy of Sciences of the United States of America *99*, 11085-11090.
Sabbagh, J.J., and Dickey, C.A. (2016). The metamorphic nature of the Tau protein: Dynamic flexibility comes at a cost. Frontiers in Neuroscience *10*.
Salek, R.M., Williams, M.A., Prodromou, C., Pearl, L.H., and Ladbury, J.E. (2002). Backbone resonance assignments of the 25kD N-terminal ATPase domain from the Hsp90 chaperone. Journal of biomolecular NMR *23*, 327-328.
Sali, A., and Blundell, T.L. (1993). Comparative protein modelling by satisfaction of spatial restraints. Journal of molecular biology *234*, 779-815.
Sato, S., Fujita, N., and Tsuruo, T. (2000). Modulation of Akt kinase activity by binding to Hsp90. Proceedings of the National Academy of Sciences of the United States of America *97*, 10832-10837.
Scherrer, L.C., Dalman, F.C., Massa, E., Meshinchi, S., and Pratt, W.B. (1990). Structural and functional reconstitution of the glucocorticoid receptor-hsp90 complex. J Biol Chem *265*, 21397-21400.
Schlecht, R., Scholz, S.R., Dahmen, H., Wegener, A., Sirrenberg, C., Musil, D., Bomke, J., Eggenweiler, H.-M., Mayer, M.P., and Bukau, B. (2013). Functional Analysis of Hsp70 Inhibitors. PloS one *8*, e78443.
Schmid, A.B., Lagleder, S., Gräwert, M.A., Röhl, A., Hagn, F., Wandinger, S.K., Cox, M.B., Demmer, O., Richter, K., Groll, M.*, et al.* (2012). The architecture of functional modules in the Hsp90 co-chaperone Sti1/Hop. The EMBO Journal *31*, 1506-1517.

Schneider, M., Rosam, M., Glaser, M., Patronov, A., Shah, H., Back, K.C., Daake, M.A., Buchner, J., and Antes, I. (2016). BiPPred: Combined sequence- and structure-based prediction of peptide binding to the Hsp70 chaperone BiP. Proteins.
Schoch, G.A., D'Arcy, B., Stihle, M., Burger, D., Bar, D., Benz, J., Thoma, R., and Ruf, A. (2010). Molecular switch in the glucocorticoid receptor: active and passive antagonist conformations. Journal of molecular biology *395*, 568-577.
Schuck, P. (2000). Size-distribution analysis of macromolecules by sedimentation velocity ultracentrifugation and lamm equation modeling. Biophys J *78*, 1606-1619.
Schuck, S.a. (2005). A Brief Introduction to the Analytical Ultracentrifugation of Proteins for Beginners. In Analytical Ultracentrifugation: Techniques and Methods, D.J. Scott, S.E. Harding, and A.J. Rowe, eds. (The Royal Society of Chemistry), pp. 1-25.
Seitz, T., Thoma, R., Schoch, G.A., Stihle, M., Benz, J., D'Arcy, B., Wiget, A., Ruf, A., Hennig, M., and Sterner, R. (2010). Enhancing the stability and solubility of the glucocorticoid receptor ligand-binding domain by high-throughput library screening. Journal of molecular biology *403*, 562-577.
Shiau, A.K., Harris, S.F., Southworth, D.R., and Agard, D.A. (2006). Structural Analysis of E. coli hsp90 reveals dramatic nucleotide-dependent conformational rearrangements. Cell *127*, 329-340.
Siligardi, G., Hu, B., Panaretou, B., Piper, P.W., Pearl, L.H., and Prodromou, C. (2004). Co-chaperone regulation of conformational switching in the Hsp90 ATPase cycle. J Biol Chem *279*, 51989-51998.
Smith, D.F. (1993). Dynamics of heat shock protein 90-progesterone receptor binding and the disactivation loop model for steroid receptor complexes. Molecular endocrinology *7*, 1418-1429.
Smith, D.F. (2004). Tetratricopeptide repeat cochaperones in steroid receptor complexes. Cell Stress Chaperones *9*, 109-121.
Smith, D.F., and Toft, D.O. (2008). Minireview: the intersection of steroid receptors with molecular chaperones: observations and questions. Molecular endocrinology (Baltimore, Md) *22*, 2229-2240.
Smock, R.G., Rivoire, O., Russ, W.P., Swain, J.F., Leibler, S., Ranganathan, R., and Gierasch, L.M. (2010). An interdomain sector mediating allostery in Hsp70 molecular chaperones. Mol Syst Biol *6*, 414.
Soroka, J., Wandinger, S.K., Mausbacher, N., Schreiber, T., Richter, K., Daub, H., and Buchner, J. (2012). Conformational switching of the molecular chaperone Hsp90 via regulated phosphorylation. Molecular cell *45*, 517-528.
Southworth, D.R., and Agard, D.A. (2008). Species-dependent ensembles of conserved conformational states define the Hsp90 chaperone ATPase cycle. Molecular cell *32*, 631-640.
Southworth, D.R., and Agard, D.A. (2011). Client-loading conformation of the Hsp90 molecular chaperone revealed in the cryo-EM structure of the human Hsp90:Hop complex. Molecular cell *42*, 771-781.
Street, T.O., Lavery, L.A., and Agard, D.A. (2011). Substrate binding drives large-scale conformational changes in the Hsp90 molecular chaperone. Molecular cell *42*, 96-105.
Studier, F.W. (2005). Protein production by auto-induction in high density shaking cultures. Protein expression and purification *41*, 207-234.
Sun, L., Edelmann, F.T., Kaiser, C.J.O., Papsdorf, K., Gaiser, A.M., and Richter, K. (2012). The Lid Domain of <italic>Caenorhabditis elegans</italic> Hsc70 Influences ATP Turnover, Cofactor Binding and Protein Folding Activity. PloS one *7*, e33980.

Surjit, M., Ganti, K.P., Mukherji, A., Ye, T., Hua, G., Metzger, D., Li, M., and Chambon, P. (2011). Widespread negative response elements mediate direct repression by agonist-liganded glucocorticoid receptor. Cell *145*, 224-241.
Svergun, D. (1992). Determination of the regularization parameter in indirect-transform methods using perceptual criteria. Journal of Applied Crystallography *25*, 495-503.
Svergun, D., Barberato, C., and Koch, M.H.J. (1995). CRYSOL - a Program to Evaluate X-ray Solution Scattering of Biological Macromolecules from Atomic Coordinates. Journal of Applied Crystallography *28*, 768-773.
Taipale, M., Jarosz, D.F., and Lindquist, S. (2010). HSP90 at the hub of protein homeostasis: emerging mechanistic insights. Nat Rev Mol Cell Biol *11*, 515-528.
Taipale, M., Krykbaeva, I., Koeva, M., Kayatekin, C., Westover, K.D., Karras, G.I., and Lindquist, S. (2012). Quantitative analysis of HSP90-client interactions reveals principles of substrate recognition. Cell *150*, 987-1001.
Tanenbaum, D.M., Wang, Y., Williams, S.P., and Sigler, P.B. (1998). Crystallographic comparison of the estrogen and progesterone receptor's ligand binding domains. Proceedings of the National Academy of Sciences of the United States of America *95*, 5998-6003.
Tortosa, E., Santa-Maria, I., Moreno, F., Lim, F., Perez, M., and Avila, J. (2009). Binding of hsp90 to tau promotes a conformational change and aggregation of tau protein. Journal of Alzheimer's Disease *17*, 319-325.
Trepel, J., Mollapour, M., Giaccone, G., and Neckers, L. (2010). Targeting the dynamic HSP90 complex in cancer. Nature reviews Cancer *10*, 537-549.
Tsai, J., and Douglas, M.G. (1996). A Conserved HPD Sequence of the J-domain Is Necessary for YDJ1 Stimulation of Hsp70 ATPase Activity at a Site Distinct from Substrate Binding. Journal of Biological Chemistry *271*, 9347-9354.
Tsai, J., Lee, J.T., Wang, W., Zhang, J., Cho, H., Mamo, S., Bremer, R., Gillette, S., Kong, J., Haass, N.K.*, et al.* (2008). Discovery of a selective inhibitor of oncogenic B-Raf kinase with potent antimelanoma activity. Proceedings of the National Academy of Sciences *105*, 3041-3046.
Tsutsumi, S., Mollapour, M., Graf, C., Lee, C.T., Scroggins, B.T., Xu, W., Haslerova, L., Hessling, M., Konstantinova, A.A., Trepel, J.B.*, et al.* (2009). Hsp90 charged-linker truncation reverses the functional consequences of weakened hydrophobic contacts in the N domain. Nature structural & molecular biology *16*, 1141-1147.
Vandevyver, S., Dejager, L., and Libert, C. (2012). On the trail of the glucocorticoid receptor: into the nucleus and back. Traffic *13*, 364-374.
Vaughan, C.K., Gohlke, U., Sobott, F., Good, V.M., Ali, M.M., Prodromou, C., Robinson, C.V., Saibil, H.R., and Pearl, L.H. (2006). Structure of an Hsp90-Cdc37-Cdk4 complex. Molecular cell *23*, 697-707.
Vaughan, C.K., Mollapour, M., Smith, J.R., Truman, A., Hu, B., Good, V.M., Panaretou, B., Neckers, L., Clarke, P.A., Workman, P.*, et al.* (2008). Hsp90-dependent activation of protein kinases is regulated by chaperone-targeted dephosphorylation of Cdc37. Molecular cell *31*, 886-895.
Vega, I.E., Cui, L., Propst, J.A., Hutton, M.L., Lee, G., and Yen, S.H. (2005). Increase in tau tyrosine phosphorylation correlates with the formation of tau aggregates. Molecular Brain Research *138*, 135-144.
Venyaminov, S.Y., Baikalov, I.A., Shen, Z.M., Wu, C.S.C., and Yang, J.T. (1993). Circular Dichroic Analysis of Denatured Proteins: Inclusion of Denatured Proteins in the Reference Set. Analytical biochemistry *214*, 17-24.

Verba, K.A., Wang, R.Y., Arakawa, A., Liu, Y., Shirouzu, M., Yokoyama, S., and Agard, D.A. (2016). Atomic structure of Hsp90-Cdc37-Cdk4 reveals that Hsp90 traps and stabilizes an unfolded kinase. Science *352*, 1542-1547.
Von Bergen, M., Barghorn, S., Li, L., Marx, A., Biernat, J., Mandelkow, E.M., and Mandelkow, E. (2001). Mutations of Tau Protein in Frontotemporal Dementia Promote Aggregation of Paired Helical Filaments by Enhancing Local β-Structure. Journal of Biological Chemistry *276*, 48165-48174.
Vranken, W.F., Boucher, W., Stevens, T.J., Fogh, R.H., Pajon, A., Llinas, M., Ulrich, E.L., Markley, J.L., Ionides, J., and Laue, E.D. (2005). The CCPN data model for NMR spectroscopy: development of a software pipeline. Proteins *59*, 687-696.
Watanabe, A., Hasegawa, M., Suzuki, M., Takio, K., Moriahima-Kawashima, M., Titani, K., Arai, T., Kosik, K.S., and Ihara, Y. (1993). In vivo phosphorylation sites in fetal and adult rat tau. Journal of Biological Chemistry *268*, 25712-25717.
Weaver, A.J., Sullivan, W.P., Felts, S.J., Owen, B.A., and Toft, D.O. (2000). Crystal structure and activity of human p23, a heat shock protein 90 co-chaperone. J Biol Chem *275*, 23045-23052.
Weikl, T., Abelmann, K., and Buchner, J. (1999). An unstructured C-terminal region of the hsp90 co-chaperone p23 is important for its chaperone function1. Journal of Molecular Biology *293*, 685-691.
Weikl, T., Muschler, P., Richter, K., Veit, T., Reinstein, J., and Buchner, J. (2000). C-terminal regions of Hsp90 are important for trapping the nucleotide during the ATPase cycle1. Journal of molecular biology *303*, 583-592.
Weingarten, M.D., Lockwood, A.H., Hwo, S.Y., and Kirschner, M.W. (1975). A protein factor essential for microtubule assembly. Proceedings of the National Academy of Sciences of the United States of America *72*, 1858-1862.
Whitesell, L., and Lindquist, S.L. (2005). HSP90 and the chaperoning of cancer. Nature reviews Cancer *5*, 761-772.
Wider, D., Peli-Gulli, M.P., Briand, P.A., Tatu, U., and Picard, D. (2009). The complementation of yeast with human or Plasmodium falciparum Hsp90 confers differential inhibitor sensitivities. Mol Biochem Parasitol *164*, 147-152.
Wood, E.J. (1983). Molecular cloning. A laboratory manual by T Maniatis, E F Fritsch and J Sambrook. pp 545. Cold Spring Harbor Laboratory, New York. 1982. $48 ISBN 0-87969-136-0. Biochemical Education *11*, 82-82.
Wu, Z., Moghaddas Gholami, A., and Kuster, B. (2012). Systematic identification of the HSP90 candidate regulated proteome. Molecular & cellular proteomics : MCP *11*, M111 016675.
Wurtz, J.M., Bourguet, W., Renaud, J.P., Vivat, V., Chambon, P., Moras, D., and Gronemeyer, H. (1996). A canonical structure for the ligand-binding domain of nuclear receptors. Nat Struct Biol *3*, 87-94.
Yoshida, H., and Ihara, Y. (1993). τ In paired helical filaments is functionally distinct from fetal τ: Assembly incompetence of paired helical filament-τ. Journal of neurochemistry *61*, 1183-1186.
Young, J.C., Agashe, V.R., Siegers, K., and Hartl, F.U. (2004). Pathways of chaperone-mediated protein folding in the cytosol. Nature Reviews Molecular Cell Biology *5*, 781-791.
Yu, X., Luo, Y., Dinkel, P., Zheng, J., Wei, G., Margittai, M., Nussinov, R., and Ma, B. (2012). Cross-seeding and conformational selection between three- and four-repeat human Tau proteins. Journal of Biological Chemistry *287*, 14950-14959.
Zhou, J., and Cidlowski, J.A. (2005). The human glucocorticoid receptor: one gene, multiple proteins and diverse responses. Steroids *70*, 407-417.

Zhu, X., Zhao, X., Burkholder, W.F., Gragerov, A., Ogata, C.M., Gottesman, M.E., and Hendrickson, W.A. (1996). Structural analysis of substrate binding by the molecular chaperone DnaK. Science *272*, 1606-1614.
Zhuravleva, A., and Gierasch, L.M. (2011). Allosteric signal transmission in the nucleotide-binding domain of 70-kDa heat shock protein (Hsp70) molecular chaperones. Proceedings of the National Academy of Sciences of the United States of America *108*, 6987-6992.
Zierer, B., Rübbelke, M., Tippel, F., Madl, T., Schopf, F.H., Rutz, D.A., Richter, K., Sattler, M., and Buchner, J. (2016 accepted). Importance of cycle timing for the function of the molecular chaperone Hsp90. Nature Structural and Molecular Biology *accepted*.

# 8 Publications

Eckl, J.M., Drazic, A., **Rutz, D.A.**, and Richter, K. (2014). Nematode Sgt1-homologue D1054.3 binds open and closed conformations of Hsp90 via distinct binding sites. Biochemistry *53*, 2505-2514.

Eckl, J.M., **Rutz, D.A.**, Haslbeck, V., Zierer, B.K., Reinstein, J., and Richter, K. (2013). Cdc37 (cell division cycle 37) restricts Hsp90 (heat shock protein 90) motility by interaction with N-terminal and middle domain binding sites. J Biol Chem *288*, 16032-16042.

Haslbeck, V., Eckl, J.M., Drazic, A., **Rutz, D.A**., Lorenz, O.R., Zimmermann, K., Kriehuber, T., Lindemann, C., Madl, T., and Richter, K. (2015). The activity of protein phosphatase 5 towards native clients is modulated by the middle- and C-terminal domains of Hsp90. Scientific reports *5*, 17058.

Lorenz, O.R., Freiburger, L., **Rutz, D.A.**, Krause, M., Zierer, B.K., Alvira, S., Cuellar, J., Valpuesta, J.M., Madl, T., Sattler, M.*, et al.* (2014). Modulation of the Hsp90 chaperone cycle by a stringent client protein. Mol Cell *53*, 941-953.

Zierer, B., Rübbelke, M., Tippel, F., Madl, T., Schopf, F.H., **Rutz, D.A.**, Richter, K., Sattler, M., and Buchner, J. (2016 accepted). Importance of cycle timing for the function of the molecular chaperone Hsp90. Nature Structural and Molecular Biology *accepted*.

# Publications

# 9 Danksagung

An erster Stelle möchte ich mich bei meinem Doktorvater Johannes Buchner für die Möglichkeit meine Doktor-Arbeit in seiner Gruppe anzufertigen, sowie für sein Vertrauen in mich und sein stetiges Engagement bedanken.
Ein großer Dank geht an die meine Kooperationspartner Michael Sattler, Lee Freiburger, Matthias Rief, Thomas Suren, Don Lamb, Daniela Wengler und Tobias Madl für die gute Zusammenarbeit.
Anja Liebscher, Bettina Richter und Margot Rubinstein sei für die stetige Unterstützung im Laboralltag, sowie der Meisterung bürokratischer Hürden gedankt.
Meinen (ehemaligen) Kollegen Oliver Lorenz, Julia Eckl, Adrian „Stanic“ Drazic, Florian H. Schopf, Katrin Back, Mathias Rosam, Klaus Richter, sowie dem gesamten Lehrstuhl für Biotechnologie danke ich für die schönen Zeiten während meiner Promotion.
Meinen Freunden Harry, Obi, Tino, Felix, Isabella und den „Stöckies“ danke ich für die vielen schönen Feiern und anderen Erfahrungen abseits des Labors.
Ganz besonders möchte ich mich bei Lisa Streitmayer, meinen Eltern Dr. Andreas Rutz und Eva Rutz, meiner Schwester Dr. Miriam Haas und ihrem Mann Markus Haas, sowie dem Rest der Familie für ihre stetige Unterstützung, vor allem auch in schwierigen Zeiten, bedanken.

# Danksagung

## 10 Eidesstattliche Erklärung

Hiermit erkläre ich an Eides statt, dass ich die vorliegende Arbeit selbständig verfasst und keine anderen als die angegebenen Quellen und Hilfsmittel verwendet habe. Die aus fremden Quellen übernommenen Gedanken sind als solche kenntlich gemacht. Die vorliegende Arbeit wurde noch keiner anderen Prüfungsbehörde vorgelegt. Teile dieser Arbeit wurden in einem wissenschaftlichen Journal veröffentlicht.

Garching, den 30.08.2016

Daniel Andreas Rutz